Contents

1.10 Analysis of Drift-Scale Thermal-Hydrological Behavior in the Repository

As was discussed in Section 1.8, decay heat, primarily from spent nuclear fuel (SNF), will play a dominant role in gas- and liquid-phase moisture movement in both the near- and far-field in the unsaturated zone (UZ) and in liquid-phase movement in a significant region of the saturated zone (SZ) at Yucca Mountain. The spatial and temporal extent of the thermal-hydrological effects of decay heat in the UZ and SZ is discussed in Chapter 10.0: Altered Zone. Chapter 1.0 (and Section 1.10 in particular) primarily focuses on the thermal-hydrological effects of decay heat at the drift scale, which includes the emplacement drifts and the rock pillars separating the emplacement drifts throughout the repository area.

1.10.1 Overview

There has been considerable discussion about the pros and cons of various thermal loading strategies, with much of the debate focused on the areal mass loading (AML, expressed in metric tons of uranium per acre, MTU/acre). While there are many competing factors (e.g., operational constraints, costs, material responses, etc.) to consider in evaluating the impacts of alternative thermal designs, some of the key considerations involve the dominant role that decay heat plays in determining the thermal-hydrological (T-H) conditions in and around the emplacement drifts and, in particular, on the WP itself. A key consideration for nuclear waste isolation is whether (or when and how) water contacts a WP, thereby affecting WP integrity, and if WPs are breached, waste form dissolution and release from the WPs. The manner in which decay heat influences the distribution of liquid saturation and liquid-phase flux within the drifts (also called the Engineered Barrier System or EBS) strongly affects radionuclide transport within the EBS and eventual radionuclide release from the EBS. The manner in which decay heat influences the distribution of liquid saturation and liquid-phase flux in the near field and altered zone affects radionuclide transport within those zones. Although not discussed in this section, the T-H effects of decay heat influence geomechanical and geochemical changes in the near field and altered zone (as a result of coupled T-H-M-C processes), which can also affect T-H flow and radionuclide transport within those zones. Coupled T-H-M-C effects will continue to influence radionuclide transport well after decay heat has stopped mobilizing gas-phase and liquid-phase flow in the UZ.

One of the most important conclusions from this study is that the details of how the WPs are configured within the repository (e.g., in a square configuration versus a line-load configuration with tight axial WP spacing and wide drift spacing) play a far greater role in determining whether near-field thermal-hydrological behavior is beneficial (versus deleterious) than the overall AML of the repository itself. One of the primary objectives of Section 1.10 is to establish functional relationships (i.e., the parametric sensitivity) between repository system parameters and near-field thermal-hydrological behavior, and thereby help develop a quantitative framework upon which thermal management principles may be incorporated into the design of the repository system. These functional relationships are also needed to (1) provide guidance for thermal-hydrological testing, (2) assist in the model abstraction process for total system performance assessment, and (3) provide a quantitative framework for comparing various alternatives that are being evaluated by the systems studies.

1.10.1.1 Background

For a nuclear waste repository in the UZ at Yucca Mountain, there are two thermal loading approaches to using decay heat constructively—that is, to substantially reduce *RH* and liquid flow near

WPs for a considerable time, and thereby limit WP degradation and radionuclide dissolution and release. "Extended dryout" (called ED) achieves these effects with a thermal load high enough to generate large-scale (coalesced) rock dryout. "Localized dryout" (called LD, which uses wide drift spacing and a thermal load too low for coalesced dryout) achieves them by maintaining a large temperature difference (ΔT_{drift}) between the WP and drift wall; this is done with close WP spacing (generating a high line-heat load) and/or low-thermal-conductivity backfill in the drift. Backfill can greatly reduce *RH* on the WP in both the localized and extended dryout approaches. Besides using decay heat constructively, localized dryout reduces the possibility that far-field temperature rise and condensate buildup above the drifts might adversely affect waste isolation. In Section 1.10.2, we examine how the major thermal design parameters (areal mass loading AML, lineal mass loading LML, drift spacing, SNF age) distinguish between the LD and ED behavior.

One of the primary issues for thermal management is to minimize the liquid-phase flux that can enter the emplacement drifts. There are two fundamental strategies to attempt to reach this goal. The minimally heated (MH) repository strategy attempts to minimize the overall magnitude of decay-heat-mobilized condensate flow, and thereby minimize the probability of adding to the liquid-phase flux into the emplacement drifts. The constructively heated (CH) repository strategy uses either the extended dryout (ED) approach and/or the localized dryout (LD) approach to decrease the likelihood that either heat-mobilized liquid-phase flux or ambient percolation flux can enter the drift (Section 1.8.2). Water may contact a WP by either liquid-phase (advective or diffusive) flow or by condensation of water vapor that forms a liquid film on the WP. There are three ways by which this contact may arise:

Drift seepage: Advective liquid-phase flow of water that enters the drift (and flows through the backfill if present) as a result of ambient percolation or decay-heat-driven condensate flow. This can include episodic nonequilibrium fracture flow or a steady weep.

Wicking: Transport of moisture driven by matric potential gradients (i.e., capillary pressure gradients). This is primarily considered to be an advective liquid-phase transport process (called imbibition); however, binary gas-phase diffusion can also play a role. Because wicking can occur as two-phase flow, it does not necessarily require a continuous liquid phase.

Cold-trap effect: Axial vapor flow and condensation within the drift is driven by axial variations in T and P_v along the drift. Water vapor is transported (by gas-phase advection and diffusion) from areas of higher temperature and P_v to areas of lower temperature and P_v where it condenses, which causes *RH* to increase (even as high as 100%). Large condensation rates can arise in the cooler areas if the following three conditions are met: (1) high *RH* in the rock at the drift wall, (2) WP heat output varies substantially from WP to WP, and (3) WPs are thermally isolated from one another. It is important to note that this mechanism does not require water to enter the drift.

For all three of these effects, we find that the most important thermal-management design factor is the WP layout (e.g., WPs placed in a square configuration versus in a line-load configuration with tight axial WP spacing and wide drift spacing) rather than the overall AML of the repository itself.

In modeling and analyzing near-field T-H behavior it is important to be cognizant of the factors that may cause temporal and spatial variability within the repository area. Of particular interest is how variability in temperature T, liquid-phase flux, and *RH* conditions around WPs, within the emplacement drifts, and in the near-field rock arises from heterogeneity in natural system and engineering conditions.

Natural system heterogeneity: Arises from variability in the following:

Percolation flux: This quantity, which is the liquid-phase flux in the host rock (the TSw2 unit), is the net result of infiltration and exfiltration and the ability of the PTn to divert the net infiltration flux which reaches the PTn unit. The temporal nature of percolation flux can range from episodic flow in fractures to steady-state flow in both the fractures and the matrix (see Sections 1.3 and 1.10.6). Imbibition in the PTn serves to dampen the influence of episodic infiltration events and thereby provide more time for exfiltration and lateral flow to influence the moisture balance in the PTn; all of which tend to reduce the percolation flux in the TSw2.

Ambient liquid saturation distribution: This quantity can be no less than what is caused by gravity-capillary-pressure equilibrium with the water table (factors that cause liquid saturation to be greater than this are discussed in Section 1.2.1). Liquid saturation increases with decreasing height above the water table (or perched water body). Liquid saturation also increases with percolation flux, particularly if that flux is steady (see Section 1.10.6).

Distribution of fracture permeability and connectivity: This affects both small-scale and large-scale vapor and condensate flow. If fracture permeability is small enough (i.e., bulk permeability k_b < 1–10 millidarcy) and/or the distance between connected fractures is large enough, then advective dryout will be throttled. If k_b > 1–10 millidarcy and the distances between well connected fractures is small enough, then advective dryout will be unthrottled. If k_b > 1–10 darcy, then buoyant gas-phase convection significantly affects the magnitude and direction of vapor flux over the length scale for which fractures are ubiquitously connected (see Section 10.1.2.2). The connected length scale of fractures also affects the scale over which repository-scale condensation redistribution can occur. Zones of highly contrasting k_b can result in focused vapor and condensate flow in the near-field rock (see Section 10.1.2.5). Note that observations of large k_b (> 1–10 darcy) being prevalent in the ESF imply that nonbuoyant or buoyant unthrottled advective dryout will prevail and that throttled advective dryout will be limited to (at most) isolated regions of the host rock.

Distribution of matrix hydrological properties: This influences small-scale gas-phase and liquid-phase flow. Of particular importance is how the imbibition properties of the matrix influence the degree to which nonequilibrium liquid-phase fracture flow can occur (see Section 1.3). The drying and rewetting characteristics of the matrix can influence the spatial extent of dryout (see Section 10.1.3). The rewetting characteristics of the matrix also strongly influence gas-phase and liquid-phase rewetting of the dryout zone (see Section 10.1.3).

Thermal conductivity K_{th} distribution in the rock: This is affected by both the K_{th} of the intact rock and the degree of fracturing.

Overburden thickness: This quantity, which is the distance between the repository and the ground surface, can vary significantly over the repository. Because this is the thickness of the "thermal blanket" that insulates the repository from the ground surface, it affects the time required to attain the peak rock temperature at the center of the repository. It also affects the vertical extent over which heat pipes may develop, with maximum vertical heat-pipe length increasing with overburden thickness. Peak temperatures at the edge of the repository are determined by the edge-cooling effect before the overburden thickness has any influence. The influence of overburden thickness on T-H behavior in the repository is discussed in Section 10.1.4 of Chapter 10.

Contribution of buoyant gas-phase convective vapor and heat flow: If k_b > 1–10 darcy, then buoyant gas-phase convection significantly affects the magnitude and direction of vapor flux over the length scale for which fractures are ubiquitously connected (see Section 10.1.2.2). If k_b > 40 darcy and fractures are ubiquitously connected over a length scale comparable to the width of the repository area, then buoyant gas-phase convection significantly affects heat flow and repository temperatures (see Section 1.8.5).

Contribution of heat-pipe-driven convective vapor and heat flow: Depending on the ambient percolation flux and on whether heterogeneity in the k_b distribution and/or heating conditions result in zones of focused condensate flow, heat-pipes can result in a significant cooling effect and cause greater liquid saturation and liquid-phase flux in the vicinity of emplacement drifts (see Sections 1.10.5.1, 1.10.6, and 10.1.2.5). For ambient percolation fluxes greater than 1.0 mm/yr, the tendency for heat pipes to cause cooler/wetter conditions near emplacement drifts increases with ambient percolation flux (Section 1.10.6).

Contribution of vapor-diffusion-driven vapor and heat flow: Depending on whether the binary diffusion of water and air is significantly enhanced (relative to "nominal" vapor diffusion), vapor diffusion can result in additional vaporization and vapor transport (relative to that driven by boiling alone) or cause significant vaporization and vapor transport after boiling has ceased (see Section 10.1.3.2).

Engineered System heterogeneity: Arises from variability in the following:

WP layout: This includes the axial spacing (along the drift) between WP centers and the lateral spacing between drift centers (called drift spacing). Section 1.10.5.1 focuses on the importance of WP layout; however, this topic is discussed throughout Sections 1.10.5 and 1.10.6.

WP heat output: This can vary substantially among spent nuclear fuel (SNF) WPs; moreover, the Defense High-Level Waste (DHLW) WPs generate an insignificant amount of heat compared to even the coolest SNF WPs. For WPs that are thermally isolated from each other, the distribution of the respective WPs along the drift can make a large difference in determining their respective environments (including T, RH, liquid-phase saturation, and liquid-phase flux). Section 1.10.5.1 focuses on the importance of WP heat output; however, this topic is discussed throughout Sections 1.10.5 and 1.10.6.

WP emissivity: This quantity determines the efficiency of thermal-radiative heat transfer from the WP to the drift wall and from WP to WP (see Section 1.10.5.3).

Backfill thermal conductivity: This quantity determines the temperature difference ΔT_{drift} between the WP and the drift wall that can substantially reduce RH on the WP surface ΔRH_{drift} (relative to that in the adjacent near-field rock). The reduction in RH is most effective if the backfill does not wick moisture back to the WP (see Section 1.10.5.5).

Backfill hydrological properties: These properties affect the degree to which wicking may transport moisture from the (cooler and more humid) near-field rock to the (hotter and less humid) WP surface. If wicking in the backfill is present, it can reduce ΔRH_{drift}. The k_b of the backfill will determine the degree to which buoyant gas-phase convection influences heat transfer between the WP and drift wall. Backfill hydrological properties also affect how effectively the drift seepage flux is able to drain out of the drift (see Section 1.10.5.4).

Backfill configuration: The important items include: (1) the percentage of the drift that is backfilled (full versus partial backfill), (2) the configuration of the upper backfill surface (sloping versus horizontal) and (3) whether backfill is allowed to fill in between WPs. The temperature difference ΔT_{drift} between the WP and the drift wall depends on the percentage of the drift that is backfilled. This may also affect the degree to which buoyant gas-phase convection influences heat transfer between the WP and drift wall (see Section 1.10.5.4).

Invert thermal conductivity: This quantity affects both the WP and drift wall temperatures. For cases with backfill, it, along with K_{th} in the backfill, determines the temperature difference ΔT_{drift} between the WP and the drift wall (see Section 1.10.5.5).

Invert hydrological properties: These properties affect the degree to which wicking may be important. If wicking in the invert is important, it can moderately reduce ΔRH_{drift}. These properties also affect how effectively the drift seepage flux is able to drain out of the drift. Radionuclide transport will also be significantly affected; particularly, as to whether transport is limited to liquid-phase diffusive transport (see Section 1.10.5.4).

Proximity to the edge of the repository: Repository edge-cooling/rewetting/shedding effects all depend on the proximity of the drift to the edge of the repository (see Section 1.10.6).

A key attribute of the EBS, affecting its ability to contribute to waste isolation, is to cause an *RH* difference (ΔRH_{drift}) between the hotter (and drier) WP and cooler (and more humid) rock at the drift wall. The drift-ΔRH effect is quantified by the relationship $RH_{wp}/RH_{dw} = P_{sat}(T_{dw})/P_{sat}(T_{wp})$, which depends primarily on the temperature difference (ΔT_{drift}) between the WP and drift wall. Therefore, the heat transfer attributes of the EBS are key in determining the extent to which *RH* can be reduced on the WP.

Engineered Barrier System (EBS) heat transfer attributes: The primary heat transfer attributes of the EBS include:

Axial WP spacing: This determines the amount of decay heat generated per unit length of drift and how efficiently heat is transferred by thermal radiation from WP to WP. This also affects the temperature distribution along the drift wall (Sections 1.10.5 and 1.10.6).

WP heat generation distribution: This, together with the axial WP spacing, determines the spatial variability of the heat flux distribution along the axis of the emplacement drift. This also affects the temperature distribution along the drift wall (Sections 1.10.5. and 1.10.6).

WP emissivity: This determines how efficiently heat is transferred by thermal radiation between a WP and (1) the drift floor, (2) the drift wall, and (3) adjacent WPs (Section 1.10.5.3).

WP thermal conductivity: For the line-load design, this may influence the efficiency of thermal homogenization along the axis of the drift. Because thermal-radiative WP-to-WP heat transfer probably limits axial heat flow along the line of WPs, WP thermal conductivity (particularly for the range of possible values) is likely to be a minor factor.

WP cross-sectional area: The percentage of the WP cross section that can conduct heat. For the line-load design, this may influence the efficiency of thermal homogenization along the axis of the drift. Because thermal-radiative WP-to-WP heat transfer probably limits axial heat flow along the line of WPs, WP cross-sectional area is likely to be a minor factor.

Percentage of drift occupied by the invert and backfill: If sufficiently low-K_{th} material is used, this determines what percentage of the drift can be devoted to insulating the WP from the near-field rock (Section 1.10.5.4).

Thermal conductivity of the invert and backfill: This, together with the drift diameter and percentage of the drift occupied by the invert and backfill, determines how effectively a WP can be insulated from the near-field rock (Section 1.10.5.5).

Drift diameter: This influences thermal-radiative heat transfer between the WP and drift wall. If backfill is used, it affects the volume of the insulation surrounding the WPs. This also affects the temperature distribution along the drift wall (Section 1.10.5.6).

Another important heat transfer attribute of the entire repository system is the overall AML of the repository area, which is discussed in Section 1.10.5.7. The AML also determines the spatial and temporal extent of significant RH reduction in the rock (ΔRH_{rock}). The AML determines the overall temperature rise of the repository rock and the vertical extent (and magnitude) of the temperature rise in the UZ (see Section 10.1.2.1) and SZ (see Section 1.10.2). The AML also determines the spatial and temporal extent of changes to the liquid-phase saturation distribution in the UZ (see Section 10.1.2.1).

Table 1.10.1.1. Percolation fluxes considered in this study and the resulting initial relative humidity and liquid saturation conditions at the repository horizon.

Infiltration flux (mm/yr)	Initial relative humidity at repository horizon (%)	Initial liquid saturation at repository horizon (%)
0.00	98.4	68
0.05	99.2	84
0.132	99.6	95
0.30	99.9	99.0
1.00	99.9	99.7
5.00	99.9	99.7

Table 1.10.1.2. Heating characteristics of the spent nuclear fuel (SNF) WP types represented in the two-dimensional model that averages the heat output from a mixture of 26-yr-old BWR WPs and 26-yr-old PWR WPs into a uniform line-heat load.

Waste package type	Percentage of WP inventory in model (%)	SNF age (yr)	MTU/WP (MTU)	Burnup (GWD/MTU)	Enrichment (%)
BWR MPCs	40.2	25.9	6.06	33,100	3.01
PWR MPCs	59.8	26.0	8.49	41,500	3.82

Table 1.10.1.3. Heating characteristics of the waste package types represented in the three-dimensional multiple-WP model.

Waste package type	Percentage of WP inventory in model (%)	SNF age (yr)	MTU/WP (MTU)	Burnup (GWD/MTU)	Enrichment (%)	Initial WP heat output (kW)
Hanford Site DHLW WP	10%	NA	2.15	NA	NA	1.56
Savannah River Site DHLW WP	20%	NA	2.15	NA	NA	2.84
Small 40-yr-old PWR WP	20%	40	4.67	35,455	3.4	3.18
Large "average" 26-yr-old BWR WP	20%	25.9	7.07	33,100	3.01	6.14
Large "average" 26-yr-old PWR WP	20%	26	8.83	41,500	3.82	9.16
Design basis fuel 10-yr-old PWR WP	10%	10	9.74	48,086	4.2%	17.85

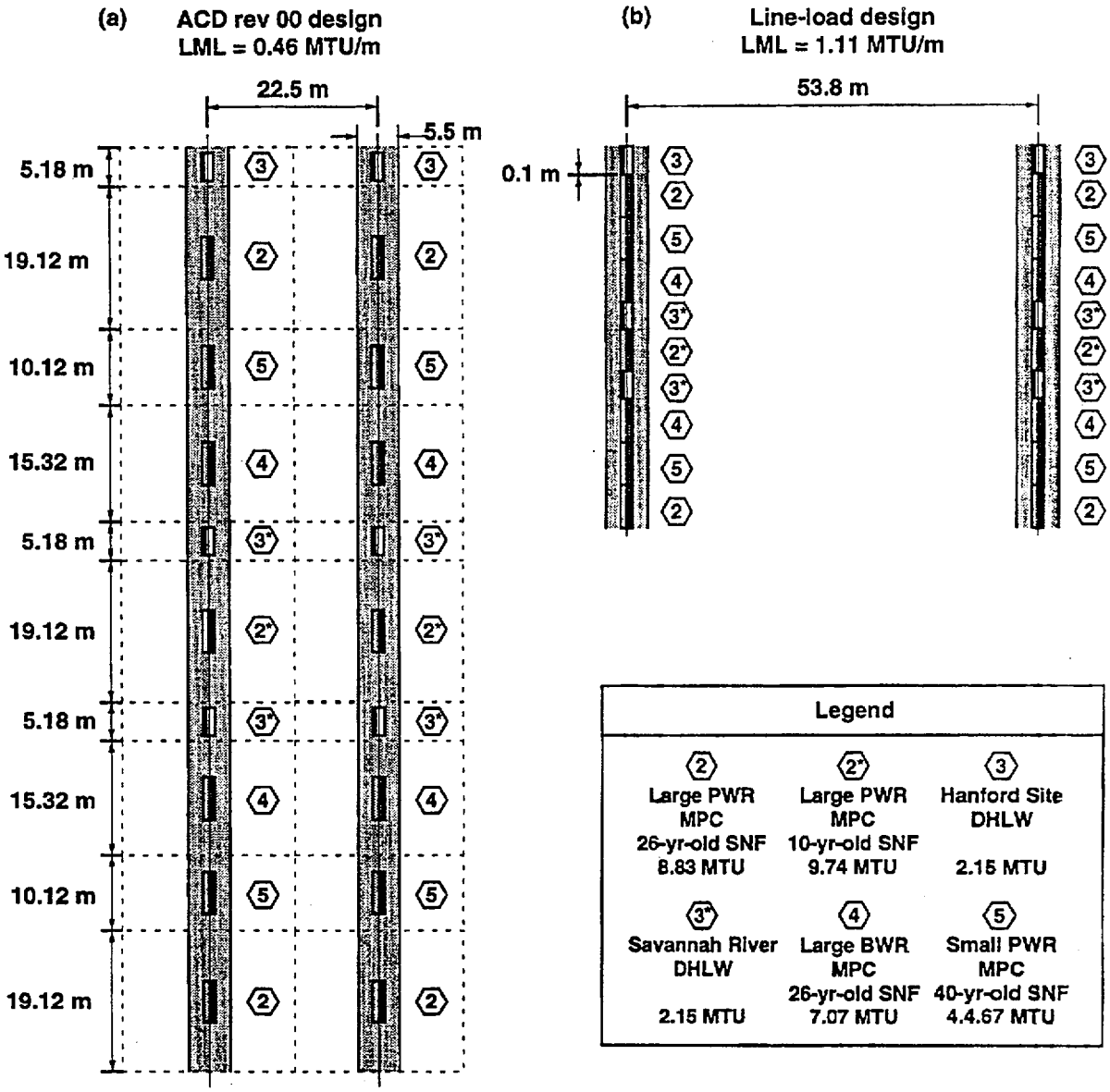

Figure 1.10.1.1. Plan view of the WP configuration that is represented by the three-dimensional, multiple-WP model for (a) the ACD rev 00 design, AML = 83.4 MTU/acre, LML = 0.46 MTU/m, and drift spacing = 22.5 m; and (b) the line-load design with AML = 83.4 MTU/acre, a 0.1-m gap between WPs, LML = 1.11 MTU/m, and drift spacing = 53.8 m.

1.10.1.2 Discussion of the Models and Sensitivity Analyses in this Section

The calculations in Section 1.10 were conducted with four different types of models:

Drift-scale ECM model: This model represents detailed three-dimensional T-H behavior in and around the emplacement drifts (including the rock pillar separating the drifts), and one-dimensional mountain-scale T-H behavior that occurs from the water table to the ground surface; it does not represent three-dimensional mountain-scale T-H behavior. This model utilizes the equivalent continuum model (ECM) to represent fracture-matrix flow. Two different drift-scale models are used, including: (1) a two-dimensional cross-sectional model, which represents (in very fine detail) the WP and emplacement drift in a plane transverse to the drift axis and which axially averages the heat output from a row of WPs (Section 1.10.5.4), and (2) a three-dimensional, multiple-WP model that represents six WPs, of which each has unique decay-heat characteristics (Sections 1.10.5 and 1.10.6).

Mountain-scale ECM model: This model represents three-dimensional mountain-scale T-H behavior with an R–Z coordinate system and represents WP decay heat by uniformly distributing the heat over a disk-shaped area; this is sometimes called a smeared-heat-source model. This model utilizes ECM to represent fracture-matrix flow (Section 1.10.6 and Sections 10.1 and 10.2).

Hybrid drift-scale–mountain-scale ECM model: This model represents both the detailed three-dimensional drift-scale effects and three-dimensional mountain-scale effects. This model is also used to check the appropriateness of the drift-scale model calculations in analyzing the performance of the entire repository area. This model utilizes ECM to represent fracture-matrix flow (Section 1.10.6).

Drift-scale DFM model: This model represents both the detailed three-dimensional drift-scale effects and one-dimensional mountain-scale effects. This model utilizes the discrete fracture-matrix model (DFM) that discretely models flow in the fractures and matrix block, and thereby accounts for nonequilibrium fracture-matrix interaction. This model is used to check the appropriateness of the drift-scale ECM model calculations in analyzing gas- and liquid-phase flow in the near field (Section 1.10.7).

Model calculations in this section were carried out using both the V-TOUGH and NUFT codes [Nitao, 1989; Nitao, 1993] and using both two- and three-dimensional drift-scale models. The models include all major hydrostratigraphic units in the UZ, which are assumed to be horizontal and of uniform thickness; the initial and boundary conditions were the same as those used in past studies [Buscheck and Nitao, 1993; Buscheck and Nitao, 1994a; Buscheck and Nitao, 1994b]. For Sections 1.10.2 through 1.10.6, we assumed k_b = 280 millidarcy. For Sections 1.10.2 and 1.10.3, we used an initial vertical liquid saturation profile based on a zero percolation flux. The initial vertical temperature and pressure distribution are consistent with the nominal geothermal flux and pneumatistatic conditions.

Higher percolation fluxes, resulting in wetter liquid saturation profiles, are considered in Sections 1.10.4 and 1.10.6 (for conditions at the repository horizon see Table 1.10.1.1). For all of the calculations, the atmospheric *RH* is assumed to be 100%, so the model allows no loss of moisture by vapor diffusion to the atmosphere. Because actual *RH* in the desert atmosphere is much lower than 100%, the model underrepresents this loss. This neglected loss may be large for high AMLs, which can steepen the temperature gradient near the ground surface by a factor of 50 relative to ambient conditions. The effect of this assumption is offset (to some degree) by the assumption of zero percolation flux made in some of the calculations. All of the drift-scale models used in this study assumed that the water table is fixed at a constant temperature, liquid saturation, and pressure. The mountain-scale and hybrid drift-scale–mountain-scale models represent thermal-hydrological flow to a depth of 1 km below the water table, which is deep enough for the model to be (effectively) infinitely deep.

Table 10.1.1. also summarizes the effect of a given percolation flux on the relative humidity *RH* and liquid saturation at the repository horizon under ambient conditions. Notice that the *RH* is extremely high regardless of infiltration flux, while liquid saturation is quite sensitive to percolation flux. For a steady-state percolation flux less than about 0.2 mm/yr, the equivalent continuum model (ECM) predicts that all of the percolation flux can be accommodated by flow in the matrix (except in the TSw3 unit where the matrix permeability may be too low to accommodate all of the flux, which results in some perching and fracture flow). In the TSw1 and TSw2 units, the matrix cannot sustain a percolation flux greater than about 0.2 mm/yr; consequently, for percolation flux greater than 0.2 mm/yr, some of the percolation flux must occur in the fractures at the repository horizon. For percolation flux greater than 0.2 mm/yr, the matrix is essentially fully saturated at the repository horizon. Note that these observations are subject to the limitations of the ECM and may not be relevant to the situation where percolation flux is focused down fault zones.

In Sections 1.10.2, 1.10.3, 1.10.4, and 1.10.5.4, drift-scale thermal-hydrological behavior is represented by a two-dimensional model that incorporates the geometric details of the WPs and emplacement drifts in a cross section transverse to the drift axes. Heat transfer in the drift occurs as thermal radiation, heat convection, and conduction. For Sections 1.10.2, 1.10.3, and 1.10.3, the WP and drift are assumed to be rectangular; however, as long as the cross-sectional areas of the WP and drift are the same as in the actual circular geometry, the model is found to accurately model heat and mass flow within the drift (see Fig. 1.10.2.1).

Because the two- and three-dimensional drift-scale models effectively assume an infinite repository area, they are applicable to the region not affected by cooling at the repository edge. Calculations for the repository edge were carried out with a two-dimensional hybrid model that imbeds a cross-sectional drift-scale model in a cross-sectional mountain-scale model. Calculations with a mountain-scale model are presented in Section 1.10.6 to examine the influence of edge-cooling/rewetting effects on temperatures and *RH* throughout the repository. Section 1.10.6 also describes a hybrid drift-scale–mountain-scale model that is an abstraction process that includes three-dimensional mountain-scale T-H behavior and detailed three-dimensional drift-scale T-H behavior driven by WPs with different decay-heat characteristics.

Section 1.8.2 describes the major thermal management strategies, including the minimally heated (MH) repository and constructively heated (CH) repository. We have identified two fundamental CH approaches for managing the T-H effects of decay heat:

Extended dryout (ED) approach: Use a high AML (>60 MTU/acre) to drive a large fraction of the initial pore water (in the rock) from the repository as a whole. The high areal power density associated with such an AML creates a thick superheated dryout zone (coalesced between emplacement drifts) and maintains above-boiling temperatures and low *RH* in the repository rock (and on WPs) for thousands of years.

Localized dryout (LD) approach: Maintain a temperature difference between the WP and the drift wall that is large enough to reduce *RH* on the WP. This is done with close axial WP spacing (generating a high line-heat load) and/or the use of low-thermal-conductivity backfill in the drift. Wide drift spacings and low to intermediate AMLs (<50–60 MTU/acre) are used to (1) prevent the boiling zones from coalescing between drifts (and thereby limiting condensate buildup above the drifts) and (2) limit far-field temperature rise (as in the MH strategy).

To determine the boundaries between the LD and ED domains (with respect to thermal design parameters), we considered AMLs of 6 to 120 MTU/acre, drift spacings L_d of 25 to 400 m, and LMLs of 0.2 to 1.25 MTU/m For Sections 1.10.2, 1.10.3, 1.10.4, and 1.10.5.4, an oldest-fuel-first (OFF) receipt scenario with 26-yr-old SNF and a mix of large BWR WPs (containing 40 BWR assemblies per WP) and large PWR WPs (containing 21 PWR assemblies per WP) was assumed for the decay-heat-generation curve (Table 1.10.1.2). Note that these WPs are called 40-BWR WPs and 21-PWR WPs, respectively. We also considered the effect of aging the SNF to ages of 40, 60, 100, and 200 yr. Cases in which the drift is backfilled at 100 yr were compared with those with no backfill.

In Section 1.10.5.4, a much more highly refined two-dimensional cross-sectional model is used that incorporates the details of the WP and emplacement drift, including the circular geometry of the WP and drift and the configuration details of the sloping-partial and level-partial backfill scenarios that were investigated in the Backfill Systems Study [Balady et al., 1996]. Heat transfer in the drift occurs as thermal radiation, heat convection, and conduction. Thermal radiation occurs between all surfaces, including thermal radiation that occurs from one drift wall (or floor) surface to another; this feature in the model is particularly important for the off-center in-drift (OCID) emplacement scenario, which results in strongly asymmetrical heating of the drift-wall surfaces. Unless otherwise stated, the models represent center-in-drift (CID) WP emplacement. We show in Section 1.10.5.4 that beyond 50 yr there is very little difference in near-field thermal-hydrological behavior between the OCID and CID emplacement scenarios. Because of the very fine degree of refinement of the numerical grid (with some grid blocks as small as 0.1 x 0.1 m) in the drift, this model can very accurately represent buoyant gas-phase convection that occurs within the drift. Unless otherwise stated, the models represented CID WP emplacement.

All previous studies of drift-scale (or sub-repository-scale) thermal-hydrological behavior [e.g., Buscheck et al., 1994; Buscheck and Nitao, 1994a; Buscheck and Nitao, 1994b; Mishra, 1994; Buscheck et al., 1995; Ho and Francis, 1996] have used two-dimensional cross-sectional models that average the heat output from rows of WPs into a uniform line-heat load. This assumption can substantially distort the representation of thermal-hydrological behavior in and around emplacement drifts for realistic WP emplacement scenarios, particularly those involving large axial WP spacing and/or a large variation in heat output from WP to WP. For such scenarios, three-dimensional calculations are required to adequately represent drift-scale thermal-hydrological behavior [Buscheck et al., 1996]. This is particularly true for the Advanced Conceptual Design (ACD) rev 00 design, which has large axial WP spacing and a WP inventory with a large degree of heat output variability from WP to WP. To carry out such calculations, a three-dimensional, drift-scale, multiple-WP model, based on the NUFT code [Buscheck et al., 1996] was developed. This is the first published thermal-hydrological model that discretely represents a mixture of WPs with different heating histories. The three-dimensional, multiple-WP model is used in Sections 1.10.5 and 1.10.6 to compare two repository designs: the ACD rev 00 design [TRW, 1996] and the line-load design, which is also called the Localized Dryout concept [Buscheck et al., 1995]. The focus of Sections 1.10.5 and 1.10.6 is on examining differences between the two designs (both with and without the use of backfill) with respect to T and RH experienced by WPs and within the drifts and the near field itself. These quantities strongly affect WP integrity and the integrity of repository components, such as steel sets that may be required for drift stability.

A mixture of WP types is examined in Sections 1.10.5 and 1,10.6, ranging from those containing very hot spent nuclear fuel (SNF) to virtually cold defense high-level waste (DHLW). The three-dimensional, multiple-WP model includes six major WP types (Table 1.10.1.3), resulting in a WP inventory that is representative of that assumed for the ACD rev 00 design, including four SNF WP types: (1) "very hot" 10-yr-old "design basis fuel" PWR WPs (comprising 10% of the WPs in the model), (2) "relatively cool" 40-yr-old PWR WPs (20% of the WPs), (3) nominal 26-yr-old PWR WPs (20% of the WPs), and (4) nominal 26-yr-old BWR WPs (20% of the WPs), and two types of DHLW, including those from the Hanford site (10% of the WPs) and those from the Savannah River site (20% of the WPs). Note that the ACD rev 00 design assumes that 27% of the WPs are DHLW WPs, while for the three-dimensional, multiple-WP model, 30% of the WPs are assumed to be DHLW WPs.

In Sections 1.10.5 and 1.10.6, the drift diameter is assumed to be 5.5 m; however, drift diameters of 3, 4, and 6.5 m are also analyzed (Section 1.10.5.6). (In Section 1.10.4, drift diameters of 5.0 and 6.77 m were considered.) Heat transfer within the drift occurs as thermal radiation, heat convection, and conduction. Thermal radiation occurs between all surfaces, including thermal radiation from WP to WP. A sensitivity study of thermal radiation in the drift considered WP emissivities of 0.3 and 0.8 (Section 1.10.5.3). For the backfill cases, a sand backfill was assumed; backfill thermal conductivity values K_{th} = 0.3 and 0.6 $W/m^{o}C$ are considered (Section 1.10.5.5). For the line-load backfill cases, it is assumed that measures are taken to prevent backfill from filling the gap separating WPs; line-load cases were also considered where backfill is allowed to fill in between WPs (Section 1.10.5.2). In addition to the reference areal mass

loading (AML=84.3 MTU/acre), AMLs of 25, 45, 100, and 120 MTU/acre are also considered (Section 1.10.5.7). Ambient percolation fluxes ranging from 0–5 mm/yr are considered in Section 1.10.6.

There are two fundamentally different ways that WPs can be arranged in the repository at Yucca Mountain. The first approach (called square spacing) attempts to uniformly distribute the WP decay heat over the repository area by placing the WPs with roughly the same axial and lateral spacing between WPs (as is done in the ACD rev 00 design). The second approach (called the line load) lineally concentrates the WP decay heat to the greatest possible extent by placing the WPs end-to-end along the emplacement drifts. For a given AML, this allows for the maximum possible spacing between emplacement drifts. (Note that the placement of more than one row of tightly spaced WPs per drift would result in an even higher line-heat load and wider drift spacing.) By utilizing each emplacement drift to the maximum possible extent, a repository that uses the line-load approach would require the minimum possible total length of emplacement drift. The two primary repository designs analyzed in Section 1.10 are:

ACD rev 00 design: This design utilizes a "square" geometry with the spacing between drift centerlines being roughly the same as the axial center-to-center spacing between SNF WPs. The ACD rev 00 has a lineal mass loading LML = 0.46 MTU/m and drift spacing = 22.5 m.

Line-load design: This approach places WPs nearly end-to-end and the drifts are spaced far apart. An example of this approach (which is emphasized in Section 1.10) assumes a 0.1-m gap between the WPs, resulting in LML = 1.11 MTU/mand drift spacing = 53.8 m; this drift spacing is used to keep the same AML (83.4 MTU/acre) as that assumed in the ACD rev 00 design. The drift spacing in this example of the line-load design is 2.4 times greater than in the ACD (see Fig. 1.10.1.1).

To examine the importance of tight axial WP spacing, we considered a line-load design with a 1.0-m gap between WPs, resulting in LML = 0.94 MTU/m and drift spacing = 46.1 m. We analyzed alternative AMLs for the 1.11-MTU/m line-load design (with a 0.1-m gap between WPs), including: (1) 120 MTU/acre, resulting in drift spacing = 37.4 m; (2) 100 MTU/acre, resulting in drift spacing = 44.9 m; (3) 45 MTU/acre, resulting in drift spacing = 100 m; (4) 25 MTU/acre, resulting in drift spacing = 180 m. We also analyzed alternative AMLs for the ACD rev 00 axial WP spacing, including: (1) 45 MTU/acre, resulting in drift spacing = 41.8 m; and (2) 25 MTU/acre, resulting in drift spacing = 25 m.

In Section 1.10.6, we examine the sensitivity of near-field thermal-hydrological behavior to ambient percolation flux. Percolation fluxes of 0.0, 0.05, 0.3, 1.0, and 5.0 mm/yr were considered. In Section 1.10.7, we make a detailed comparison of drift-scale therm
al-hydrological behavior calculated by the discrete fracture-matrix model and the equivalent continuum model (ECM), which is the approximation for fracture-matrix interaction used throughout most of our thermal-hydrological calculations. A comparison of the discrete fracture-matrix model with the ECM in representing thermal-hydrological behavior is also described in Section 1.9.7.

1.10.2 Analysis of Localized and Extended Dryout Regimes

The major features of the localized dryout (LD) and extended dryout (ED) approaches are discussed in Section 1.8.2. A primary concern for the ED approach is whether condensate buildup above the boiling zone has a deleterious effect on waste isolation. For both the ED and LD approaches, this buildup is affected by several key factors:

1. **Exfiltration flux:** This may be strongly affected by how much the decay-heat-steepened temperature gradient near the ground surface increases the exfiltration flux to the atmosphere (moisture loss by advective and diffusive vapor transport).
2. **Infiltration flux:** This is precipitation that does not run off the area overlying the repository, and is not evaporated or transpired before it reaches a depth below the zone of evapo-transpiration.
3. **Percolation flux:** This quantity, which is the liquid-phase flux in the host rock (the TSw2 unit), is the net result of infiltration and exfiltration and the ability of the PTn to divert the net infiltration flux which reaches the PTn unit.

4. **Buoyant versus nonbuoyant advective vapor transport:** This determines what fraction of the water vaporized by decay heat is driven above the boiling zone. If vapor flow is dominated by buoyant gas-phase convection, up to 100% of the vapor can end up above the boiling zone (where it condenses). If vapor flow is dominated by boiling-driven advective transport, then 50% of the vapor will end up above the boiling zone.
5. **Decay-heat-driven vaporization rate:** The rate at which pore water in the rock is vaporized by decay heat and transported above the boiling zone (where it condenses). This is affected by AML and by the major thermal-hydrological regime that dominates vaporization and vapor transport. The major T-H regimes are: (1) throttled, nonbuoyant advective vapor transport, (2) unthrottled, nonbuoyant advective vapor transport, and (3) unthrottled, buoyant advective vapor transport (see Section 1.8.5). The extent to which vapor diffusion is enhanced will also affect the vaporization rate.
6. **Condensate shedding:** How effectively does liquid-phase drainage around the boiling zone (or zones) mitigate condensate buildup above the boiling zone(s).

Factors 1 through 5 determine the liquid-phase flux that reaches the top of boiling zone(s); factor 6 influences how much of that flux drains around (and below) the boiling zone(s). The ED approach (and, to a lesser extent, the LD approach) may increase exfiltration flux (factor 1). The LD approach will limit the AML dependence of the condensate flux (factor 5) and prevent the boiling zones from coalescing between drifts, thereby allowing condensate to drain between the drifts (factor 6).

Figure 1.10.2.1a,c gives the maximum vertical distance ΔZ_{max} of the upper boiling front from the repository horizon as a function of AML for various SNF ages. The boiling zones are initially cylindrical (centered at the drift axis) with a radius equal to ΔZ_{max}; after they coalesce (in the ED approach), the coalesced zone is tabular (centered at the repository horizon) with a vertical thickness of $2\Delta Z_{max}$. Examination of the temperature fields for a wide range of cases shows that uncoalesced (cylindrical) boiling (that is, localized dryout) persists as long as the radial dimension of the boiling zone (ΔZ_{max}) is less than half the drift spacing ($\Delta Z_{max} < L_d/2$); coalesced (tabular) boiling (that is, extended dryout) occurs for $\Delta Z_{max} > L_d/2$. This observation permits us to distinguish between the LD and ED domains in Fig. 1a,c; all values of ΔZ_{max} lying below the $\Delta Z_{max} = L_d/2$ curve are in the LD domain, and all values lying above this curve are in the ED domain. Figure 1.10.2.2 gives the maximum AML (AML_{max}) for uncoalesced boiling as a function of SNF age for two values of lineal mass loading (LML). The range of AMLs amenable to the LD approach is increased by (1) wider drift spacings (higher LMLs), (2) SNF aging, and (3) drift ventilation.

Another benefit of wide drift spacing (high LMLs) is that peak WP (and drift-wall) temperature T_{peak} is insensitive to AML (Fig. 1.10.2.1b,d). This means that WPs could be emplaced in every other drift, and the decision of whether to fill the remaining drifts deferred until enough information about T-H behavior was available from *in situ* thermal tests [Buscheck and Nitao, 1995] and repository performance monitoring. Because T_{peak} in the near field is insensitive to AML for high LMLs, similar near-field environment (NFE) design assumptions concerning T_{peak} will be applicable to a wide range of thermal loading (and WP emplacement) options. These results also indicate that T_{peak} in the near field is insensitive to proximity to the repository edge; NFE design assumptions concerning T_{peak} will therefore be similar for the entire repository area. Another advantage for high LMLs is that the total length of emplacement drifts depends on LML and is independent of AML (and repository area). Some of the potential cost savings in constructing a high-AML repository could also be realized in a low-AML repository that uses the same LML.

Still another benefit of wide drift spacing is that the drift-ΔRH effect is maximized for any given AML. Figure 1.10.2.3b shows this effect for a 40-MTU/acre example of the LD approach. Higher LMLs increase ΔT_{drift} and thereby increase ΔRH_{drift}. This increase in ΔRH_{drift} occurs even though far-field temperatures are nearly identical for these cases (not shown in Fig. 1.10.2.3) and near-field temperatures are similar after about 2000 yr (Fig. 1.10.2.3a). Thus, it is possible with the LD approach to substantially reduce RH on the WP while limiting far-field temperature rise.

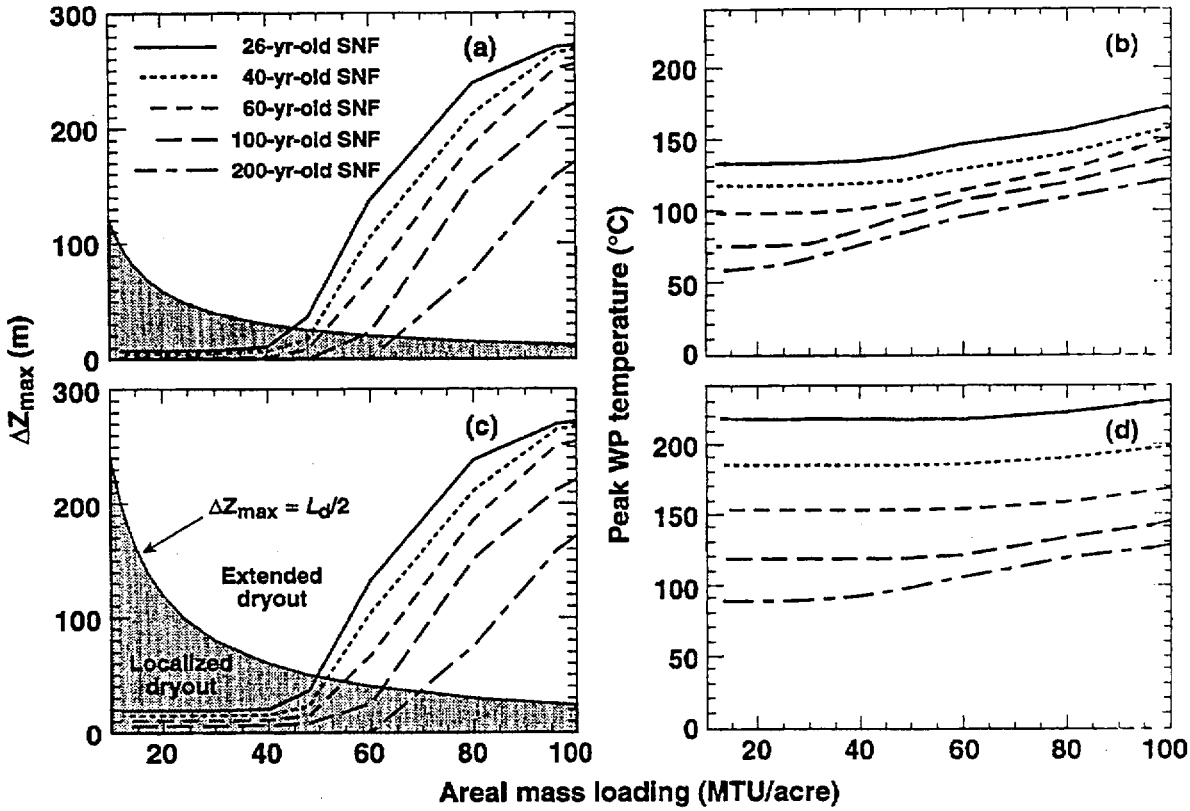

Figure 1.10.2.1. (a) Maximum vertical distance ΔZ_{max} of the upper boiling front from the repository horizon and (b) peak temperature on the WP as a function of AML for various SNF ages, LML = 0.63 MTU/m, no backfill, bulk permeability k_b = 280 millidarcy, and vapor diffusion tortuosity factor τ_{eff} = 0.2. Curves are also shown (c,d) for LML = 1.25 MTU/m and WP spacing = 6 m. In (a) and (c), the curve separating the ED and LD domains corresponds to ΔZ_{max} equal to one-half the drift spacing $L_d/2$.

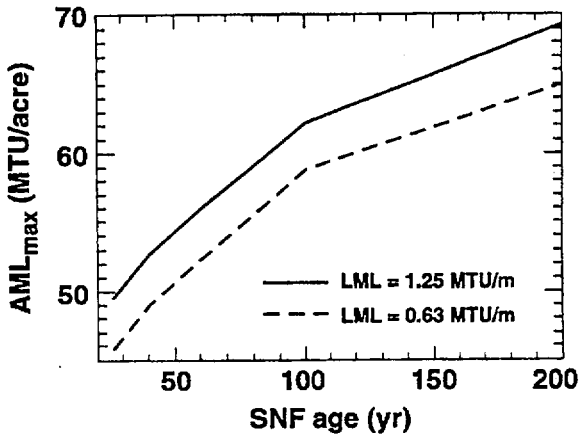

Figure 1.10.2.2. The maximum AML (AML_{max}) for uncoalesced boiling as a function of SNF age. Combinations of AML and SNF age lying below a given curve result in uncoalesced (cylindrical) boiling zones (that is, localized dryout); combinations lying above a given curve result in coalesced (tabular) boiling zones (that is, extended dryout). Higher LMLs (and larger L_d) and older SNF increase the range of AMLs amenable to the LD approach. The effect of emplacing older SNF may also be achieved (with younger SNF) by ventilating the emplacement drifts to remove water vapor (and its associated latent heat) from the drifts and from the repository rock.

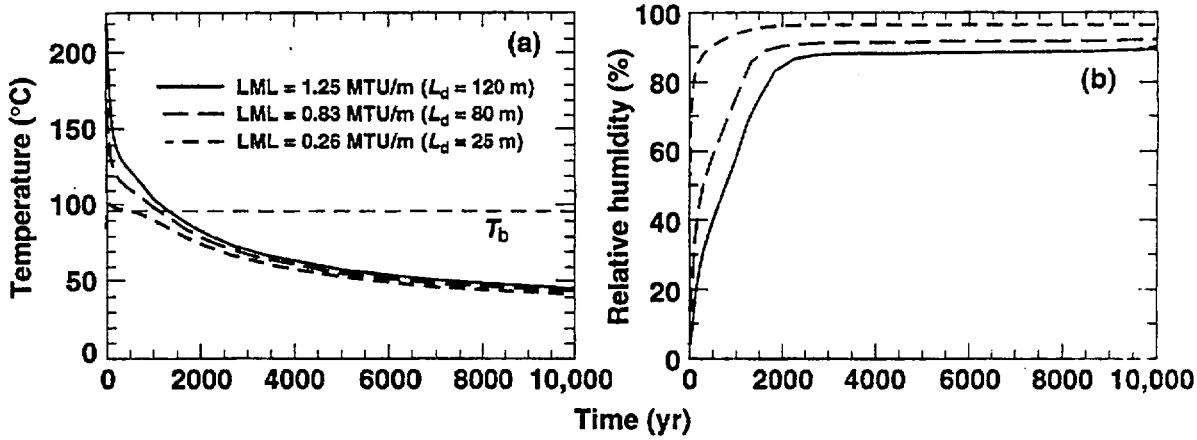

Figure 1.10.2.3 (a) Temperature and (b) relative humidity on the WP surface for AML = 40 MTU/acre, 26-yr-old SNF, no backfill, bulk permeability k_b = 280 millidarcy, and vapor diffusion tortuosity factor τ_{eff} = 0.2 for three values of LML.

1.10.3 Performance Attributes of Engineered Backfill

We analyzed the effect of a granular backfill on ΔRH_{drift} for the LD approach (Fig. 1.10.3.1a,b). We assumed that the intergranular porosity of a crushed PTn tuff backfill can be treated like fractures in the equivalent continuum model [Buscheck and Nitao, 1994a] with k_b = 40 darcy. The hydrological properties of the intragranular porosity are assumed to be those of the intact rock matrix, and the drying curves measured by Peters et al. [1984] are assumed to be applicable to matrix imbibition; both assumptions probably overrepresent the tendency of water to be wicked back to the WP and are therefore conservative. For most of the calculations, the dry and wet values of K_{th} were assumed to be one-half the intact PTn values (0.305 and 0.425 W m^{-1} $°C^{-1}$, respectively).

After backfill is emplaced at t = 100 yr, T_{wp} increases abruptly from 100 to 210°C (Fig. 1.10.3.1a), decreasing RH_{wp} from 62 to 2.7% (Fig. 1.10.3.1b). Because of the low AML (24 MTU/acre), RH reduction that results from rock dryout (ΔRH_{rock}) is negligible (Table 1.10.3.1). Because of the larger ΔT_{drift}, backfill results in a much larger ΔRH_{drift} than when backfill is not used. At t = 10,000 yr, RH_{wp} = 71 and 93% for backfill and no backfill, respectively (Fig. 1.10.3.1b). An important benefit of backfill is that RH_{wp} may remain low until T_{wp} is quite low. With backfill (at t = 21,000 yr), RH_{wp} = 81% and T_{wp} = 34°C; with no backfill (at t = 715 yr), RH_{wp} = 81% and T_{wp} = 77°C; backfill can therefore substantially reduce the T_{wp} associated with a given RH_{wp}.

On the basis of ongoing sensitivity analyses, seven potentially beneficial performance attributes have been identified for a well-selected engineered backfill:

1. Persistent steep (predictable) temperature difference ΔT_{drift} between the WP and drift wall that substantially reduces RH on the WP surface ΔRH_{drift} (relative to that in the adjacent host rock). The reduction in RH is most effective if the backfill does not wick moisture back to the WP.
2. Capillary barrier that attenuates (spreads) focused liquid flux (including nonequilibrium fracture flow).
3. High heat capacity (relative to air) and large ΔT_{drift} that evaporates the (attenuated) liquid flux and equilibrates the absolute humidity (partial pressure of water vapor P_v) in the drift with conditions in the adjacent host rock.
4. Minimized liquid contact on the WP that prevents an evaporative buildup of salts on the WP.
5. Minimized (gas- and liquid-phase) moisture contact on the WP that reduces the potential for radionuclide dissolution and release from the WP.
6. Minimized liquid saturation that reduces the potential for the diffusive transport of radionuclides within the EBS (and radionuclide release from the EBS).
7. Minimized liquid flux near the waste package that reduces the potential for the advective transport of radionuclides within the EBS (and radionuclide release from the EBS).

We also analyzed the effect of backfill on ΔRH_{drift} for the ED approach (Fig. 1.10.3.1c,d). After backfill is emplaced at t = 100 yr, T_{wp} increases abruptly from 148 to 266°C (Fig. 1.10.3.1c), reducing RH_{wp} from 22 to 1.8% (Fig. 1.10.3.1d). Table 1.10.3.1 summarizes ΔRH_{rock} and ΔRH_{drift}. Because the 24- and 80-MTU/acre cases share the same LML and because ΔT_{drift} is proportional to LML (except for early time, when thermal radiation in the drift is also sensitive to absolute temperature), ΔT_{drift} is the same in both cases. The ratio RH_{wp}/RH_{dw} is insensitive to AML for t > 2000 yr. [From Eq. 2 in Section 1.8.3.1, we have $RH_{wp}/RH_{dw} = P_{sat}(T_{dw})/P_{sat}(T_{wp})$.] Later, the difference in absolute temperature

between the two cases decreases, so that $P_{sat}(T_{dw})/P_{sat}(T_{wp})$ depends primarily on ΔT_{drift}; therefore, RH_{wp}/RH_{dw} depends primarily on LML and the thermal properties of the backfill and is insensitive to AML, drift spacing, and location in the repository (i.e., proximity to the edge).

For the LD approach, ΔRH_{drift} is always the major contributor to *RH* reduction on the WP (Table 1.10.3.1) everywhere in the repository (including the edge). For the ED approach, ΔRH_{rock} can play an important role in *RH* reduction during the first 10,000 yr in the central half of the repository and during the first 1000–2000 yr at the repository edge (particularly if the percolation is low). For the 80-MTU/acre repository, ΔRH_{drift} becomes the major contributor to *RH* reduction for $t > 10{,}000$ yr in the central half of the repository and for $t > 2000$ yr at the edge. At late time, *RH* reduction depends primarily on the thermal and hydrological properties of the backfill (notably K_{th} and rewetting diffusivity) and is insensitive to AML, drift spacing, and location in the repository. At late time, *RH* reduction for a high-AML repository is similar to that of a low-AML repository having the same LML.

Table 1.10.3.1. Temperature and relative humidity on the upper drift wall and the upper WP surface for LML = 0.63 MTU/m, crushed PTn tuff invert, full crushed PTn backfill at 100 yr with K_{th} = 0.305 W/m°C, WP emissivity = 0.3, and percolation flux = 0 mm/yr. Calculations were done with a two-dimensional model that averages the heat output from a mixture of 26-yr-old BWR WPs and 26-yr-old PWR WPs into a uniform line-heat load. Also listed is the *RH* reduction contributed by repository rock dryout (ΔRH_{rock}) and by the drift-ΔRH effect (ΔRH_{drift}).

AML		time(yr)							
		60	100	2000	10,000	20,000	40,000	60,000	100,000
24 MTU/acre	RH_{wp} (%)	46	2.7	53	71	80	89	92	94
	T_{wp} (°C)	118	210	69	42	34	29	27	26
	RH_{dw} (%)	82	96	98.6	98.5	98.4	98.4	98.4	98.4
	RH_{wp} /RH_{dw}	0.56	0.03	0.54	0.72	0.81	0.90	0.94	0.96
	ΔT_{drift} (°C)	17	131	15	7.1	4.3	2.1	1.4	0.9
	ΔRH_{rock} (%)	16	2	0	0	0	0	0	0
	ΔRH_{drift} (%)	36	94	46	27	18	9	6	4
	ΔRH_{total} (%)	52	96	46	27	18	9	6	4
80 MTU/acre	RH_{wp} (%)	19	1.8	33	46	59	78	90	94
	T_{wp} (°C)	153	266	127	64	47	35	31	28
	RH_{dw} (%)	27	30	54	64	73	87	96	98
	RH_{wp} /RH_{dw}	0.70	0.06	0.61	0.72	0.81	0.90	0.94	0.96
	ΔT_{drift} (°C)	12	131	15	7.1	4.3	2.1	1.4	0.9
	ΔRH_{rock} (%)	71	69	44	34	25	11	2	0
	ΔRH_{drift} (%)	8	28	21	18	14	9	6	4
	ΔRH_{total} (%)	79	97	65	52	39	20	8	4

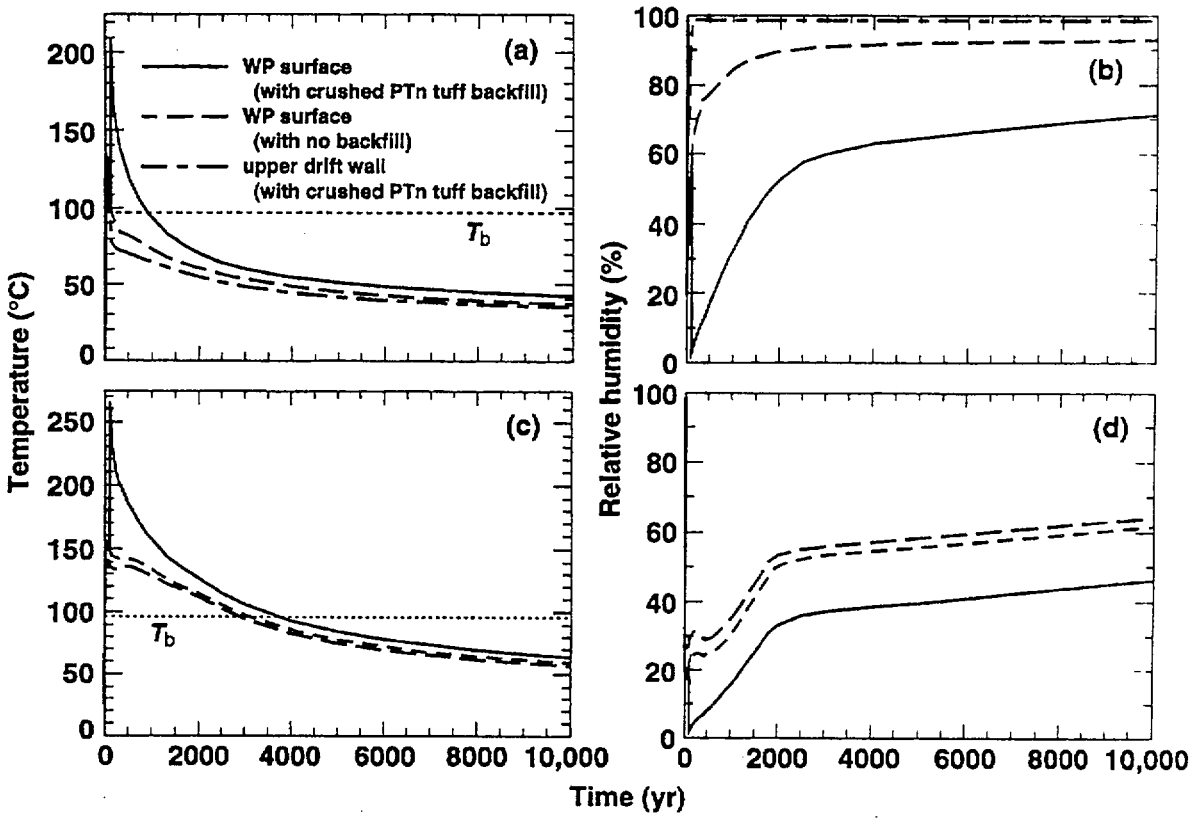

Figure 1.10.3.1. (a) Temperature and (b) relative humidity on the WP surface and in the rock at the upper drift wall for AML = 24 MTU/acre, 26-yr-old SNF, LML = 0.63 MTU/m, L_d = 100 m, bulk permeability k_b = 280 millidarcy, and vapor diffusion tortuosity factor τ_{eff} = 0.2. (c, d) Same as (a, b) except for AML = 80 MTU/acre and L_d = 30 m. Curves are shown for backfill emplaced at t = 100 yr and no backfill. Temperature and relative humidity at the upper drift wall with no backfill is very similar to that shown for the case with backfill.

1.10.4 Analysis of Engineered Backfill Scenarios for the FY95 Total Systems Performance Assessment (TSPA95)

Calculations of drift-scale thermal-hydrological behavior were conducted with the NUFT code in support of TSPA95 [Andrews et al., 1995]. The temperature and relative humidity *RH* on the WP for a case with AML = 80 MTU/acre and LML = 0.53 MTU/m (similar to the 0.63-MTU/m case in Buscheck et al., [1995]) were compared with the reference 83.4-MTU/acre case (with LML = 0.47 MTU/m) in TSPA95. The reference 83.4-MTU/acre TSPA case was found to have significantly lower WP temperature and significantly higher *RH* than the 80-MTU/acre, 0.53-MTU/m case. A thermal-hydrological analysis was conducted to identify and quantify the factors leading to the differences between the two calculations (Table 1.10.4.1). The major contributors to the differences fall in two categories: (1) thermal design assumptions and (2) whether or not rock dryout was assumed to contribute to *RH* reduction on the WP. Figure 1.10.4.1 clearly shows that whether the WP and emplacement drift are represented as being circular in cross section or represented as a square with the same cross-sectional area as the actual circular cross-sectional geometry has no effect on either the WP temperature or the temperature difference between the WP and drift wall ΔT_{drift} (items 1 and 2 in Table 1.10.4.1).

Figure 1.10.4.2 breaks down the contributions of each of the three differing thermal design assumptions on *RH* reduction. By focusing on the ratio RH_{wp}/RH_{dw}, which is the ratio of *RH* on the WP surface divided by *RH* on the drift wall, it is possible to isolate the contribution of each of the thermal design assumptions from the contribution of the assumption concerning *RH* reduction by rock dryout (ΔRH_{rock}). Recall that thermal design assumptions in the drift primarily affect the drift-ΔRH effect, which is measured by RH_{wp}/RH_{dw}, (see Eq. 2 in Section 1.8.3.1). Because TSPA95 effectively neglected ΔRH_{rock} (i.e., $RH_{dw} \approx 99\%$), RH_{wp}/RH_{dw} is nearly equal to RH_{wp} . The difference in the assumed cross-sectional area of the drift (or drift diameter) causes a 32% difference in ΔT_{drift}, which results in a 4% difference in RH_{wp} at 2000 yr (Fig. 1.10.4.2c and item 3 in Table 1.10.4.1). The difference in the assumed thermal conductivity K_{th} of the backfill causes ΔT_{drift} to differ by a factor of 1.9, which results in an 11% difference in RH_{wp} at 2000 yr (Fig. 1.10.4.2a and item 4 in Table 1.10.4.1). The difference in the assumed LML causes ΔT_{drift} to differ by 11%, which results in a 1% difference in RH_{wp} at 2000 yr (Fig. 1.10.4.2b and item 5 in Table 1.10.4.1). Altogether, the differences in thermal design assumptions caused a 24% difference in RH_{wp} at 2000 yr (Fig. 1.10.4.2d).

A sensitivity analysis was conducted to investigate the sensitivity of WP temperature, ΔT_{drift}, ΔRH_{rock}, RH_{wp}, and RH_{wp}/RH_{dw} to percolation flux for AMLs of 24 and 80 MTU/acre (Figs. 1.10.4.3–1.10.4.6). At early time, WP temperatures are about 50°C higher for the 80-MTU/acre cases than for the 24-MTU/acre cases (compare Figs. 1.10.4.3a and 1.10.4.4a; see also Table 1.10.3.1). Although WP (and rock) temperatures are considerably different for the 24- and 80-MTU/acre cases, ΔT_{drift} is virtually the same (compare Figs. 1.10.4.3c and 1.10.4.4c; see also Table 1.10.3.1). The temperature difference between the WP and drift wall ΔT_{drift} is insensitive to AML; consequently, it is also independent of the proximity of the drift to the edge of the repository. Notice that ΔT_{drift} is also insensitive to ambient percolation flux.

The *RH* calculations for the reference TSPA95 cases assume that the partial pressure of water vapor P_v on the WP is the same as P_v at the dryout front (assumption 6 in Table 1.10.4.1). This is a conservative assumption because it is equivalent to assuming that the contribution of rock dryout to *RH* reduction on the WP is negligible (i.e., $\Delta RH_{rock} = 0$). Figures 1.10.4.3b and 1.10.4.4b show the sensitivity of ΔRH_{rock} to percolation flux. Figure 1.10.4.4b shows that *RH* reduction due to rock dryout is negligible for 24 MTU/acre. In general, ΔRH_{rock} decreases with increasing percolation flux (as shown in Fig. 1.10.4.3b). For the 80-MTU/acre, 0.63-MTU/m case, ΔRH_{rock} is 43, 31, 25, and 14% at 2000 yr for

percolation fluxes of 0, 0.05, 0.132, and 0.3 mm/yr, respectively. The percolation flux would have to be larger than 0.3 mm/yr in order for the assumption of a negligible ΔRH_{rock} (assumption 6 in Table 1.10.4.1) not to be too overly conservative.

Because of assumption 6A in Table 1.10.4.1, assumption 7A (that the backfill capillary properties are similar to typical gravel) cannot have any impact on the *RH* calculations for the reference TSPA95 cases. Assumption 6A effectively negates the influence of thermal-hydrological effects inside the dryout front, including any effects occurring inside the backfilled emplacement drift. Consequently, the capillary properties of the backfill are not reflected in the analysis of the reference TSPA95 cases. As regards assumption 6B in Table 1.10.4,1, comparisons of calculations made for a 10-darcy sand and crushed TSw2 tuff backfill indicate the potential importance of wicking of moisture back to the WP on the drift-ΔRH effect. Calculations for crushed PTn tuff (which was found to wick less than crushed TSw2 tuff) indicated for high percolation flux and/or low AMLs that wicking eventually obviates much of the drift-ΔRH effect (Figs. 1.10.4.5c, 1.10.4.5d, 1.10.4.6c, and 1.10.4.6d). Because the 10-darcy sand backfill does not result in significant moisture wicking back to the WP, the drift-ΔRH effect remains intact for percolation flux at least as great as 0.3 mm/yr (Figs. 1.10.4.5a, 1.10.4.5b, 1.10.4.6a, and 1.10.4.6b).

The use of a granular backfill with nonporous grains (such as quartz sand) and sufficiently large grain size (such as a medium to coarse sand) may be required to prevent the wicking of moisture back to the WP. The wicking of moisture calculated for the crushed tuff backfill is facilitated by the capillary properties of the porous grains of the crushed tuff. The wicking of moisture through porous grains (however small) may eventually obviate the benefit of the drift-ΔRH effect. The fines contained in poorly sorted crushed rock may also facilitate moisture wicking and may also settle onto the surface of the WP, facilitating capillary or osmotic condensation of water vapor on the WP. Consequently, it may be desirable to have a well-sorted backfill.

Note that the conservative assumption was made that the characteristic curves for PTn and TSw2, which were obtained under drying conditions, are applicable to rewetting. Analyses of imbibition experiments [Buscheck and Nitao, 1987] had previously shown that the drying curves may overpredict rewetting by a factor of 40. However, even a factor of 40 reduction in wicking rate would not be large enough to eliminate the eventual deleterious consequences of moisture wicking back to the WP. However, additional analyses and laboratory and field experiments (e.g., in conjunction with the drift-scale thermal test) will be required to determine whether the wicking of moisture back to the WP may obviate the drift-ΔRH effect for various candidate backfill types.

Because of assumption 6A in Table 1.10.4.1, assumption 8A (that the backfill bulk permeability k_b = 50 millidarcy) cannot have any impact on the *RH* calculations for the reference TSPA95 cases. Assumption 6A negates the influence of thermal-hydrological behavior inside the backfilled emplacement drift. Consequently, the assumed hydrological properties of the backfill have no influence on the RH_{wp} calculated for the reference TSPA95 cases. As regards assumption 8B, the effect of the k_b of the backfill will require further investigation. Of particular interest is determining whether the backfill k_b could be large enough to cause buoyant gas-phase convection to significantly contribute to heat transfer between the WP and drift wall. If buoyant gas-phase convection significantly contributes to heat transfer between the WP and drift wall, then ΔT_{drift} and ΔRH_{drift} will be reduced relative to the case where the heat transfer is largely limited to conduction.

Table 1.10.4.1. Summary of the influence of model assumptions and level of model refinement on relative humidity calculations supporting the FY95 Total Systems Performannce Assessment (TSPA95).

	Assumption/ refinement	A: TSPA95	B: LLNL (Buscheck et al. 1995)	Effect
1	Geometry	Circular	Square	None
2	WP cross section	2.6 m^2	2.6 m^2	NA
3	Drift cross section	19.6 m^2	36 m^2	Larger backfill cross section increases ΔT_{drift} by 32%, thereby increasing ΔRH_{drift}
4	Backfill thermal conductivity K_{th}	0.6 W/m °C	0.305 W/m °C	Lower K_{th} increases ΔT_{drift} by factor of 1.9, significantly increasing ΔRH_{drift}
5	Lineal mass loading (LML)	0.47 MTU/m	0.53 MTU/m	Higher LML increases ΔT_{drift} by 11%
6	*RH* calculations	P_v (WP) = P_v (dryout front)	Explicitly calculated throughout model domain, including WP surface	Explicit calculation of *RH* is necessary to account for the influence of rock dryout and moisture flow in the drift
7	Backfill capillary properties	Similar to typical gravel	Similar to fractured PTn tuff	Assumption 5A makes assumption 6A irrelevant Assumption 6B is being assessed
8	Backfill bulk permeability k_b	50 millidarcy	40 darcy	Assumption 5A makes assumption 7A irrelevant Assumption 7B is being assessed

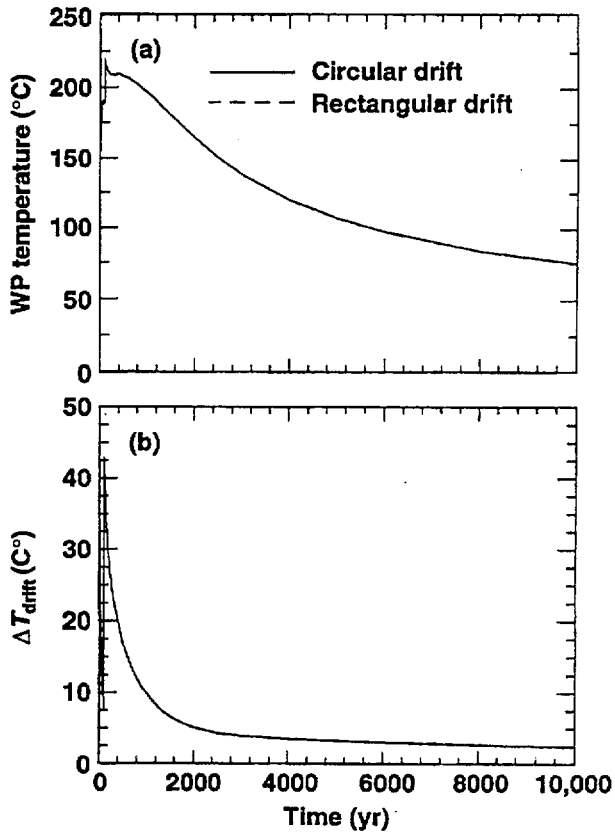

Figure 1.10.4.1. Temperature on the WP surface (a) and temperature difference between the WP and drift wall ΔT_{drift} (b) for the TSPA95 reference case with AML = 83.4 MTU/acre, LML = 0.47 MTU/m, and drift spacing = 22.5 m. Calculations were done with a two-dimensional heat-conduction model that averages the heat output from a mixture of 26-yr-old BWR WPs and 26-yr-old PWR WPs into a uniform line-heat load. Note that the curves for the circular drift and rectangular drift plot directly on top of each other.

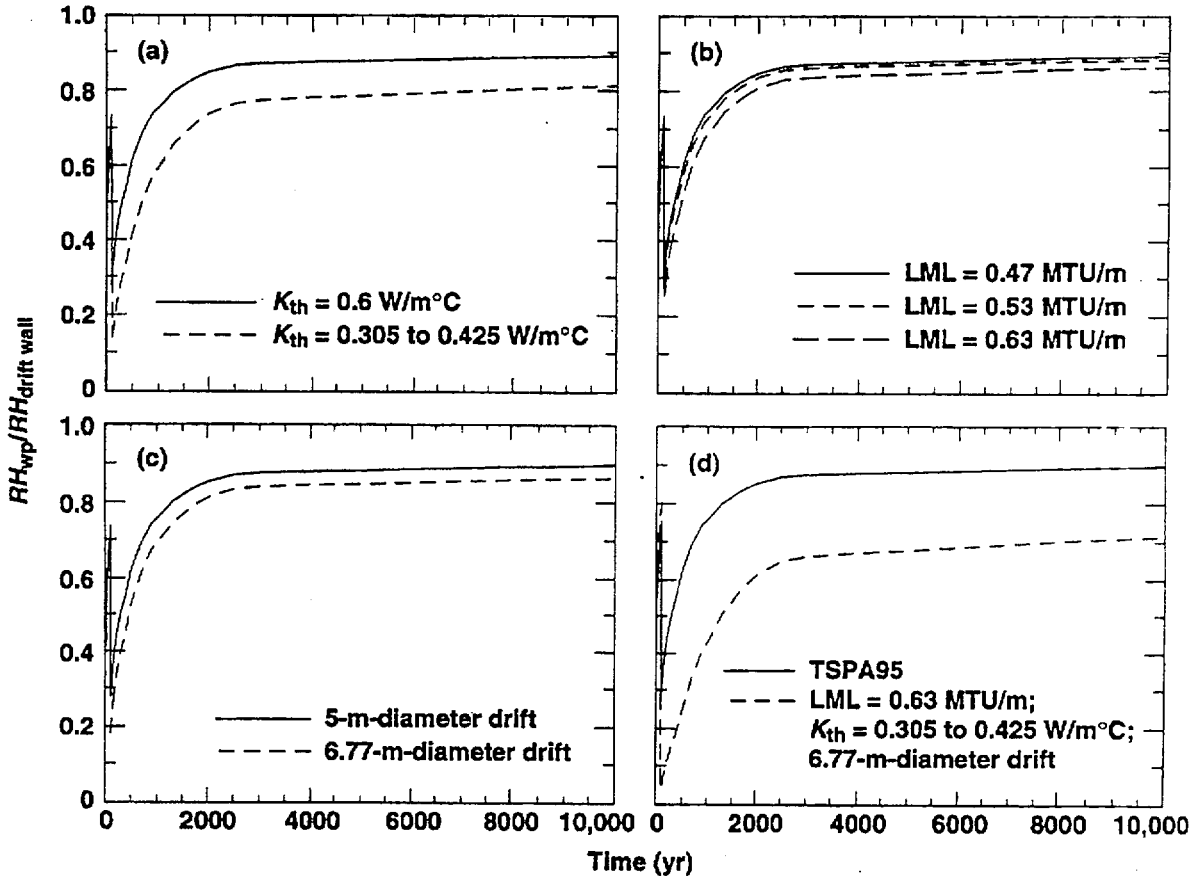

Figure 1.10.4.2. The ratio of WP relative humidity to drift wall relative humidity RH_{wp}/RH_{dw} for the TSPA95 reference backfill case with AML = 83.4 MTU/acre and backfill at 100 yr is compared with other 83.4-MTU/acre cases that each differ from the reference TSPA95 case by one thermal design assumption: (a) backfill thermal conductivity K_{th}, (b) lineal mass loading LML, and (c) drift diameter. The combined effect of all of these design assumptions (d) on RH_{wp}/RH_{dw} is also shown. The TSPA95 reference case has a backfill K_{th} = 0.6 W/m°C, LML = 0.47 MTU/m, and drift diameter = 5.0 m. The 0.53-MTU/m and 0.63-MTU/m (b) have drift spacings of 25 and 30 m, respectively. Calculations were done with a two-dimensional model that averages the heat output from a mixture of 26-yr-old BWR WPs and 26-yr-old PWR WPs into a uniform line-heat load.

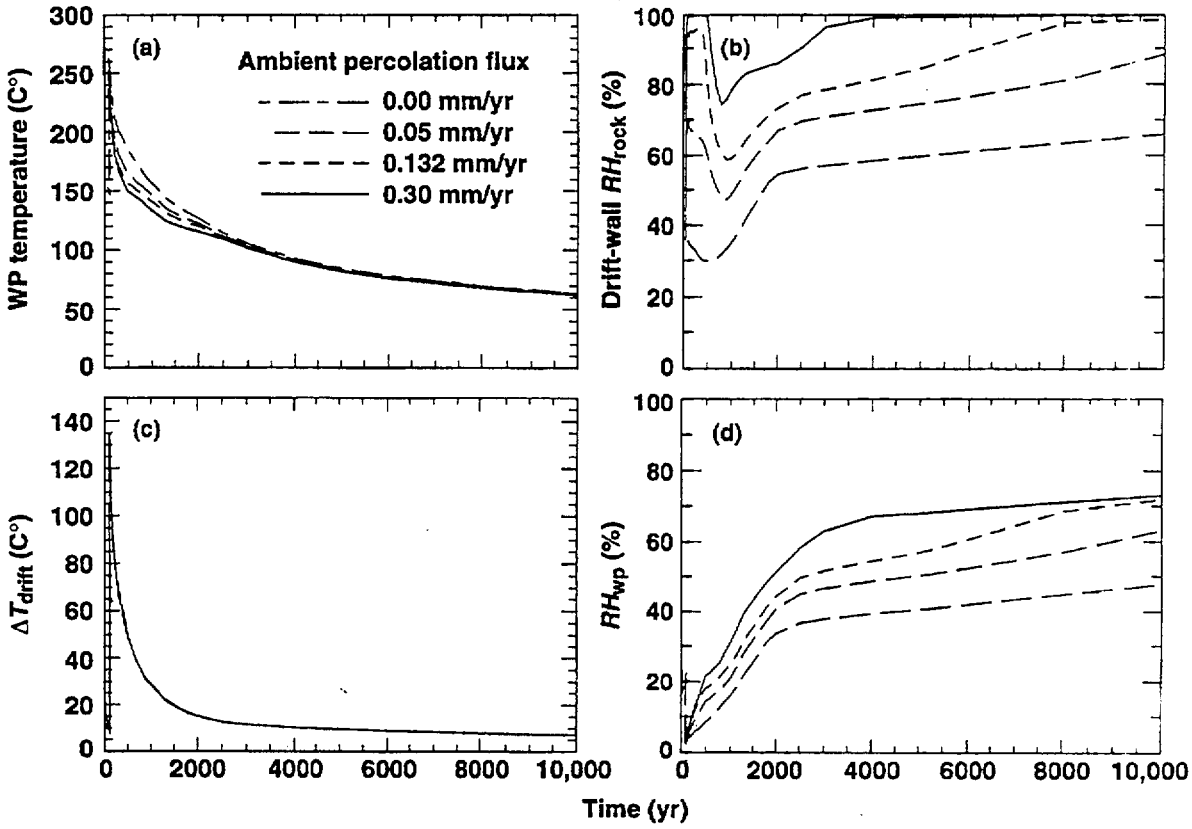

Figure 1.10.4.3. Temperature on theWP (a), relative humidity in the rock at the upper drift wall (b), temperature difference between the WP and drift wall ΔT_{drift} (c), and relative humidity on the WP for AML = 80 MTU/acre, LML = 0.63 MTU/acre, drift spacing = 30 m, backfill at 100 yr, backfill thermal conductivity K_{th} = 0.305 to 0.425 W/m°C, drift diameter = 6.77 m, and various ambient percolation fluxes. Curves are plotted for 10-darcy sand backfill (a,b) and 40-darcy crushed PTn tuff backfill (c,d). Calculations were done with a two-dimensional model that averages the heat output from a mixture of 26-yr-old BWR WPs and 26-yr-old PWR WPs into a uniform line-heat load.

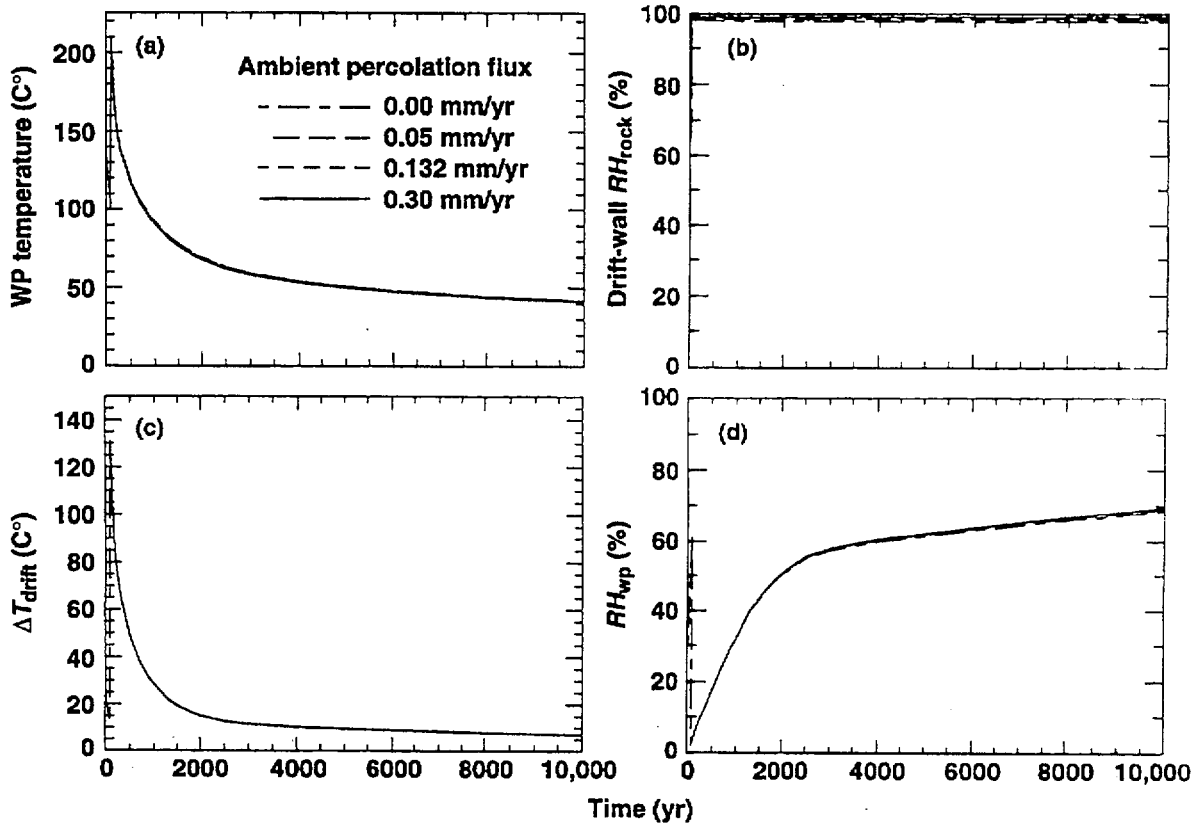

Figure 1.10.4.4. Temperature on the WP (a), relative humidity in the rock at the upper drift wall (b), temperature difference between the WP and drift wall ΔT_{drift} (c), and relative humidity on the WP for AML = 24 MTU/acre, LML = 0.63 MTU/acre, drift spacing = 100 m, backfill at 100 yr, backfill thermal conductivity K_{th} = 0.305 to 0.425 W/m°C, drift diameter = 6.77 m, and various ambient percolation fluxes. Curves are plotted for 10-darcy sand backfill (a,b) and 40-darcy crushed PTn tuff backfill (c,d). Calculations were done with a two-dimensional model that averages the heat output from a mixture of 26-yr-old BWR WPs and 26-yr-old PWR WPs into a uniform line-heat load. Note the curves for the respective ambient percolation flux cases plot directly on top of one another.

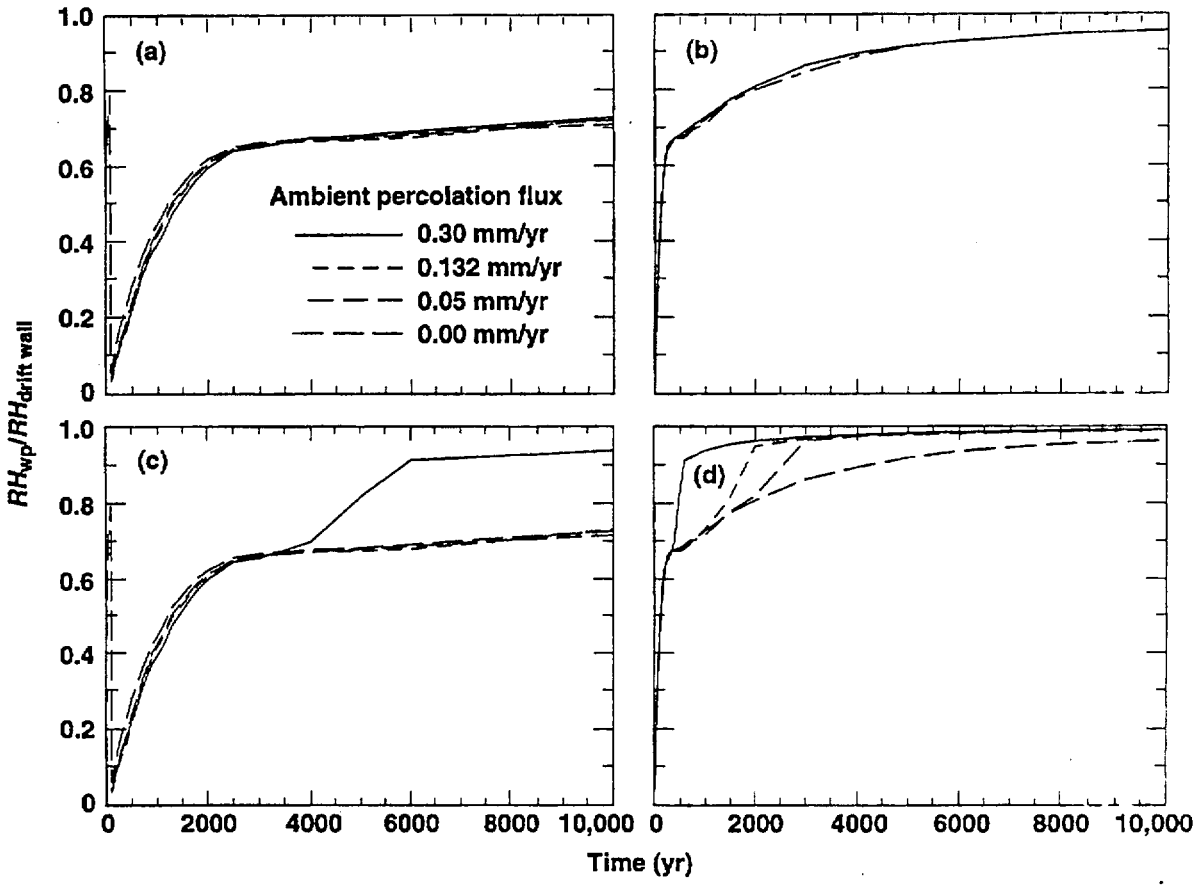

Figure 1.10.4.5. The ratio of WP relative humidity to drift wall relative humidity RH_{wp}/RH_{dw} for AML = 80 MTU/acre, LML = 0.63 MTU/acre, drift spacing = 30 m, backfill at 100 yr, backfill thermal conductivity K_{th} = 0.305 to 0.425 W/m°C, drift diameter = 6.77 m, and various ambient percolation fluxes. Curves are plotted for 10-darcy sand backfill (a,b) and 40-darcy crushed PTn tuff backfill (c,d). Calculations were done with a two-dimensional model that averages the heat output from a mixture of 26-yr-old BWR WPs and 26-yr-old PWR WPs into a uniform line-heat load. Note that the curves for percolation fluxes of 0.0, 0.05, and 0.132 mm/yr plot nearly on top of one another (b,c).

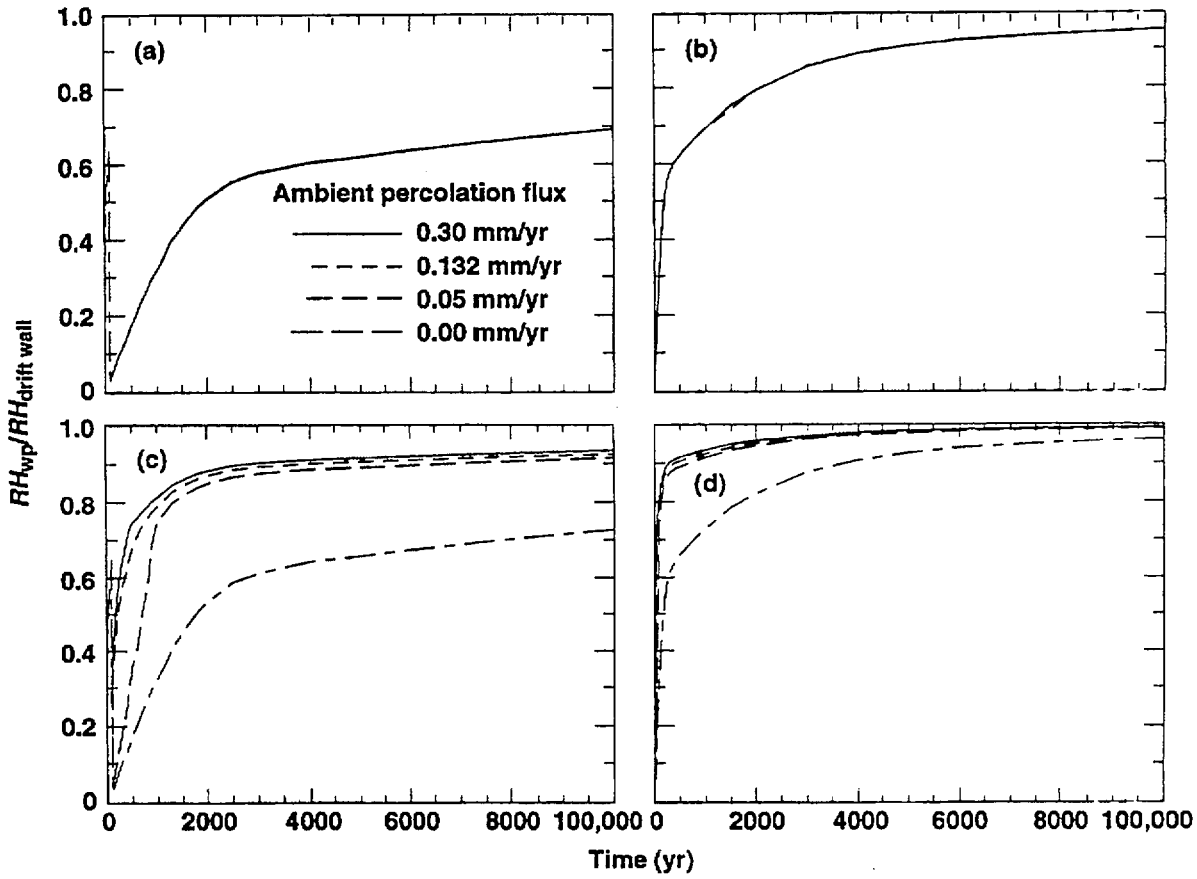

Figure 1.10.4.6. The ratio of WP relative humidity to drift wall relative humidity RH_{wp}/RH_{dw} for AML = 24 MTU/acre, LML = 0.63 MTU/acre, drift spacing = 100 m, backfill at 100 yr, backfill thermal conductivity K_{th} = 0.305 to 0.425 W/m°C, drift diameter = 6.77 m, and various ambient percolation fluxes. Curves are plotted for 10-darcy sand backfill (a,b) and 40-darcy crushed PTn tuff backfill (c,d). Calculations were done with a two-dimensional model that averages the heat output from a mixture of 26-yr-old BWR WPs and 26-yr-old PWR WPs into a uniform line-heat load.

1.10.5 Influence of Repository Design on Thermal-Hydrological Behavior

1.10.5.1 Influence of Axial Waste Package Spacing and Drift Spacing

There are two fundamentally different ways that WPs can be arranged in the repository at Yucca Mountain. The first approach (called square spacing) attempts to uniformly distribute the WP decay heat over the repository area by placing the WPs with roughly the same axial and lateral spacing between WPs (as is done in the ACD rev 00 design). The second approach (called the line load) lineally concentrates the WP decay heat to the greatest possible extent by placing the WPs end-to-end along the emplacement drifts. For a given AML, this allows for the maximum possible spacing between emplacement drifts. By utilizing each emplacement drift to the maximum possible extent, a repository that uses the line-load approach would require the minimum possible total length of emplacement drift. The three primary repository designs analyzed in Section 1.10 are:

ACD rev 00 design: This design utilizes a "square" geometry with the spacing between drift centerlines being roughly the same as the axial center-to-center spacing between SNF WPs. The ACD rev 00 has a lineal mass loading LML = 0.46 MTU/m and drift spacing = 22.5 m.

1.11-MTU/m line-load design: This design assumes a 0.1-m gap between the WPs, resulting in LML = 1.11 MTU/m and drift spacing = 53.8 m; this drift spacing is used to keep the same AML (83.4 MTU/acre) as that assumed in the ACD rev 00 design. The drift spacing in this example of the line-load design is 2.4 times greater than in the ACD (see Fig. 1.10.1.1).

0.94-MTU/m line-load design: This design assumes a 1.0-m gap between the WPs, resulting in LML = 0.94 MTU/m and drift spacing = 46.1 m; this drift spacing is used to keep the same AML (83.4 MTU/acre) as that assumed in the ACD rev 00 design. The drift spacing in this example of the line-load design is 2.05 times greater than in the ACD. This example is considered to examine the importance of tight axial WP spacing.

Using the three-dimensional, multiple-WP model (using the NUFT code), the WP inventory listed in Table 1.10.1.3, and an assumed ambient percolation flux of 0.3 mm/yr, we start with an analysis of "no-backfill" cases in which engineered backfill (also called backfill) is never used. We assume the center-in-drift (CID) WP configuration. Note that the off-center-in-drift (OCID) configuration is compared with the CID WP configuration in Section 1.10.5.4. It should also be noted that these calculations do not account for the potential dryout effects that may occur as a result of drift ventilation. At the time that the WPs are emplaced in the drifts, *RH* in the drift is in equilibrium with ambient humid conditions (see Table 1.10.1.1).

Figure 1.10.5.1.1 shows the temperature distributions at 100 and 500 yr for the ACD rev 00 design and the 1.11-MTU/m line-load design. For Figs. 1.10.5.1a,b,d, temperatures below 112°C are transparent to help illustrate the relatively hot regions in the near field. For Fig. 1.10.5.1c, temperatures below 110°C are transparent. For an ambient percolation flux of 0.3 mm/yr, rock temperatures above 105°C were found to correspond to a reduction in *RH* (Figure 1.8-4). Therefore the opaque regions in Figure 1.10.5.1.1 can be considered to be zones of superheated conditions, in which temperatures are sufficiently hotter than the nominal boiling point (96°C) so that moisture conditions are drier than ambient. In general, condensate drainage will occur around the opaque zones in Fig. 1.10.5.1.1. For the line-load design (Figs. 1.10.5.1.1b,d), condensate shedding occurs in a cylindrical fashion, with condensate flux at the repository horizon only occurring in the rock pillars separating the emplacement drifts.

The large axial WP spacing in the ACD rev 00 design thermally isolates the WPs from one another, causing the heat flux at the drift surfaces to vary substantially along the drift axis. As will be further discussed, this results in substantial variations in WP and rock temperatures and *RH* along the axis of the drift. This also causes rock dryout and condensate shedding to occur in a spherical fashion (Figs.

1.10.5.1.1a,c), with condensate flux at the repository horizon occurring within the drifts as well as in the rock pillars separating the drifts. Accordingly, condensate seepage into the drift occurs above the relatively cooler DHLW WPs in the ACD rev 00 design (Fig. 1.10.5.1.2a). For the Hanford Site DHLW WP, the liquid-phase drift seepage flux is 65, 16, 8, and 5 mm/yr at 10, 100, 200, and 300 yr, respectively. Note that these liquid-phase fluxes are much greater than the ambient percolation flux of 0.3 mm/yr assumed in this calculation. With the exception of very early time for the 40-yr-old PWR WP in the ACD rev 00 design, the drift seepage flux above the SNF WPs is always zero. For the 1.11-MTU/m line-load, the drift seepage flux is always zero for all WPs, including the DHLW WPs. It is important to point out that the model assumes that ambient percolation flux is both uniform and steady-state. Therefore, the model does not represent the possibility of either episodic nonequilibrium fracture flow or heterogeneous steady-state fracture flow; further work is required to address such possibilities.

In the ACD rev 00 design, the size of any given spherically shaped superheated zone is directly correlated with the heat output of the WP associated with that zone (Figs. 1.10.5.1.1a,c). Only half of the WPs generate enough decay heat to develop a superheated zone at 100 yr; the other half, including both DHLW WPs and the 40-yr-old PWR WP, do not generate enough decay heat to cause temperatures to reach 112°C. The "design basis fuel" 10-yr-old PWR WP (in the foreground of Figs. 1.10.5.1.1a,c) is associated with the largest superheated zone. Notice that the superheated zones associated with the 10-yr-old PWR WPs coalesce with those of the neighboring drifts (Fig. 1.10.5.1a). The 26-yr-old PWR and 26-yr-old BWR WPs generate much smaller superheated zones, which are indicative of their respective heat outputs. At 500 yr, drift-wall temperatures are very close to the nominal boiling point (96°C) all along the drift. In Fig. 1.10.5.1.1c, only the immediate vicinity of the two hottest WPs (the 10-yr-old PWR WP and the 26-yr-old PWR WP) is opaque (indicating local temperatures slightly above 110°C). For the ACD rev 00 design, only a very small portion of the repository can be considered to be in a marginally superheated state at 500 yr.

The close axial WP spacing in the 1.11-MTU/m line-load design facilitates highly efficient WP-to-WP thermal-radiative heat transfer along the axis of the emplacement drift, resulting in heat being delivered to the drift surfaces (and surrounding rock) in a highly uniform fashion. Accordingly, the superheated zone surrounding the drift is virtually invariant in the axial direction (Figs. 1.10.5.1.1b,d). The higher LML (and more uniform axial heat flux distribution) in the 1.11-MTU/m line-load design results in more locally intensive (and uniform) rock dryout around the drifts, and the larger drift spacing allows for more effective condensate shedding around the superheated zones (through the rock pillars separating the drifts), thereby facilitating less condensate buildup above the line-load drifts. As is discussed in Section 1.10.7, the tendency for condensate shedding is greater if the local heat flux (and resulting local condensate flux) is greater. Consequently, the line-load is associated with a much larger superheated volume (compare Figs. 1.10.5.1.1b,d with 1.10.5.1.1a,c) than the ACD rev 00, even though the two designs share the same AML.

Figures 1.10.5.1.3–1.10.5.1.5 and Table 1.10.5.1.1 describe the temperature and *RH* conditions in the rock at the upper drift wall during the first 10,000 yr after emplacement at various WP locations along the drift for the ACD rev 00 and 1.11-MTU/m line-load designs. Table 1.10.5.1 also describes a 0.94-MTU/m line-load design with a 1.0-m gap between WPs, which will be discussed later. For a percolation flux of 0.3 mm/yr, the LML in the ACD rev 00 design is not large enough to partially dry out, even for a limited period of time, all portions of the rock adjacent to the drift walls; consequently, humid ambient conditions always prevail along the portions of the drifts containing the cooler WPs. Moreover, the wetter (as well as cooler) portions of the ACD rev 00 drifts experience heat-pipe conditions in the overlying rock, resulting in condensate seepage flux into the drift (and onto the cooler WPs). By placing the WPs in a square pattern, the ACD rev 00 design (perhaps unintentionally) attempts to heat (and thereby presumably dry out) all regions of the repository as evenly as possible. The ACD rev 00 axial WP spacing tries to uniformly maintain 0.46 MTU/m along the axis of the drift, which, together with the 22.5-m drift spacing, results in a heat flux distribution that is as close to a smeared-out uniform heat source as possible for an 83.4-MTU/acre repository. On the other hand, the line-load (or localized dryout) approach attempts to localize (as much as possible) the heat flux distribution in the drifts themselves, while heating the rock pillars to a much lesser extent. This

results in much more locally intensive rock dryout in the vicinity of the line-load drifts and a much greater tendency for drainage in the cooler rock pillars.

In theoretical studies of the effect of decay heat on condensate flux [Nitao and Bradford, 1996], it was found that the tendency for either hot and dry conditions prevailing (rather than hot and wet conditions) depends on whether there is enough heat flux locally that is capable of evaporating the local liquid-phase flux. The local heat flux q_H (which, during the initial heat-up period is proportional to LML) will prevail over the local liquid-phase flux q_{liq} if the following holds:

$$q_H > q_{liq}\rho_{liq}h_{fg}\,, \tag{1}$$

where ρ_{liq} is the mass density of water and h_{fg} is the latent heat of vaporization. As discussed later in Section 1.10.6, both the ACD rev 00 design and the 1.11-MTU/m line-load design generate the same magnitude of condensate flux. So on average, both designs have the same liquid-phase flux returning to the repository horizon. Because larger drift spacing in the line-load design allows more effective condensate shedding, the liquid-phase flux in the heat-pipe zone directly above the emplacement drifts is less than in the ACD rev 00 design during the first 600 yr (see Fig. 1.10.6.1). During the initial heat-up period (before coalescence of the heat flow field with the neighboring drifts), q_H is proportional to LML, while at later time, it is proportional to AML. Because in the vicinity of the 1.11-MTU/m line-load emplacement drifts q_H is initially 2.4 times greater than in the ACD rev 00 design, there is a much greater tendency to generate hot and dry (rather than hot and wet) conditions in the vicinity of the line-load drifts.

A consequence of the ACD design spreading the decay heat out as evenly as possibly is that for any given repository location it is much more likely that Eq. (1) will not hold true, thereby resulting in only a very small portion of the repository footprint being drier than ambient at 500 yr (Fig. 1.10.5.1.1c). The line-load design attempts to increase the likelihood that superheated (dry) conditions be maintained around the drifts and to decrease the likelihood that superheated conditions be maintained in the midpoint of the rock pillars separating drifts, thereby facilitating condensate shedding in the pillars. The more effective condensate shedding in the line-load design results in a smaller liquid-phase flux directly above the emplacement drifts during the first 600 yr (Fig. 1.10.6.1).

The axial WP spacing in the ACD is large enough to thermally isolate the WPs from one another, so that some WP locations are very hot and dry, while others are cooler and much more humid (Table 1.10.5.1). The range in peak drift-wall temperatures is 65°C, while it is only 23°C for the 1.11-MTU/m line-load design. Because of the efficient WP-to-WP heat transfer, the maximum peak drift-wall temperature is only 19°C higher in the 1.11-MTU/m line-load than in the ACD rev 00 design, even though its LML is 2.4 times greater. The high thermal conductivity of the WPs and the efficient thermal-radiative WP-to-WP heat transfer (which was facilitated by the close axial WP spacing) allows heat flow to be efficiently distributed along the line of WPs. A very large axial heat flux occurs from WP-to-WP; in effect, relatively cool WPs function like "cooling fins" or heat-flow conduits (or distributors), receiving the heat generated by hotter neighboring WPs and distributing that heat to adjacent drift wall surfaces and (in some cases) to the next WP along the drift. For example, the Savannah River DHLW WP functioned like an axial heat-flow conduit, by receiving the excess heat generated from the 10-yr-old PWR WP located next to one of its ends, and delivering some of that excess heat to the 26-yr-old BWR located at its opposite end (see Fig. 1.10.5.1 for details of the WP layout). Even though the Savannah River DHLW WP generated much less heat than the 26-yr-old BWR WP, it still served to supply heat to (rather than receive heat from) the 26-yr-old BWR WP, because of the excess heat flow that it was receiving from its other neighboring WP (the 10-yr-old PWR WP).

During the pre-closure period (t < 100 yr) as well as during the post-closure period, the coolest and most humid location in the 1.11-MTU/m line-load drift has a lower *RH* than the hottest and least humid location in the ACD rev 00 drift (Table 1.10.5.1). All locations in the 1.11-MTU/m line-load design quickly decline to very dry (and uniform) *RH* conditions. Temperature conditions in the rock along the drift also become very uniform, with only a 6°C range in temperature at 100 yr. Pre-closure *RH* conditions in the drift are an important consideration in selecting and designing mechanical support

for the drifts. All locations of the ACD rev 00 drift wall have rewetted to ambient humid conditions within about 2500 yr (Fig. 1.10.5.1.5c), whereas it takes about 5000 yr for the drift wall in the 1.11-MTU/m drift wall to rewet to ambient *RH* conditions.

Figures 1.10.5.1.6–1.10.5.1.9 and Tables 1.10.5.1.2 –1.10.5.1.4 describe the temperature and *RH* conditions on WPs during the first 100,000 yr after emplacement for the ACD rev 00 and 1.11-MTU/m line-load designs. Table 1.10.5.2 also describes a 0.94-MTU/m line-load design with a 1.0-m gap between WPs, which will be discussed later. The large axial WP spacing in the ACD rev 00 design thermally isolates the WPs from one another so that some WPs are very hot and dry, while others (particularly the DHLW) are much cooler and much more humid. The range in peak WP temperature is 85°C, while it is only 29°C for the 1.11-MTU/m line-load design. Because of the efficient WP-to-WP heat transfer, the maximum peak WP temperature is only 11°C higher in the 1.11-MTU/m line-load than in the ACD rev 00 design, even though its LML is 2.4 times greater. The coolest and most humid WP (the Hanford Site DHLW WP) in the 1.11-MTU/m line-load design has a lower *RH* than the hottest (the "design basis fuel" 10-yr-old PWR WP) in the ACD rev 00 design.

For the ACD rev 00 design, the liquid-phase drift seepage flux is zero above all WPs from 350 to 2500 yr (Fig. 1.10.5.2.1b). Prior to 350 yr, focused drainage is able to overwhelm the superheated zone overlying the Hanford Site DHLW WP, resulting in a substantial drift seepage flux (Fig. 1.10.5.2.1a). Model calculations have indicated that the general thermal-hydrological behavior of the repository system can be divided into three sequential periods: drying, quasi-steady, and rewetting [Buscheck and Nitao, 1993a, 1993b]. The concept of these three periods is applicable over dynamically changing *spatial* regimes. Therefore, at a given time, certain locations in a repository (such as the perimeter) may already be in the rewetting regime while other locations (such as the center of the repository) may remain in the drying regime. During the first 500–1000 yr, the center of the repository (for which the drift-scale model is most applicable) is in the drying period (refer to Section 1.7.2). During the drying period, the cumulative volume of water removed from the WP zone increases monotonically; the upper vertical extent of the nominal dryout front (on average) also grows monotonically during this period. As the upper extent of the average dryout front moves further above the repository horizon, it becomes increasing difficult for focused liquid-phase flow to penetrate the superheated region and reach the repository horizon. For the ACD rev 00 design and an ambient percolation flux of 0.3 mm/yr, it takes 350 yr for the standoff between the emplacement drift and the average dryout front location to be large enough to be able to completely vaporize the focused "down spout" of condensate that was resulting in liquid-phase seepage into the drift above the Hanford Site DHLW WP.

For the ACD rev 00 design, the surface temperature of both DHLW WPs declines below the nominal boiling point (96°C) at 2100 yr, while the neighboring SNF WPs remain above the boiling point. Because the drift-wall and WP surfaces are below the boiling point in the vicinity of the DHLW WPs, water vapor preferentially flows to these locations, where it condenses, thereby depositing a considerable quantity of latent heat and condensate. The cooler regions of the drift function as "cold traps" in that they attract vapor flow (from the hotter regions of the drift) as a result of their lower gas-phase pressure. This process of vapor flow and condensation in the drifts results in the transport of a considerable quantity of moisture and latent heat to the cold traps. For 2000–60,000 yr, the surfaces of the DHLW WPs experience $RH = 100\%$ because of the presence of liquid water (condensate) on the surfaces of those WPs. In general, the cold-trap effect arises from:

Axial vapor flow and condensation within the drift: This effect is driven by axial variations in temperature T and P_V along the drift. Water vapor is transported (by gas-phase advection and diffusion) from areas of higher T and P_V to areas of lower T and P_V where it condenses, which causes *RH* to increase (even as high as 100%). Because there is so little resistance to vapor flow along the drift, large vapor fluxes can occur along the drift and large condensation rates can arise in the cooler areas if the following three conditions are met: (1) high *RH* in the rock at the drift wall, (2) WP heat output varies substantially from WP to WP, and (3) WPs are thermally isolated from one another.

The condensate flux generated by the cold-trap effect contributes to the seepage flux at the drift wall (and on the drift floor) at these locations (Fig. 1.10.5.1.2b). Although the WPs are thermally

isolated from one another, they are not thermal-hydrologically isolated from one another; from 0–350 yr and from 2000–60,000 yr, the decay-heat from the hot WPs drives condensate onto the cooler WPs (as a result of the cold-trap effect) in the ACD rev 00 design.

The last two rows of Tables 1.10.5.1.2–1.10.5.1.4 list the time required to rewet to *RH* = 65% and 90%; these RH thresholds are listed because corrosion studies of the candidate WP materials indicate that the critical *RH* for atmospheric corrosion is 65% if an evaporitic salt is present on the WP or 90% if the WP surface is free of salt [Gdowski, 1996]. For the ACD rev 00 design, the Hanford Site DHLW WP never is below the *RH* = 65% threshold, while the Savannah River Site DHLW WP and the 40-yr-old PWR WP require only 130 and 140 yr to reach the 65% threshold (Table 1.10.5.1.3). For the 1.11-MTU/m line-load design (Table 1.10.5.1.4), the Savannah River Site DHLW WP takes the least time (1450 yr) to reach the 65% threshold, which is still considerably longer than the time (630 yr) for the relatively hot 10-yr-old PWR WP to reach the 65% threshold in the ACD rev 00 design (Table 1.10.5.1.3). The time required for the ACD rev 00 WPs to reach the *RH* = 90% threshold ranges from 1170 to 2330 yr, while for the 1.11-MTU/m line-load WPs, the range is 4030 to 4680 yr (Table 1.10.5.1.2).

Temperature and *RH* conditions in the rock at the upper drift wall and on the WPs for the 0.94-MTU/m line-load design with a 1.0-m gap between WPs is given in Figs. 1.10.5.1.10–1.10.5.1.13. Because of the larger gaps between WPs, axial WP-to-WP heat transfer is a little less efficient than in the 1.11-MTU/m line-load design. This results in a slightly larger range in peak drift-wall temperatures (34°C versus 23°C; see Table 1.10.5.1.1) and in a larger range in peak WP temperatures (43°C versus 31°C; see Table 1.10.5.2); however, the drift-wall and WP temperature range is still considerably less than in the ACD rev 00 design. Because of the efficient WP-to-WP heat transfer, the maximum peak WP temperature is only 5°C higher in the 0.94-MTU/m line-load than in the ACD rev 00 design, even though its LML is 2 times greater. The coolest (and most humid) WP in the 0.94-MTU/m line-load design is only slightly more humid than the hottest and (driest) WP in the ACD rev 00 design (Table 1.10.5.1.2). Table 1.10.5.1.5 summarizes temperature and *RH* on the WPs in the 0.94-MTU/m line-load design. The coolest (and most humid) WP (the Savannah River Site DHLW WP) in the 0.94-MTU/m line-load design is much less humid than the hottest (and driest) WP (the 10-yr-old PWR WP) in the ACD rev 00 design. Consequently, the Savannah River Site DHLW WP in the 0.94-MTU/m design requires more time to reach the *RH* = 65% and 90% thresholds than the the 10-yr-old PWR WP in the ACD rev 00 design.

Table 1.10.5.1.1. Temperature and relative humidity in rock at upper drift wall for AML = 83.4 MTU/acre, drift diameter = 5.5 m, sand invert, no backfill, WP emissivity = 0.8, and percolation flux = 0.3 mm/yr.

Repository design	**ACD rev 00**	**Line load**	**Line load**
LML	0.46 MTU/m	1.11 MTU/m	0.94 MTU/m
Drift spacing	22.5 m	53.8 m	46.1 m
Gap between WPs	varies	0.1 m	1.0 m
T_{peak} (t < 100 yr)	100–165°C	161–184°C	139–173°C
RH_{max} (t < 100 yr)	36–98%	21–25%	28–37%
T_{peak} (t > 100 yr)	100–129°C	142–148°C	129–139°C
RH (t = 120 yr)	36–97%	23–27%	31–39%
RH (t = 2000 yr)	90–97%	76–77%	82–83%
RH (t = 10,000 yr)	99.8–99.8%	99.1–99.1%	99.4–99.4%

Table 1.10.5.1.2. Temperature and relative humidity on upper WP surface for AML = 83.4 MTU/acre, drift diameter = 5.5 m, sand invert, no backfill, WP emissivity = 0.8, and percolation flux = 0.3 mm/yr.

Repository design	ACD rev 00	Line load	Line load
LML	0.46 MTU/m	1.11 MTU/m	0.94 MTU/m
Drift spacing	22.5 m	53.8 m	46.1 m
Gap between WPs	varies	0.1 m	1.0 m
T_{peak} (t < 100 yr)	107–192°C	172–203°C	151–197°C
RH_{max} (t < 100 yr)	25–86%	16–21%	20–32%
T_{peak} (t > 100 yr)	104–144°C	147–158°C	134–150°C
RH (t = 120 yr)	29–85%	18–23%	23–33%
RH (t = 2000 yr)	86–97%	72–76%	78–82%
RH (t = 10,000 yr)	92–99.9%	94–98%	94–99%
$t(RH = 65\%)$	0–630 yr	1450–1620 yr	990–1270 yr
$t(RH = 90\%)$	1170–2330 yr	4030–4680 yr	2790–3540 yr

Table 1.10.5.1.3. Temperature and relative humidity on upper WP surface for AML = 83.4 MTU/acre, a line-load design with a 0.1-m gap between WPs, LML = 1.11 MTU/m, drift spacing = 53.8 m,sand invert, no backfill, drift diameter = 5.5 m, WP emissivity = 0.8, and percolation flux = 0 mm/yr.

Waste package type	Hanford Site DHLW	Savannah River Site DHLW	40-yr-old PWR MPC	26-yr-old BWR MPC	26-yr-old PWR MPC	10-yr-old PWR MPC
T_{peak} (t < 100 yr)	187°C	198°C	185°C	188°C	192°C	216°C
RH_{max} (t < 100 yr)	16%	15%	15%	15%	14%	12%
T_{peak} (t > 100 yr)	160°C	162°C	161°C	163°C	164°C	170°C
RH (t = 120 yr)	17%	17%	17%	17%	14%	14%
RH (t = 2000 yr)	58%	59%	57%	58%	57%	56%
RH (t = 10,000 yr)	69%	70%	69%	69%	68%	67%
$t(RH$ = 65%)	6840 yr	6290 yr	7370 yr	7210 yr	8150 yr	8480 yr
$t(RH$ = 90%)	26,250 yr	25,850 yr	26,720 yr	26,680 yr	27,360 yr	27,680 yr

Table 1.10.5.1.4. Temperature and relative humidity on upper WP surface for AML = 83.4 MTU/acre, a line-load design with a 0.1-m gap between WPs, LML = 1.11 MTU/m, drift spacing = 53.8 m,sand invert, no backfill, drift diameter = 5.5 m, WP emissivity = 0.8, and percolation flux = 0.3 mm/yr.

Waste package type	Hanford Site DHLW	Savannah River Site DHLW	40-yr-old PWR MPC	26-yr-old BWR MPC	26-yr-old PWR MPC	10-yr-old PWR MPC
T_{peak} (t < 100 yr)	171°C	184°C	171°C	174°C	178°C	203°C
RH_{max} (t < 100 yr)	21%	21%	21%	21%	19%	16%
T_{peak} (t > 100 yr)	147°C	149°C	148°C	148°C	151°C	158°C
RH (t = 120 yr)	23%	23%	23%	22%	21%	18%
RH (t = 2000 yr)	75%	76%	76%	74%	73%	72%
RH (t = 10,000 yr)	97%	98%	98%	96%	95%	94%
$t(RH$ = 65%)	1510 yr	1450 yr	1550 yr	1540 yr	1610 yr	1620 yr
$t(RH$ = 90%)	4180 yr	4030 yr	4320 yr	4290 yr	4540 yr	4680 yr

Table 1.10.5.1.5. Temperature and relative humidity on upper WP surface for AML = 83.4 MTU/acre, a line-load design with a 1.0-m gap between WPs, LML = 0.94 MTU/m, drift spacing = 46.1 m, sand invert, no backfill, drift diameter = 5.5 m, WP emissivity = 0.8, and percolation flux = 0.3 mm/yr.

Waste package type	Hanford Site DHLW	Savannah River Site DHLW	40-yr-old PWR MPC	26-yr-old BWR MPC	26-yr-old PWR MPC	10-yr-old PWR MPC
T_{peak} (t < 100 yr)	151°C	165°C	149°C	156°C	162°C	197°C
RH_{max} (t < 100 yr)	32%	32%	30%	29%	26%	20%
T_{peak} (t > 100 yr)	134°C	136°C	136°C	138°C	141°C	150°C
RH (t = 120 yr)	33%	32%	32%	31%	26%	23%
RH (t = 2000 yr)	82%	83%	80%	81%	79%	78%
RH (t = 10,000 yr)	99%	99%	97%	97%	95%	94%
$t(RH$ = 65%)	1040 yr	990 yr	1110 yr	1120 yr	1230 yr	1280 yr
$t(RH$ = 90%)	2860 yr	2790 yr	2990 yr	2990 yr	3310 yr	3540 yr

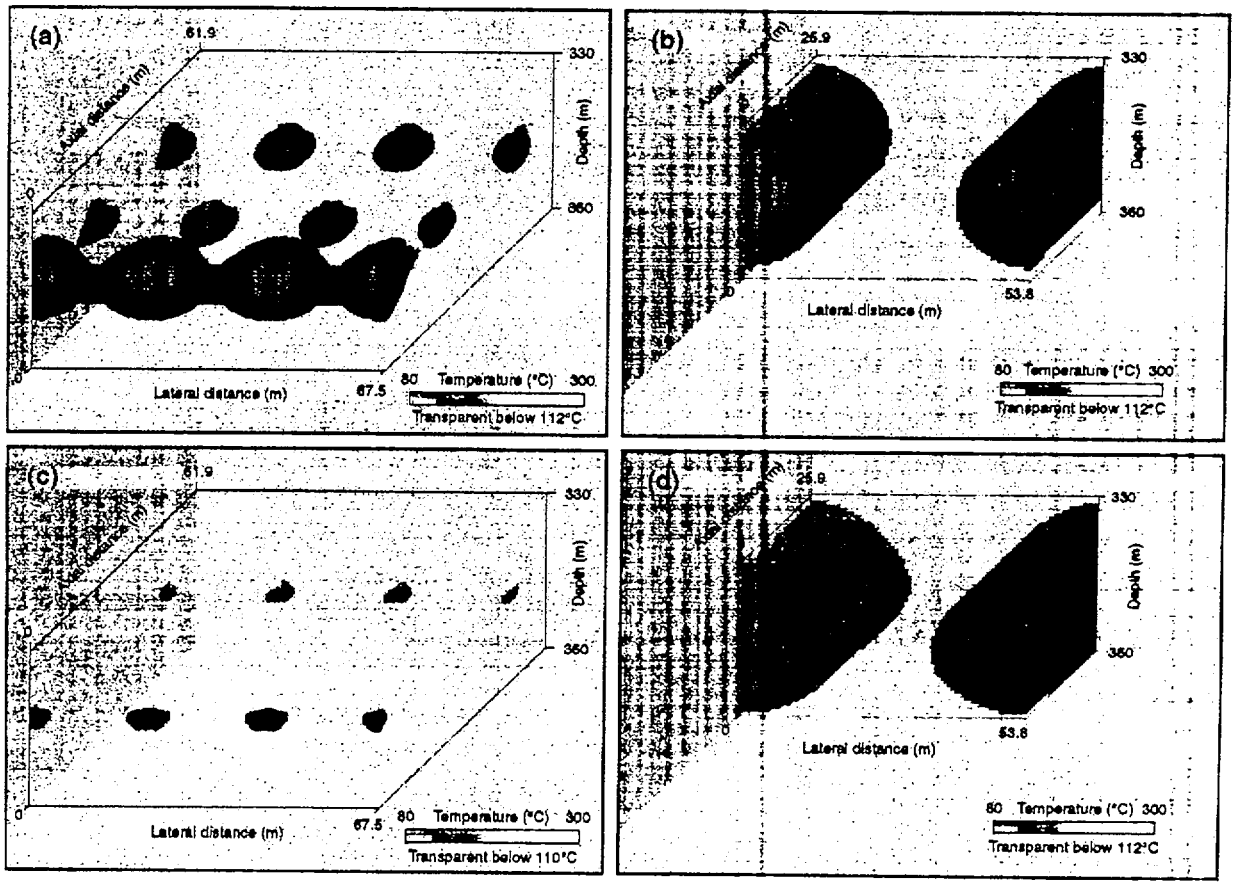

Figure 1.10.5.1.1. Temperature distribution for the ACD rev 00 design (a,c) with LML = 0.46 MTU/m and drift spacing = 22.5 m; and the line-load design (b,d) with 0.1-m gaps between WPs, LML = 1.11 MTU/m, and drift spacing = 53.8 m. For both cases, AML = 83.4 MTU/acre, sand invert, no overfill, drift diameter = 5.5 m, WP emissivity = 0.8, and ambient percolation flux = 0.3 mm/yr. Temperature distributions are plotted at 100 yr (a,b) and 500 yr (c,d). Temperatures less than 112°C are transparent (a,b,d). Temperatures less than 110°C are transparent (c). Note that the emplacement drifts are parallel to the axial distance axis. For the ACD rev 00 design, the drift axes are located at lateral distances of 0, 22.5, 45, and 67.5 m. For the line-load design, the drift axes are located at lateral distances of 0 and 53.8 m.

Table 1.10.5.2.6. Temperature and relative humidity on upper WP surface for AML = 83.4 MTU/acre, a line-load design with a 1.0-m gap between WPs, LML = 0.94 MTU/m, drift spacing = 46.1 m, sand invert, full sand backfill at 100 yr with K_{th} = 0.6 W/m°C, drift diameter = 5.5 m, WP emissivity = 0.8, and percolation flux = 0.3 mm/yr.

Waste package type	Hanford Site DHLW	Savannah River Site DHLW	40-yr-old PWR MPC	26-yr-old BWR MPC	26-yr-old PWR MPC	10-yr-old PWR MPC
T_{peak} (t < 100 yr)	151°C	165°C	149°C	156°C	162°C	197°C
RH_{max} (t < 100 yr)	32%	32%	30%	29%	26%	20%
T_{peak} (t > 100 yr)	194°C	205°C	206°C	203°C	213°C	221°C
RH (t = 120 yr)	8%	7%	6%	7%	5%	5%
RH (t = 2000 yr)	66%	65%	60%	62%	57%	59%
RH (t = 10,000 yr)	86%	85%	81%	82%	77%	78%
$t(RH$ = 65%)	1990 yr	2000 yr	2440 yr	2310 yr	2740 yr	2600 yr
$t(RH$ = 90%)	17,490 yr	19,100 yr	27,700 yr	26,180 yr	35,110 yr	32,740 yr

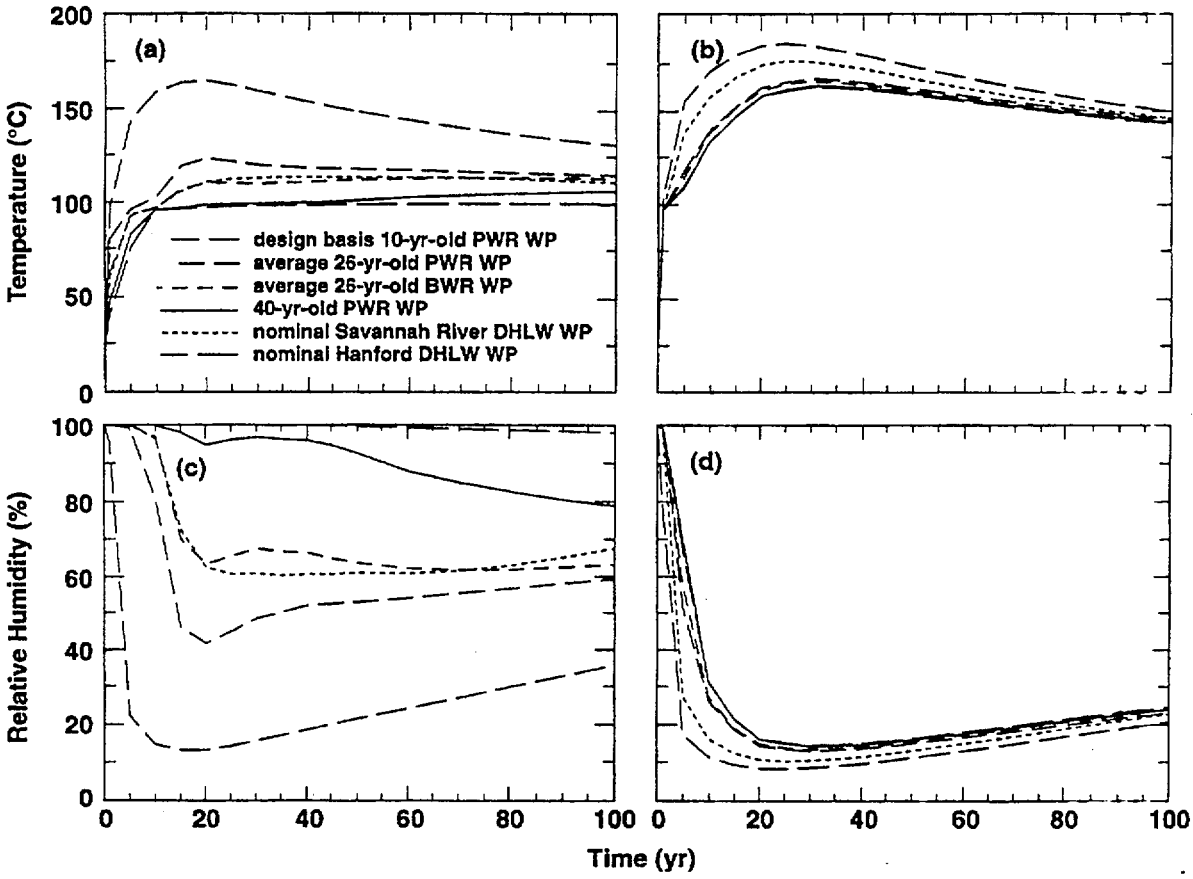

Figure 1.10.5.1.3. Temperature and relative humidity in rock at upper drift wall at various WP locations for AML = 83.4 MTU/acre, sand invert, drift diameter = 5.5 m, WP emissivity = 0.8, and ambient percolation flux = 0.3 mm/yr. Curves are plotted for the ACD rev 00 design (a,c) with LML = 0.46 MTU/m, and a line-load design (b,d) with a 0.1-m gap between WPs and LML = 1.11 MTU/m.

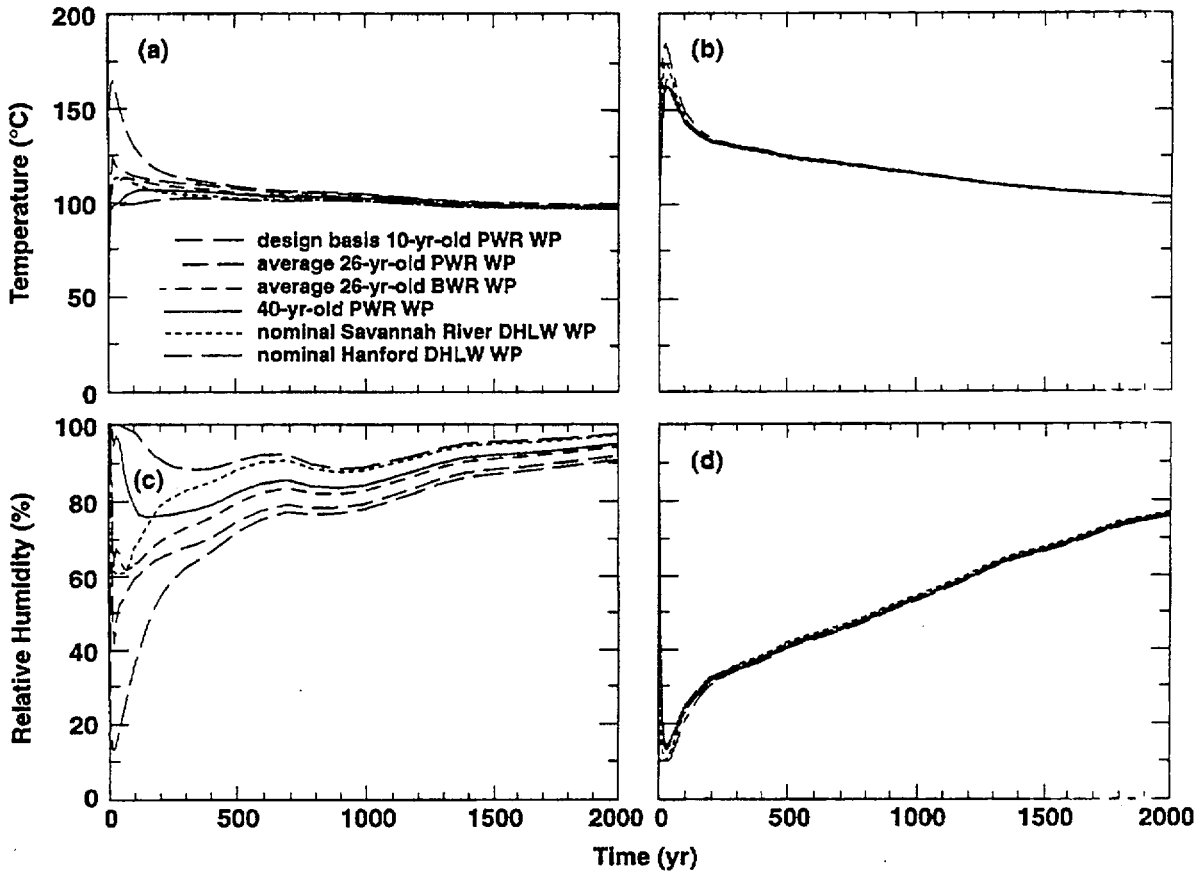

Figure 1.10.5.1.4. Temperature and relative humidity in rock at upper drift wall at various WP locations for AML = 83.4 MTU/acre, sand invert, no overfill, drift diameter = 5.5 m, WP emissivity = 0.8, and ambient percolation flux = 0.3 mm/yr. Curves are plotted for the ACD rev 00 design (a,c) with LML = 0.46 MTU/m, and a line-load design (b,d) with a 0.1-m gap between WPs and LML = 1.11 MTU/m.

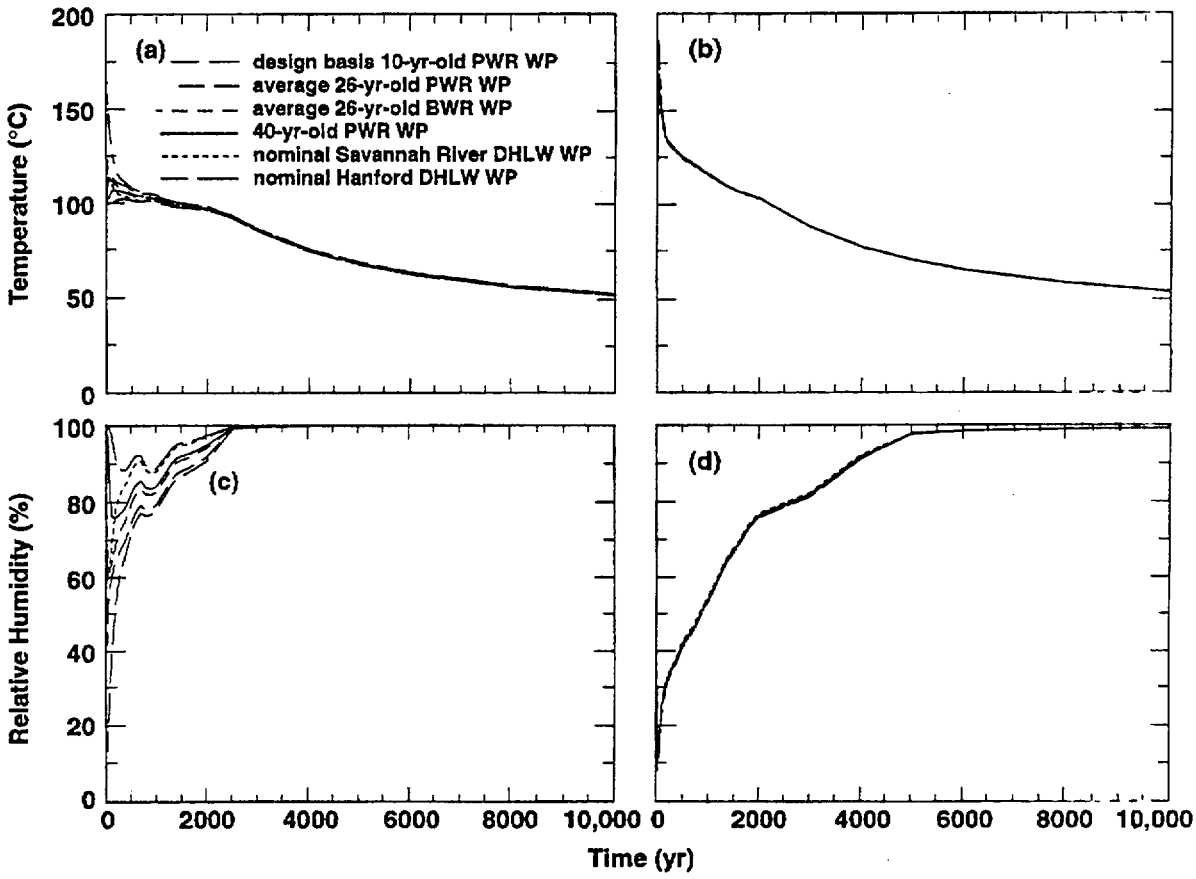

Figure 1.10.5.1.5. Temperature and relative humidity in rock at upper drift wall at various WP locations for AML = 83.4 MTU/acre, sand invert, no overfill, drift diameter = 5.5 m, WP emissivity = 0.8, and ambient percolation flux = 0.3 mm/yr. Curves are plotted for the ACD rev 00 design (a,c) with LML = 0.46 MTU/m, and a line-load design (b,d) with a 0.1-m gap between WPs and LML = 1.11 MTU/m.

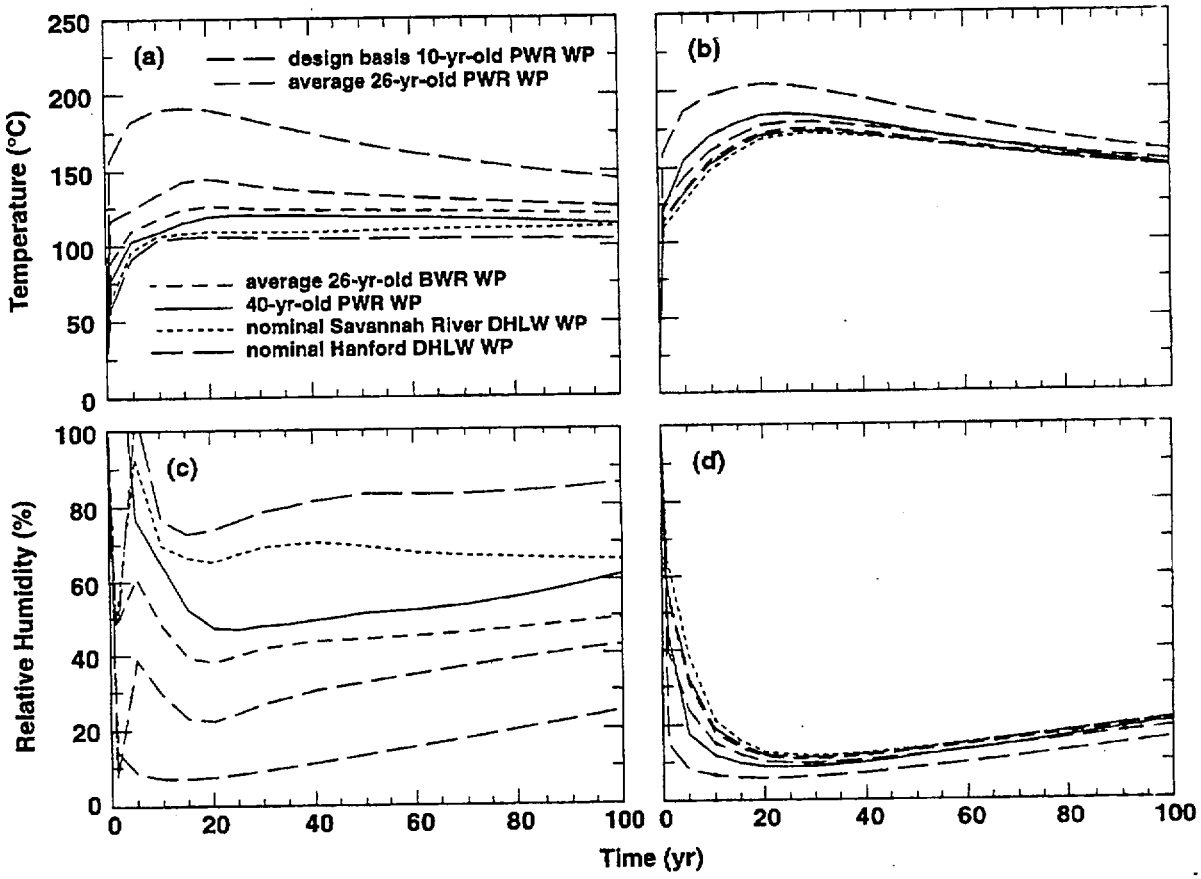

Figure 1.10.5.1.6. Temperature and relative humidity on upper surface of WP for AML = 83.4 MTU/acre, sand invert, drift diameter = 5.5 m, WP emissivity = 0.8, and ambient percolation flux = 0.3 mm/yr. Curves are plotted for the ACD rev 00 design (a,c) with LML = 0.46 MTU/m, and a line-load design (b,d) with a 0.1-m gap between WPs and LML = 1.11 MTU/m.

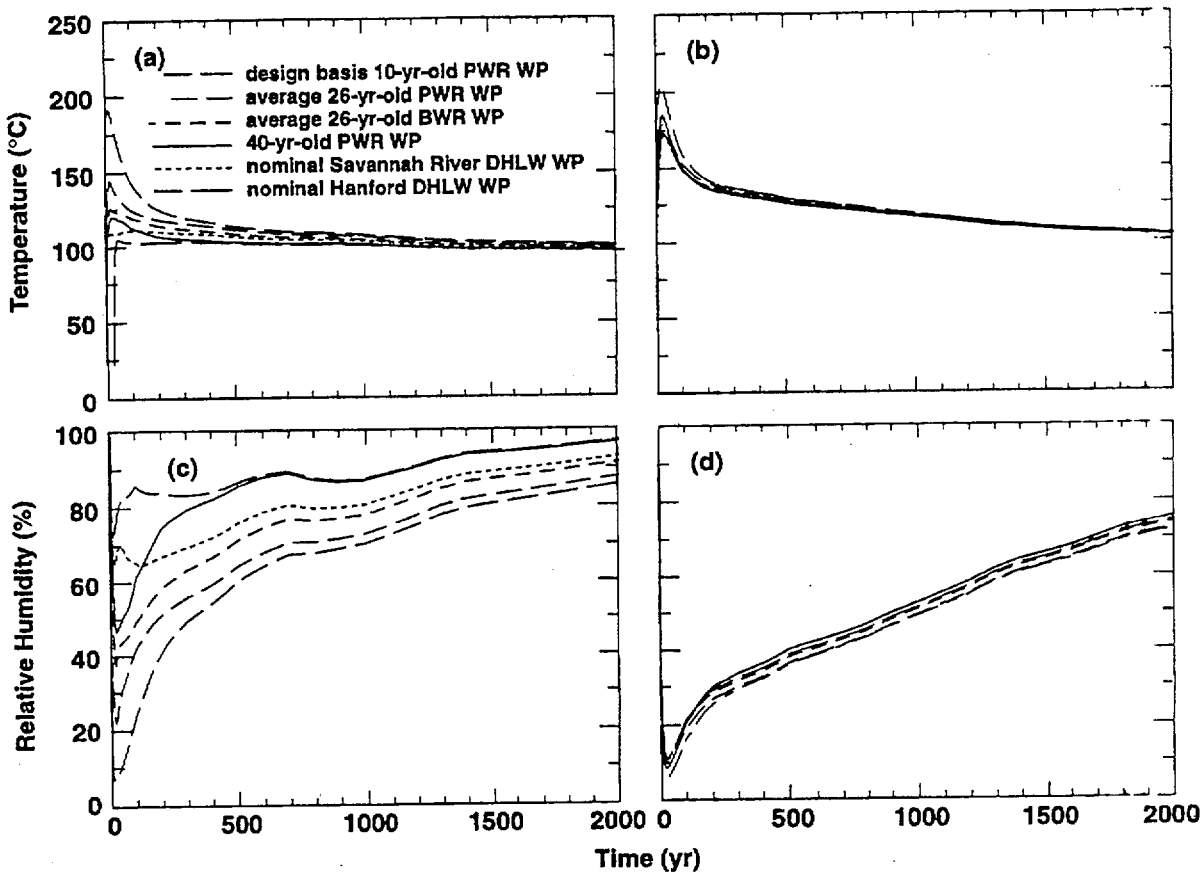

Figure 1.10.5.1.7. Temperature and relative humidity on upper surface of WP for AML = 83.4 MTU/acre, sand invert, no overfill, drift diameter = 5.5 m, WP emissivity = 0.8, and ambient percolation flux = 0.3 mm/yr. Curves are plotted for the ACD rev 00 design (a,c) with LML = 0.46 MTU/m, and a line-load design (b,d) with a 0.1-m gap between WPs and LML = 1.11 MTU/m.

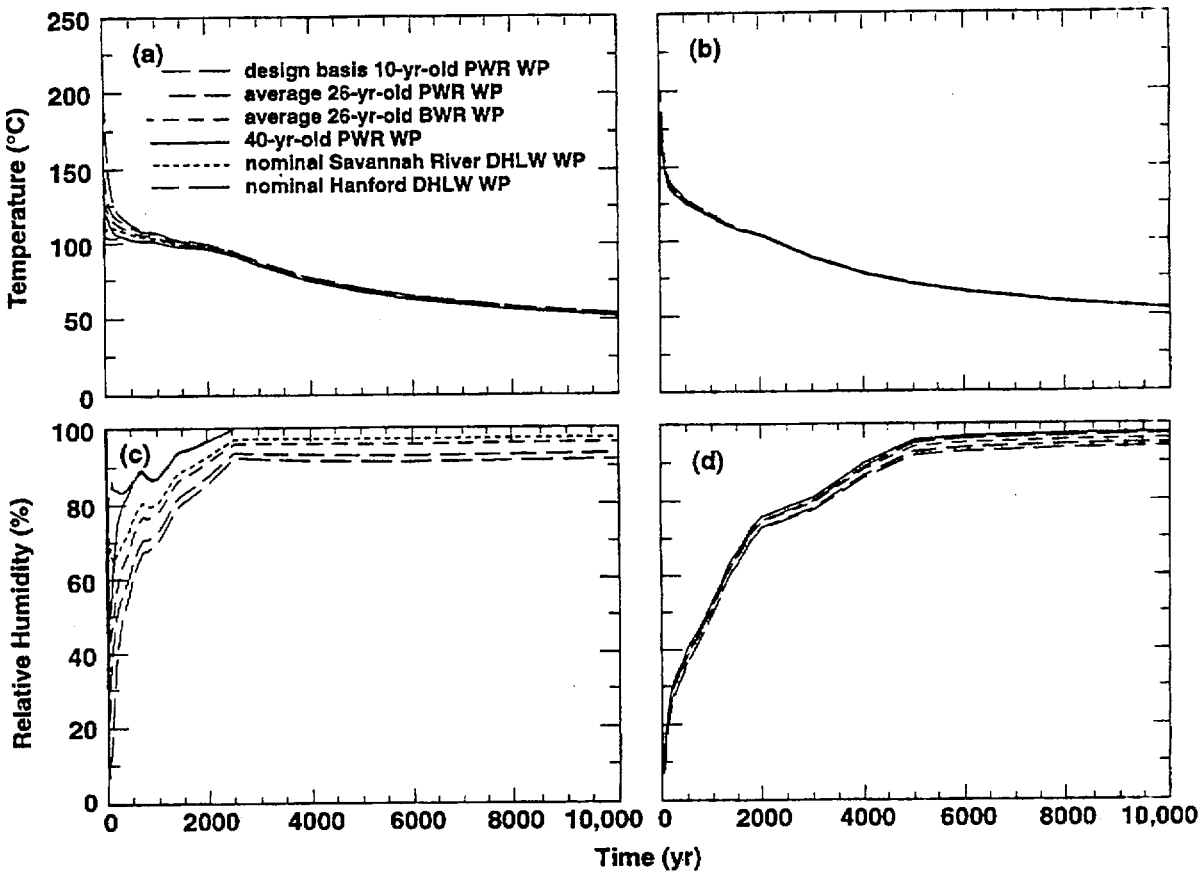

Figure 1.10.5.1.8. Temperature and relative humidity on upper surface of WP for AML = 83.4 MTU/acre, sand invert, no overfill, drift diameter = 5.5 m, WP emissivity = 0.8, and ambient percolation flux = 0.3 mm/yr. Curves are plotted for the ACD rev 00 design (a,c) with LML = 0.46 MTU/m, and a line-load design (b,d) with a 0.1-m gap between WPs and LML = 1.11 MTU/m.

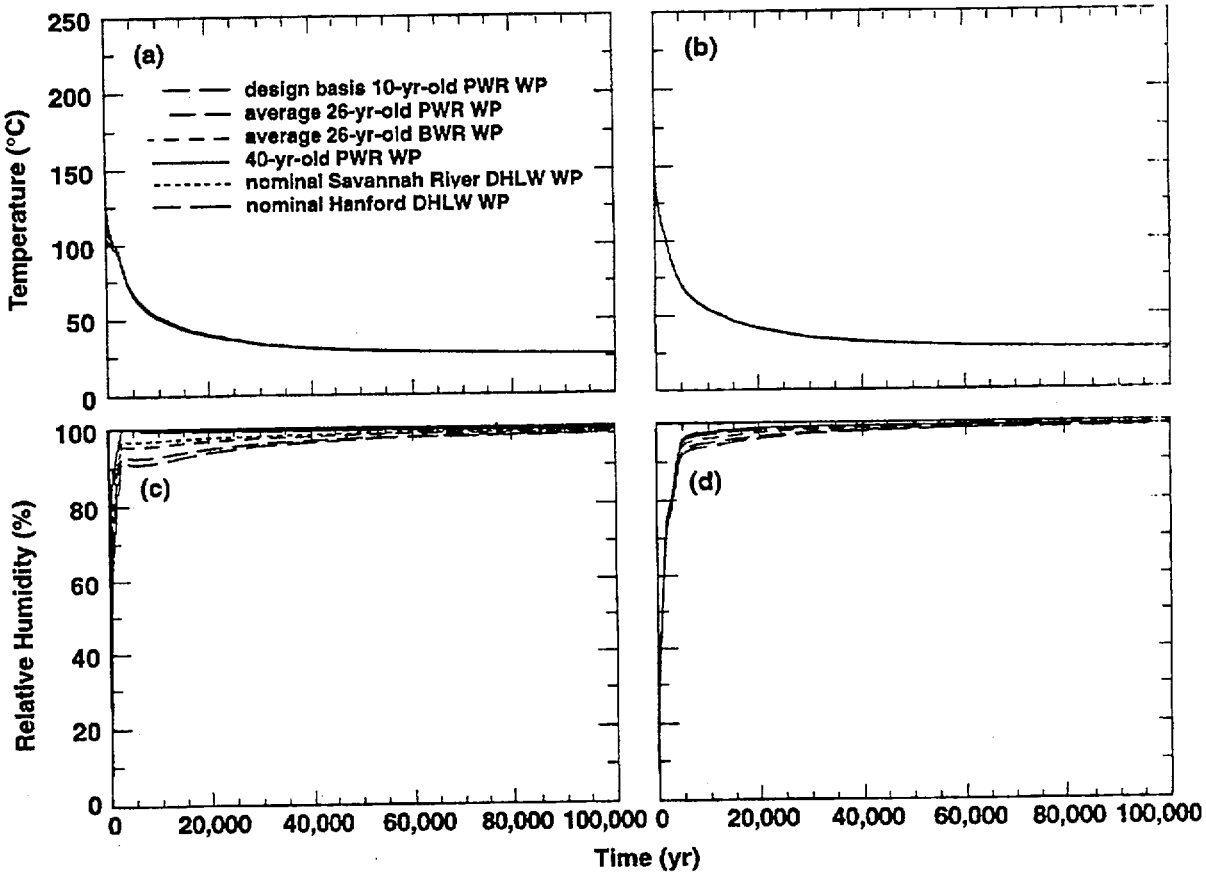

Figure 1.10.5.1.9. Temperature and relative humidity on upper surface of WP for AML = 83.4 MTU/acre, sand invert, no overfill, drift diameter = 5.5 m, WP emissivity = 0.8, and ambient percolation flux = 0.3 mm/yr. Curves are plotted for the ACD rev 00 design (a,c) with LML = 0.46 MTU/m, and a line-load design (b,d) with a 0.1-m gap between WPs and LML = 1.11 MTU/m.

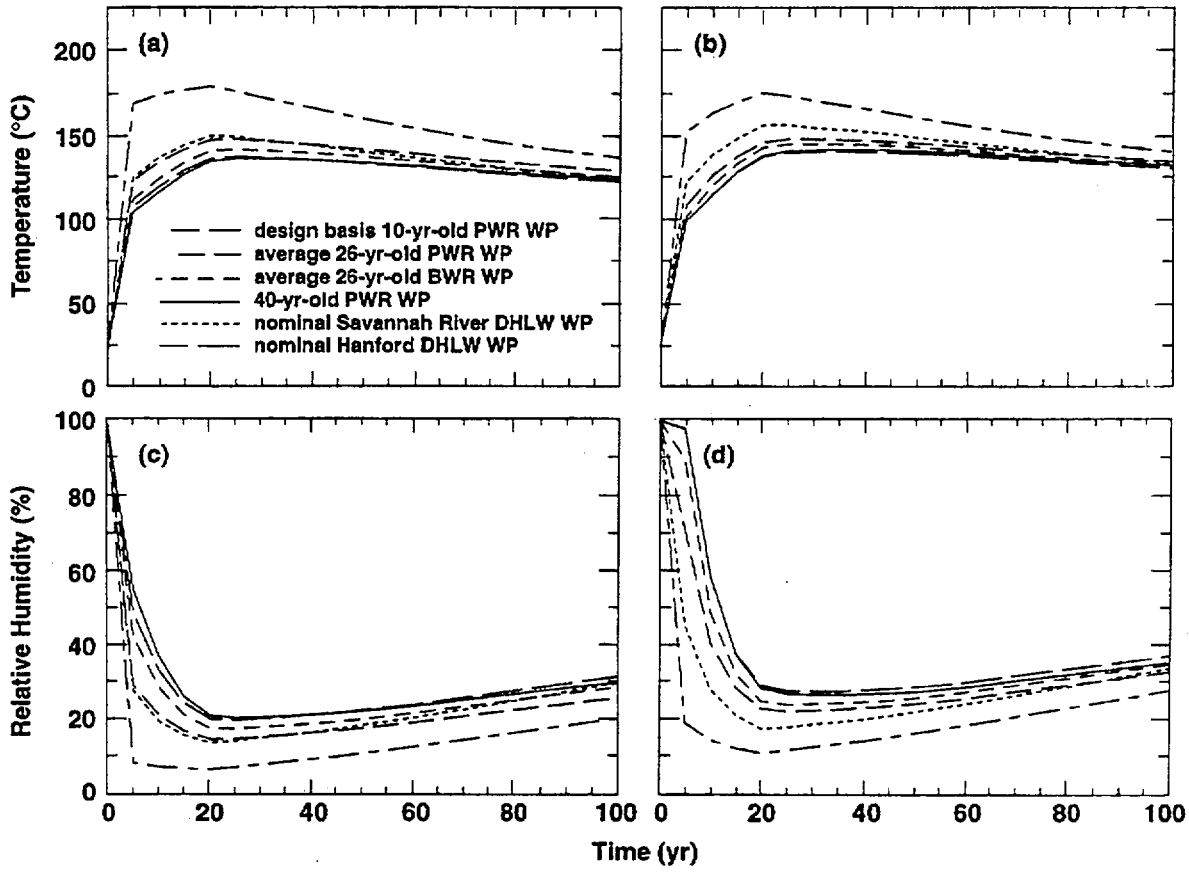

Figure 1.10.5.1.10. Temperature and relative humidity on upper WP surface (a,c) and in rock at upper drift wall (b,d) at various WP locations for AML = 83.4 MTU/acre, a line-load design with a 1.0-m gap between WPs, LML = 0.94 MTU/m, sand invert, drift diameter = 5.5 m, WP emissivity = 0.8, and ambient percolation flux = 0.3 mm/yr.

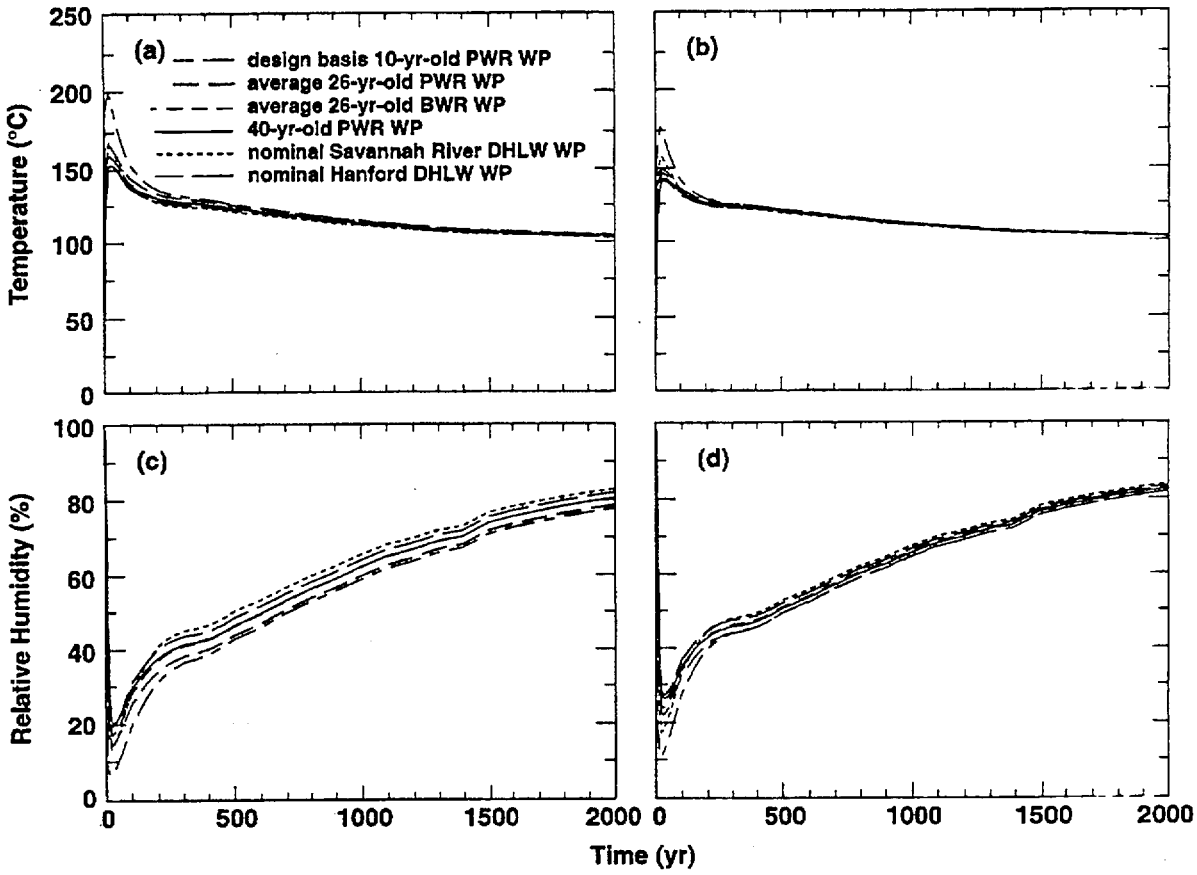

Figure 1.10.5.1.11 Temperature and relative humidity on upper WP surface (a,c) and in rock at upper drift wall (b,d) at various WP locations for AML = 83.4 MTU/acre, a line-load design with a 1.0-m gap between WPs, LML = 0.94 MTU/m, sand invert, no overfill, drift diameter = 5.5 m, WP emissivity = 0.8, and ambient percolation flux = 0.3 mm/yr.

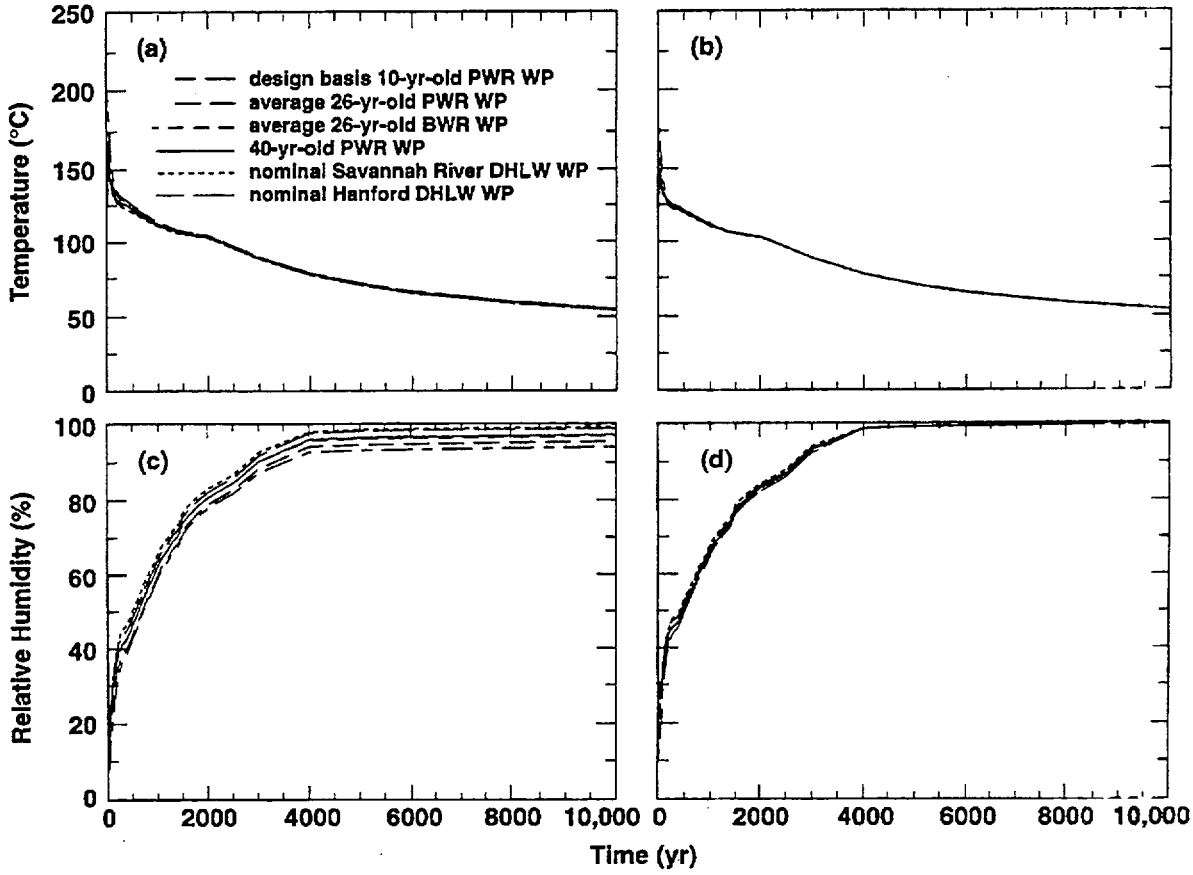

Figure 1.10.5.1.12. Temperature and relative humidity on upper WP surface (a,c) and in rock at upper drift wall (b,d) at various WP locations for AML = 83.4 MTU/acre, a line-load design with a 1.0-m gap between WPs, LML = 0.94 MTU/m, sand invert, no overfill, drift diameter = 5.5 m, WP emissivity = 0.8, and ambient percolation flux = 0.3 mm/yr.

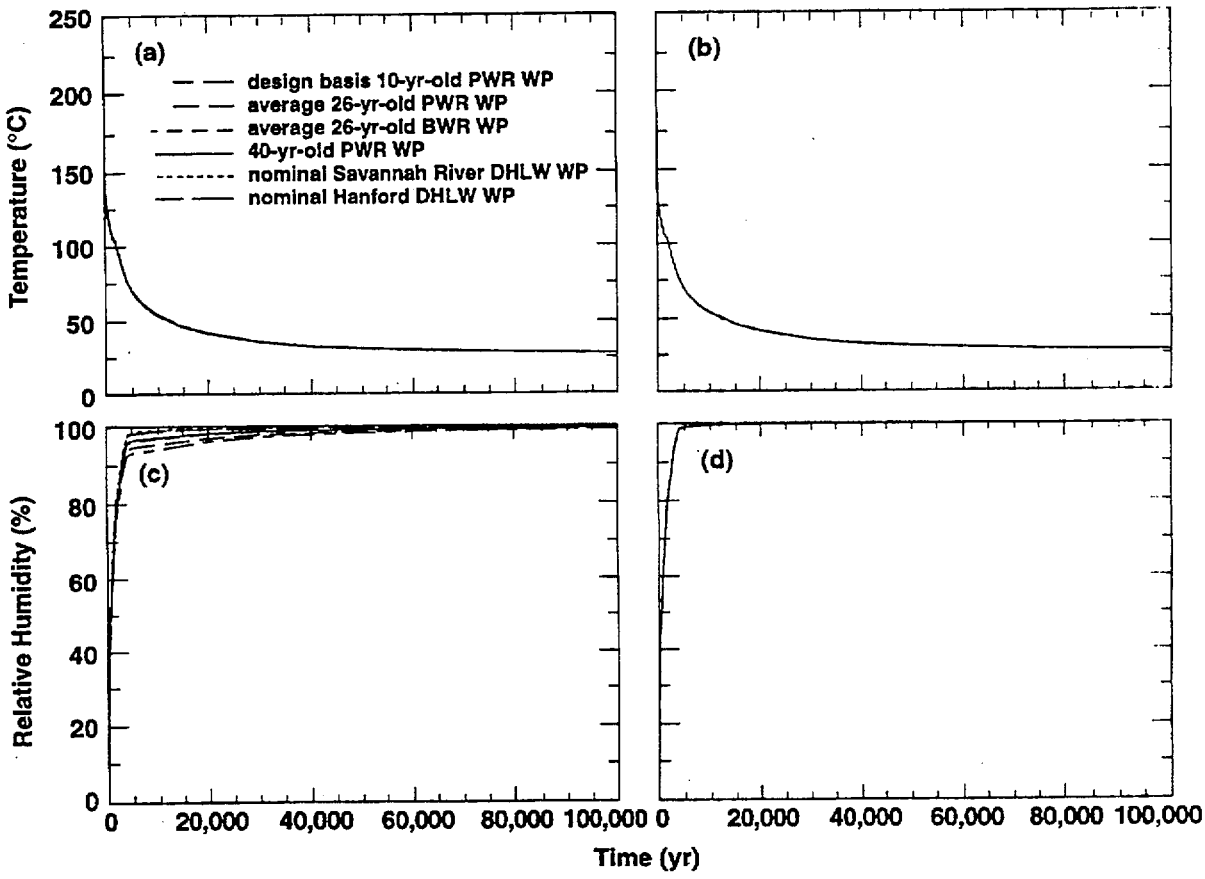

Figure 1.10.5.1.13. Temperature and relative humidity on upper WP surface (a,c) and in rock at upper drift wall (b,d) at various WP locations for AML = 83.4 MTU/acre, a line-load design with a 1.0-m gap between WPs, LML = 0.94 MTU/m, sand invert, no overfill, drift diameter = 5.5 m, WP emissivity = 0.8, and ambient percolation flux = 0.3 mm/yr.

1.10.5.2 Influence of Engineered Backfill

The cases analyzed in this section utilize the same assumptions analyzed in Section 1.10.5.1, with the exception of being backfilled at 100 yr with a full sand "backfill," which is to say that the drifts are fully filled with the backfill (or overfill). The hydrological properties of the backfill are representative of a fine to medium sand. However, other backfill materials, such as crushed tuff or basalt gravel, may be found to exhibit similar hydrological properties. The important hydrological feature of sand or "sand-like" backfill that was assumed in these calculations is that it does not wick moisture in from the near-field rock unless the matric potential of the adjacent rock is nearly zero (nearly saturated conditions). This arises largely from the sand having zero intragranular porosity (i.e., the sand grains are essentially nonporous). It is assumed that when the backfill is emplaced, its moisture content (matric potential and *RH*) will be drier than ambient pre-emplacement conditions at the repository horizon. Moreover, as was shown in Section 1.10.5.1 for the line-load, conditions in the drift will be extremely dry when backfill is emplaced at 100 yr. Therefore, for some time after the emplacement of backfill, the backfill will be subjected to *RH* conditions that are much drier than ambient pre-emplacement conditions at the repository horizon. Moreover, after backfill is emplaced, the temperature in the backfill will abruptly rise to well above the nominal boiling point. Altogether, these effects tend to cause the backfill *RH* to be much drier than ambient pre-emplacement conditions.

The most critical consideration for engineered backfill concerns the magnitude and duration of the *RH* reduction on the WP, relative to RH conditions in the adjacent near-field rock. The reduction in *RH* is affected by three key factors:

Drift-ΔRH effect: This effect is based on the relationship: $RH_{wp}/RH_{dw} = P_{sat}(T_{dw})/P_{sat}(T_{wp})$, which holds if the partial pressure of water vapor P_v on the WP is in equilibrium with P_v in the rock at the drift wall (see Section 1.8.3.1). Therefore, this effect is governed by the magnitude and duration of the temperature difference ΔT_{drift} between the WP and (cooler) drift wall (see Section 1.10.3). To the extent that P_v on the WP is greater than P_v at the drift wall, *RH* reduction on the WP is negated. If the drift is not backfilled, thermal-radiative heat transfer will dominate ΔT_{drift}; if backfill is used, thermal conduction in the backfill will dominate ΔT_{drift}. In both cases, it is important to determine whether the gas-phase buoyant convection contributes signficantly to heat transfer between the WP and drift wall.

Net moisture flux into the drift: This is the net result of mechanisms that cause water to enter the drift (drift seepage and wicking) and mechanisms that cause water to leave the drift (drainage and evaporation). If the net flux of moisture into the drift is high enough, P_v on the WP will be higher than P_v in the rock at the drift wall, thereby negating some (or possibly all) of the drift-ΔRH effect. Net moisture flux will be influenced by the hydrological properties of the backfill/invert system.

Axial vapor flow and condensation within the drift: This effect (called the "cold-trap effect" in Section 1.10.5.1) is driven by axial variations in temperature *T* and P_v along the drift. Water vapor is transported (by gas-phase advection and diffusion) from areas of higher *T* and P_v to areas of lower *T* and P_v where it condenses, which causes *RH* to increase (even as high as 100%). Because there is so little resistance to vapor flow along the drift, large vapor fluxes can occur along the drift and large condensation rates can arise in the cooler areas if the following three conditions are met: (1) high *RH* in the rock at the drift wall, (2) WP heat output varies substantially from WP to WP, and (3) WPs are thermally isolated from one another. This effect will be influenced by whether backfill is allowed to fill in between the WPs, thereby causing greater thermal isolation between WPs.

The following are the two primary mechanisms that cause water to enter the drift:

Drift seepage: Advective liquid-phase flow of water that enters the drift (and flows through the backfill) as a result of ambient percolation or decay-heat driven condensate flow. This can include episodic nonequilibrium fracture flow or a steady weep. This process is not significantly affected by the presence (or absence) of backfill.

Wicking: This effect requires the presence of a porous material (i.e., backfill and/or a porous invert) in the drift. Wicking involves the transport of moisture, driven by matric potential gradients (i.e., capillary pressure gradients) from high to low matric potential. Because the host rock is generally wetter than the backfill and/or porous invert, it has a higher matric potential than the backfill/invert. This is primarily considered to be an advective liquid-phase transport process (called imbibition); however, binary gas-phase diffusion can also play a role. Because wicking can occur as two-phase flow, it does not necessarily require a continuous liquid phase.

The following are the two primary mechanisms that cause water to leave the drift:

Drainage: Advective liquid-phase flow of water that leaves the drift. Net drainage will be affected by (a) the rate at which water enters the drift (e.g., episodically versus a steady weep), (b) the capillary properties of the intragranular and intergranular porosity of the backfill (in particular, how strongly capillary forces tend to retain moisture), and (c) whether fractures at the bottom of the drift readily drain or cause water to pond.

Evaporation: Heat flow through the backfill will be capable of maintaining an evaporation rate (or evaporative capacity). This evaporative capacity depends on the WP heat generation rate, which will decay with time. The water vapor generated by this evaporation will be transported out of the drift by gas-phase advection, driven by gas-phase pressure gradients, and by the gas-phase diffusion of water vapor and air, possibly including enhanced diffusion. While the backfill is above the boiling point, gas-phase advection will be an important means of transporting vapor out of the drift. After the backfill has dropped below the boiling point, gas-phase diffusion may be the primary means of transporting vapor out of the drift.

If the combined effects of the evaporative capacity and drainage exceed the combined effects of drift seepage and wicking, then the backfill will be maintained in a state in which P_V in the backfill (and on the WP surface) tends to be in equilibrium with P_V in the near-field rock adjacent to the drift. If drift seepage occurs episodically, the net moisture gain in the backfill will be minimized if the backfill and the fractures at the base of the drift (i.e., base of the invert) facilitate rapid drainage.

If the backfill has intragranular porosity, wicking can occur as a result of the matric potential gradients that occur within the porous grains. Minimal asperity contact area between grains does not prevent wicking, because it can occur as a two-phase flow process, involving vapor transport in the air between grains and liquid flow within grains. These grains do not need to be in solid-phase contact with one another for this process to occur because water can evaporate from the wetter grain, be transported by vapor diffusion through the air gap between the grains from the wetter to the drier grain, and then condense on the drier grain.

If the backfill has no intragranular porosity, then wicking is limited to film flow along the surfaces of the grains. If the intragranular porosity is effectively zero and the intergranular porosity is sufficiently coarse, then water retention in the backfill will be limited to the asperity contacts. Unless *RH* in the backfill is high enough to cause continuous surface films of water to exist on the surfaces of the grains, then the liquid phase will be discontinuous, limited to the pendular water at the asperities. The discontinuous liquid phase will be incapable of supporting a wicking flux from the relatively wetter near-field rock, through the relatively drier backfill, and onto to the WPs. As seen in the experimental testing of backfill [Conca, 1996], the relative permeability for this discontinuous saturation condition can be extremely low. It should also be pointed out that hysteresis effects in the capillary pressure and relative permeability characteristics of the backfill will make it easier for water to drain from the backfill than for water to wick back (i.e., rewet) from the wetter near-field

rock, through the backfill, and onto the WP. Because of hysteresis effects, it is important that data obtained under drainage conditions not be applied to rewetting behavior of the backfill. The combination of (1) minimized water retention in the drift, (2) rapid drainage of episodic fracture flow, and (3) extremely low relative permeability of the backfill all tend to favor having P_v on the WP being in equilibrium with P_v in the adjacent near-field rock.

In Section 1.10.4 it was found for either high percolation flux and/or for low AMLs that wicking in a PTn tuff gravel backfill eventually obviates much of the drift-ΔRH effect (Figs. 1.10.4.5c, 1.10.4.5d, 1.10.4.6c, and 1.10.4.6d). Calculations for a TSw2 gravel backfill had an even greater tendency to wick than the PTn gravel backfill. The sand backfill did not wick enough moisture to have any effect on the drift-ΔRH effect for any of the AMLs and percolation fluxes considered in Section 1.10.4 (Figs. 1.10.4.5a,b and Figs. 1.10.4.6a,b).

The four backfill cases analyzed in this section assume center-in-drift (CID) WP configuration and a "full backfill" backfill configuration, using a sand backfill with a thermal conductivity K_{th} of 0.6 W/m^{o}C. In Section 1.10.5.4, a comparison is made between CID WP emplacement and off-center-in-drift (OCID) WP configuration. Three different backfill configurations, including full backfill, level-partial backfill, and sloping-partial backfill are also compared in Section 1.10.5.4. The influence of backfill K_{th} is addressed in Section 1.10.5.5. Because the drift-scale model effectively assumes an infinite repository area, it does not directly address the influence of the edge-cooling/rewetting effects. The hybrid drift-scale–mountain-scale model (described in Section 1.10.6) addresses these effects.

For all but one of the line-load cases considered in this report, it is assumed that measures are taken to prevent backfill from filling in between the gaps separating the WPs. Such measures might involve the use of a "skirt" or an overhang at one of the ends of the WPs and/or the use of a drip shield, which, in addition to preventing backfill from filling in between WPs, would also prevent backfill from settling on the WP itself. For all of the ACD rev 00 cases analyzed in this report and for one of the 1.11-MTU/m line-load cases analyzed in this section, it is assumed that backfill is allowed to fill in the gap separating WPs. As discussed below, the presence of low-K_{th} backfill between the WPs causes the WPs to be thermally isolated from one another. This is particularly true for the large axial gaps between WPs in the ACD rev 00 design.

Figure 1.10.5.2.1 shows the temperature distributions at 101 and 500 yr for the ACD rev 00 design and the 1.11-MTU/m line-load design. Temperatures below 112^{o}C are made transparent to help illustrate the relatively hot regions in the near field rock and emplacement drifts. For an ambient percolation flux of 0.3 mm/yr, rock temperatures above 105^{o}C were found to correspond to a reduction in RH (Figure 1.8-4). Therefore the opaque regions in Figure 1.10.5.2.1 can be considered to be zones of superheated conditions, in which temperatures are sufficiently above the nominal boiling point (96^{o}C) to cause moisture conditions to be drier than ambient. In general, condensate drainage will occur around the opaque zones in Fig. 1.10.5.2.1. For the line-load design (Figs. 1.10.5.2.1b,d), condensate shedding occurs in a cylindrical fashion, with condensate flux at the repository horizon only occurring in the rock pillars.

The large axial WP spacing in the ACD rev 00 design thermally isolates the WPs from one another, causing the heat flux at the drift wall to vary substantially along the drift axis. As will be discussed further, this results in substantial variations in WP and rock temperatures and RH along the axis of the drift. This also causes rock dryout and condensate shedding to occur in a spherical fashion (Figs. 1.10.5.2.1a,c), with condensate flux at the repository horizon occurring within the drifts as well as in the rock pillars separating the drifts. Accordingly, condensate seepage into the drift occurs above the relatively cooler DHLW WPs in the ACD rev 00 design (Fig. 1.10.5.1.2a). For the Hanford Site DHLW WP, the liquid-phase drift seepage flux is 65.4 , 16.1, 7.5, and 5.0 mm/yr at 10, 100, 200, and 300 yr, respectively. Note that these liquid-phase fluxes are much greater than the ambient percolation flux of 0.3 mm/yr assumed in this calculation. With the exception of very early time for the 40-yr-old PWR WP in the ACD rev 00 design, the drift seepage flux above the SNF WPs is always zero. For the 1.11-MTU/m line-load, the drift seepage flux is always zero for all WPs, including the DHLW WPs. It is important to point out that the model assumes that ambient percolation flux is both uniform and steady-state. Therefore, the model does not represent the possibility of either episodic nonequilibrium

fracture flow or heterogeneous steady-state fracture flow; further work is required to address such possibilities.

Figure 1.10.5.2.2 illustrates the relationship between the temperature difference between the WP and drift wall (ΔT_{drift}) and the *RH* difference between the drift wall and WP (ΔRH_{drift}). If no backfill is used, thermal radiation dominates heat transfer from the WP to the drift wall; because thermal radiation is fairly efficient (as compared to conduction in the rock or backfill), ΔT_{drift} is relatively small, resulting in a relatively small ΔRH_{drift}. Heat flow in the backfill will be dominated by conduction unless the bulk permeability k_b of the backfill is large enough to allow buoyant gas-phase convection to substantially contribute to heat flow. For the 10-yr-old WP and a backfill thermal conductivity K_{th} of 0.6 W/m°C, ΔT_{drift} is 129°C at the time backfill is emplaced (t = 100 yr), resulting in a large ΔRH_{drift} (Fig. 1.10.5.2.2a,b). For K_{th} = 0.3 W/m°C, ΔT_{drift} = 227°C at the time of backfill, resulting in an even larger (and more persistent) ΔRH_{drift}.

For a given heat-of-decay heat generation curve, there is a linear relationship between ΔT_{drift} at any given time and the ΔT_{drift} at the time of backfill. It is likely that there will be a maximum allowable WP temperature, perhaps constrained by the maximum allowable zircoloy cladding temperature. Given a maximum allowable WP temperature and the rock temperature that is calculated to occur at the time of backfill, this will determine a maximum allowable ΔT_{drift} at the time of backfill. Based on the relevant heat-of-decay curve and the maximum allowable WP temperature, it is then possible to estimate the maximum theoretical RH_{wp}/RH_{dw} that can be achieved at any given time (recall that RH_{wp}/RH_{dw} was shown in Sections 1.10.3 and 1.10.4 to best quantify the drift-ΔRH effect). There is a trade-off between maximizing the benefits of *RH* reduction and adhering to system constraints on the peak allowable WP temperature. The relationship between ΔT_{drift} at time of backfill and RH_{wp}/RH_{dw} implies an optimization process, which can be applied to maximizing the *RH*-reduction benefits of backfill. For example, the use of a lower AML will reduce the drift-wall temperature at the time of backfill, thereby increasing the maximum allowable ΔT_{drift}. Illustrations of how this optimization process may be applied are described in Section 1.10.5.7.

Figures 1.10.5.2.3 and 1.10.5.2.4 (and the first two cases of Table 1.10.5.2.1) describe temperature and *RH* conditions in the rock at the upper drift wall at various WP locations along the drift for the ACD rev 00 design and the 1.11-MTU/m line-load design. A comparison with the "no-backfill" cases (Figs. 1.10.5.1.2 and 1.10.5.1.3 and Table 1.10.5.1.1) shows that backfill effectively insulates the rock above the drift from decay heat for a number of years following its emplacement, causing the drift-wall temperature to be slightly cooler than in the no-backfill cases. Effectively, the addition of backfill creates a low-K_{th} "thermal blanket" lying above and to the sides of the WP, which causes a moderately larger fraction of the WP heat flux to be directed downward towards the invert, relative to the no-backfill case. Note that for the no-backfill case, a low-K_{th} invert effectively creates a thermal blanket beneath the WP, which focuses more of the overall WP heat flux (upward) towards the drift-wall surfaces, relative to the case where a WP is sitting directly on the host rock or on an invert with a K_{th} similar to that of the rock.

The hiatus in heating the rock after backfill is emplaced and the refocusing (downward) of WP heat flux cause a small decrease in ΔRH_{rock} at the upper drift wall. The much higher (and more uniform) heat flux conditions along the 1.11-MTU/m line-load design result in much more locally intensive (and more uniform) rock dryout along the drift than in the ACD rev 00 design. After backfill is emplaced, the 1.11-MTU/m line-load case results in even more homogeneous rock dryout along the drift than in the no-backfill line-load case. This more uniform rock dryout behavior is the result of two effects that arise from the use of backfill:

Focused axial heat flow: Because heat conduction in the low-K_{th} backfill results in a much higher impedance to radial heat flow (than results from thermal radiation in the no-backfill case), heat flow is more likely to flow axially along the line of WPs, in effect, seeking the "path of least resistance" to heat flow. Backfill acts like a cylindrical "blanket" that literally forces heat to flow axially to where (because of relatively cooler conditions) it experiences less impedance to radial heat flow.

Enhanced axial thermal-radiative heat flow: Because the low-K_{th} backfill substantially raises the WP temperatures, it substantially improves the efficiency of thermal-radiative WP-to-WP heat transfer. Thermal radiation is driven by the T^4 difference, where T is the absolute temperature (^{o}K). Higher absolute temperatures result in more efficient thermal radiation. This effect will also be seen in Section 1.10.6, where it is found that higher AMLs (resulting in higher WP temperatures) are associated with better thermal homogenization along the drifts. Therefore, one of the benefits of backfill is to facilitate even more effective thermal homogenization along the drifts in the line-load design.

Figures 1.10.5.2.5 through 1.10.5.2.7 (and the first two cases of Table 1.10.5.2.2) describe temperature and *RH* on WPs for the ACD rev 00 design and the 1.11-MTU/m line-load design. Tables 1.10.5.2.3 and 1.10.5.2.4 summarize temperature and *RH* on WPs for all of the WPs considered in the model. For the ACD rev 00 design, the effect of low-K_{th} is to further exaggerate the axial variability of temperature and *RH* along the drift and on WPs. The range in WP temperatures at the time that backfill is emplaced is 236^{o}C for the ACD rev 00 design, while it is only 26^{o}C for the 1.11-MTU/m line-load design (Table 1.10.5.2.2), which is nearly a factor of 10 difference in axial variability between the two designs. Accordingly, the range in RH_{WP} is 56% for the ACD rev 00 design, while it is only 1% for the 1.11-MTU/m line-load design. At 2000 yr, the range in RH_{WP} is 55% for the ACD rev 00 design, while it is only 2% for the 1.11-MTU/m line-load design. At 10,000 yr, the range in RH_{WP} is 40% for the ACD rev 00 design, while it is only 4% for the 1.11-MTU/m line-load design. For the line-load design, the WP-to-WP variability in RH_{WP} grows slowly with time, because the declining WP temperatures result in somewhat less efficient thermal-radiative WP-to-WP heat transfer, which modestly reduces the effectiveness of thermal homogenization along the line of WPs.

The last two rows of Tables 1.10.5.2.2–1.10.5.2.6 list the time required to rewet to *RH* = 65% and 90%; these RH thresholds are listed because corrosion studies of the candidate WP materials indicate that the critical *RH* for atmospheric corrosion is 65% if an evaporitic salt is present on the WP or 90% if the WP surface is free of salt [Gdowski, 1996]. For the ACD rev 00 design, the Hanford Site and Savannah River Site DHLW WPs are never below the *RH* = 65% threshold prior to the time that backfill is emplaced at 100 yr (Table 1.10.5.2.3). The abrupt increase in WP temperatures after backfill is emplaced causes an abrupt decrease in *RH* on all WPs (including the DHLW WPs). Because the DHLW WPs generate very little heat and because WPs in the ACD rev 00 design are thermally isolated from one another, *RH* on both of the DHLW WPs falls below 65% for only a brief period; the Hanford Site and Savannah River Site DHLW WPs take only 160 and 210 yr to rewet to the *RH* = 65% threshold, respectively, and only 950 and 860 yr to reach the *RH* = 90% threshold.

For the 1.11-MTU/m line-load design (Table 1.10.5.2.4), highly efficient WP-to-WP heat transfer allows the DHLW WPs to share virtually the same temperature behavior as the spent nuclear fuel (SNF) WPs. Consequently, the Hanford Site and Savannah River Site DHLW WPs take 3930 and 3730 yr to reach the *RH* = 65% threshold, respectively, while taking 33,320 and 30,480 yr to reach the *RH* = 90% threshold (Table 1.10.5.2.4), which is very similar to the time it takes for the SNF WPs to reach these *RH* thresholds. The 26-yr-old BWR, 40-yr-old PWR, 26-yr-old PWR, and 10-yr-old PWR WPs take 3960, 4250, 4580, and 4600 yr, respectively, to reach the *RH* = 65% threshold, while taking 34,890, 36,800, 39,920, and 39,820 yr to reach the *RH* = 90% threshold (Table 1.10.5.2.4). For the ACD rev 00 design, the 26-yr-old BWR, 40-yr-old PWR, 26-yr-old PWR, and 10-yr-old PWR WPs take 2250, 1590, 9480, and 13,660 yr, respectively, to reach the *RH* = 65% threshold, while taking 35,690, 25,870, 54,690, and 62,680 yr to reach the *RH* = 90% threshold (Table 1.10.5.2.3). For the 1.11-MTU/m line-load design, the temporal variability in the time it takes to reach the *RH* = 65% and 90% thresholds is 23% and 31%, respectively (when all WPs are considered), while the temporal variability is only 16% and 14% (when only the SNF WPs are considered). For the ACD rev 00 design, the temporal variability for reaching the *RH* = 65% and 90% thresholds is a factor of 85 and 73, respectively (when all WPs are considered), while the temporal variability is a factor of 8.6 and 2.4 (when only the SNF WPs are considered).

In order to benefit from the drift-ΔRH effect, a WP must be capable of driving heat flow from its skin, radially out into the drift (or backfill). This heat must be generated directly by the WP itself or

heat that can be delivered to that WP (by virtue of axial WP-to-WP heat flow) from other (hotter) WPs in the drift. Integrated over time, the SNF WPs (in these calculations, assumed to be 70% of the total number of WPs) generate nearly 100% of the total decay heat. The DHLW WPs cannot, by themselves, generate a ΔT_{drift} between their skin and the adjacent drift wall. Therefore, thermal isolation of the WPs in the ACD rev 00 design effectively prevents the DHLW WPs from sharing in the benefits of *RH* reduction; instead, it allows the SNF WPs to benefit from essentially 100% of the aggregate drift-ΔRH effect. This is contrasted with the line-load design, which, because of its high axial heat conductance, allows the decay heat to be shared (almost equally) by all of the WPs; consequently, the WPs in the line-load design (SNF and DHLW alike) benefit (almost equally) from the drift-ΔRH effect. This causes WPs in the line-load design to generate, on average, 30% less radial heat flux than the average SNF WP in the ACD rev 00 design.

At late time, when *RH* reduction is dominated by the drift-ΔRH effect (rather than rock dryout), this fundamental difference in how decay heat is shared causes the average to hotter-than-average SNF WPs in the ACD rev 00 to be somewhat hotter (and drier) than the average to hotter-than-average SNF WP in the line-load design. This is illustrated by comparing the 26-yr-old PWR WPs (considered to be an "average-heat-output" WP) for these two designs (compare Tables 1.10.5.2.3. and 1.10.5.2.4). The time to reach the *RH* = 65% and 90% is longer for the line-load design. On the other hand, a colder-than-average WP (e.g., the 40-yr-old PWR WP) in the line-load design is hotter and drier than in the ACD rev 00 design. At early time when rock dryout (ΔRH_{rock}) plays a significant role in *RH* reduction, a larger percentage of the line-load SNF WPs tends to be drier than the ACD rev 00 SNF WPs, because of the more effective rock dryout associated with the line-load design.

It should be noted that the drier *RH* associated with the hottest WPs in the ACD rev 00 design comes at the expense of much higher peak temperatures than in the line-load design (e.g., 353°C versus 266°C for the 10-yr-old PWR WP). The higher WP temperatures might generate some off-setting effects that are detrimental to total systems performance. It is important that the peak allowable skin temperatures on the WPs be established on the basis of total systems performance assessment rather than some rigid criteria. For the situation where there is a high degree of variability in peak WP temperature, the peak temperature constraint will cause many of the (much cooler) WPs to benefit from only a small fraction of the maximum theoretical drift-ΔRH effect. For the line-load design, the small degree of variability in peak WP temperature allows even the coolest WP to benefit from a large fraction of the maximum theoretical drift-ΔRH effect (as constrained by the peak allowable WP temperature).

So far, it has been shown that axial homogenization of temperature and *RH* along the drift is quite effective if the WPs are axially spaced very close together (0.1-m gaps) and if backfill is not allowed to fill the gaps between the WPs. It is important to establish how dependent effective axial homogenization is on the 0.1-m gaps being free of low-K_{th} backfill. Figures 1.10.5.2.8 through 1.10.5.2.10 and Table 1.10.5.2.5 summarize the temperature and *RH* on the upper drift wall and upper WP surface for a 1.11-MTU/m line-load design in which the 0.1-m gaps between the WPs are filled with 0.6 W/m°C backfill at 100 yr.

At the time that backfill is emplaced at 100 yr, the range in peak WP temperature is only 16°C if the 0.1-m gaps between the WPs are free of backfill, whereas backfilling these gaps causes the post-emplacement peak WP temperature range to increase to 83°C (Table 1.10.5.2). Note that this is still much less than the 236°C peak WP temperature range for the ACD rev 00 design. Although the range in WP temperature and *RH* increases somewhat when the 0.1-m gaps are backfilled, temperature and *RH* conditions in the rock along the drift wall continue to be very uniform (Figs. 1.10.5.2.8–1.10.5.2.10). Rock dryout is just as locally intensive (and effective) as it was for the case with no backfill between WPs. The variability in the time it takes to reach the *RH* = 65% and 90% thresholds becomes greater when backfill is allowed to fill the 0.1-m gaps. In effect, the hottest WPs share a little less of their decay heat with the coolest WPs. Consequently, the time to reach the *RH* = 65% threshold increases (from 4600 to 7130 yr) for the 10-yr-old PWR WP and decreases (from 3730 to 3110 yr) for the Savannah River Site DHLW WP (compare Tables 1.10.5.2.4 and 1.10.5.2.5). The time to reach the *RH* = 90% threshold

increases (from 39,920 to 46,460 yr) for the 26-yr-old PWR WP and decreases (from 30,480 to 26,330 yr) for the Savannah River DHLW WP.

So far, it has been shown that axial homogenization of temperature and *RH* along the drift is quite effective if the WPs are placed very close together (0.1-m gaps). It is important to establish how dependent effective axial homogenization is on axial WP spacing. In particalar, to establish whether effective axial homogenization requires very tight WP spacing or whether the axial spacing requirement could be relaxed somewhat (perhaps up to 1 meter) and still provide for an effective level of homogenization. Figures 1.10.5.2.11 through 1.10.5.2.13 and Table 1.10.5.2.6 summarize the temperature and *RH* on the upper drift wall and upper WP surface for a 0.94-MTU/m line-load design in which the 1.0-m gaps between the WPs are not filled with backfill at 100 yr.

At the time that backfill is emplaced at 100 yr, the range in peak WP temperature is only increased slightly (from 16 to 27°C) if the 1.0-m gaps between the WPs are used instead of 0.1 m (Table 1.10.5.2). Because of the lower LML (0.94 MTU/m), all post-emplacement peak WP temperatures are decreased (compare Tables 1.10.5.2.4 and 1.10.5.2.6). Although the range in WP temperature and *RH* increases slightly when the 1.0-m gaps are used, temperature and *RH* conditions in the rock along the drift wall continue to be very uniform (Figs. 1.10.5.2.11–1.10.5.2.13 and Table 1.10.5.2.1). Because of the lower LML, rock dryout is less locally intensive than it is for the 1.11-MTU/m cases, resulting in higher *RH* in the rock along the drift (41–43% versus 31% at 120 yr; and 84% versus 78% at 2000 yr). Because the overall line-load heat flux is 18% less intense per unit length of drift, the drift-ΔRH effect is also less. Consequently, it takes less time for the WPs in the 0.94-MTU/m case to reach the *RH* = 65% and 90% thresholds than in the 1.11-MTU/m cases.

The high effective axial heat conductance facilitated by close axial WP spacing results in the line-load effectively working as a heat flow "homogenizer" as well as a preferential heat flow "conduit." These two functions provide a number of very important benefits to the waste isolation system.

Heat flow homogenizer: This prevents large variations in WP heat output along the drift from imposing heterogeneous heat flux conditions at the drift wall, resulting in:

- Uniform rock dryout along the drift wall.
- Uniform rock temperatures at the drift wall.
- Uniform WP temperatures.

Preferential heat-flow conduit: This allows heat to be effectively delivered to otherwise vulnerable areas of the emplacement drifts, such as the following:

- Areas influenced by edge-cooling effects.
- Areas affected by high (or focused) liquid-phase flux.
- Areas of enhanced cooling as a result of the heat-pipe effect.

Waste isolation system impacts: From a total systems point of view, close axial WP spacing can result in the following benefits:

- A large reduction (up to 58%) in the required total length of emplacement drifts.
- Allows for backfilling the drifts with lower K_{th} material (than in the ACD rev 00 design) without exceeding WP thermal goals.
- A large reduction in the range of temperature and *RH* for which natural and engineered materials must be tested and for which performance analyses must be performed.
- The benefits of *RH* reduction are shared nearly equally by all WPs (including DHLW).
- Allows for low-AML options of using decay heat constructively.

These potential benefits are being evaluated by the total systems performance assessment [Andrews et al., 1996] and by various system studies [Balady et al., 1996; Saterlie et al., 1996].

Table 1.10.5.2.1. Temperature and relative humidity in rock at upper drift wall for AML = 83.4 MTU/acre, drift diameter = 5.5 m, sand invert, full sand backfill at 100 yr with K_{th} = 0.6 W/m°C, WP emissivity = 0.8, and percolation flux = 0.3 mm/yr.

Repository design	**ACD rev 00**	**Line load**	**Line load**	**Line load**
LML	0.46 MTU/m	1.11 MTU/m	1.11 MTU/m	0.94 MTU/m
Drift spacing	22.5 m	53.8 m	53.8 m	46.1 m
Gap between WPs	varies	0.1 m	0.1 m	1.0 m
Gap between WPs	backfilled at 100 yr	remains empty	backfilled at 100 yr	remains empty
T_{peak} (t < 100 yr)	100–165°C	161–184°C	161–184°C	139–173°C
RH (t < 100 yr)	36–98%	21–25%	21–25%	28–37%
T_{peak} (t > 100 yr)	100–123°C	135–137°C	135–137°C	125–128°C
RH (t = 120 yr)	45–99%	31–31%	31–31%	41–43%
RH (t = 2000 yr)	92–99%	78–78%	78–78%	84–84%
RH(t = 10,000 yr)	99.8–99.8%	99.1–99.1%	99.1–99.1%	99.5–99.5%

Table 1.10.5.2.2. Temperature and relative humidity on upper WP surface for AML = 83.4 MTU/acre, drift diameter = 5.5 m, sand invert, full sand backfill at 100 yr with K_{th} = 0.6 W/m°C, WP emissivity = 0.8, and percolation flux = 0.3 mm/yr.

Repository design	**ACD rev 00**	**Line load**	**Line load**	**Line load**
LML	0.46 MTU/m	1.11 MTU/m	1.11 MTU/m	0.94 MTU/m
Drift spacing	22.5 m	53.8 m	53.8 m	46.1 m
Gap between WPs	varies	0.1 m	0.1 m	1.0 m
Gap between WPs	backfilled at 100 yr	remains empty	backfilled at 100 yr	remains empty
T_{peak} (t < 100 yr)	107–192°C	172–203°C	172–203°C	149–197°C
RH (t < 100 yr)	25–86%	16–21%	16–21%	20–32%
T_{peak} (t > 100 yr)	117–353°C	250–266°C	231–314°C	194–221°C
RH (t = 120 yr)	1–57%	2–3%	1–4%	5–8%
RH (t = 2000 yr)	43–98%	49–51%	44–57%	59–66%
RH(t = 10,000 yr)	60–99.7%	73–77%	68–81%	78–86%
t(RH = 65%)	160*–13,330 yr	3730–4600 yr	3110–7130 yr	1990–2600 yr
t(RH = 90%)	860–62,680 yr	30,480–39,920 yr	26,330–46,460 yr	17,490–32,740 yr

Table 1.10.5.2.3. Temperature and relative humidity on upper WP surface for AML = 83.4 MTU/acre, the ACD rev 00 design with LML = 0.46 MTU/m, drift spacing = 22.5 m, sand invert, full sand backfill at 100 yr with K_{th} = 0.6 W/m°C, drift diameter = 5.5 m, WP emissivity = 0.8, and percolation flux = 0.3 mm/yr.

Waste package type	Hanford Site DHLW	Savannah River Site DHLW	40-yr-old PWR MPC	26-yr-old BWR MPC	26-yr-old PWR MPC	10-yr-old PWR MPC
T_{peak} (t < 100 yr)	106°C	121°C	112°C	127°C	145°C	192°C
RH_{max} (t < 100 yr)	86%	61%	65%	50%	42%	25%
T_{peak} (t > 100 yr)	117°C	136°C	172°C	222°C	272°C	353°C
RH (t = 120 yr)	57%	34%	13%	5%	2%	1%
RH (t = 2000 yr)	98%	97%	71%	62%	50%	43%
RH (t = 10,000 yr)	99.7%	99.2%	82%	76%	66%	60%
$t(RH = 65\%)$	160* yr	210* yr	1590 yr	2250 yr	9480 yr	13,660 yr
$t(RH = 90\%)$	950 yr	860 yr	25,870 yr	35,690 yr	54,680 yr	62,670 yr
* RH is never less than 65% prior to backfill						

Table 1.10.5.2.4. Temperature and relative humidity on upper WP surface for AML = 83.4 MTU/acre, a line-load design with a 0.1-m gap between WPs, LML = 1.11 MTU/m, drift spacing = 53.8 m,sand invert, full sand backfill at 100 yr with K_{th} = 0.6 W/m°C, drift diameter = 5.5 m, WP emissivity = 0.8, and percolation flux = 0.3 mm/yr.

Waste package type	Hanford Site DHLW	Savannah River Site DHLW	40-yr-old PWR MPC	26-yr-old BWR MPC	26-yr-old PWR MPC	10-yr-old PWR MPC
T_{peak} (t < 100 yr)	171°C	184°C	171°C	174°C	178°C	203°C
RH_{max} (t < 100 yr)	21%	21%	21%	21%	19%	16%
T_{peak} (t > 100 yr)	252°C	258°C	250°C	251°C	256°C	266°C
RH (t = 120 yr)	3%	3%	3%	3%	3%	2%
RH (t = 2000 yr)	51%	52%	50%	51%	49%	49%
RH (t = 10,000 yr)	76%	77%	74%	76%	73%	73%
t(RH = 65%)	3930 yr	3730 yr	4250 yr	3960 yr	4580 yr	4600 yr
t(RH = 90%)	33,320 yr	30,480 yr	36,800 yr	34,890 yr	39,920 yr	39,820 yr

Table 1.10.5.2.5. Temperature and relative humidity on upper WP surface for AML = 83.4 MTU/acre, a line-load design with a 0.1-m gap between WPs, LML = 1.11 MTU/m, drift spacing = 53.8 m,sand invert, full sand backfill at 100 yr with K_{th} = 0.6 W/m°C, drift diameter = 5.5 m, WP emissivity = 0.8, and percolation flux = 0.3 mm/yr. Backfill is allowed to fill the gap between WPs.

Waste package type	Hanford Site DHLW	Savannah River Site DHLW	40-yr-old PWR MPC	26-yr-old BWR MPC	26-yr-old PWR MPC	10-yr-old PWR MPC
T_{peak} (t < 100 yr)	171°C	184°C	171°C	174°C	178°C	203°C
RH_{max} (t < 100 yr)	21%	21%	21%	21%	19%	16%
T_{peak} (t > 100 yr)	231°C	239°C	239°C	248°C	271°C	314°C
RH (t = 120 yr)	4%	4%	3%	3%	2%	1%
RH (t = 2000 yr)	55%	57%	52%	51%	46%	44%
RH (t = 10,000 yr)	79%	81%	76%	76%	71%	68%
$t(RH$ = 65%)	3360 yr	3110 yr	3840 yr	3830 yr	5300 yr	7130 yr
$t(RH$ = 90%)	28,940 yr	26,330 yr	35,260 yr	34,770 yr	43,670 yr	46,460 yr

Table 1.10.5.2.6. Temperature and relative humidity on upper WP surface for AML = 83.4 MTU/acre, a line-load design with a 1.0-m gap between WPs, LML = 0.94 MTU/m, drift spacing = 46.1 m, sand invert, full sand backfill at 100 yr with K_{th} = 0.6 W/m°C, drift diameter = 5.5 m, WP emissivity = 0.8, and percolation flux = 0.3 mm/yr.

Waste package type	Hanford Site DHLW	Savannah River Site DHLW	40-yr-old PWR MPC	26-yr-old BWR MPC	26-yr-old PWR MPC	10-yr-old PWR MPC
T_{peak} (t < 100 yr)	151°C	165°C	149°C	156°C	162°C	197°C
RH_{max} (t < 100 yr)	32%	32%	30%	29%	26%	20%
T_{peak} (t > 100 yr)	194°C	205°C	206°C	203°C	213°C	221°C
RH (t = 120 yr)	8%	7%	6%	7%	5%	5%
RH (t = 2000 yr)	66%	65%	60%	62%	57%	59%
RH (t = 10,000 yr)	86%	85%	81%	82%	77%	78%
t(RH = 65%)	1990 yr	2000 yr	2440 yr	2310 yr	2740 yr	2600 yr
t(RH = 90%)	17,490 yr	19,100 yr	27,700 yr	26,180 yr	35,110 yr	32,740 yr

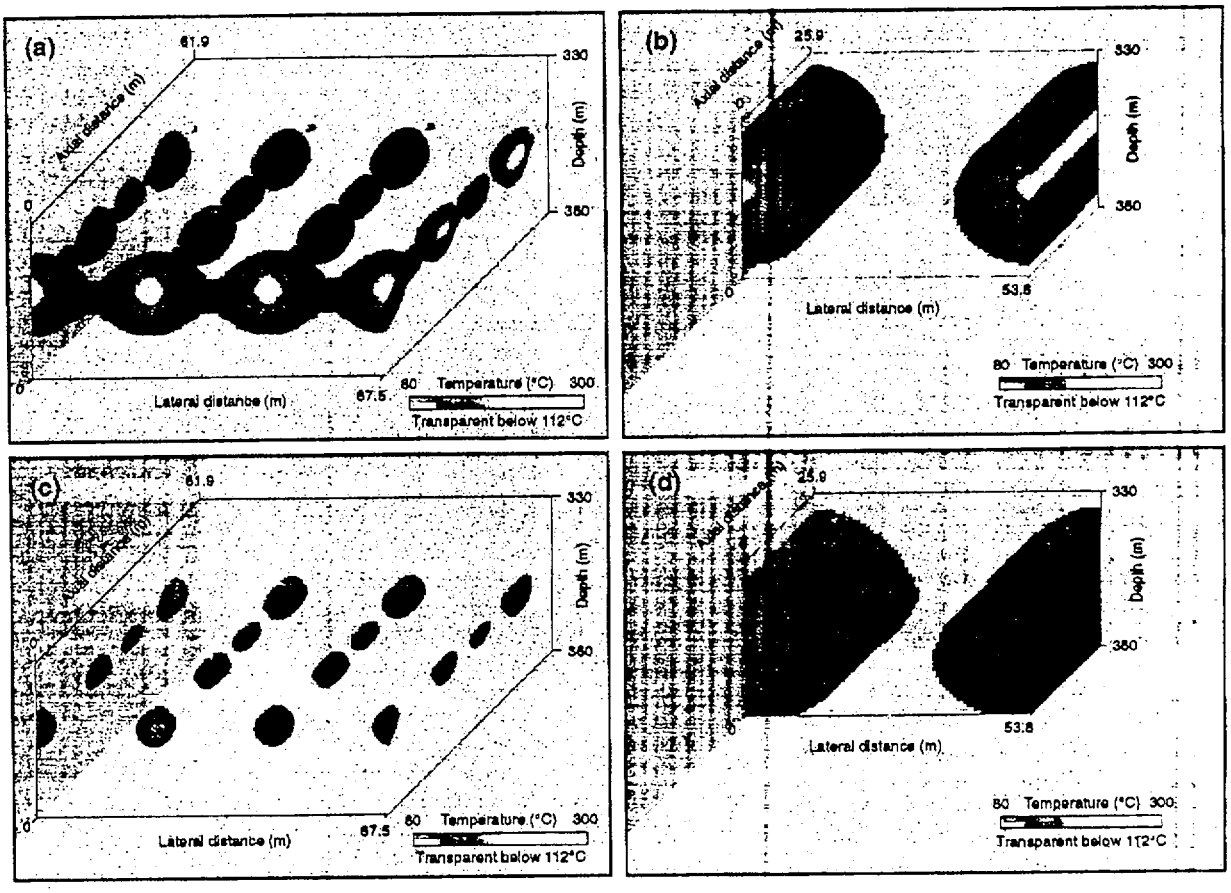

Figure 1.10.5.2.1. Temperature distribution for the ACD rev 00 design (a,c) with LML = 0.46 MTU/m and drift spacing = 22.5 m; and the line-load design (b,d) with 0.1-m gaps between WPs, LML = 1.11 MTU/m, and drift spacing = 53.8 m. For both cases, AML = 83.4 MTU/acre, sand invert, full sand backfill at 100 yr with K_{th} = 0.6 W/m°C, drift diameter = 5.5 m, WP emissivity = 0.8, and ambient percolation flux = 0.3 mm/yr. Temperature distributions are plotted at 101 yr (a,b) and 500 yr (c,d). Temperatures less than 112°C are transparent. Note that the emplacement drifts are parallel to the axial distance axis. For the ACD rev 00 design, the drift axes are located at lateral distances of 0, 22.5, 45, and 67.5 m. For the line-load design, the drift axes are located at lateral distances of 0 and 53.8 m.

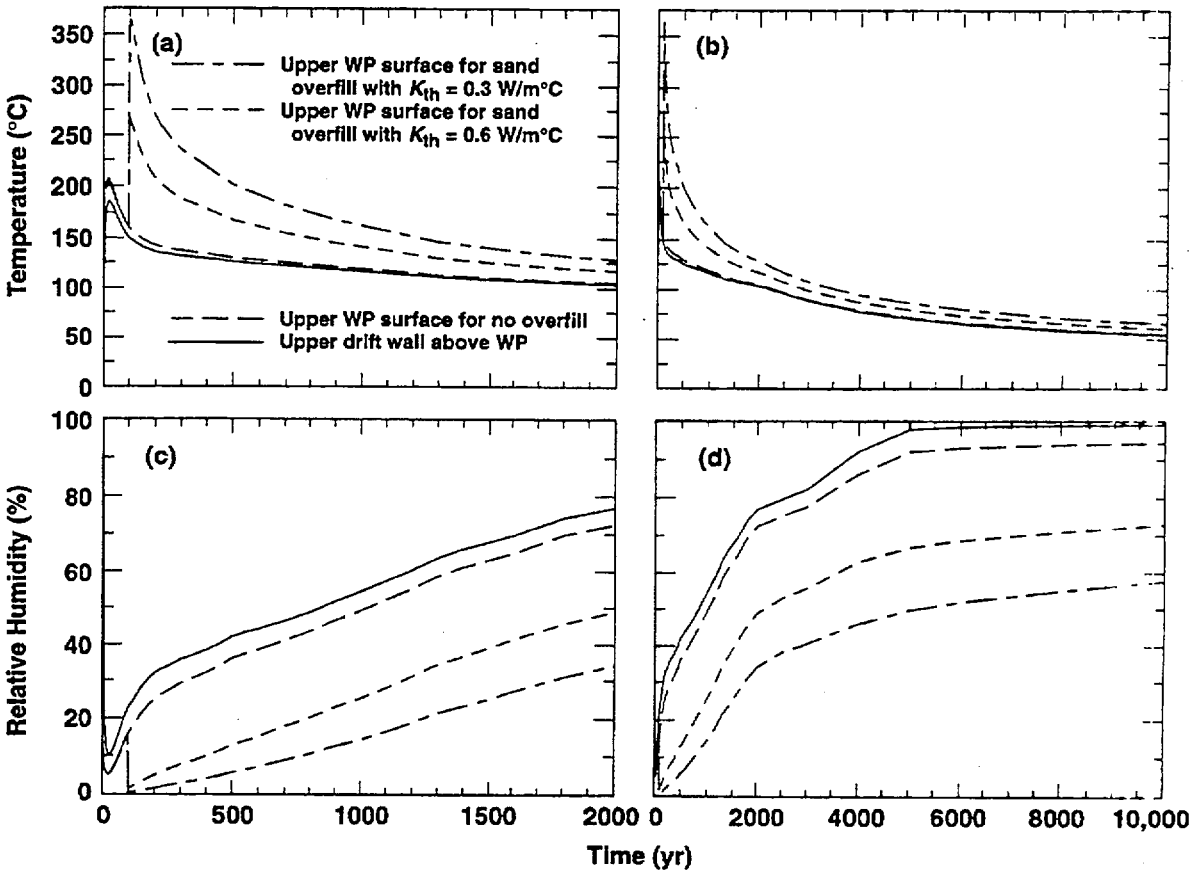

Figure 1.10.5.2.2. Temperature (a,b) and relative humidity (c,d) in the vicinity of a design basis 10-yr-old large PWR WP, AML = 83.4 MTU/acre, a line-load design with a 0.1-m gap between WPs, LML = 1.11 MTU/m, drift spacing = 53.8 m, sand invert, drift diameter = 5.5 m, WP emissivity = 0.8, and ambient percolation flux = 0.3 mm/yr. Curves are plotted for a case with no backfill and for two cases with sand overfill at 100 yr.

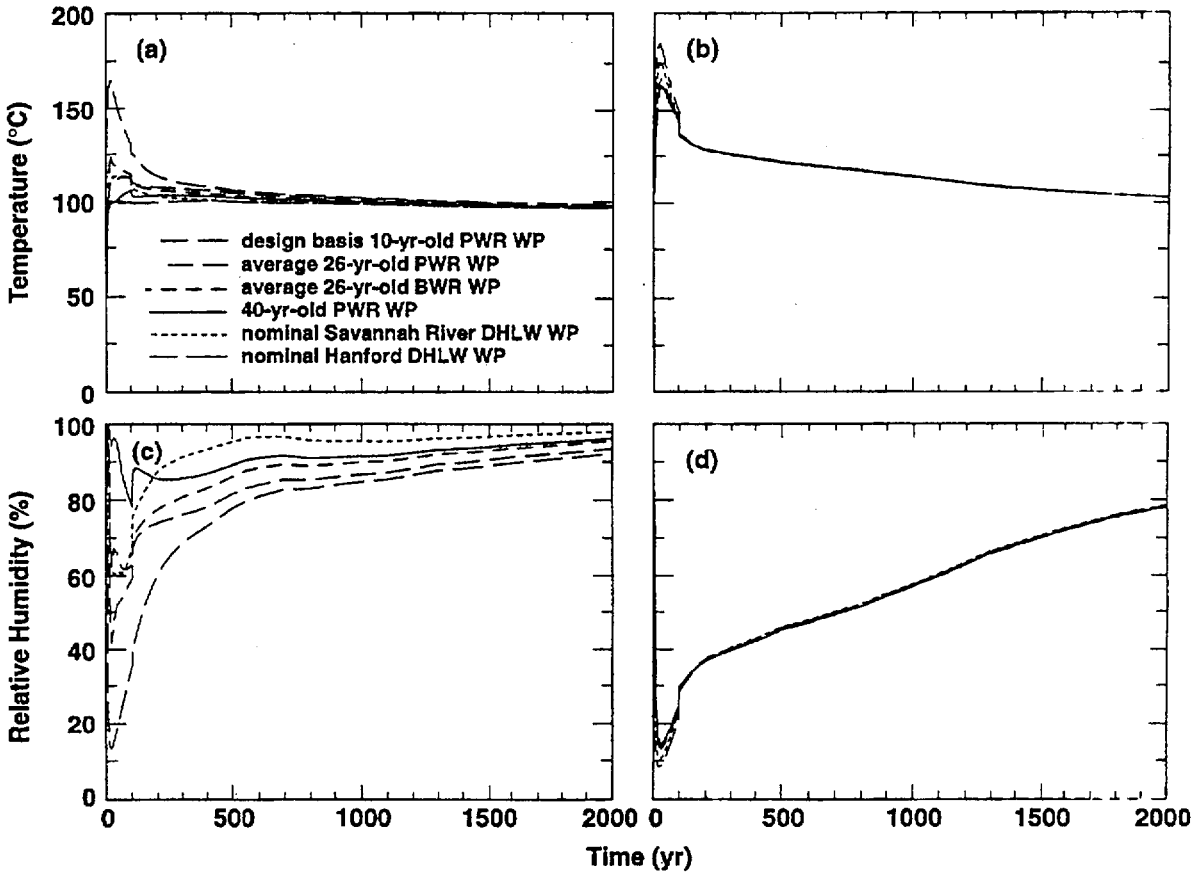

Figure 1.10.5.2.3. Temperature and relative humidity in rock at upper drift wall at various WP locations for AML = 83.4 MTU/acre, sand invert, full sand backfill at 100 yr with K_{th} = 0.6 W/m°C, drift diameter = 5.5 m, WP emissivity = 0.8, and ambient percolation flux = 0.3 mm/yr. Curves are plotted for the ACD rev 00 design (a,c) with LML = 0.46 MTU/m, and a line-load design (b,d) with a 0.1-m gap between WPs and LML = 1.11 MTU/m.

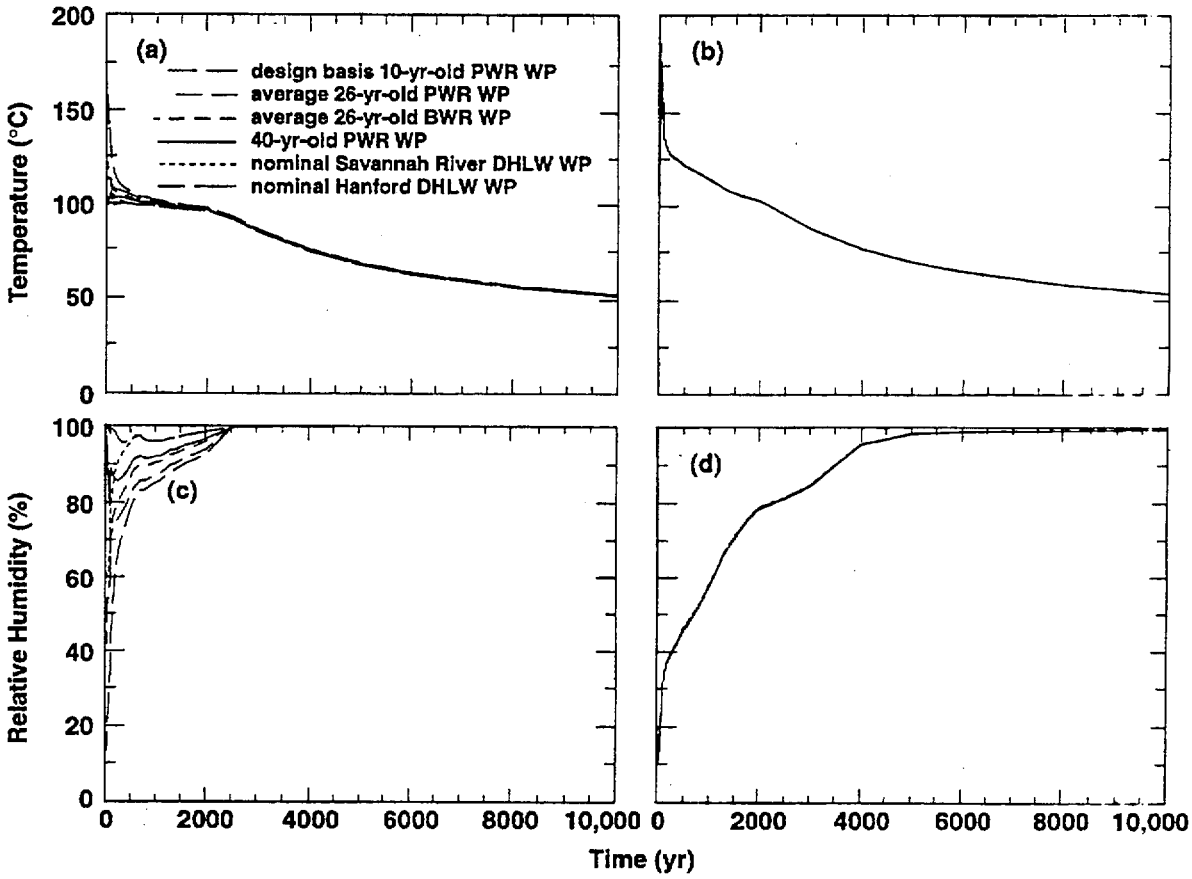

Figure 1.10.5.2.4. Temperature and relative humidity in rock at upper drift wall at various WP locations for AML = 83.4 MTU/acre, sand invert, full sand backfill at 100 yr with K_{th} = 0.6 W/m°C, drift diameter = 5.5 m, WP emissivity = 0.8, and ambient percolation flux = 0.3 mm/yr. Curves are plotted for the ACD rev 00 design (a,c) with LML = 0.46 MTU/m, and a line-load design (b,d) with a 0.1-m gap between WPs and LML = 1.11 MTU/m.

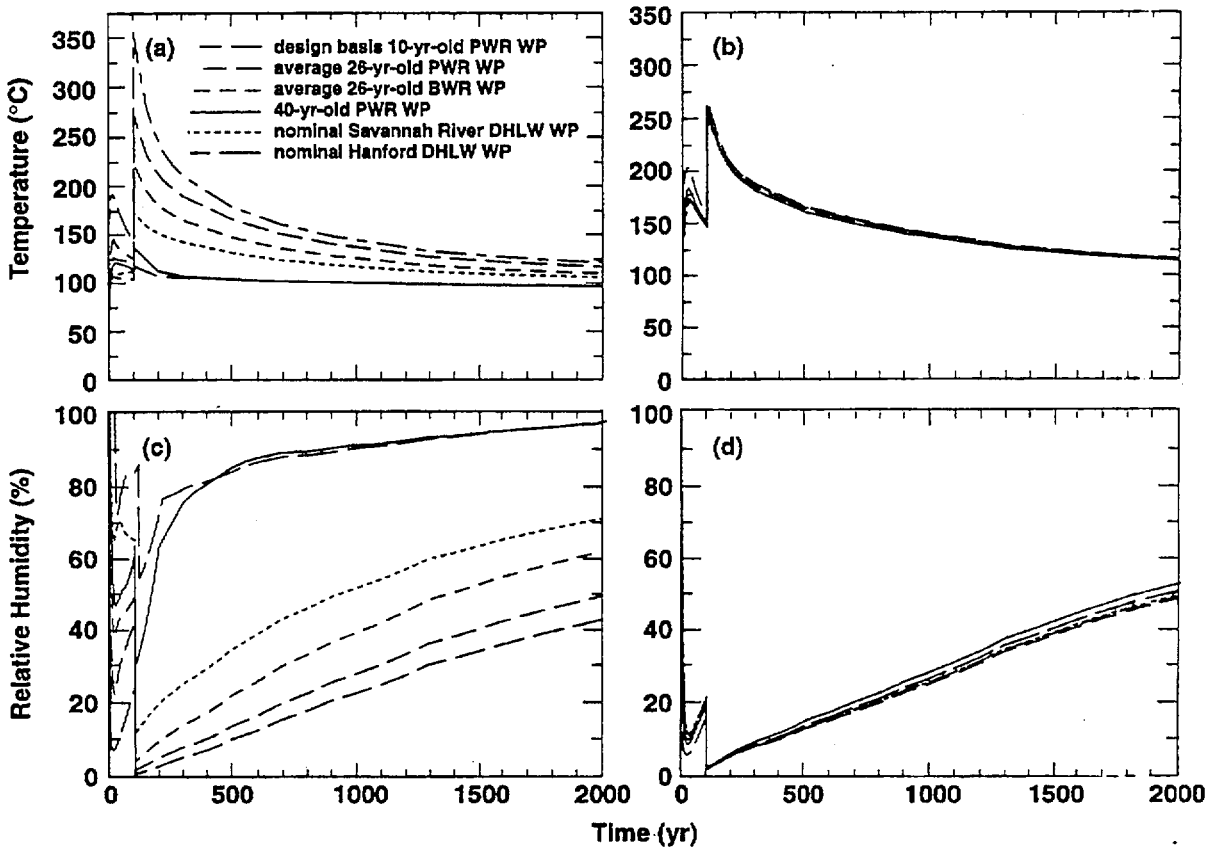

Figure 1.10.5.2.5. Temperature and relative humidity on upper surface of WP for AML = 83.4 MTU/acre, sand invert, full sand backfill at 100 yr with K_{th} = 0.6 W/m°C, drift diameter = 5.5 m, WP emissivity = 0.8, and ambient percolation flux = 0.3 mm/yr. Curves are plotted for the ACD rev 00 design (a,c) with LML = 0.46 MTU/m, and a line-load design (b,d) with a 0.1-m gap between WPs and LML = 1.11 MTU/m.

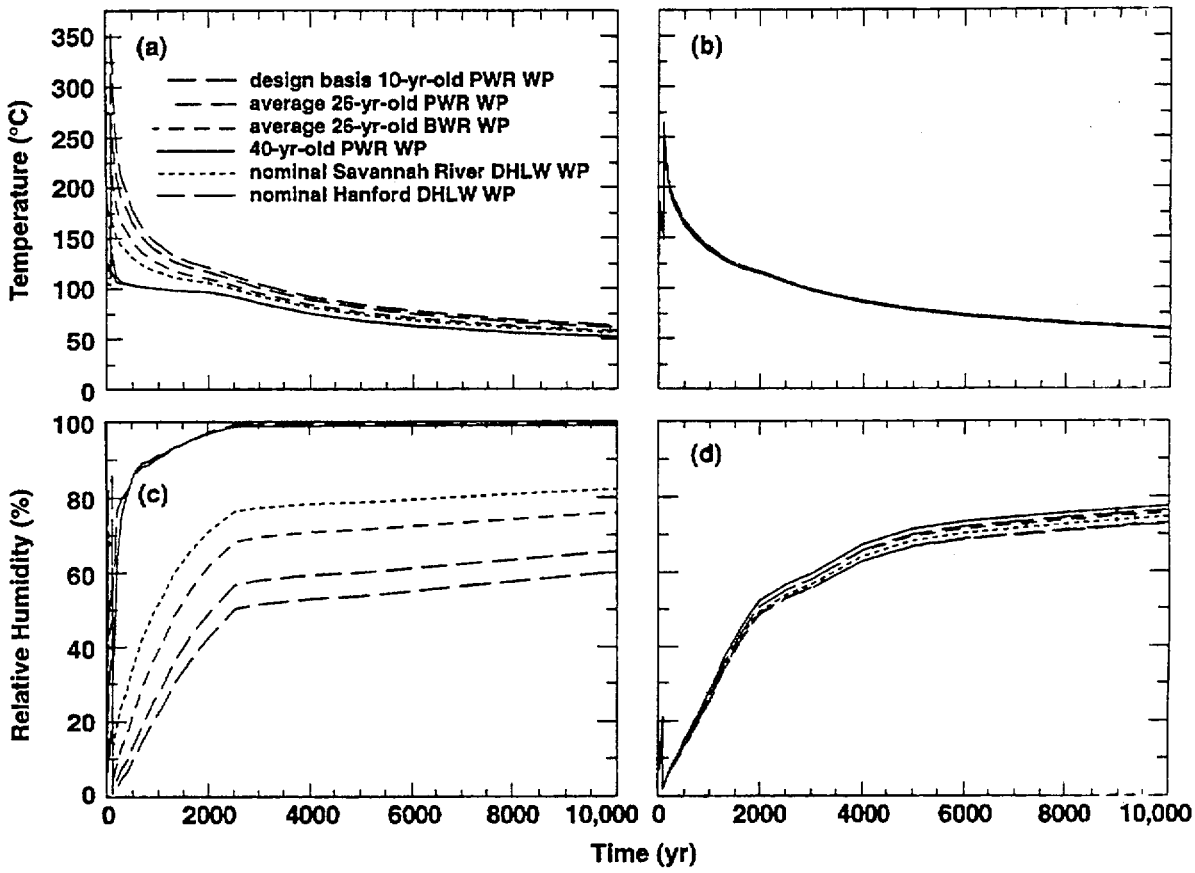

Figure 1.10.5.2.6. Temperature and relative humidity on upper surface of WP for AML = 83.4 MTU/acre, sand invert, full sand backfill at 100 yr with K_{th} = 0.6 W/m°C, drift diameter = 5.5 m, WP emissivity = 0.8, and ambient percolation flux = 0.3 mm/yr. Curves are plotted for the ACD rev 00 design (a,c) with LML = 0.46 MTU/m, and a line-load design (b,d) with a 0.1-m gap between WPs and LML = 1.11 MTU/m.

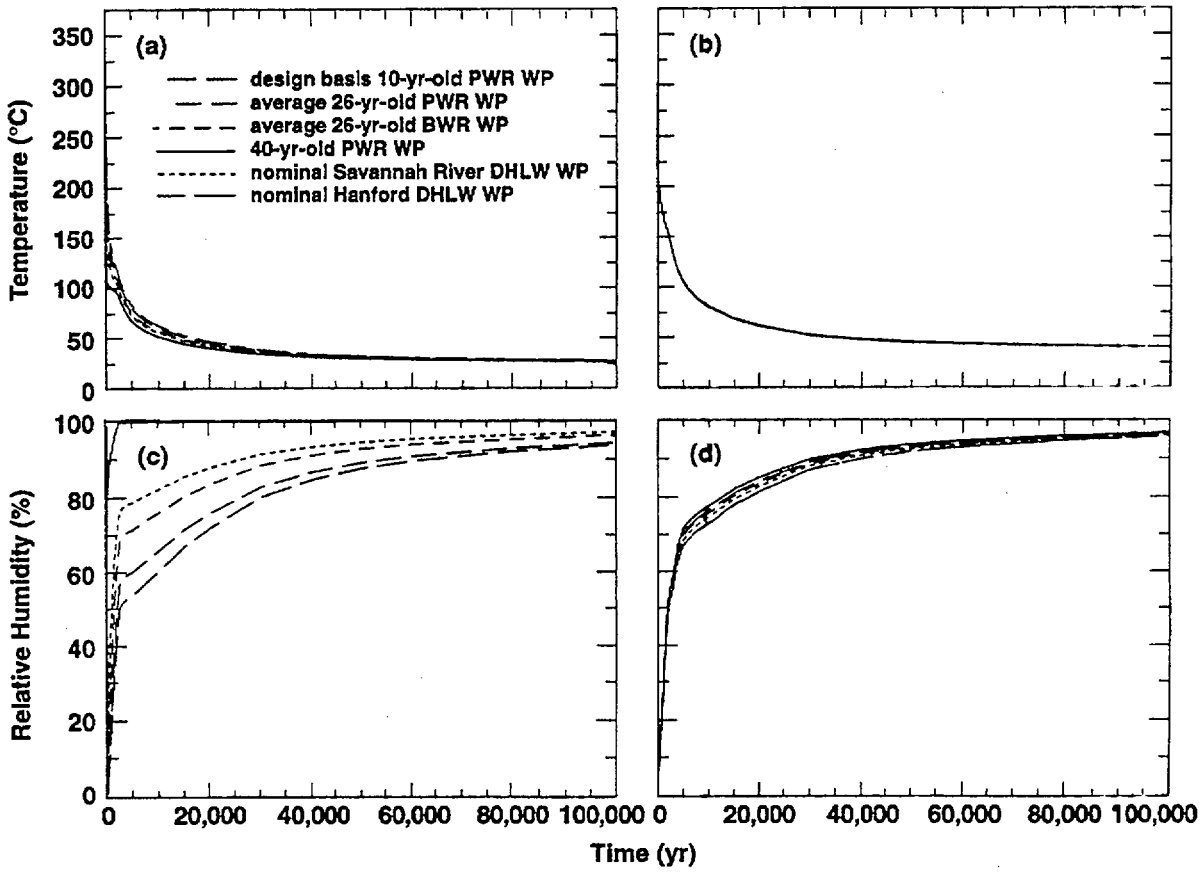

Figure 1.10.5.2.7. Temperature and relative humidity on upper surface of WP for AML = 83.4 MTU/acre, sand invert, full sand backfill at 100 yr with K_{th} = 0.6 W/m°C, drift diameter = 5.5 m, WP emissivity = 0.8, and ambient percolation flux = 0.3 mm/yr. Curves are plotted for the ACD rev 00 design (a,c) with LML = 0.46 MTU/m, and a line-load design (b,d) with a 0.1-m gap between WPs and LML = 1.11 MTU/m.

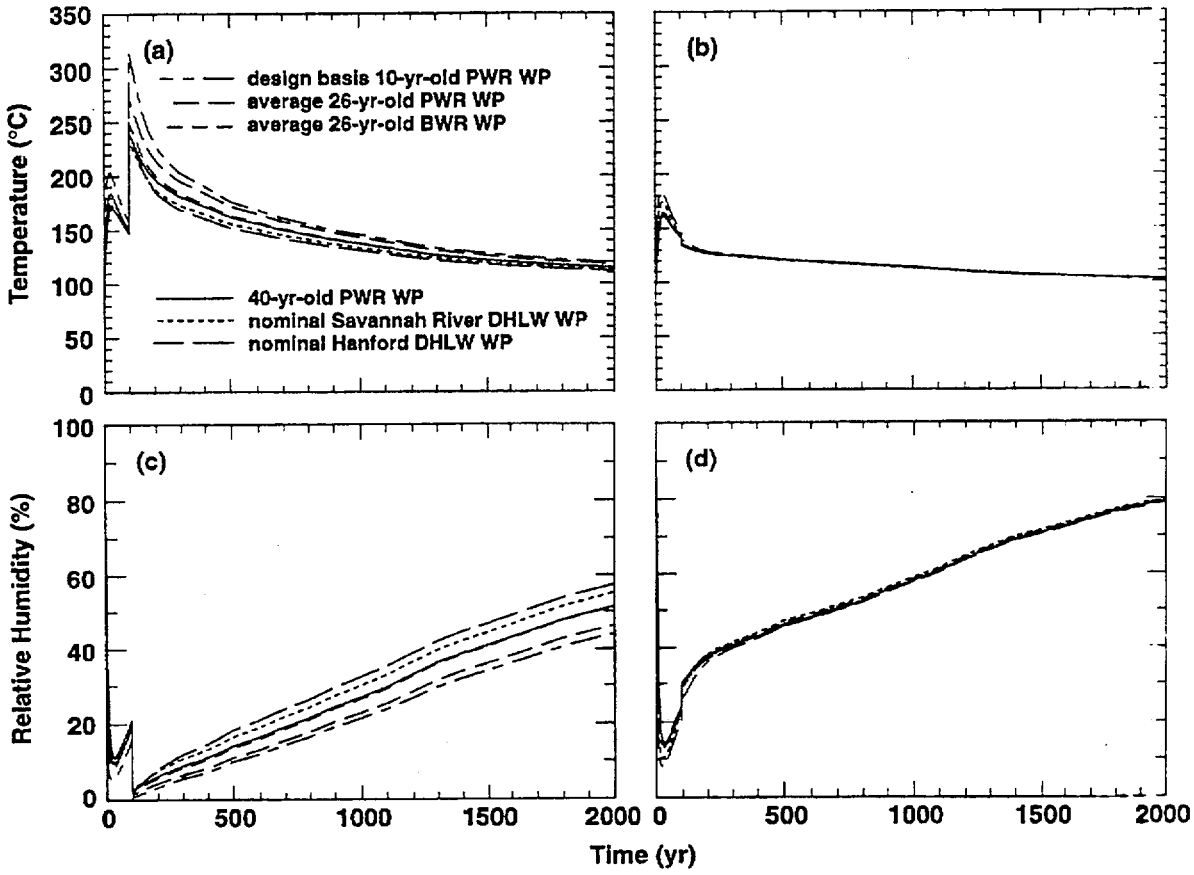

Figure 1.10.5.2.8. Temperature and relative humidity on upper WP surface (a,c) and in rock at upper drift wall (b,d) at various WP locations for AML = 83.4 MTU/acre, a line-load design with a 0.1-m gap between WPs, LML = 1.11 MTU/m, sand invert, full sand backfill at 100 yr with K_{th} = 0.6 W/m°C, drift diameter = 5.5 m, WP emissivity = 0.8, and ambient percolation flux = 0.3 mm/yr. Sand overfill is allowed to fill the gap separating the WPs at 100 yr.

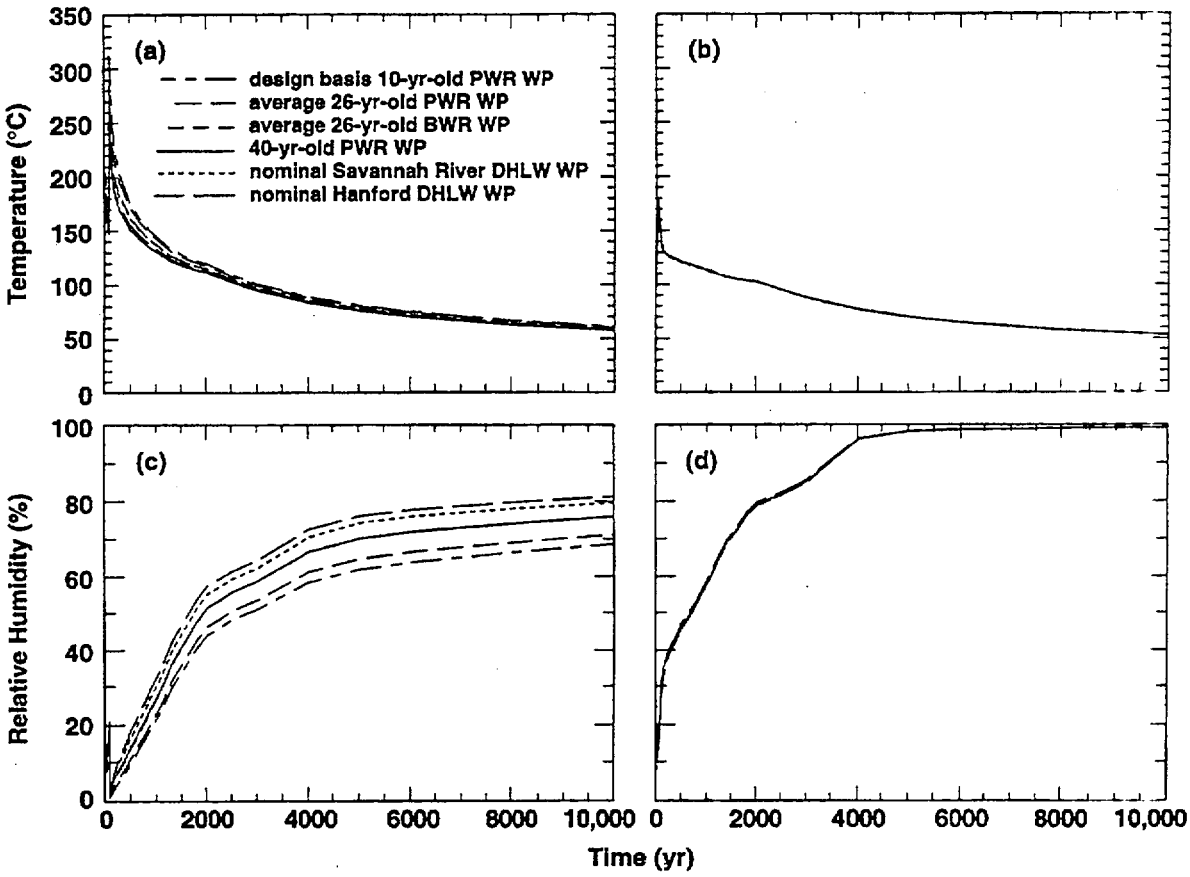

Figure 1.10.5.2.9. Temperature and relative humidity on upper WP surface (a,c) and in rock at upper drift wall (b,d) at various WP locations for AML = 83.4 MTU/acre, a line-load design with a 0.1-m gap between WPs, LML = 1.11 MTU/m, sand invert, full sand backfill at 100 yr with K_{th} = 0.6 W/m°C, drift diameter = 5.5 m, WP emissivity = 0.8, and ambient percolation flux = 0.3 mm/yr. Sand overfill is allowed to fill the gap separating the WPs at 100 yr.

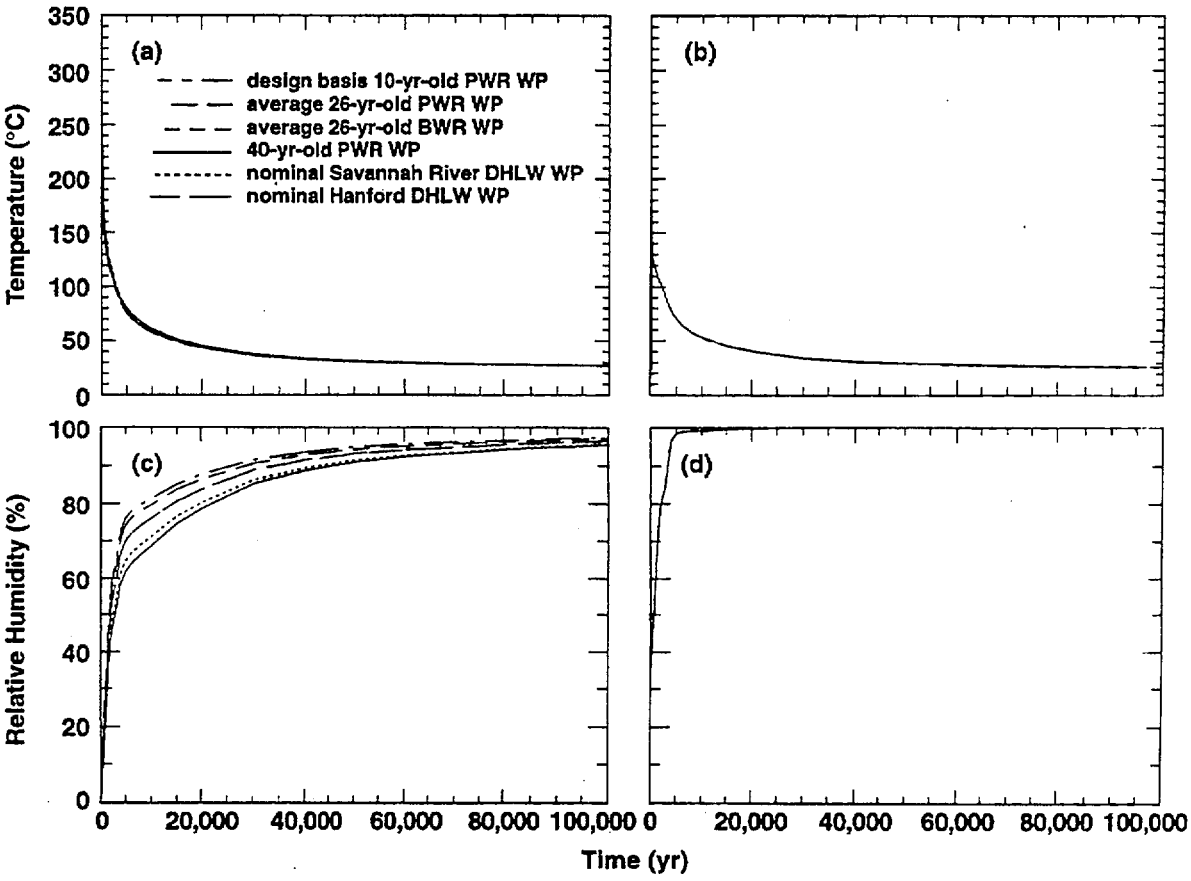

Figure 1.10.5.2.10. Temperature and relative humidity on upper WP surface (a,c) and in rock at upper drift wall (b,d) at various WP locations for AML = 83.4 MTU/acre, a line-load design with a 0.1-m gap between WPs, LML = 1.11 MTU/m, sand invert, full sand backfill at 100 yr with K_{th} = 0.6 W/m°C, drift diameter = 5.5 m, WP emissivity = 0.8, and ambient percolation flux = 0.3 mm/yr. Sand overfill is allowed to fill the gap separating the WPs at 100 yr.

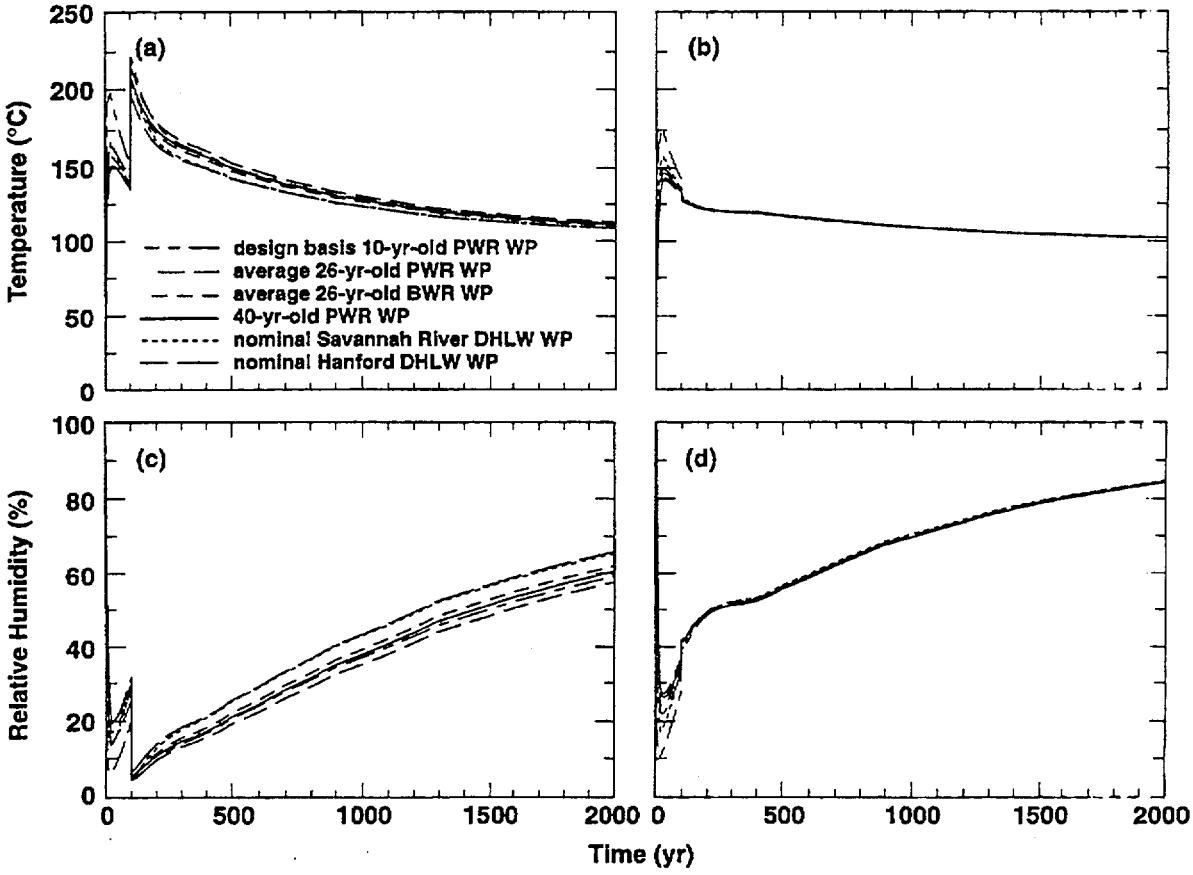

Figure 1.10.5.2.11. Temperature and relative humidity on upper WP surface (a,c) and in rock at upper drift wall (b,d) at various WP locations for AML = 83.4 MTU/acre, a line-load design with a 1.0-m gap between WPs, LML = 0.94 MTU/m, sand invert, full sand backfill at 100 yr with K_{th} = 0.6 W/m°C, drift diameter = 5.5 m, WP emissivity = 0.8, and ambient percolation flux = 0.3 mm/yr.

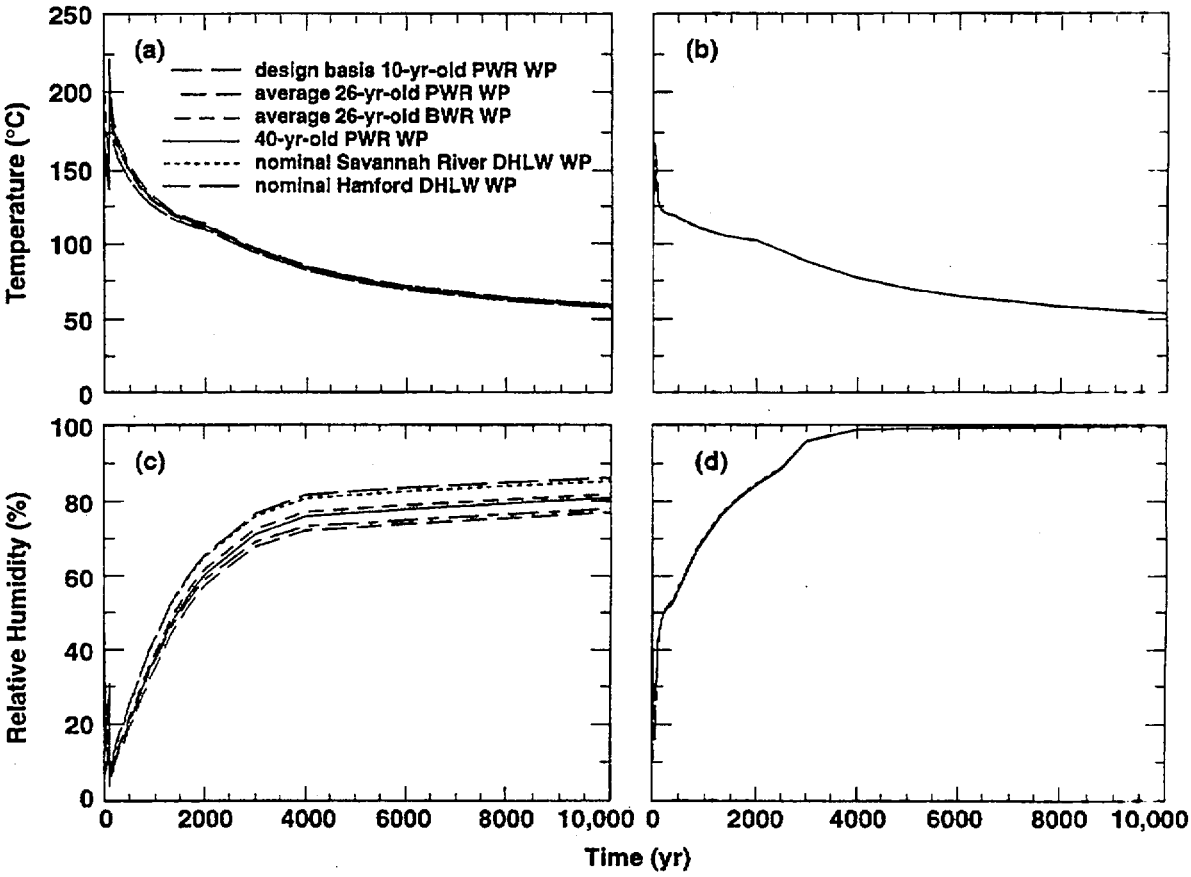

Figure 1.10.5.2.12. Temperature and relative humidity on upper WP surface (a,c) and in rock at upper drift wall (b,d) at various WP locations for AML = 83.4 MTU/acre, a line-load design with a 1.0-m gap between WPs, LML = 0.94 MTU/m, sand invert, full sand backfill at 100 yr with K_{th} = 0.6 W/m°C, drift diameter = 5.5 m, WP emissivity = 0.8, and ambient percolation flux = 0.3 mm/yr.

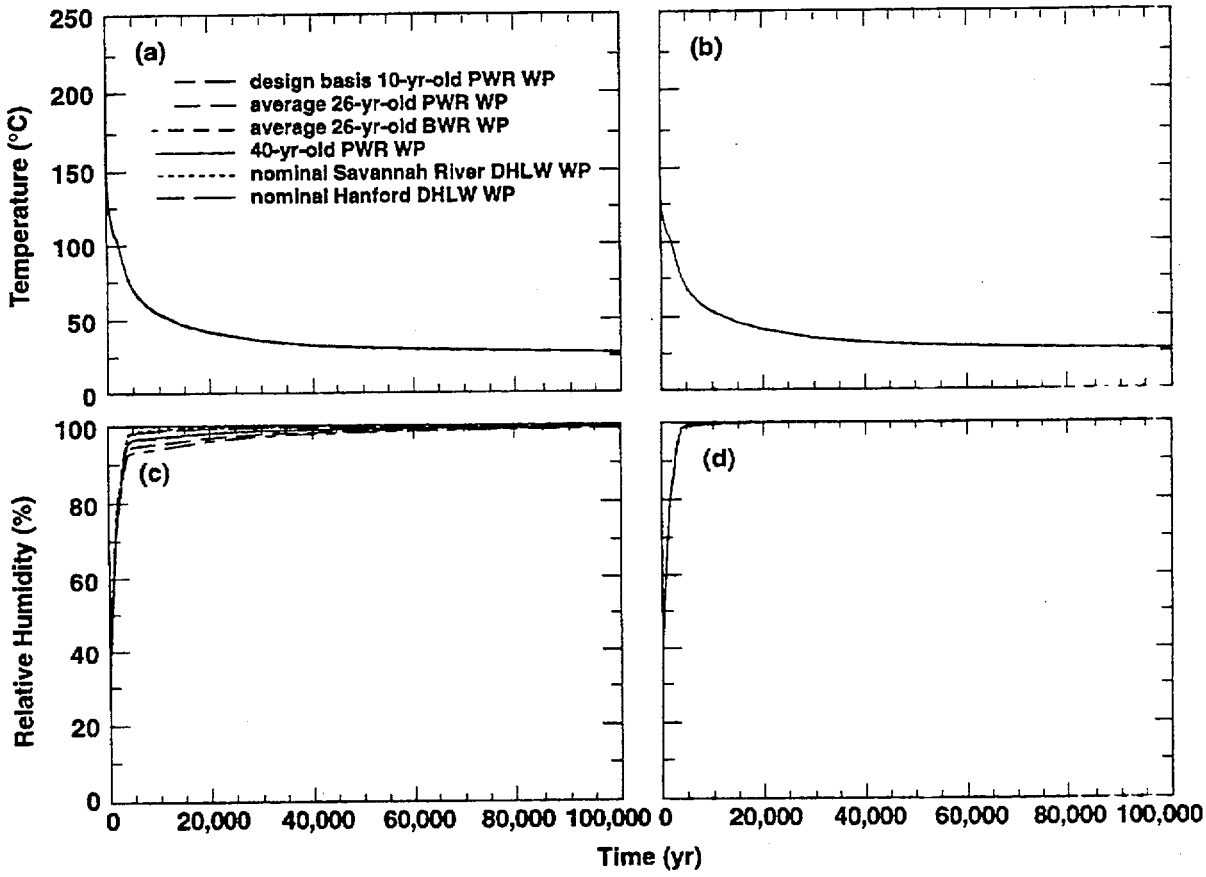

Figure 1.10.5.2.13. Temperature and relative humidity on upper WP surface (a,c) and in rock at upper drift wall (b,d) at various WP locations for AML = 83.4 MTU/acre, a line-load design with a 1.0-m gap between WPs, LML = 0.94 MTU/m, sand invert, full sand backfill at 100 yr with K_{th} = 0.6 W/m°C, drift diameter = 5.5 m, WP emissivity = 0.8, and ambient percolation flux = 0.3 mm/yr

1.10.5.3 Influence of Waste Package Emissivity

In Sections 1.10.5.1 and 1.10.5.2, the WP emissivity was assumed to be 0.8, which is the same as that assumed by Bahney [1996]. Emissivity ε, which can vary between 0 and 1, quantifies how efficiently heat is transferred to a surface by thermal radiation. An emissivity of 1.0 corresponds to a blackbody, which is a perfect absorber of thermal radiation. An emissivity of 0 corresponds to a perfectly reflective surface. Emissivity can vary significantly among engineered materials and it can also vary in time; for example, as a metallic surface oxidizes it tends to reflect less and absorb thermal radiation more efficiently. The cases analyzed in this section utilize the same assumptions used in Sections 1.10.5.1 and 1.10.5.2 with the exception that the WP emissivity is assumed to be 0.3 instead of 0.8. Note that the range of ε from 0.3 to 0.8 covers a fairly wide spectrum of metallic surfaces; therefore a comparison of calculations conducted in Sections 1.10.5.1 and 1.10.5.2 with those of this section (Section 1.10.5.3) should bracket much of the sensitivity of drift-scale T-H behavior to WP emissivity. Section 1.1.3.5 discusses the details of how thermal-radiative heat transfer is treated in the drift-scale models.

Although emissivity of the rock can be 0.85 to 0.95, a value of 1.0 was assumed in all of the calculations with the three-dimensional multiple-WP model. This assumption can be justified on the basis of the relationship [Holman, 1990] for radiation heat exchange q between two concentric cylindrical surfaces:

$$q = \frac{\sigma A_1\left(T_1^4 - T_2^4\right)}{1/\varepsilon_1 + (A_1/A_2)(1/\varepsilon_2 - 1)}, \qquad (2)$$

where A_1 and A_2 are the areas, T_1 and T_2 are the temperatures, and ε_1 and ε_2 are the emissivities of the inner and outer cylindrical surfaces, and σ is the Stephan-Boltzmann constant. If the outer cylinder is much larger than the inner cylinder, A_1/A_2 approaches 0, or if ε_2 is close to 1, then Eq. (2) becomes:

$$q = \sigma A_1 \varepsilon_1\left(T_1^4 - T_2^4\right), \qquad (3)$$

which is readily applied to calculate the radiation heat transfer from a hot object to a large room. In effect, the hot object (or WP) functions as a nonblackbody (also called a graybody) with a given emissivity ε_1 and area A_1, while the surfaces of the room (or emplacement drift) function as though they were blackbodies.

A comparison of Tables 1.10.5.3.1 and 1.10.5.3.2 with Tables 1.10.5.1.1 and 1.10.5.1.2 shows the influence of WP emissivity on T and RH on the upper drift wall and upper WP surface for the no-backfill cases, including the ACD rev 00 design and the 1.11- and 0.94-MTU/m line-load designs. Figure 1.10.5.3.1 summarizes the influence of WP emissivity on the maximum peak WP and rock temperatures prior to closure. A smaller WP emissivity increases the resistance to thermal-radiative heat transfer from the WP to the drift wall, thereby increasing the temperature difference ΔT_{drift} between the WP and the drift wall. Consequently, the maximum peak WP temperature increases from 192 to 233°C for the ACD rev 00 design and increases from 203 to 239°C for the 1.11-MTU/m line-load design.

The WP emissivity also affects the range in peak WP temperature; higher WP emissivity causes more effective thermal homogenization, which reduces the range in peak WP temperatures (Fig. 1.10.5.3.1c), particularly for the line-load design. For the ACD rev 00 design, the range in peak WP temperature is 117 and 85°C for WP emissivities of 0.3 and 0.8, respectively. Because of the importance of WP-to-WP thermal-radiative heat transfer for close axial WP spacing, WP emissivity significantly affects the range in peak WP temperatures in the line-load design. The importance of WP emissivity on the effectiveness of WP-to-WP thermal-radiative heat transfer can be seen in the relationship [Holman, 1990] for the net radiation heat exchange q_{net} between parallel disks:

$$q_{net} = \frac{\sigma A_1 \left(T_1^4 - T_2^4 \right)}{(1-\varepsilon_1)/\varepsilon_1 A_1 + 1/A_1 F_{12} + (1-\varepsilon_2)/e_2 A_2}, \quad (4)$$

where A_1 and A_2 are the areas, T_1 and T_2 are the temperatures, ε_1 and ε_2 are the emissivities of the disks, F_{12} is the radiation shape factor between the disks, and σ is the Stephan-Boltzmann constant. The radiation shape factor F_{12} can be determined on the basis of the ratio d/x, where d is the diameter of the disks and x is the separation distance between the disks, and a graphical relationship given in Holman [1990]. For the 1.11-MTU/m line-load design, $d/x = 18$, which results in $F_{12} = 1$. For $\varepsilon_1 = \varepsilon_2 = 0.8$, $q_{net} = 0.667\sigma A_1$, while for $\varepsilon_1 = \varepsilon_2 = 0.3$, $q_{net} = 0.298\sigma A_1$; consequently, WP-to-WP thermal-radiative heat transfer is 2.24 times more efficient for the case with $\varepsilon = 0.8$ (than for the case with $\varepsilon = 0.3$). Consequently, the range in peak WP temperatures is reduced by a factor of two (31 versus 60°C) when WP emissivity is increased from 0.3 to 0.8 (Fig. 1.10.5.3.1c).

The maximum peak drift-wall temperature is insensitive to WP emissivity (Fig. 1.10.5.3.1b) for all LML. However, because WP emissivity influences the effectiveness of thermal homogenization for close axial WP spacing, the range in peak drift-wall temperature is moderately sensitive to WP emissivity for the line-load design. Higher WP emissivity causes more effective thermal homogenization, which reduces the range in peak drift-wall temperatures. For the ACD rev 00 design, the WPs are too far apart (and are too thermally isolated from one another) for WP emissivity to have any influence on the range in drift-wall temperatures.

Because WP emissivity plays a minor role in determining how decay heat is delivered to the drift wall and floor surfaces in the ACD rev 00 design, it only weakly influences the intensity and distribution of rock dryout along the drift (compare Tables 1.10.5.1 and 1.10.5.3.1). Although it may not be significant, the higher WP emissivity ($\varepsilon = 0.8$) case results in slightly drier rock *RH* along the drift. For the line-load cases, WP emissivity plays a more significant role in determining how decay heat is delivered to the drift wall and floor surfaces. The more efficient thermal homogenization associated with the higher WP emissivity ($\varepsilon = 0.8$) case results in slightly more uniform and more intensive rock dryout along the drift.

A smaller WP emissivity increases the resistance to thermal-radiative heat transfer from the WP to the drift wall, increasing the magnitude and duration of the temperature difference ΔT_{drift} between the WP and drift wall for the cases with the lower WP emissivity ($\varepsilon = 0.3$). This results in a larger and more persistent *RH* difference ΔRH_{drift} between the WP and drift wall. For the ACD rev 00 design, this causes the hotter-than-average WPs to be drier for the $\varepsilon = 0.3$ case, while the average to cooler-than-average WPs are only slightly drier for the $\varepsilon = 0.3$ case (compare Tables 1.10.5.3.3 and 1.10.5.1.3). For example, the time for the hottest WP (the 10-yr-old PWR WP) to reach the *RH* = 65% threshold is longer (1030 yr) for the $\varepsilon = 0.3$ case than for the $\varepsilon = 0.8$ case (630 yr). At later time, the WP emissivity has an even greater effect on ΔRH_{drift}, with the time for the 10-yr-old PWR WP to reach the *RH* = 90% threshold taking 20,860 yr (compared with only 2330 yr for the $\varepsilon = 0.8$ case).

For the line-load design, a reduction in the WP emissivity causes two effects: (1) increases, on average, ΔT_{drift} for all WPs and (2) moderately reduces the tendency for the WPs to equally share the decay heat. For the cooler-than-average WPs (the DHLW, the 40-yr-old PWR, and the 26-yr-old BWR WPs) these two effects compensate for each other and the WPs have about the same *RH* histories for the $\varepsilon = 0.3$ case as in the $\varepsilon = 0.8$ case (compare Tables 1.10.5.3.4 and 1.10.5.1.4). For the average to hotter-than-average WPs (the 26-yr-old PWR and 10-yr-old PWR WPs), these effects cause the *RH* histories to be considerably drier for the $\varepsilon = 0.3$ case than in the $\varepsilon = 0.8$ case, particularly at late time. Consequently, the time to reach the *RH* = 90% threshold increases substantially for these WPs.

For the 0.94-MTU/acre line-load design, a reduction in the WP emissivity has a similar effect on WP *RH* histories as in the 1.11-MTU/m case. For the cooler-than-average WPs (the DHLW, the 40-yr-old PWR, and the 26-yr-old BWR WPs), the WPs have slightly drier *RH* histories for the $\varepsilon = 0.3$ case than in the $\varepsilon = 0.8$ case (compare Tables 1.10.5.3.5 and 1.10.5.1.5). For the average to hotter-than-average WPs (the 26-yr-old PWR and 10-yr-old PWR WPs), the *RH* histories are considerably drier

for the $\varepsilon = 0.3$ case than in the $\varepsilon = 0.8$ case, particularly at late time. Consequently, the time to reach the RH = 90% threshold increases substantially for these WPs.

The influence of WP emissivity on T and RH on the upper drift wall and WP surface for the backfill cases is shown by a comparison of Tables 1.10.5.3.6 and 1.10.5.3.7 with Tables 1.10.5.2.1 and 1.10.5.2.2. Because the presence of backfill prevents thermal-radiative heat transfer between the WPs and drift wall, WP emissivity has little influence on how decay heat is delivered to the drift wall after backfill is emplaced at 100 yr, other than affecting how well the line-load homogenizes the radial heat flux leaving the respective WPs. Consequently, there is very little difference in T and RH in the near-field rock between the $\varepsilon = 0.3$ case and $\varepsilon = 0.8$ case (compare Tables 1.10.5.3.6 and 1.10.5.1.1). Because the WPs in the ACD rev 00 design are completely surrounded by backfill, WP emissivity plays no role in heat transfer from the WPs after 100 yr. Consequently, for the ACD rev 00 design, there are virtually no differences in the respective T and RH histories for the WPs in the $\varepsilon = 0.3$ and 0.8 cases (compare Tables 1.10.5.3.8 and 1.10.5.1.3).

After backfill is emplaced in the line-load designs, WP emissivity influences T and RH on WPs by affecting how well the radial heat flux leaving the respective WPs is homogenized. The 1.11-MTU/m line-load is most affected by the efficiency of WP-to-WP thermal-radiative heat transfer. A reduction in WP emissivity (from 0.8 to 0.3) causes the range in post-closure (> 100 yr) peak WP temperatures to increase from 16°C to 36°C, with the maximum peak WP temperature increasing from 266 to 280°C. The moderate decrease in the efficiency of radiative WP-to-WP heat transfer causes an increase in the temporal variability in the time it takes to reach the RH = 65% and 90% thresholds. The cooler-than-average WPs (the DHLW WPs) in the $\varepsilon = 0.3$ case take less time to reach the RH = 65% and 90% thresholds than in the $\varepsilon = 0.3$ case (compare Tables 1.10.5.3.9 and 1.10.5.2.4). The cooler-than-average to average WPs (the 40-yr-old BWR and 26-yr-old BWR WPs) in the $\varepsilon = 0.3$ case take nearly the same time to reach the RH = 65% and 90% thresholds as in the $\varepsilon = 0.3$ case. The hotter-than-average WPs (the 26-yr-old PWR and 10-yr-old PWR WPs) in the $\varepsilon = 0.3$ case take more time to reach the RH = 65% and 90% thresholds than in the $\varepsilon = 0.3$ case.

For the 0.94-MTU/m line-load design, a reduction in WP emissivity (from 0.8 to 0.3) causes the range in post-closure (> 100 yr) peak WP temperatures to increase from 27°C to 46°C, with the maximum peak WP temperature increasing from 221 to 237°C. The moderate decrease in the efficiency of radiative WP-to-WP heat transfer causes an increase in the temporal variability in the time it takes to reach the RH = 65% and 90% thresholds. The cooler-than-average WPs (the DHLW WPs) in the $\varepsilon = 0.3$ case take a little less time to reach the RH = 65% and 90% thresholds than in the $\varepsilon = 0.3$ case (compare Tables 1.10.5.3.10 and 1.10.5.2.6). The cooler-than-average to average WPs (the 40-yr-old BWR and 26-yr-old BWR WPs) in the $\varepsilon = 0.3$ case take nearly the same time to reach the RH = 65% and 90% thresholds as in the $\varepsilon = 0.3$ case. The hotter-than-average WPs (the 26-yr-old PWR and 10-yr-old PWR WPs) in the $\varepsilon = 0.3$ case take more time to reach the RH = 65% and 90% thresholds than in the $\varepsilon = 0.3$ case.

In this section, we considered a range in WP emissivity that probably more than adequately spans the range of possible values for the potential repository system at Yucca Mountain. The influence of WP emissivity on rock temperatures and RH is minor (almost negligible). The influence of WP emissivity on WP temperatures and RH for the ACD rev 00 design with backfill is also negligible. The two most significant effects influenced by WP emissivity are:

Drift-ΔRH effect for cases with no backfill: The temperature difference ΔT_{drift} between the WP and drift wall depends on the efficiency of thermal-radiative heat transfer between the WP and drift wall, which depends strongly on WP emissivity. WP emissivity does not strongly affect RH_{WP} until late time when RH approaches 90%.

Heat flow homogenization for line-load cases: The efficiency of radiative WP-to-WP heat transfer depends on WP emissivity, which affects the extent to which T and RH on WPs is homogenized. Even for the lower WP emissivity ($\varepsilon = 0.3$) case, the line-load is found to effectively homogenize T and RH along the drift.

Table 1.10.5.3.1. Temperature and relative humidity in rock at upper drift wall for AML = 83.4 MTU/acre, drift diameter = 5.5 m, sand invert, no backfill, WP emissivity = 0.3 and percolation flux = 0.3 mm/yr.

Repository design	ACD rev 00	Line load	Line load
LML	0.46 MTU/m	1.11 MTU/m	0.94 MTU/m
Drift spacing	22.5 m	53.8 m	46.1 m
Gap between WPs	varies	0.1 m	1.0 m
T_{peak} (t < 100 yr)	100–164°C	155–185°C	134–172°C
RH_{max} (t < 100 yr)	40–99.7%	22–28%	30–41%
T_{peak} (t > 100 yr)	100–129°C	138–146°C	126–136°C
RH (t = 120 yr)	45–99.6%	24–29%	33–42%
RH (t = 2000 yr)	94–99%	77–78%	82–84%
RH (t = 10,000 yr)	99.9–99.9%	99.1–99.1%	99.4–99.4%

Table 1.10.5.3.2. Temperature and relative humidity on upper WP surface for AML = 83.4 MTU/acre, drift diameter = 5.5 m, sand invert, no backfill, WP emissivity = 0.3, and percolation flux = 0.3 mm/yr.

Repository design	**ACD rev 00**	**Line load**	**Line load**
LML	0.46 MTU/m	1.11 MTU/m	0.94 MTU/m
Drift spacing	22.5 m	53.8 m	46.1 m
Gap between WPs	varies	0.1 m	1.0 m
T_{peak} (t < 100 yr)	116–233°C	179–239°C	160–230°C
RH_{max} (t < 100 yr)	17–86%	11–20%	14–29%
T_{peak} (t > 100 yr)	104–144°C	149–172°C	137–165°C
RH (t = 120 yr)	29–85%	13–22%	16–31%
RH (t = 2000 yr)	86–97%	68–75%	73–81%
RH (t = 10,000 yr)	92–99.9%	88–96%	88–97%
$t(RH$ = 65%)	60–1030 yr	1400–1800 yr	1020–1510 yr
$t(RH$ = 90%)	180–20,860 yr	3780–14,520 yr	2840–14,370 yr

Table 1.10.5.3.3. Temperature and relative humidity on upper WP surface for AML = 83.4 MTU/acre, the ACD rev 00 design with LML = 0.46 MTU/m, drift spacing = 22.5 m, sand invert, no backfill, drift diameter = 5.5 m, WP emissivity = 0.3, and percolation flux = 0.3 mm/yr.

Waste package type	Hanford Site DHLW	Savannah River Site DHLW	40-yr-old PWR MPC	26-yr-old BWR MPC	26-yr-old PWR MPC	10-yr-old PWR MPC
T_{peak} (t < 100 yr)	116°C	127°C	121°C	146°C	170°C	233°C
RH_{max} (t < 100 yr)	86%	64%	60%	41%	31%	17%
T_{peak} (t > 100 yr)	104°C	111°C	114°C	125°C	133°C	152°C
RH (t = 120 yr)	86%	67%	61%	43%	34%	20%
RH (t = 2000 yr)	99%	99%	93%	90%	85%	81%
RH (t = 10,000 yr)	99.9%	99.8%	95%	93%	88%	86%
$t(RH = 65\%)$	60 yr	130 yr	190 yr	410 yr	700 yr	1030 yr
$t(RH = 90\%)$	180 yr	320 yr	1680 yr	1970 yr	14,390 yr	20,860 yr

Table 1.10.5.3.4 Temperature and relative humidity on upper WP surface for AML = 83.4 MTU/acre, a line-load design with a 0.1-m gap between WPs, LML = 1.11 MTU/m, drift spacing = 53.8 m,sand invert, no backfill, drift diameter = 5.5 m, WP emissivity = 0.3 and percolation flux = 0.3 mm/yr.

Waste package type	Hanford Site DHLW	Savannah River Site DHLW	40-yr-old PWR MPC	26-yr-old BWR MPC	26-yr-old PWR MPC	10-yr-old PWR MPC
T_{peak} (t < 100 yr)	179°C	192°C	176°C	184°C	195°C	239°C
RH_{max} (t < 100 yr)	20%	20%	19%	18%	15%	11%
T_{peak} (t > 100 yr)	149°C	150°C	151°C	154°C	160°C	172°C
RH (t = 120 yr)	22%	22%	21%	20%	17%	13%
RH (t = 2000 yr)	75%	76%	73%	72%	70%	68%
RH (t = 10,000 yr)	96%	97%	94%	93%	90%	88%
$t(RH = 65\%)$	1470 yr	1400 yr	1560 yr	1580 yr	1720 yr	1800 yr
$t(RH = 90\%)$	3910 yr	3780 yr	4410 yr	4580 yr	8330 yr	14,520 yr

Table 1.10.5.3.5. Temperature and relative humidity on upper WP surface for AML = 83.4 MTU/acre, a line-load design with a 1.0-m gap between WPs, LML = 0.94 MTU/m, drift spacing = 46.1 m, sand invert, no backfill, drift diameter = 5.5 m, WP emissivity = 0.3, and percolation flux = 0.3 mm/yr.

Waste package type	Hanford Site DHLW	Savannah River Site DHLW	40-yr-old PWR MPC	26-yr-old BWR MPC	26-yr-old PWR MPC	10-yr-old PWR MPC
T_{peak} (t < 100 yr)	160°C	175°C	157°C	168°C	182°C	230°C
RH_{max} (t < 100 yr)	29%	28%	26%	24%	20%	14%
T_{peak} (t > 100 yr)	137°C	139°C	140°C	144°C	151°C	164°C
RH (t = 120 yr)	31%	30%	28%	26%	22%	16%
RH (t = 2000 yr)	81%	82%	78%	78%	75%	73%
RH (t = 10,000 yr)	97%	98%	94%	93%	91%	88%
$t(RH = 65\%)$	1120 yr	1020 yr	1240 yr	1260 yr	1380 yr	1500 yr
$t(RH = 90\%)$	2940 yr	2840 yr	3410 yr	3560 yr	6850 yr	14,360 yr

Table 1.10.5.3.6. Temperature and relative humidity in rock at upper drift wall for AML = 83.4 MTU/acre, drift diameter = 5.5 m, sand invert, full sand backfill at 100 yr with K_{th} = 0.6 W/m°C, WP emissivity = 0.3, and percolation flux = 0.3 mm/yr.

Repository design	ACD rev 00	Line load	Line load
LML	0.46 MTU/m	1.11 MTU/m	0.94 MTU/m
Drift spacing	22.5 m	53.8 m	46.1 m
Gap between WPs	varies	0.1 m	1.0 m
T_{peak} (t < 100 yr)	100–164°C	155–185°C	135–172°C
RH_{max} (t < 100 yr)	40–99.7%	22–28%	30–41%
T_{peak} (t > 100 yr)	100–124°C	134–137°C	123–128°C
RH (t = 120 yr)	49–99%	31–33%	41–45%
RH (t = 2000 yr)	97–99.4%	79–79%	84–84%
RH (t = 10,000 yr)	99.8–99.8%	99.1–99.1%	99.4–99.5%

Table 1.10.5.3.7 Temperature and relative humidity on upper WP surface for AML = 83.4 MTU/acre, drift diameter = 5.5 m, sand invert, full sand backfill at 100 yr with K_{th} = 0.6 W/m°C, WP emissivity = 0.3, and percolation flux = 0.3 mm/yr.

Repository design	ACD rev 00	Line load	Line load
LML	0.46 MTU/m	1.11 MTU/m	0.94 MTU/m
Drift spacing	22.5 m	53.8 m	46.1 m
Gap between WPs	varies	0.1 m	1.0 m
T_{peak} (t < 100 yr)	116–233°C	176–239°C	160–230°C
RH_{max} (t < 100 yr)	17–86%	11–20%	14–29%
T_{peak} (t > 100 yr)	116–348°C	244–280°C	191–237°C
RH (t = 120 yr)	1–61%	2–3%	4–7%
RH (t = 2000 yr)	45–99%	46–56%	54–67%
RH (t = 10,000 yr)	60–99.7%	68–81%	73–87%
$t(RH = 65\%)$	140–13,440 yr	3200–6890 yr	1890–3240 yr
$t(RH = 90\%)$	400–62,060 yr	24,750–48,270 yr	14,760–40,350 yr

Table 1.10.5.3.8. Temperature and relative humidity on upper WP surface for AML = 83.4 MTU/acre, the ACD design with LML = 0.46 MTU/m, drift spacing = 22.5 m, sand invert, full sand backfill at 100 yr with K_{th} = 0.6 W/m°C, drift diameter = 5.5 m, WP emissivity = 0.3, and percolation flux = 0.3 mm/yr.

Waste package type	Hanford Site DHLW	Savannah River Site DHLW	40-yr-old PWR MPC	26-yr-old BWR MPC	26-yr-old PWR MPC	10-yr-old PWR MPC
T_{peak} (t < 100 yr)	116°C	127°C	121°C	146°C	170°C	233°C
RH_{max} (t < 100 yr)	86%	64%	60%	41%	31%	17%
T_{peak} (t > 100 yr)	116°C	134°C	168°C	218°C	268°C	348°C
RH (t = 120 yr)	61%	38%	15%	5%	2%	1%
RH (t = 2000 yr)	99%	99%	73%	64%	52%	45%
RH (t = 10,000 yr)	99.7%	99.2%	82%	76%	66%	60%
$t(RH = 65\%)$	140* yr	190 yr	1460 yr	2090 yr	9270 yr	13,440 yr
$t(RH = 90\%)$	400 yr	430 yr	25,500 yr	35,180 yr	54,070 yr	62,060 yr
* RH is never less than 65% prior to backfill						

Table 1.10.5.3.9. Temperature and relative humidity on upper WP surface for AML = 83.4 MTU/acre, a line-load design with a 0.1-m gap between WPs, LML = 1.11 MTU/m, drift spacing = 54.8 m, sand invert, full sand backfill at 100 yr with K_{th} = 0.6 W/m°C, drift diameter = 5.5 m, WP emissivity = 0.3, and percolation flux = 0.3 mm/yr.

Waste package type	Hanford Site DHLW	Savannah River Site DHLW	40-yr-old PWR MPC	26-yr-old BWR MPC	26-yr-old PWR MPC	10-yr-old PWR MPC
T_{peak} (t < 100 yr)	179°C	192°C	176°C	184°C	195°C	239°C
RH_{max} (t < 100 yr)	20%	20%	19%	18%	15%	11%
T_{peak} (t > 100 yr)	244°C	253°C	248°C	249°C	259°C	280°C
RH (t = 120 yr)	3%	3%	3%	3%	2%	2%
RH (t = 2000 yr)	54%	56%	51%	51%	47%	46%
RH (t = 10,000 yr)	80%	81%	76%	76%	71%	68%
$t(RH$ = 65%)	3370 yr	3200 yr	3830 yr	3800 yr	5200 yr	6890 yr
$t(RH$ = 90%)	26,450 yr	24,750 yr	34,390 yr	34,640 yr	45,300 yr	48,270 yr

Table 1.10.5.3.10. Temperature and relative humidity on upper WP surface for AML = 83.4 MTU/acre, a line-load design with a 1.0-m gap between WPs, LML = 0.94 MTU/m, drift spacing = 46.1 m, sand invert, full sand backfill at 100 yr with K_{th} = 0.6 W/m°C, drift diameter = 5.5 m, WP emissivity = 0.3, and percolation flux = 0.3 mm/yr.

Waste package type	Hanford Site DHLW	Savannah River Site DHLW	40-yr-old PWR MPC	26-yr-old BWR MPC	26-yr-old PWR MPC	10-yr-old PWR MPC
T_{peak} (t < 100 yr)	160°C	175°C	157°C	168°C	182°C	230°C
RH_{max} (t < 100 yr)	29%	28%	26%	20%	14%	14%
T_{peak} (t > 100 yr)	191°C	206°C	208°C	208°C	225°C	237°C
RH (t = 120 yr)	9%	7%	6%	4%	4%	4%
RH (t = 2000 yr)	67%	66%	60%	60%	54%	54%
RH (t = 10,000 yr)	87%	86%	80%	80%	73%	73%
$t(RH$ = 65%)	1890 yr	1940 yr	2510 yr	2450 yr	3270 yr	3240 yr
$t(RH$ = 90%)	17,490 yr	16,550 yr	28,360 yr	28,380 yr	40,700 yr	40,350 yr

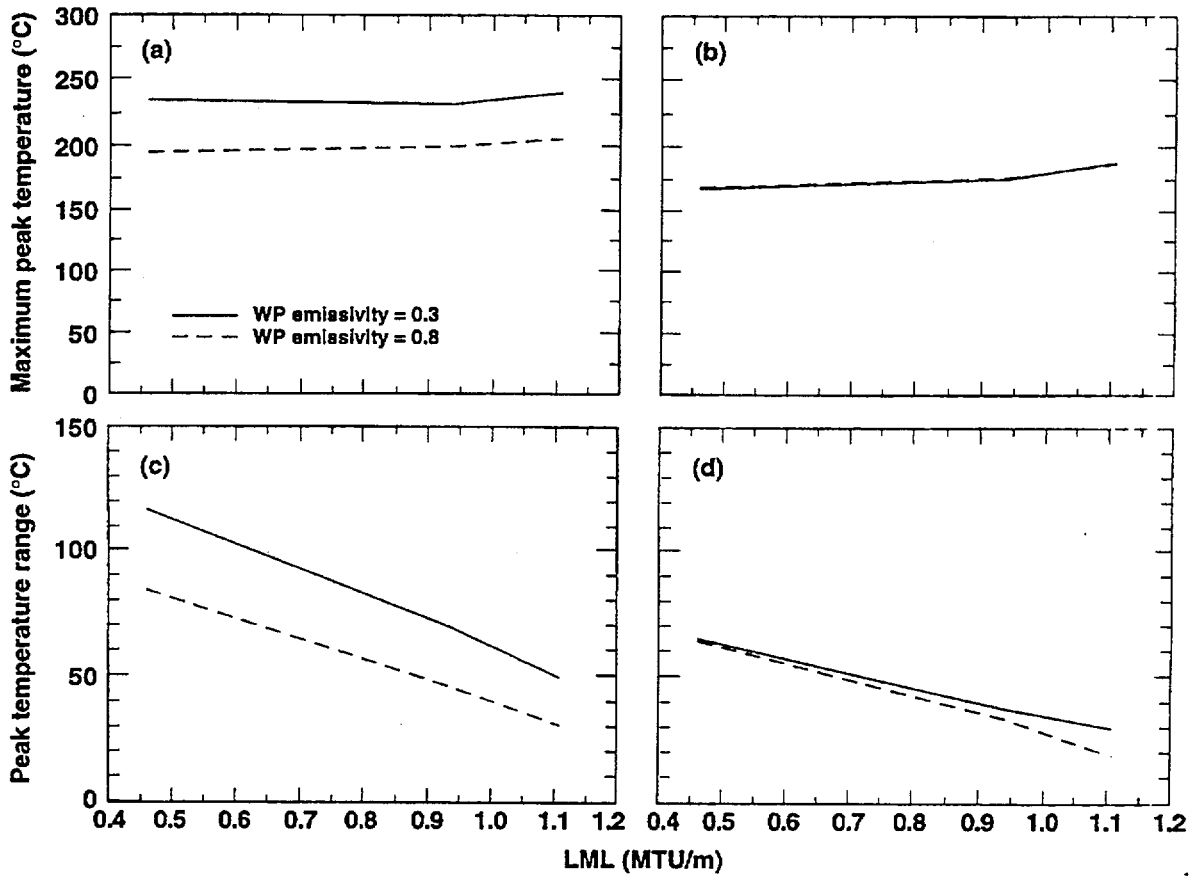

Figure 1.10.5.3.1. Maximum peak temperature on upper WP surface (a,c) and in rock at upper drift wall (b,d) for AML = 83.4 MTU/acre, sand invert, no backfill, drift diameter = 5.5 m, and ambient percolation flux = 0.3 mm/yr. Peak temperatures are also applicable to the pre-closure period for cases that are backfilled at 100 yr.

1.10.5.4 Influence of Waste Package and Backfill Configuration

The drift-scale analyses described in Sections 1.10.5.1 through 1.10.5.3 (as well as in the following sections) assume the center-in-drift (CID) WP configuration and, for the backfill (or overfill) cases, it was assumed that the drifts are completely filled with backfill. Because of operational constraints, it may be found that it is not possible (particularly if backfill is to be emplaced) to utilize the CID configuration [Balady, 1996]. Instead, it may be necessary to place the WPs to one side of the drift in the off-center-in-drift (OCID) WP configuration (Fig. 1.10.4.1a). Operational limitations may also prevent the drifts from being completely filled with backfill. In addition to the full backfill configuration (Fig. 1.10.4.1d), various partial backfill configurations have been analyzed for the backfill systems study [Balady, 1996], including the sloping-partial backfill (Fig. 1.10.4.1.b) and level-partial backfill (Fig. 1.10.4.1.c).

The drift-scale analyses in Sections 1.10.5.1 through 1.10.5.3 (as well as in the following sections) assume that both the invert and backfill are filled with a sand or "sand-like" granular material with respect to its rewetting (or wicking) characteristics. (Note that many of these calculations were conducted in support of the backfill systems study [Balady, 1996], which focused on the evaluation of granular invert and backfill materials.) The assumption of a sand-like granular material is not limited to the use of sand. By sand-like, it is meant that the granular material be of similar coarseness (i.e., grain size distribution) and have a negligible porosity (i.e., nonporous grains). A granular material with coarser grain sizes, such as a basalt or granite gravel, would exhibit even more favorable non-wicking qualities than the sand-like granular material assumed in these calculations. In this section, we address the possibility of using crushed TSw2 tuff (or gravel) in the invert. A TSw2 gravel differs from a sand-like material primarily by virtue of its having a significant intragranular porosity that may influence wicking. In Section 1.10.4, a comparison of a crushed PTn tuff and a sand backfill indicated that the crushed tuff had a greater tendency (than sand) to wick moisture back into the drift.

As in the previous three sections, calculations in this section assume an AML of 83.4 MTU/acre and an ambient percolation flux of 0.3 mm/yr. The analysis of alternative backfill configurations was conducted using a two-dimensional cross-sectional model that represents, in fine detail, the emplacement drift and pillar in a plane transverse to the drift. The model averages the heat output from a mixture of 26-yr-old BWR WPs and 26-yr-old PWR WPs into a uniform line-heat load. The WP decay heat characteristics are described in Table 1.10.1.2 and are based on a WP receipt analysis by King [1994]. Because of the large number of grid blocks required to represent the detail of the alternative WP and backfill configurations (Fig. 1.10.5.4.1), it was not feasible to conduct these calculations with a three-dimensional model that explicitly represents multiple WPs. Instead, it was necessary to utilize a two-dimensional model.

The two-dimensional model, in effect, averages (or smears) out the differences in heat output generated by the respective WPs. Moreover, the two-dimensional model cannot represent heat flow in the third (axial) dimension; consequently, it cannot adequately represent heat and fluid flow generated by the ACD rev 00 design. However, because close axial (end-to-end) WP spacing effectively homogenizes the distribution of radial heat flow leaving the respective WPs (causing them to function as though they shared the same decay heat generation curve), the two-dimensional model is a very reasonable representation of the line-load design. In spite of the large differences in heat generation among the various WPs, the high effective axial heat conductance facilitated by the end-to-end WP spacing causes the line of WPs to function as though it were a (nearly) uniform line-heat load. Because the two-dimensional drift-scale model is much better suited to analyzing the line-load design (rather than the ACD rev 00 design, we focus much of the analysis in this section (that requires the use of the two-dimensional model) on the line-load design.

The major geometric attributes of the alternative backfill configurations analyzed in this section are shown in Figs. 1.10.5.4.1 and 1.10.5.4.2. Table 1.10.5.4.1 gives the percentages of the emplacement drift cross section occupied by the major components of the Engineered Barrier Systems (EBS) for a drift

diameter of 5.5 m and a WP diameter of 1.8 m. Notice that 16% of the drift is occupied by the invert, while the WP occupies 10.7%. For the sloping-partial backfill configuration, the backfilled portion (36.9%) and unfilled portion (35.4%) are roughly equal; in total, 64.6% of the drift cross section is occupied (primarily with the invert and backfill material). For the level-partial backfill configuration, 56.6% of the drift cross section is backfilled at 100 yr, while only 15.7% is left unfilled; in total, 84.3% of the drift cross section is occupied. The full backfill configuration fills 100% of the drift.

All of the two-dimensional calculations assume a WP emissivity $\varepsilon = 0.3$, which is different from the value ($\varepsilon = 0.8$) assumed in most of the three-dimensional, multiple-WP model calculations presented in Sections 1.10.5 and 1.10.6. (At the time the two-dimensional calculations were conducted, which was prior to when the three-dimensional calculations were conducted, $\varepsilon = 0.3$ was judged to be appropriate for the WPs; since then, $\varepsilon = 0.8$ has been assumed for the WPs in the reference case.) Because thermal radiation controls ΔT_{drift} for the no-backfill case, the smaller value of ε (0.3) assumed in this section results in a moderately greater ΔT_{drift} as compared to the cases with $\varepsilon = 0.8$. As discussed in Section 1.10.5.3, the larger ΔT_{drift} for the no-backfill cases with $\varepsilon = 0.3$ results in a greater drift-ΔRH effect, particularly at late time ($t > 5000$ yr).

For the sloping-partial and level-partial backfill cases, thermal radiation occurs between all of the surfaces surrounding the unfilled drift cavity that overlies the backfill. An emissivity of 0.9 was assumed for the rock surfaces and the upper surface of the partially filled backfill. As discussed in Section 1.10.5.3, it does not make much difference whether $\varepsilon = 0.9$ or 1.0 is assumed for the rock-wall surfaces of the drift. For the no-backfill cases, the two-dimensional model represents thermal-radiative heat transfer between all of the surfaces in the drift, including: (1) the WP, (2) the WP cart, (3) the drift floor, and (4) the drift walls. The low-K_{th} invert causes the drift floor to become relatively hot (compared with the drift walls), resulting in significant thermal-radiative heat transfer from the drift floor to drift walls. Similarly, the asymmetrical geometry of the OCID WP configuration causes the left-side drift wall to be hotter than the right-side drift wall; consequently, there is significant thermal-radiative heat transfer from the right-side drift wall to the left-side drift wall.

The near-field *RH* distribution at 120 yr (20 yr after backfill is emplaced) for the ACD rev 00 design with LML = 0.47 MTU/m and drift spacing = 22.5 m is shown in Fig. 1.10.5.4.1. Because of the relatively low LML, *RH* reduction by rock dryout (ΔRH_{rock}) is minimal; virtually all of the *RH* reduction occurs inside of the drift, driven by ΔT_{drift}, which results in the drift-ΔRH effect. Notice that most of the *RH* reduction occurs within the backfill; the unfilled portions of the drift in the sloping-partial and level-partial backfill configurations (Figs. 1.10.5.4.1b,c) have a less steep *RH* gradient than inside of the backfill. The OCID configuration results in there being much more low-K_{th} backfill insulating the left side of the WP than the right side (Fig. 1.10.5.4.1); consequently, the rock to the left of the drift is more insulated from heat flow than the rock to the right of the drift. The asymmetrical insulation surrounding the WP causes more of the WP decay heat to flow to the rock at the right side of the drift than to the left side, causing higher rock temperatures and greater rock dryout in the rock pillar to the right of the drift than to the left (Figs. 1.8-4 and 1.10.5.4.1). This effect, together with the overall weak rock dryout generated by 0.47 MTU/m, results in there being very little rock dryout at 120 yr in the pillar to the left of the drift.

The near-field *RH* distribution at 120 yr for the line-load design with LML = 0.94 MTU/m and drift spacing = 45 m is shown in Fig. 1.10.5.4.2. The higher LML results in much more locally intensive rock dryout and a much larger ΔRH_{rock} than in the ACD rev 00 design. The unbackfilled 0.94-MTU/m case (Fig. 1.10.5.4.2a) results in a lower *RH* on the WP than any of the ACD rev 00 cases with backfill (Fig. 1.10.5.4.1). Figure 1.10.5.4.3 shows the temperature *T* and *RH* on the WP for the four backfill configurations. At the time of backfill, ΔT_{drift} is 57, 48, and 39°C for the full, level-partial, and sloping-partial backfill cases, respectively. For the level-partial backfill case, ΔT_{drift} is 84% of that for the full backfill case, while for the sloping-partial backfill case, ΔT_{drift} is 68% of that for the full backfill case. The percentage of the ΔT_{drift} relative to the full backfill case is nearly the same as the percentages of the drift that are occupied with low-K_{th} invert and backfill material. Therefore,

ΔT_{drift} approximately scales as the percentage of the drift that is filled. The drift-ΔRH effect (as measure by RH_{wp}/RH_{dw}) also scales as the percentage of the drift that is filled.

Figure 1.10.5.4.4 compares *T* and *RH* on the WP for the CID and OCID WP configurations for the line-load design with LML = 0.94 MTU/m, drift spacing = 45 m, and full backfill at 100 yr. Notice that the asymmetrical geometry in the OCID configuration does not result in significant differences in *T* and *RH* on the WP relative to the symmetrical CID configuration. The higher heat flux to the right side of the drift causes a steeper T and RH gradient to the right of the WP relative to the left side of the WP. The steeper *T* and *RH* gradients compensate for there being less low-K_{th} backfill to the right of the WP, resulting in roughly the same ΔT_{drift} and ΔRH_{drift} (which is best quantified by RH_{wp}/RH_{dw}) on both sides of the WP. Moreover, because *RH* in the rock at the right-side drift wall is somewhat lower than at the left-side drift wall, this compensates for any minor reduction in ΔT_{drift} and RH_{wp}/RH_{dw} that occurs to the right of the WP (relative to that on the left side). In general, the insulating effect of the low-K_{th} material on ΔT_{drift} and RH_{wp}/RH_{dw} is dependent on the total cross-sectional area of the low-K_{th} material, not on its precise geometric details. Consequently, there are minor differences in the *RH* histories on the WP for the OCID and CID WP configurations (as is shown by a comparison the last two columns of Table 1.10.6.4.3).

Table 1.10.5.4.2 summarizes *T* and *RH* on the WP for the four backfill configurations analyzed for the 0.47-MTU/m ACD rev 00 design (Fig. 1.10.5.4.1). Table 1.10.5.4.3 summarizes *T* and *RH* on the WP for the four backfill configurations analyzed for the 0.94-MTU/m line-load design (Fig. 1.10.5.4.2). The 0.94-MTU/m line-load design results in significantly higher *T* and lower *RH* on WPs than the 0.47-MTU/m ACD rev 00 design (as is shown by a comparison of Tables 1.10.5.4.2 and 1.10.5.4.3). As noted earlier, the two-dimensional model cannot accurately represent the three-dimensional character of heat flow around the ACD rev 00 WPs. In effect, the ACD rev 00 WPs function as point-heat sources, causing "spherical" heat flow in the drift and near-field rock. The two-dimensional model smears this heat flow into a uniform line-heat source that results in radial (or cylindrical) heat flow in the drift and near-field rock. On the other hand, the line-load design results in a uniform line-heat source and radial heat flow in the near field that is well represented by the two-dimensional model.

For the ACD rev 00 design, the calculations of *T* and *RH* on WPs using the two-dimensional model compare poorly with those calculated with the three-dimensional model (a comparison of Tables 1.10.5.1.3 and 1.10.5.2.3 with Table 1.10.5.4.2 illustrates this point). On the other hand, a comparison of Tables 1.10.5.3.5 and 1.10.5.3.10 (calculated with the three-dimensional model) with Table 1.10.5.4.3 (calculated with the two-dimensional model) illustrates how well the two-dimensional model can represent *T* and *RH* on the WPs in the line-load design. A comparison of the 26-yr-old PWR WP (fifth column in Table 1.10.3.5) with the first column in Table 1.10.5.4.3 indicates good agreement between the two models for the case without backfill. (Because 60% of the WPs are assumed to be 26-yr-old PWR WPs in the two-dimensional model, it is best to compare the 26-yr-old PWR WP in the three-dimensional model with the two-dimensional model.) The slightly drier condition calculated in the two-dimensional model is a result of the fact that all of the MTUs in the two-dimensional model come from spent nuclear fuel (SNF), while some of the MTUs in the three-dimensional model come from defense high-level waste (DHLW). In the three-dimensional model, 11.25% of the MTUs come from the DHLW WPs, with the remaining 88.75% coming from SNF WPs. Because the DHLW WPs hardly generate any heat, the LML of the significant heat-producing WPs in the three-dimensional model is 83.4 MTU/m for the 0.94-MTU/m line-load case. If one were to calculate a "composite" 26-yr-old WP, based on 40% of the WPs being BWR WPs and 60% being PWR WPs, in Table 1.10.5.3.5, the composite WP would be somewhat cooler and more humid than the composite 26-yr-old WP represented in Table 1.10.5.4.3. This is not surprising because the three-dimensional model has about 11% less decay heat (than the two-dimensional model) being generated per unit length of emplacement drift.

As discussed earlier, most of the drift-scale calculations have assumed that a sand or "sand-like" invert is used. For the ACD rev 00 design, *RH* on the upper and lower WP surfaces is shown for a sand invert and a TSw2 gravel invert for the full backfill configuration (Fig. 1.10.5.4.4) and the sloping-partial backfill configuration (Fig. 1.10.5.4.5). There is virtually no difference in *RH* on the upper WP surface, while the TSw2 gravel inverts cause more humid *RH* on the lower WP surface. The higher *RH*

associated with the TSw2 gravel invert is the result of greater wicking of moisture in the TSw2 gravel. Because rock dryout reduces *RH* in the near-field rock for the first 3000 yr, the effects of wicking in the TSw2 gravel do not begin until after 3000 yr. The effects of this wicking on increasing *RH* on the lower surface of the WP are mitigated by the fact that the 0.3-m gap between the underside of the WP cart and the drift floor is backfilled with sand, which has a much lesser tendency to wick moisture than the TSw2 gravel in the invert. The sand backfill separating the WP from the invert functions as a buffer that lessens the effect of more humid invert *RH* conditions on *RH* conditions on the WP. Had the WP been sitting directly on the drift floor, it would have more fully felt the effects of the more humid conditions in the invert.

Because the two-dimensional model artificially smears out the WP heat generation into a line-heat load, thereby reducing the apparent ΔT_{drift} and ΔRH_{drift} effects for the ACD rev 00 design, the differences in WP *RH* between the TSw2 gravel and sand invert cases are less than those calculated by the three-dimensional model. Table 1.10.5.4.4 shows *T* and *RH* on WPs calculated with the three-dimensional model for the ACD rev 00 design and a TSw2 gravel invert. Wicking (and more humid *RH*) in the TSw2 gravel invert causes a moderate increase in *RH* on WPs at later time (t > 5000 yr), relative to the case with a sand invert (a comparison of Tables 1.10.5.3.8 and 1.10.5.4.4 illustrates this point). Consequently, the time it takes to reach the *RH* = 90% threshold decreases by about 17–18% for SNF WPs. For the DHLW WPs, the time to reach the *RH* = 90% thresholds is decreased by 44–45%. For the hottest WPs (the 26-yr-old PWR and 10-yr-old PWR WPs), the time to reach *RH* = 65% is decreased by 30–48%.

Table 1.10.5.4.5 shows *T* and *RH* on WPs calculated with the three-dimensional model for the 1.11-MTU/m line-load design and a TSw2 gravel invert. A comparison of Table 1.10.5.2.4 and 1.10.5.4.5 indicates that wicking (and more humid *RH*) in the TSw2 gravel causes a moderate increase in *RH* on WPs at later time (t > 5000 yr), relative to the case with a sand invert (a comparison of Tables 1.10.5.3.9 and 1.10.5.4.5 illustrates this point). Consequently, the time it takes to reach the *RH* = 90% threshold decreases by about 19–20%.

When backfill is not used, the effect of greater wicking (and more humid *RH*) in the TSw2 gravel invert is to increase *RH* on both the upper and lower WP surfaces (Fig. 1.10.5.4.6). This occurs because there is no sand backfill "buffer" between the more humid TSw2 gravel invert and the WP. Because of the limitations of the two-dimensional model in representing the ΔT_{drift} and ΔRH_{drift} effects for the ACD rev 00 design, the differences in *RH* shown for the WPs in Figure 1.10.5.4.6 probably underrepresent the actual effects.

It should be noted that we have not discussed the consequences on *T* and *RH* on WPs of using an invert that is entirely (or partially) made up of concrete. With respect to *T* on WPs, K_{th} for intact concrete (i.e., unaltered by high *T* and very low *RH*) is closer to that of the near-field rock than that of the granular (sand or crushed TSw2) invert. Consequently, intact concrete would create less of a thermal-blanket effect beneath the WPs, which would moderately reduce ΔT_{drift} relative to the case with a granular invert. However, it is likely that because a concrete invert would be subjected to high *T* and very low *RH*, a certain degree of degradation (fracturing and spalling as a result of thermal stresses and dehydration) would occur that would decrease K_{th} for altered concrete. In its altered condition, K_{th} of the concrete may be closer to K_{th} of the granular invert materials rather than K_{th} of the near-field rock. Therefore, a concrete invert may not cause *T* on WPs to deviate significantly from what has been presented in Section 1.10. With respect to *RH* on WPs, it is likely that the wicking characteristics of a concrete invert would be closer to those of the crushed TSw2 gravel invert than those of the sand-like invert. The primary reason for this conclusion is that the pore sizes in concrete (which govern capillary wicking) will be much closer to those of the intragranular porosity of the TSw2 gravel than those of the intergranular porosity of the sand (recall that the quartz sand assumed in these calculations has no intragranular porosity). Moreover, as the concrete dehydrates, fine fractures in the concrete could also contribute to wicking. It should also be pointed out that strong osmotic gradients are likely to occur in the concrete as it rehydrates, which would also contribute to wicking.

Table 1.10.5.4.1. Percentages of the emplacement drift cross section occupied by the major EBS components for drift diameter = 5.5 m, WP diameter = 1.8 m, and alternative WP and backfill configurations.

WP configuration	Off-center (OCID)	Off-center (OCID)	Off-center (OCID)	Off-center (OCID)	Centered (CID)
Backfill configuration	No backfill	Sloping-partial	Level-partial	Full	Full
Unfilled drift	72.3%	35.4%	15.7%	0%	0%
Backfill	0%	36.9%	56.6%	72.3%	72.3%
WP	10.7%	10.7%	10.7%	10.7%	10.7%
WP cart	1.0%	1.0%	1.0%	1.0%	1.0%
Invert	16.0%	16.0%	16.0%	16.0%	16.0%
Filled drift	27.7%	64.6%	84.3%	100%	100%

Table 1.10.5.4.2. Temperature and relative humidity on upper surface of WP for AML = 83.4 MTU/acre, the ACD rev 00 design, drift spacing = 22.5 m, LML = 0.47 MTU/m, drift diameter = 5.5 m, TSw2 gravel invert, sand backfill at 100 yr with K_{th} = 0.6 W/m°C, WP emissivity = 0.3, and percolation flux = 0.3 mm/yr. Calulations were done with a two-dimensional model that averages the heat output from a mixture of 26-yr-old BWR WPs and 26-yr-old PWR WPs into a uniform line-heat load.

WP configuration	Off-center (OCID)	Off-center (OCID)	Off-center (OCID)	Off-center (OCID)
Backfill configuration	No backfill	Sloping-partial	Level-partial	Full
T_{peak} (t < 100 yr)	141°C	141°C	141°C	141°C
RH_{max} (t < 100 yr)	58%	58%	58%	58%
T_{peak} (t > 100 yr)	116°C	132°C	137°C	141°C
RH (t = 120 yr)	61%	40%	36%	32%
RH (t = 2000 yr)	79%	77%	74%	72%
RH (t = 10,000 yr)	96%	93%	92%	91%
$t(RH = 65\%)$	140 yr	1140 yr	1280 yr	1370 yr
$t(RH = 90\%)$	3310 yr	3770 yr	4190 yr	6620 yr

Table 1.10.5.4.3. Temperature and relative humidity on upper surface of WP for AML = 83.4 MTU/acre, a line-load design, drift spacing = 45 m, LML = 0.94 MTU/m, drift diameter = 5.5 m, sand invert, sand backfill at 100 yr with K_{th} = 0.6 W/m°C, WP emissivity = 0.3, and percolation flux = 0.3 mm/yr. Calulations were done with a two-dimensional model that averages the heat output from a mixture of 26-yr-old BWR WPs and 26-yr-old PWR WPs into a uniform line-heat load.

WP configuration	**Off-center (OCID)**	**Off-center (OCID)**	**Off-center (OCID)**	**Off-center (OCID)**	**Centered (CID)**
Backfill configuration	**No backfill**	**Sloping-partial**	**Level-partial**	**Full**	**Full**
T_{peak} (t < 100 yr)	199°C	199°C	199°C	199°C	224°C
RH_{max} (t < 100 yr)	20%	20%	20%	20%	15%
T_{peak} (t > 100 yr)	153°C	187°C	196°C	205°C	211°C
RH (t = 120 yr)	20%	10%	8%	6%	6%
RH (t = 2000 yr)	64%	56%	53%	52%	52%
RH (t = 10,000 yr)	91%	87%	85%	83%	81%
$t(RH$ = 65%)	2100 yr	3200 yr	3840 yr	4130 yr	3640 yr
$t(RH$ = 90%)	7140 yr	17,300 yr	20,920 yr	23,930 yr	27,710 yr

Table 1.10.5.4.4. Temperature and relative humidity on upper WP surface for AML = 83.4 MTU/acre, the ACD rev 00 design with LML = 0.46 MTU/m, drift spacing = 22.5 m, TSw2 gravel invert, full sand backfill at 100 yr with K_{th} = 0.6 W/m°C, drift diameter = 5.5 m, WP emissivity = 0.8, and percolation flux = 0.3 mm/yr.

Waste package type	Hanford Site DHLW	Savannah River Site DHLW	40-yr-old PWR MPC	26-yr-old BWR MPC	26-yr-old PWR MPC	10-yr-old PWR MPC
T_{peak} (t < 100 yr)	105°C	120°C	110°C	126°C	143°C	191°C
RH_{max} (t < 100 yr)	89%	64%	72%	52%	44%	26%
T_{peak} (t > 100 yr)	116°C	135°C	170°C	220°C	271°C	351°C
RH (t = 120 yr)	59%	36%	14%	5%	2%	1%
RH (t = 2000 yr)	98%	98%	72%	63%	50%	44%
RH (t = 10,000 yr)	99.7%	99.2%	85%	79%	70%	66%
$t(RH = 65\%)$	140* yr	200* yr	1540 yr	2120 yr	4920 yr	9540 yr
$t(RH = 90\%)$	520 yr	490 yr	21,440 yr	29,410 yr	45,440 yr	52,080 yr
* RH is never less than 65% prior to backfill						

Table 1.10.5.4.5. Temperature and relative humidity on upper WP surface for AML = 83.4 MTU/acre, a line-load design with a 0.1-m gap between WPs, LML = 1.11 MTU/m, drift spacing = 53.8 m, TSw3 gravel invert, full sand backfill at 100 yr with K_{th} = 0.6 W/m°C, drift diameter = 5.5 m, WP emissivity = 0.8, and percolation flux = 0.3 mm/yr.

Waste package type	Hanford Site DHLW	Savannah River Site DHLW	40-yr-old PWR MPC	26-yr-old BWR MPC	26-yr-old PWR MPC	10-yr-old PWR MPC
T_{peak} (t < 100 yr)	172°C	184°C	171°C	174°C	178°C	203°C
RH_{max} (t < 100 yr)	21%	20%	21%	21%	19%	16%
T_{peak} (t > 100 yr)	252°C	258°C	254°C	251°C	256°C	266°C
RH (t = 120 yr)	3%	3%	3%	3%	3%	2%
RH (t = 2000 yr)	51%	52%	49%	51%	48%	49%
RH (t = 10,000 yr)	80%	81%	78%	79%	76%	76%
$t(RH$ = 65%)	3970 yr	3770 yr	4270 yr	4010 yr	4540 yr	4560 yr
$t(RH$ = 90%)	26,760 yr	25,070 yr	29,330 yr	28,080 yr	31,910 yr	32,170 yr

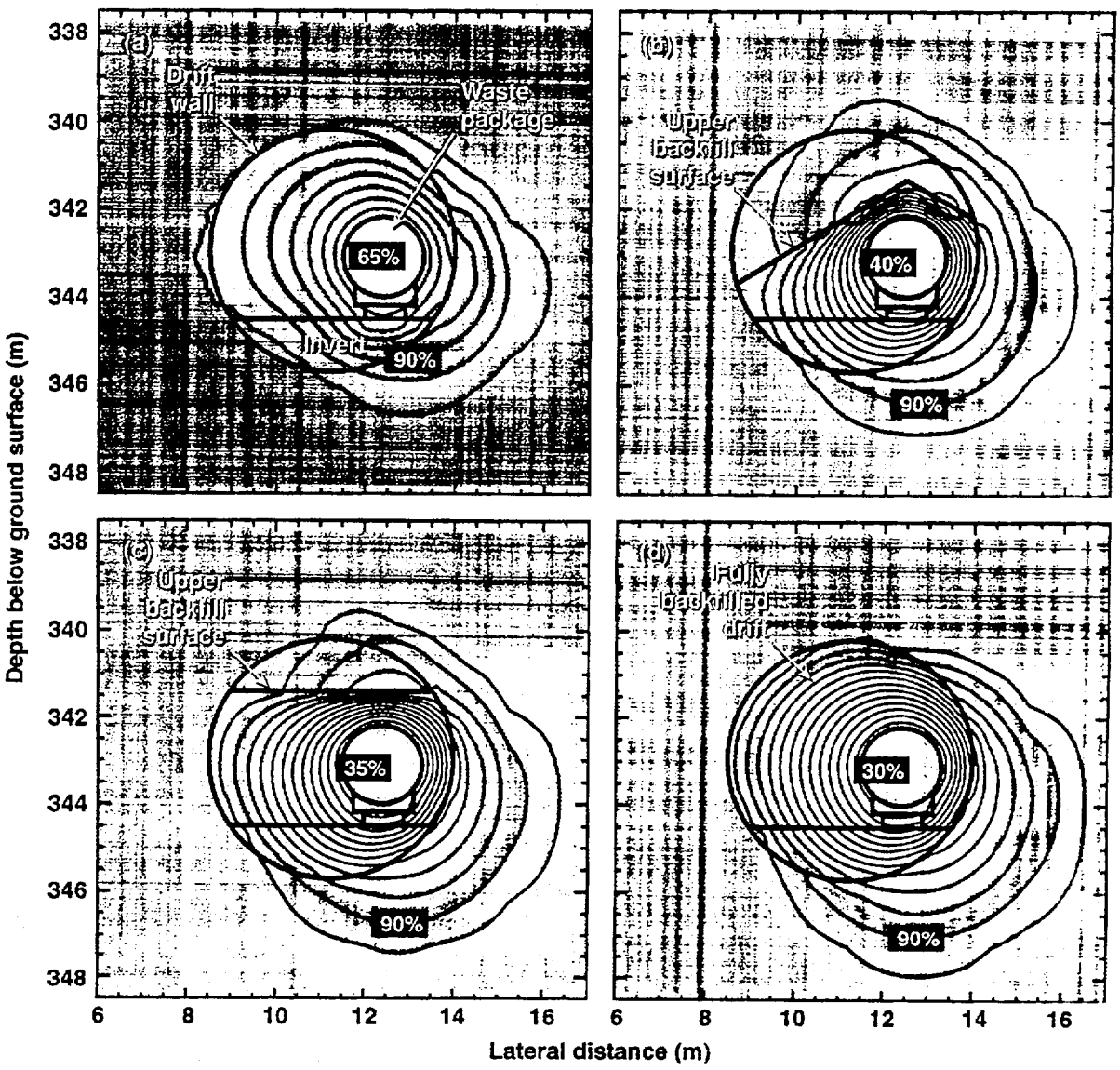

Figure 1.10.5.4.1. Near-field relative humidity *RH* distribution at t = 120 yr for the ACD rev 00 design, AML = 83.4 MTU/acre, LML = 0.46 MTU/m, drift spacing = 22.5 m, 40-darcy TSw2 tuff gravel invert, 10-darcy sand overfill at 100 yr with K_{th} = 0.6 W/m°C, off-center in-drift (OCID) emplacement, drift diameter = 5.5 m, WP emissivity = 0.3, and ambient percolation flux = 0.3 mm/yr. Calculations were done with a two-dimensional model that averages the heat output from a mixture of 26-yr-old BWR WPs and 26-yr-old PWR WPs into a uniform line-heat load. Three backfill configurations are shown: (a) no backfill, (b) sloping-partial backfill, (c) level-partial backfill, and (d) full backfill. The *RH* contour interval is 5%.

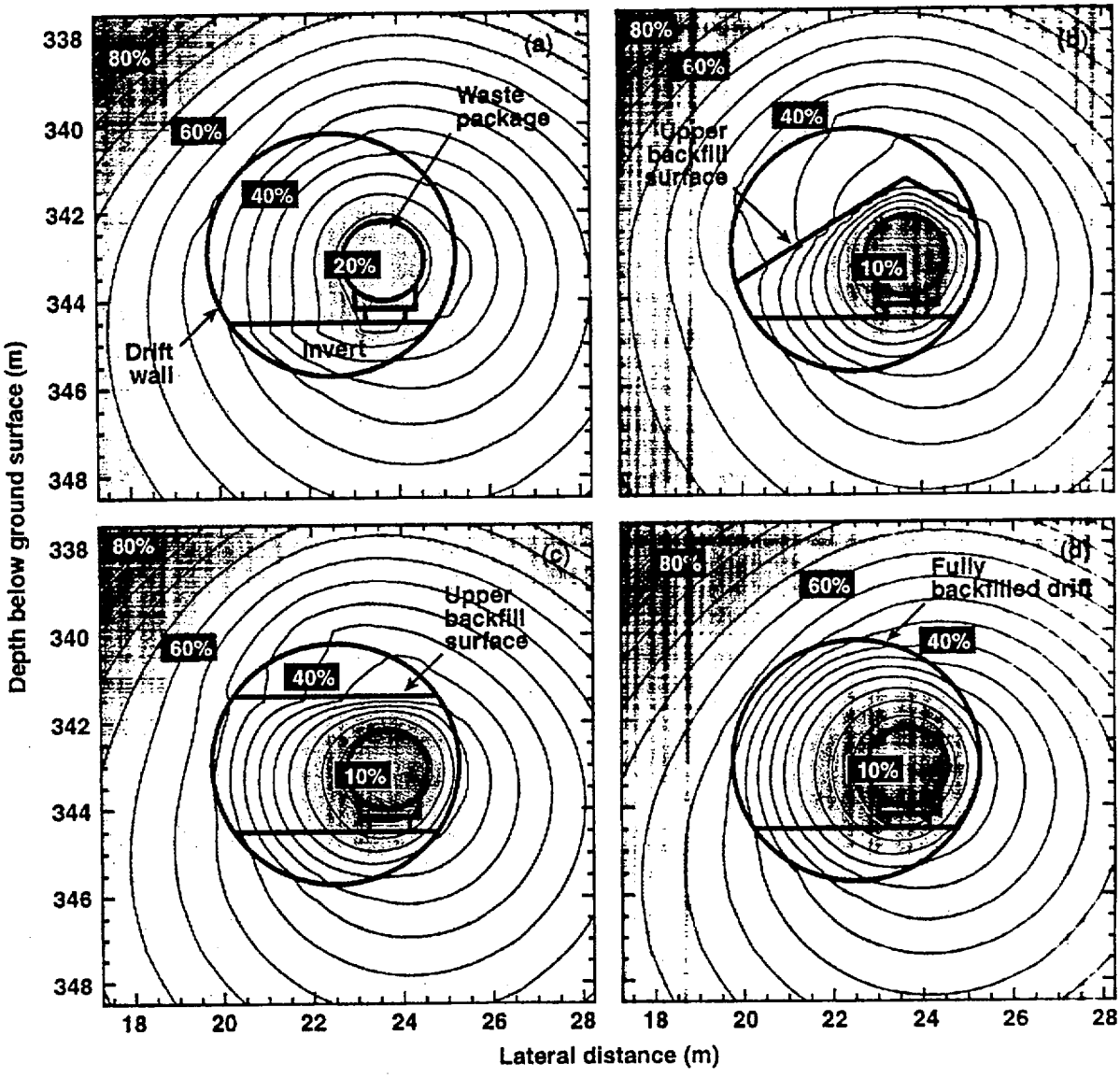

Figure 1.10.5.4.2. Near-field relative humidity *RH* distribution at t = 120 yr for the line-load design, AML = 83.4 MTU/acre, LML = 0.94 MTU/m, drift spacing = 45 m, 10-darcy sand invert, 10-darcy sand overfill at 100 yr with K_{th} = 0.6 W/m°C, off-center in-drift (OCID) emplacement, drift diameter = 5.5 m, WP emissivity = 0.3, and percolation flux = 0.3 mm/yr. Calculations were done with a two-dimensional model that averages the heat output from a mixture of 26-yr-old BWR WPs and 26-yr-old PWR WPs into a uniform line-heat load. Four backfill configurations are shown: (a) no backfill, (b) sloping-partial backfill, (c) level-partial backfill, and (d) full backfill. The *RH* contour interval is 5%.

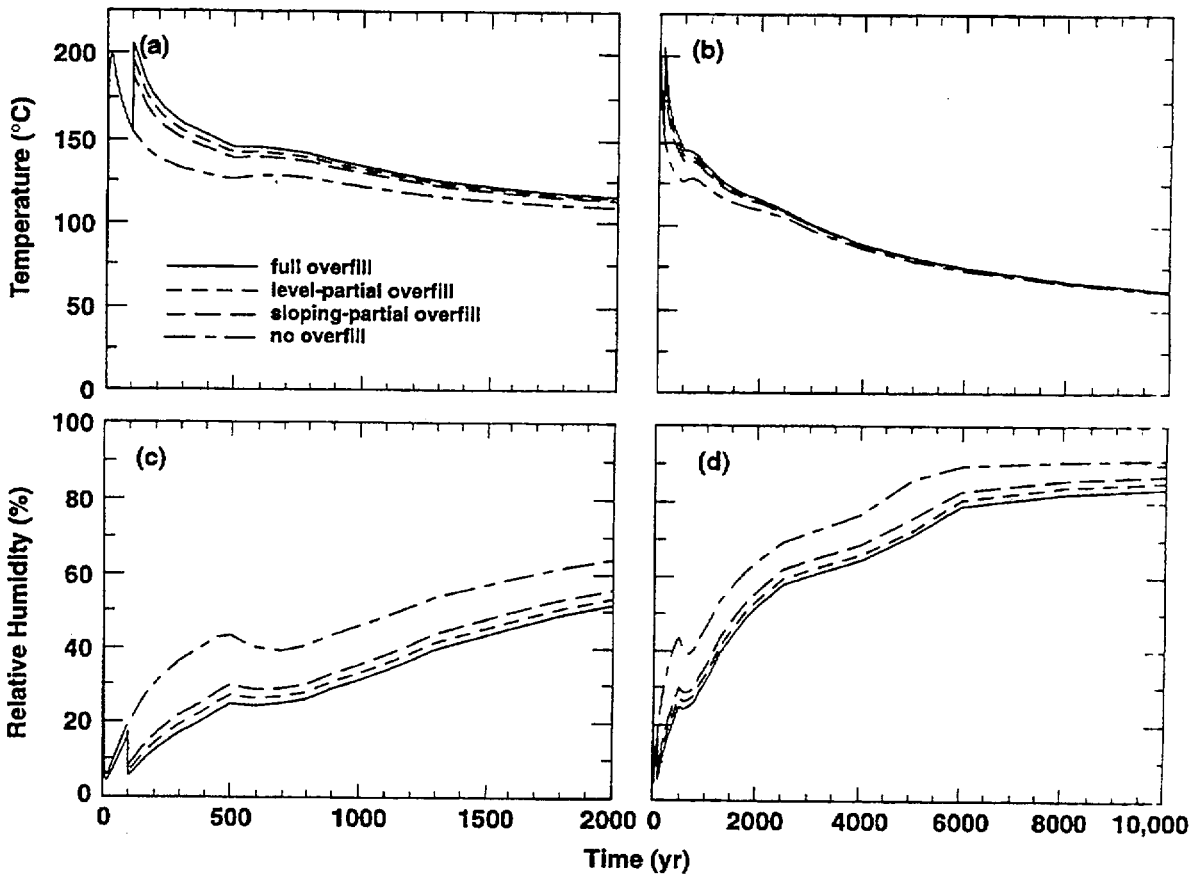

Figure 1.10.5.4.3. Temperature (a,b) and relative humidity (c,d) on upper surface of WP for AML = 83.4 MTU/acre, a line-load design, drift spacing = 45 m, LML = 0.94 MTU/m, off-center in-drift (OCID) emplacement, drift diameter = 5.5 m, sand invert, sand backfill at 100 yr with K_{th} = 0.6 W/m°C, WP emissivity = 0.3, and ambient percolation flux = 0.3 mm/yr. Curves are plotted for four backfill configurations: (1) no backfill, (2) sloping-partial backfill, (3) level-partial backfill, and (4) full backfill. Calculations were done with a two-dimensional model that averages the heat output from a mixture of 26-yr-old BWR WPs and 26-yr-old PWR WPs into a uniform line-heat load.

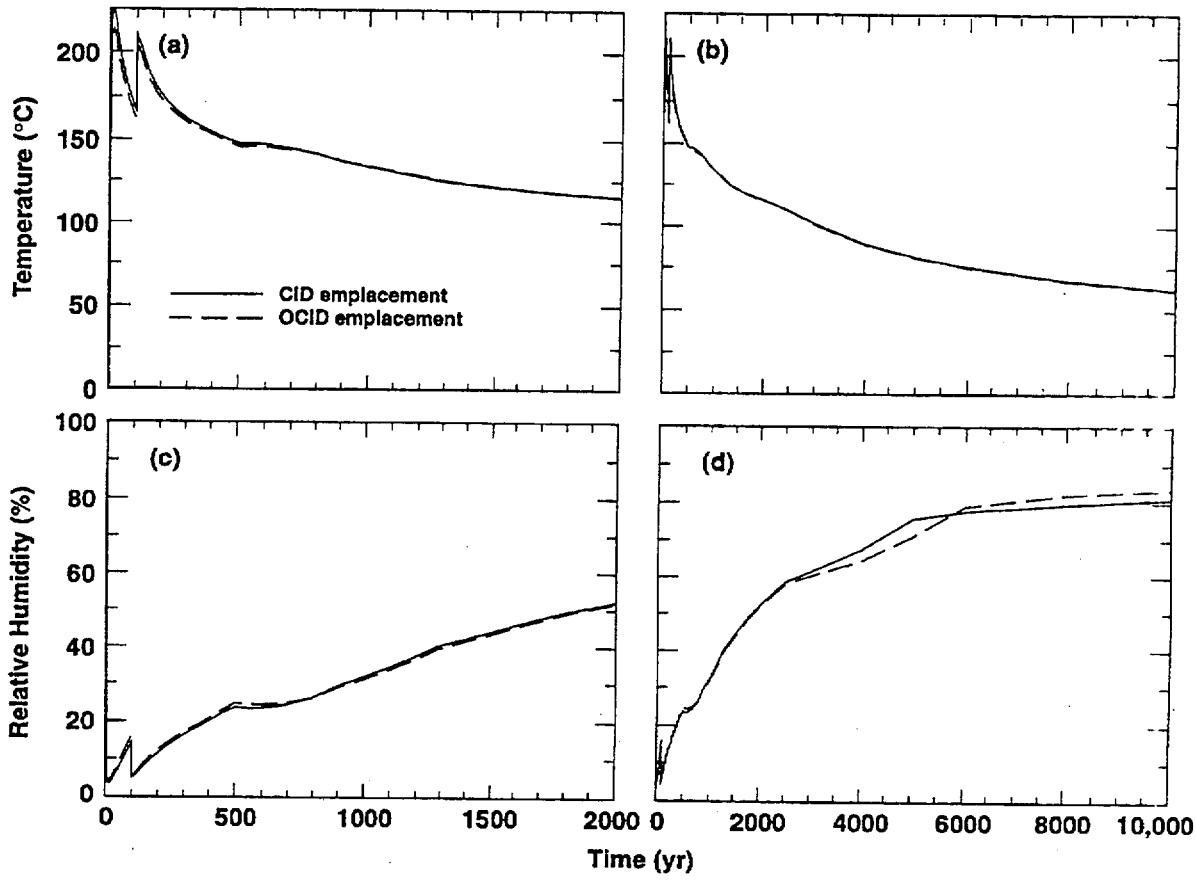

Figure 1.10.5.4.4. Temperature (a,b) and relative humidity (c,d) on upper surface of WP for AML = 83.4 MTU/acre, a line-load design, drift spacing = 45 m, LML = 0.94 MTU/m, off-center in-drift (OCID) emplacement, drift diameter = 5.5 m, sand invert, full sand backfill at 100 yr with K_{th} = 0.6 W/m°C, WP emissivity = 0.3, and ambient percolation flux = 0.3 mm/yr. Curves are plotted for two WP configurations: (1) off-center in-drift (OCID) emplacement and (2) centered in-drift (CID) emplacement. Calculations were done with a two-dimensional model that averages the heat output from a mixture of 26-yr-old BWR WPs and 26-yr-old PWR WPs into a uniform line-heat load.

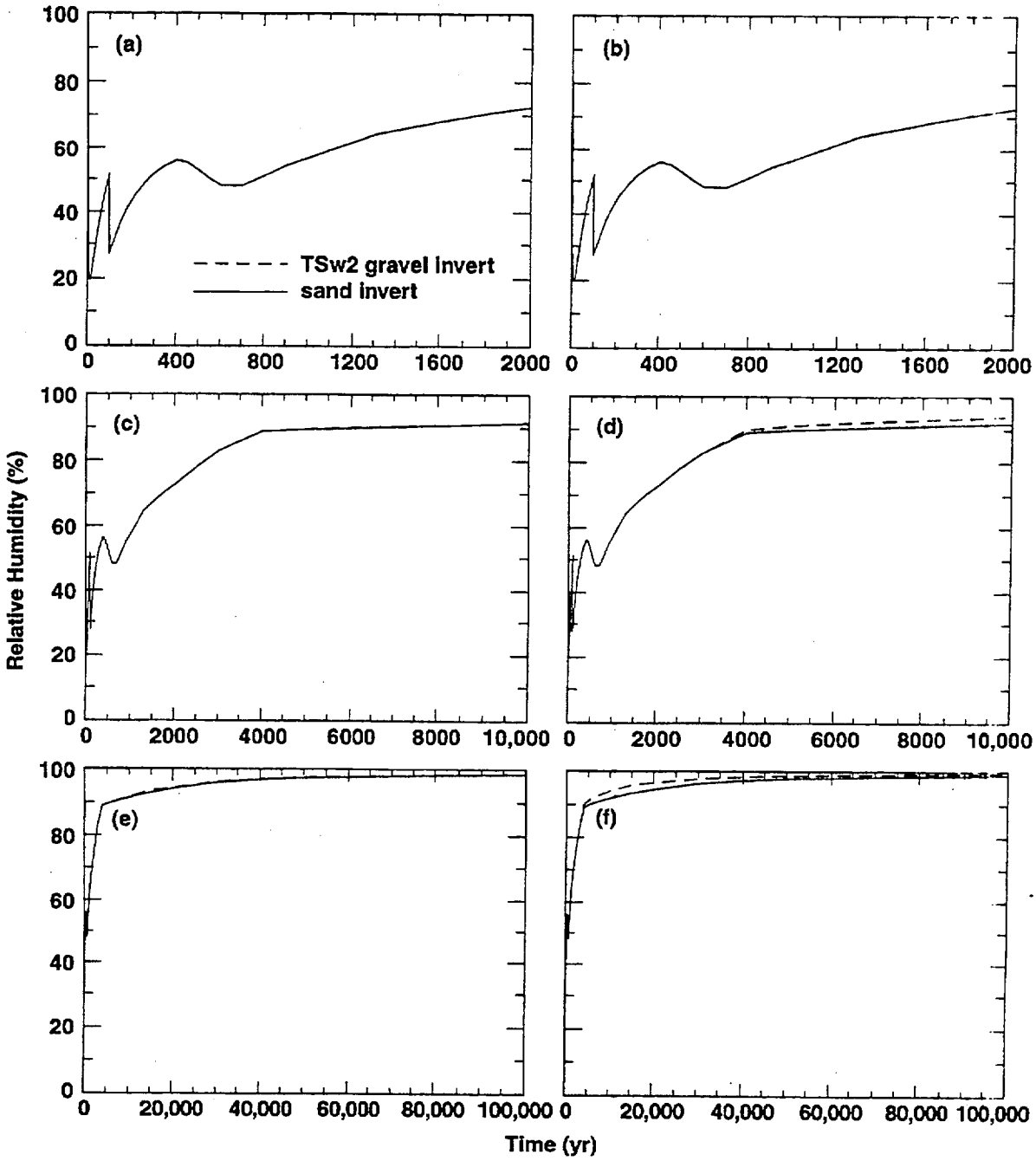

Figure 1.10.5.4.5. Relative humidity on upper WP surface (a,c,e) and on lower WP surface (b,d,f) for AML = 83.4 MTU/acre, the ACD rev 00 design, LML = 0.47 MTU/m, drift spacing = 45 m, off-center in-drift (OCID) emplacement, drift diameter = 5.5 m, full sand backfill at 100 yr with bulk permeability k_b = 10 darcy K_{th} = 0.6 W/m°C, WP emissivity = 0.3, and ambient percolation flux = 0.3 mm/yr. Curves are plotted for two invert types: (1) TSw2 gravel with k_b = 40 darcy and K_{th} = 0.6 W/m°C; and (2) sand with k_b = 10 darcy and K_{th} = 0.6 W/m°C. Calculations were done with a two-dimensional model that averages the heat output from a mixture of 26-yr-old BWR WPs and 26-yr-old PWR WPs into a uniform line-heat load.

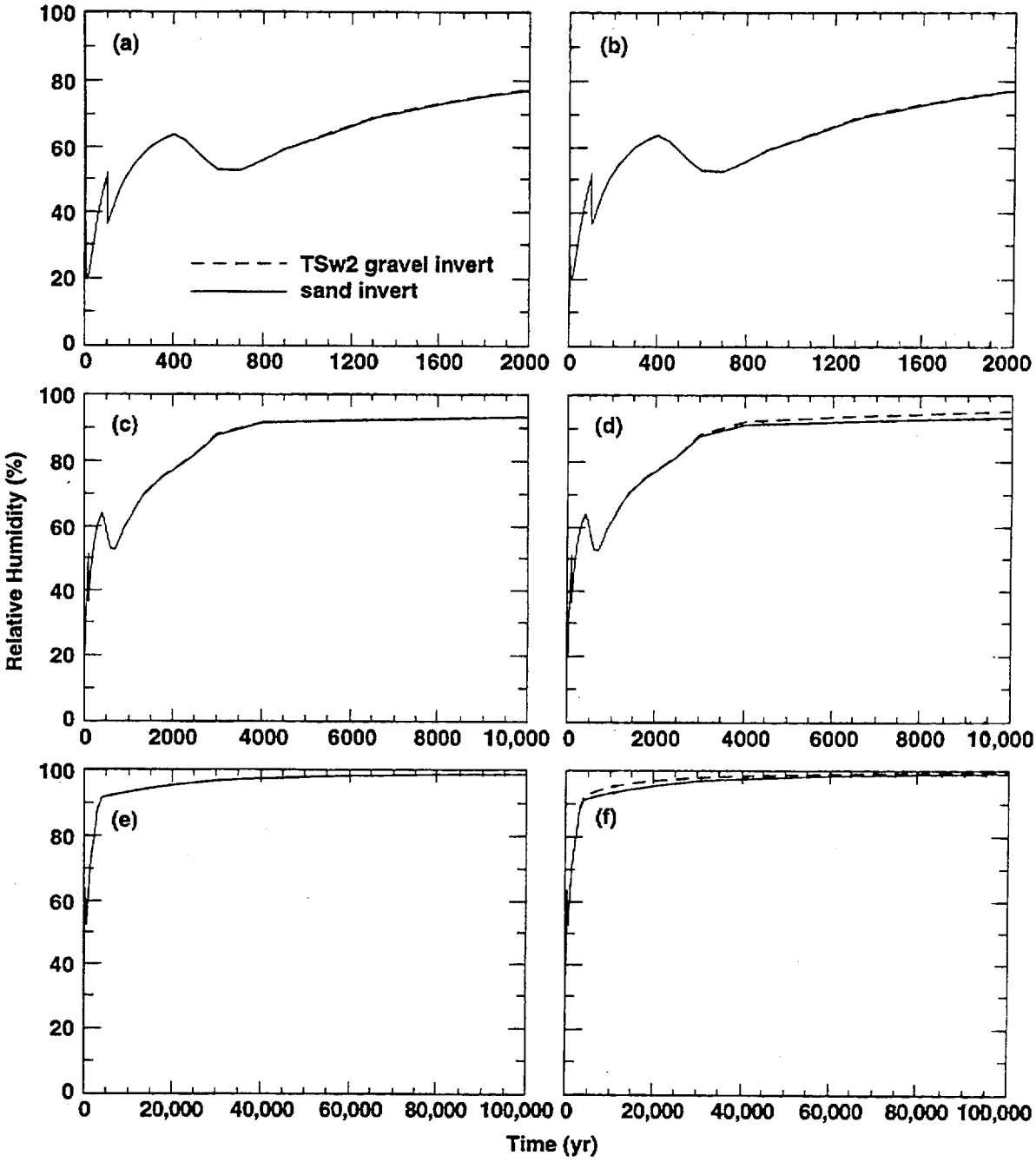

Figure 1.10.5.4.6. Relative humidity on upper WP surface (a,c,e) and on lower WP surface (b,d,f) for AML = 83.4 MTU/acre, the ACD rev 00 design, LML = 0.47 MTU/m, drift spacing = 45 m, off-center in-drift (OCID) emplacement, drift diameter = 5.5 m, sloping-partial sand backfill at 100 yr with bulk permeability k_b = 10 darcy K_{th} = 0.6 W/m°C, WP emissivity = 0.3, and ambient percolation flux = 0.3 mm/yr. Curves are plotted for two invert types: (1) TSw2 gravel with k_b = 40 darcy and K_{th} = 0.6 W/m°C; and (2) sand with k_b = 10 darcy and K_{th} = 0.6 W/m°C. Calculations were done with a two-dimensional model that averages the heat output from a mixture of 26-yr-old BWR WPs and 26-yr-old PWR WPs into a uniform line-heat load.

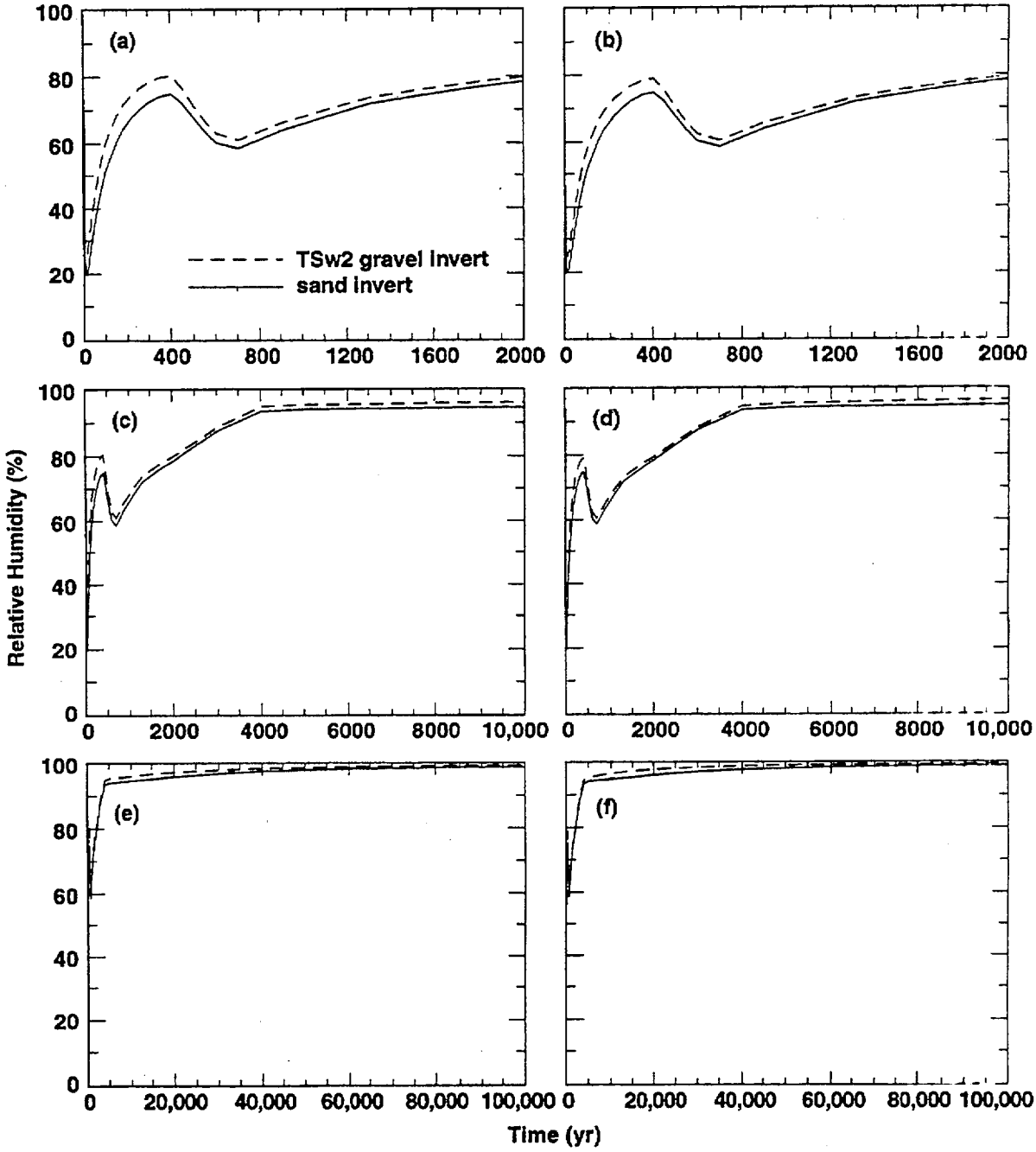

Figure 1.10.5.4.7. Relative humidity on upper WP surface (a,c,e) and on lower WP surface (b,d,f) for AML = 83.4 MTU/acre, the ACD rev 00 design, LML = 0.47 MTU/m, drift spacing = 45 m, off-center in-drift (OCID) emplacement, drift diameter = 5.5 m, no backfill, WP emissivity = 0.3, and ambient percolation flux = 0.3 mm/yr. Curves are plotted for two invert types: (1) TSw2 gravel with k_b = 40 darcy and K_{th} = 0.6 W/m°C; and (2) sand with k_b = 10 darcy and K_{th} = 0.6 W/m°C. Calculations were done with a two-dimensional model that averages the heat output from a mixture of 26-yr-old BWR WPs and 26-yr-old PWR WPs into a uniform line-heat load.

1.10.5.5 Influence of Engineered Backfill Thermal Conductivity

As discussed in the previous three sections, the key function of backfill (or overfill) is to cause a *RH* difference (ΔRH_{drift}) between the hotter (and drier) WP and cooler (and more humid) rock at the drift wall. The drift-ΔRH effect is quantified by the relationship $RH_{wp}/RH_{dw} = P_{sat}(T_{dw})/P_{sat}(T_{wp})$, which depends primarily on the temperature difference (ΔT_{drift}) between the WP and drift wall. Therefore, to function effectively, the backfill (and invert) must insulate the WP from the drift wall. To be effective insulators, heat transfer in the backfill and invert should be dominated by conduction (i.e., heat convection by heat pipes and buoyant gas-phase convection should not contribute significantly), and the thermal conductivity K_{th} of these materials should be less than that of the near-field rock. The insulating effect of the low-K_{th} (backfill and invert) materials primarily depends on the quantity of these materials and their K_{th}. The quantity of the backfill and invert depends on the diameter of the emplacement drift and the percentage of the drift that is occupied by the backfill and invert. Section 1.10.5.4 addresses the influence of the percentage of the drift that is filled on the drift-ΔRH effect. Section 1.10.5.6 addresses the influence of drift diameter on the drift-ΔRH effect. This section (Section 1.10.5.5) addresses the influence of invert and backfill K_{th}.

The three cases presented in this section are equivalent to the three primary cases presented in Section 1.10.5.2 (the ACD rev 00 case and the line-load cases with no backfill between the WPs), with the only difference being that K_{th} of the invert and backfill has been reduced by a factor of two. Backfill (and invert) K_{th} has virtually no effect on *T* and *RH* in the near-field rock (compare Tables 1.10.5.5.1 and 1.10.5.2.1). The lack of sensitivity stems from the fact that K_{th} has little effect on the spatial or temporal distribution of heat flux in the rock except that for the line-load cases, a reduction in K_{th} further improves thermal homogenization along the drift, causing *T* and *RH* in the near-field rock to be even more uniform.

Backfill (and invert) K_{th} strongly influences *T* and *RH* on WPs (compare Tables 1.10.5.5.2 and 1.10.5.2.2; also compare Figs. 1.10.5.5.1–1.10.5.5.3 with Figs. 1.10.5.2.5–1.10.5.2.8). For the ACD rev 00 design, a reduction in K_{th} increases the range in *T* and *RH* on WPs, while for the line-load cases, the range in *T* and *RH* is reduced. Because of the increase in ΔT_{drift}, the benefits of *RH* reduction on WPs can be substantially improved with the use of a low-K_{th} material in the invert and backfill.

A 50% reduction in K_{th} dramatically increases the peak WP temperature on the spent nuclear fuel (SNF) WPs for the ACD rev 00 design (compare Tables 1.10.5.5.3 and 1.10.5.2.3). The peak temperature on the 10-yr-old PWR WP increases by 197°C (from 353 to 550 °C), while the peak temperature on the Hanford Site DHLW WP increases by only 13°C (from 117 to 130°C). Consequently, the variability in *T* on the respective WPs increases from 236°C (for K_{th} = 0.6 W/m°C) to 420°C (for K_{th} = 0.3 W/m°C). Because of the large increase in ΔT_{drift} for the SNF WPs, the drift-ΔRH effect improves substantially for the SNF WPs, while the very small increase in ΔT_{drift} for the DHLW WPs means that the drift-ΔRH effect for the DHLW WPs continues to be negligible.

The reduction in K_{th} increases the temporal variability in the time required for WPs to reach the *RH* = 65% and 90% thresholds. For the K_{th} = 0.6 W/m°C case, the temporal variability for reaching the *RH* = 65% and 90% thresholds is a factor of 85 and 73, respectively (when all WPs are considered), while the temporal variability is a factor of 8.6 and 2.4 (when only the SNF WPs are considered). For the K_{th} = 0.3 W/m°C case, the temporal variability for reaching the *RH* = 65% and 90% thresholds is a factor of 152 and 114, respectively (when all WPs are considered), while the temporal variability is a factor of 4.9 and 2.2 (when only the SNF WPs are considered). Therefore, when only the SNF WPs are taken into account, a reduction in K_{th} causes a small reduction in the temporal variability for reaching the *RH* thresholds. A reduction in K_{th} (from 0.6 to 0.3 W/m°C) increases the time to reach the *RH* = 65% by a factor of 2.1 for the 10-yr-old PWR WP and by a factor of only 1.2 for the Hanford DHLW WP. A reduction in K_{th} (from 0.6 to 0.3 W/m°C) increases the time to reach *RH* = 90% by a factor of 1.7 for the 10-yr-old PWR WP and by a factor of only 1.2 for the Hanford DHLW WP.

For the 1.11-MTU/m line-load design, a 50% reduction in K_{th} increases the peak WP temperature on all WPs to an almost equal extent (compare Tables 1.10.5.5.4 and 1.10.5.2.4). The peak temperature on the 10-yr-old PWR WP increases by 96°C (from 266 to 362°C); the Hanford Site DHLW WP experiences a similar (100°C) increase in peak temperature (from 252 to 352°C). The fact that the Hanford Site DHLW WP experiences a slightly larger increase in peak temperature than the 10-yr-old PWR WP stems from the fact that a reduction in K_{th} causes a moderate improvement in thermal homogenization. This improvement comes from two effects:

Focused axial heat flow : Because of the higher impedance to radial heat flow in the K_{th} = 0.3 W/m°C case, compared to the K_{th} = 0.6 W/m°C case, decay heat has a greater tendency to flow axially along the line of WPs, seeking the location where the impedance to radial heat flow is least (in the vicinity of the coolest WPs). Backfill functions like a cylindrical "blanket" that focuses heat flow along the axis of the drift to the coolest WP locations. A reduction in K_{th} improves this heat flow focusing effect.

Enhanced axial thermal-radiative heat flow: Because the K_{th} = 0.3 W/m°C case substantially increases the WP temperatures, as compared to the K_{th} = 0.6 W/m°C case, the efficiency of thermal-radiative WP-to-WP heat transfer is improved. Thermal radiation is driven by the T^4 difference, where T is the absolute temperature (°K). Higher absolute temperatures result in more efficient thermal radiation. Therefore, one of the benefits of a low-K_{th} backfill (and a low-K_{th} invert) is the improvement of thermal homogenization along the drifts.

The combined effects of having the low-K_{th} backfill focus heat flow along the axis of the drifts and the higher WP temperatures improve radiative WP-to-WP heat transfer are to reduce the variability in T on the respective WPs.

Because of the large increase in ΔT_{drift} for all of the WPs in the 1.11-MTU/m line-load design, the drift-ΔRH effect improves substantially for all WPs (compare Tables 1.10.5.5.4 and 1.10.5.2.4). The improvement is somewhat larger for the coolest WPs than for the hottest WPs. A reduction in K_{th} (from 0.6 to 0.3 W/m°C) increases the time to reach the RH = 65% by a factor of 3.4 for the 10-yr-old PWR WP and by a factor of 3.5 for the Hanford DHLW WP. A reduction in K_{th} (from 0.6 to 0.3 W/m°C) increases the time to reach RH = 90% by a factor of 1.8 for the 10-yr-old PWR WP and by a factor of 2.0 for the Hanford DHLW WP. The larger improvement in RH history for the cooler WPs (than the hotter WPs) stems from the fact that a reduction in K_{th} enhances thermal homogenization between the WPs (as explained above), allowing the decay heat to be more equally shared by the WPs.

For the 0.94-MTU/m line-load design, a 50% reduction in K_{th} increases the peak WP temperature on all WPs to an almost equal extent (compare Tables 1.10.5.5.5 and 1.10.5.2.6). The peak temperature on the 10-yr-old PWR WP increases by 56°C (from 221 to 277°C); the Hanford Site DHLW WP experiences a similar (60°C) increase in peak temperature (from 194 to 254°C). The fact that the Hanford Site DHLW WP experiences a slightly larger increase in peak temperature than the 10-yr-old PWR WP stems from the fact that a reduction in K_{th} causes a moderate improvement in thermal homogenization.

Because of the large increase in ΔT_{drift} for all of the WPs in the 0.94-MTU/m line-load design, the drift-ΔRH effect improves substantially for all WPs (compare Tables 1.10.5.5.5 and 1.10.5.2.6). The improvement is somewhat larger for the coolest WPs than for the hottest WPs. A reduction in K_{th} (from 0.6 to 0.3 W/m°C) increases the time to reach the RH = 65% by a factor of 3.1 for the 10-yr-old PWR WP and by a factor of 1.7 for the Hanford DHLW WP. A reduction in K_{th} (from 0.6 to 0.3 W/m°C) increases the time to reach the RH = 90% by a factor of 1.6 for the 10-yr-old PWR WP and by a factor of 2.1 for the Hanford DHLW WP. The larger improvement in RH history for the hotter WPs (than the cooler WPs) is the opposite of the trend noted for the 1.11-MTU m line-load case (where the cooler WPs experienced a larger improvement than the hotter WPs). The cause of this difference is the larger gap separating the WPs (1.0 versus 0.1 m). Because the larger (1.0-m) gap causes less efficient radiative WP-to-WP heat transfer (than the 0.1-m gap), decay heat is not as equally shared in the 0.94-MTU/m case as it is in the 1.11-MTU/m case. Because thermal homogenization is somewhat less effective, the hotter WPs cannot "give up" as much of their excess decay heat to the cooler WPs (as in the case with 0.1-m gaps). It should be noted that thermal homogenization in the 0.94-MTU/m case is still far more effective than in the ACD rev 00 design.

Table 1.10.5.5.1. Temperature and relative humidity in rock at upper drift wall for AML = 83.4 MTU/acre, drift diameter = 5.5 m, sand invert, full sand backfill at 100 yr with K_{th} = 0.3 W/m°C, WP emissivity = 0.8, and percolation flux = 0.3 mm/yr.

Repository design	ACD rev 00	Line load	Line load
LML	0.46 MTU/m	1.11 MTU/m	0.94 MTU/m
Drift spacing	22.5 m	53.8 m	46.1 m
Gap between WPs	varies	0.1 m	1.0 m
T_{peak} (t < 100 yr)	100–168°C	163–187°C	141–176°C
RH_{max} (t < 100 yr)	35–98%	20–24%	26–35%
T_{peak} (t > 100 yr)	100–125°C	134–135°C	126–128°C
RH (t = 120 yr)	87–99.3%	31–32%	40–41%
RH (t = 2000 yr)	93–98%	78–78%	84–84%
RH (t = 10,000 yr)	99.8–99.8%	99.1–99.1%	99.4–99.4%

Table 1.10.5.5.2. Temperature and relative humidity on upper WP surface for AML = 83.4 MTU/acre, drift diameter = 5.5 m, sand invert, full sand backfill at 100 yr with K_{th} = 0.3 W/m°C, WP emissivity = 0.8, and percolation flux = 0.3 mm/yr.

Repository design	ACD rev 00	Line load	Line load
LML	0.46 MTU/m	1.11 MTU/m	0.94 MTU/m
Drift spacing	22.5 m	53.8 m	46.1 m
Gap between WPs	varies	0.1 m	1.0 m
T_{peak} (t < 100 yr)	107–195°C	175–206°C	153–200°C
RH_{max} (t < 100 yr)	24–86%	16–20%	19–30%
T_{peak} (t > 100 yr)	130–550°C	348–362°C	254–278°C
RH (t = 120 yr)	0.5–40%	1–1%	2–3%
RH (t = 2000 yr)	24–97%	34–37%	46–53%
RH (t = 10,000 yr)	40–99.5%	57–61%	65–75%
$t(RH$ = 65%)	190*–28,850 yr	12,700-15,590 yr	3420–8060 yr
$t(RH$ = 90%)	940–107,450 yr	55,030-72,440 yr	35,980–56,840 yr
* RH is never less than 65% prior to backfill			

Table 1.10.5.5.3. Temperature and relative humidity on upper WP surface for AML = 83.4 MTU/acre, the ACD design with LML = 0.46 MTU/m, drift spacing = 22.5 m,sand invert, full sand backfill at 100 yr with K_{th} = 0.3 W/m°C, drift diameter = 5.5 m, WP emissivity = 0.8, and percolation flux = 0.3 mm/yr.

Waste package type	Hanford Site DHLW	Savannah River Site DHLW	40-yr-old PWR MPC	26-yr-old BWR MPC	26-yr-old PWR MPC	10-yr-old PWR MPC
T_{peak} (t < 100 yr)	107°C	122°C	112°C	128°C	147°C	195°C
RH_{max} (t < 100 yr)	86%	61%	65%	49%	42%	24%
T_{peak} (t > 100 yr)	130°C	158°C	228°C	318°C	412°C	550°C
RH (t = 120 yr)	40%	20%	4%	1%	0.5%	0.5%
RH (t = 2000 yr)	97%	97%	55%	43%	30%	24%
RH (t = 10,000 yr)	99.5%	99%	69%	60%	46%	40%
$t(RH$ = 65%)	190 yr	270 yr	5890 yr	13,770 yr	24,800 yr	28,850 yr
$t(RH$ = 90%)	1120 yr	940 yr	48,280 yr	65,930 yr	99,310 yr	107,450 yr

Table 1.10.5.5.4. Temperature and relative humidity on upper WP surface for AML = 83.4 MTU/acre, a line-load design with a 0.1-m gap between WPs, LML = 1.11 MTU/m, drift spacing = 53.8 m,sand invert, full sand backfill at 100 yr with K_{th} = 0.3 W/m°C, drift diameter = 5.5 m, WP emissivity = 0.8, and percolation flux = 0.3 mm/yr.

Waste package type	Hanford Site DHLW	Savannah River Site DHLW	40-yr-old PWR MPC	26-yr-old BWR MPC	26-yr-old PWR MPC	10-yr-old PWR MPC
T_{peak} (t < 100 yr)	175°C	186°C	173°C	176°C	181°C	206°C
RH_{max} (t < 100 yr)	21%	20%	20%	20%	19%	16%
T_{peak} (t > 100 yr)	352°C	357°C	351°C	348°C	352°C	362°C
RH (t = 120 yr)	1%	1%	1%	1%	1%	1%
RH (t = 2000 yr)	35%	37%	34%	35%	34%	35%
RH (t = 10,000 yr)	60%	61%	58%	60%	57%	58%
$t(RH$ = 65%)	13,890 yr	12,700 yr	14,740 yr	13,870 yr	15,950 yr	15,560 yr
$t(RH$ = 90%)	65,030 yr	59,570 yr	68,370 yr	65,020 yr	72,440 yr	70,220 yr

Table 1.10.5.5.5. Temperature and relative humidity on upper WP surface for AML = 83.4 MTU/acre, a line-load design with a 1.0-m gap between WPs, LML = 0.94 MTU/m, drift spacing = 46.1 m,sand invert, full sand backfill at 100 yr with K_{th} = 0.3 W/m°C, drift diameter = 5.5 m, WP emissivity = 0.8, and percolation flux = 0.3 mm/yr.

Waste package type	Hanford Site DHLW	Savannah River Site DHLW	40-yr-old PWR MPC	26-yr-old BWR MPC	26-yr-old PWR MPC	10-yr-old PWR MPC
T_{peak} (t < 100 yr)	153°C	167°C	152°C	158°C	165°C	200°C
RH_{max} (t < 100 yr)	30%	28%	28%	27%	24%	19%
T_{peak} (t > 100 yr)	254°C	266°C	267°C	263°C	270°C	277°C
RH (t = 120 yr)	3%	2%	2%	2%	2%	2%
RH (t = 2000 yr)	53%	52%	48%	49%	46%	47%
RH (t = 10,000 yr)	75%	74%	69%	70%	65%	67%
$t(RH$ = 65%)	3420 yr	3590 yr	6550 yr	5100 yr	9610 yr	8060 yr
$t(RH$ = 90%)	35,980 yr	37,610 yr	48,260 yr	45,180 yr	56,840 yr	51,770 yr

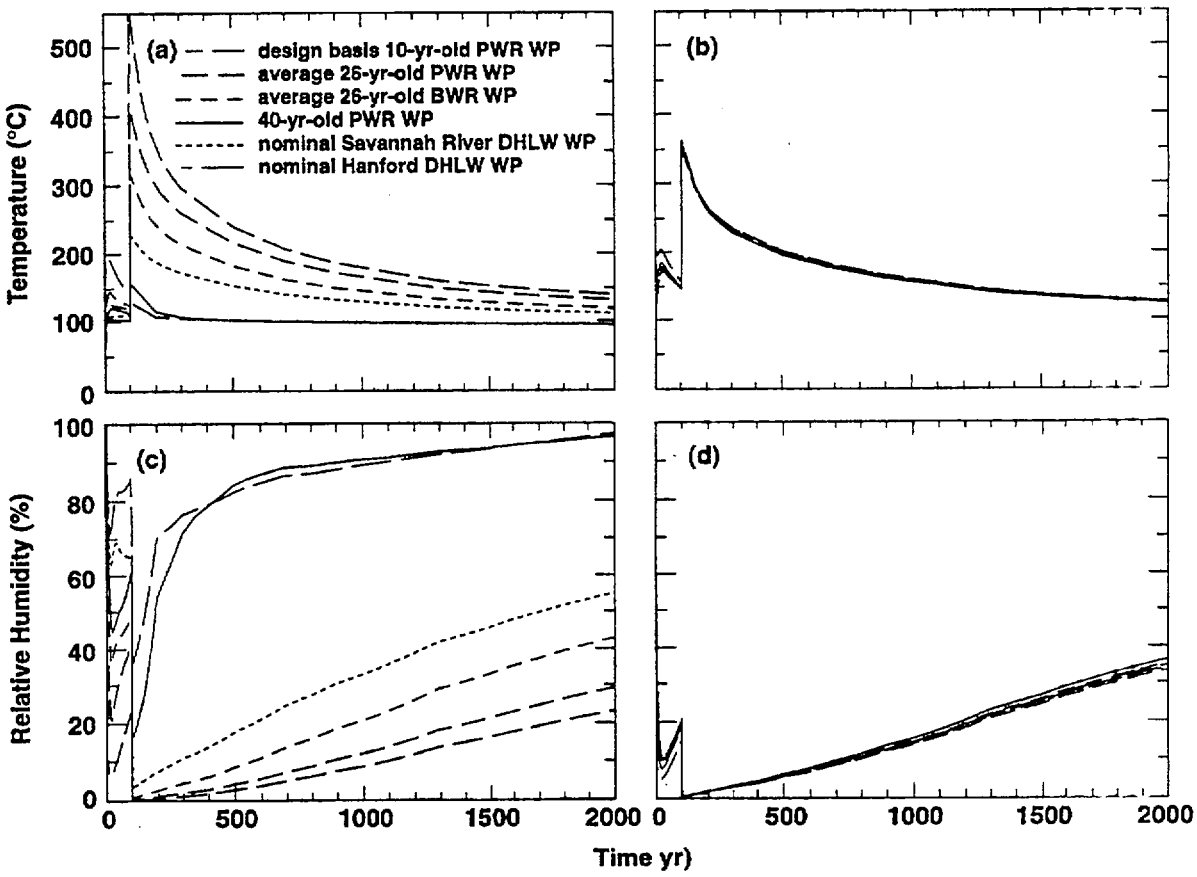

Figure 1.10.5.5.1. Temperature and relative humidity on upper surface of WP for AML = 83.4 MTU/acre, sand invert, full sand backfill at 100 yr with K_{th} = 0.3 W/m°C, drift diameter = 5.5 m, WP emissivity = 0.8, and ambient percolation flux = 0.3 mm/yr. Curves are plotted for the ACD rev 00 design (a,c) with LML = 0.46 MTU/m, and a line-load design (b,d) with a 0.1-m gap between WPs and LML = 1.11 MTU/m.

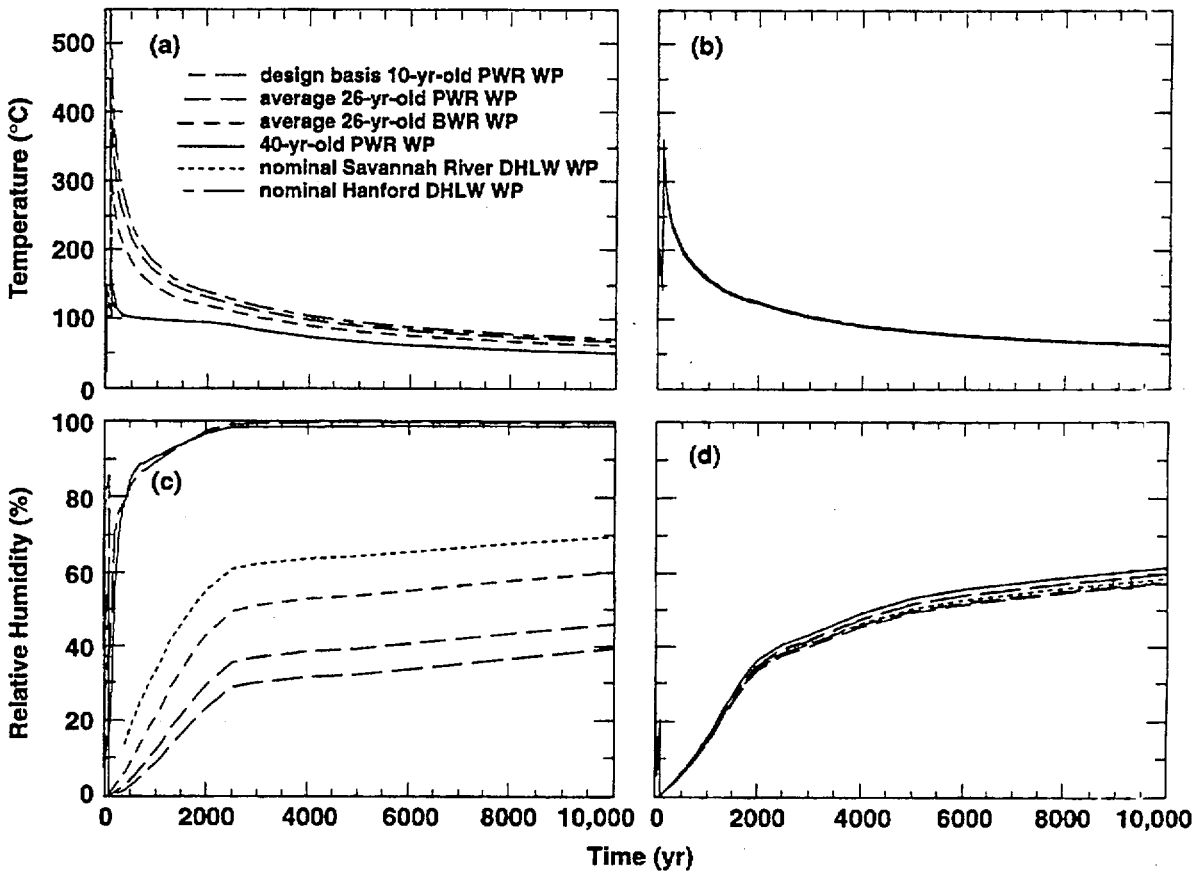

Figure 1.10.5.5.2. Temperature and relative humidity on upper surface of WP for AML = 83.4 MTU/acre, sand invert, full sand backfill at 100 yr with K_{th} = 0.3 W/m°C, drift diameter = 5.5 m, WP emissivity = 0.8, and ambient percolation flux = 0.3 mm/yr. Curves are plotted for the ACD rev 00 design (a,c) with LML = 0.46 MTU/m, and a line-load design (b,d) with a 0.1-m gap between WPs and LML = 1.11 MTU/m.

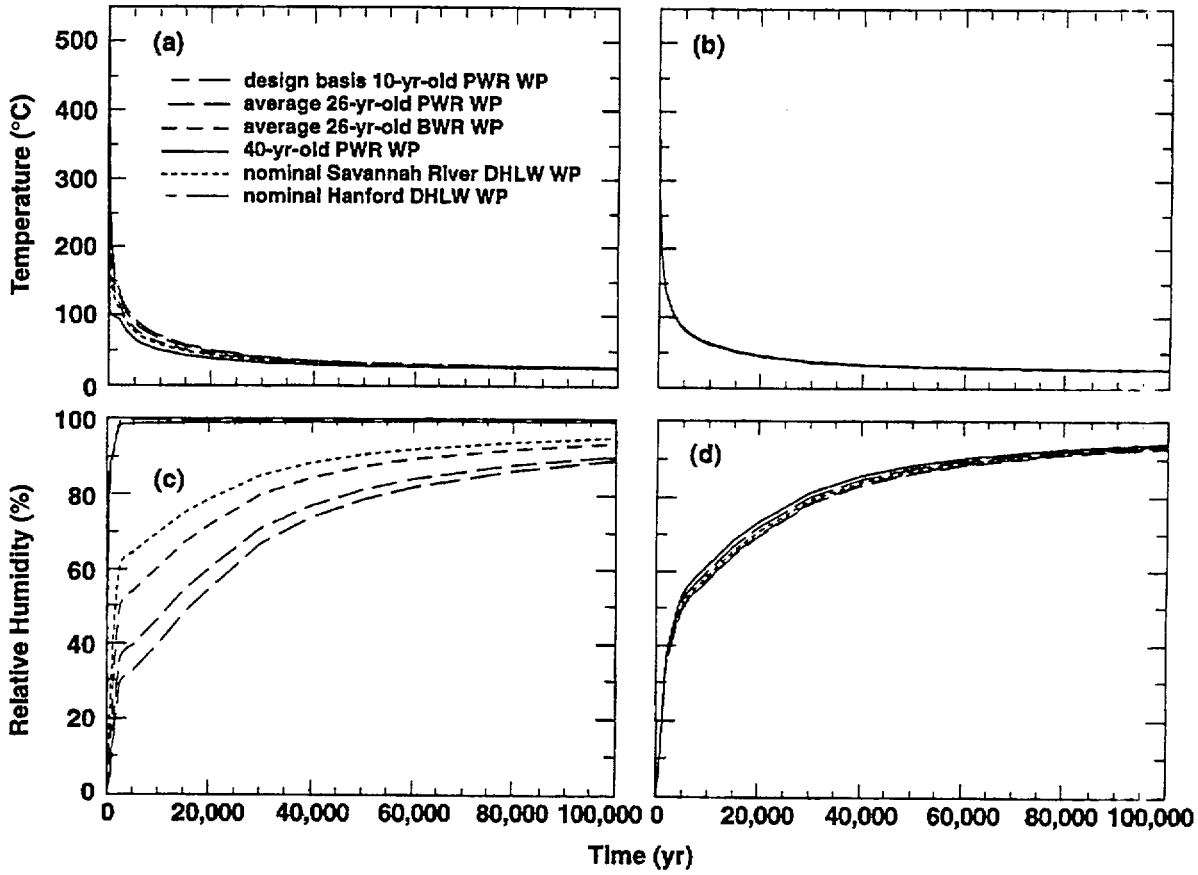

Figure 1.10.5.5.3. Temperature and relative humidity on upper surface of WP for AML = 83.4 MTU/acre, sand invert, full sand backfill at 100 yr with K_{th} = 0.3 W/m°C, drift diameter = 5.5 m, WP emissivity = 0.8, and ambient percolation flux = 0.3 mm/yr. Curves are plotted for the ACD rev 00 design (a,c) with LML = 0.46 MTU/m, and a line-load design (b,d) with a 0.1-m gap between WPs and LML = 1.11 MTU/m.

1.10.5.6 Influence of Drift Diameter

As discussed in the previous four sections, a key attribute of the EBS, affecting its ability to contribute to waste isolation, is to cause an *RH* difference (ΔRH_{drift}) between the hotter (and drier) WP and cooler (and more humid) rock at the drift wall. The drift-ΔRH effect is quantified by the relationship $RH_{wp}/RH_{dw} = P_{sat}(T_{dw})/P_{sat}(T_{wp})$, which depends primarily on the temperature difference (ΔT_{drift}) between the WP and drift wall. Therefore, the heat-transfer attributes of the EBS are key in determining the extent to which *RH* can be reduced on the WP. The primary heat transfer attributes of the EBS include:

Axial WP spacing: This determines the amount of decay heat generated per unit length of drift and how efficiently heat is transferred by thermal radiation from WP to WP. This also affects the temperature distribution along the drift wall (Sections 1.10.5.1-1.10.5.7 and Section 1.10.6).

WP heat generation distribution: This, together with the axial WP spacing, determines the spatial variability of the heat flux distribution along the axis of the emplacement drift. This also affects the temperature distribution along the drift wall (Sections 1.10.5.1-1.10.5.7 and Section 1.10.6).

WP emissivity: This determines how efficiently heat is transferred by thermal radiation between a WP and (1) the drift floor, (2) the drift wall, and (3) adjacent WPs (Section 1.10.5.3).

WP thermal conductivity: For the line-load design, this may influence the efficiency of thermal homogenization along the axis of the drift. Because radiative WP-to-WP heat transfer probably limits axial heat flow along the line of WPs, WP thermal conductivity (particularly for the range of possible values) is likely to be a minor factor.

WP cross-sectional area: The percentage of the WP cross section that can conduct heat. For the line-load design, this may influence the efficiency of thermal homogenization along the axis of the drift. Because radiative WP-to-WP heat transfer probably limits axial heat flow along the line of WPs, WP cross-sectional area is likely to be a minor factor.

Percentage of drift occupied by the invert and backfill: If sufficiently low-*K*th material is used, this determines what percentage of the drift can be devoted to insulating the WP from the near-field rock (Section 1.10.5.4).

Thermal conductivity of the invert and backfill: This, together with the drift diameter and percentage of the drift occupied by the invert and backfill, determines how effectively a WP can be insulated from the near-field rock (Section 1.10.5.5).

Drift diameter: This influences thermal radiative-heat transfer between the WP and drift wall. If backfill is used, it affects the volume of the insulation surrounding the WPs. This also affects the temperature distribution along the drift wall (Section 1.10.5.6).

This section (Section 1.10.5.6) addresses the influence of drift diameter on *T* and *RH* in the rock at the drift wall and on the WPs for the 1.11-MTU/m line-load design.

Figure 1.10.5.6.1 summarizes *T* and *RH* in the rock at the drift wall and on WPs for the 1.11-MTU/m line-load design and no backfill (also see Tables 1.10.5.6.1 and 1.10.5.6.2). Drift diameter influences: (1) the maximum peak drift-wall temperature, (2) the maximum peak WP temperature, (3) the range in peak drift-wall temperature, (4) the range in peak WP temperature, and (5) the intensity of local rock dryout and the magnitude of *RH* reduction in the rock around the drift (ΔRH_{rock}). Items 1 through 5 all increase with decreasing drift diameter as a result of the following effects:

Surface area exposed to heat flux from WPs: The drift-wall and floor surface areas (over which the heat flux from the WPs is distributed) decrease with drift diameter. A smaller drift diameter results in more intensive heating per unit area of drift-wall and floor surface, which results in generally higher drift-wall and WP temperatures (and higher peak drift-wall and peak WP

temperatures). The more intensive heating (and higher drift-wall temperatures) causes more locally intensive rock dryout around the drift.

Thermal radiation view factor between the WPs and drift wall: Thermal-radiative heat transfer between two finite surface elements depends on the view factor, which increases with the angles of incidence on the respective surfaces. If the drift diameter is large, then there is a longer interval along the drift wall for which the angles of incidence on the drift wall and WP are not shallow. Effectively, the WP can "see" a longer interval of the drift wall, which allows for more (axial) spreading of WP heat along the drift wall. If the drift diameter is small, then there is a shorter interval along the drift wall for which the angles of incidence are not shallow; consequently, there is less (axial) spreading of heat from the WP. Because increased thermal spreading facilitates more axial homogenization, there is less spatial variability in drift-wall and WP temperatures along the drift (and less variability in peak drift-wall and peak WP temperatures) with increasing drift diameter.

Time to reach peak drift-wall temperatures: The time to reach peak temperature decreases with decreasing drift diameter. Decreasing the time to reach peak temperature reduces the time during which thermal homogenization can develop. In general, a shorter time scale for thermal homogenization is associated with a shorter length scale for thermal homogenization. If the time and length scales for thermal homogenization are short, then the temperature at a given location of the drift wall (or a given WP) is influenced by conditions occurring over a shorter interval of the drift. If the time and length scales were longer (as they are with the larger drift diameter), then the temperature at any given location would be influenced by a longer interval of the drift. Consequently, a shorter time to peak temperature results in a larger range in peak temperatures and a greater maximum peak temperature for the drift wall and WPs (as compared to a case with a longer time to peak temperature).

The maximum peak drift-wall temperature is only 180°C for a drift diameter of 6.5 m, while it is 241 and 217°C for drift diameters of 3.0 and 4.0 m, respectively. The range in peak temperatures is only 22°C for a drift diameter of 6.5 m, while it is 44 and 38°C for drift diameters of 3.0 and 4.0 m, respectively. The maximum peak WP temperature is only 203°C for a drift diameter of 6.5 m, while it is 243 and 223°C for drift diameters of 3.0 and 4.0 m, respectively. The range in peak temperatures is 32°C for a drift diameter of 6.5 m, while it is 44 and 39°C for drift diameters of 3.0 and 4.0 m, respectively.

At 100 yr, *RH* in the rock is 23–27% for a drift diameter of 6.5 m, while it is only 12–17% and 15–20% for drift diameters of 3.0 and 4.0 m, respectively (Table 1.10.5.6.1). Differences in rock *RH* between the respective diameters decreases with time. At 2000 yr, *RH* in the rock is 78% for a drift diameter of 6.5 m, while it is 72–74% and 73–75% for drift diameters of 3.0 and 4.0 m, respectively. At 100 yr, *RH* on the WPs is 17–22% for a drift diameter of 6.5 m, while it is 12–16% and 14–19% for drift diameters of 3.0 and 4.0 m, respectively (Table 1.10.5.6.2). At 2000 yr, the range of *RH* on WPs is 74–76% for a drift diameter of 6.5 m, while it is 71–74% and 72–74% for drift diameters of 3.0 and 4.0 m, respectively. In general, *RH* on WPs is relatively insensitive to drift diameter for the cases with no backfill.

For the 1.11-MTU/m line-load cases with backfill, *T* in the rock at the drift wall is similar to the no-backfill cases, except that for drift diameters of 4.0, 5.5, and 6.5 m, *T* is lower for some period of time after the emplacement of backfill than in the no-backfill cases (Tables 1.10.5.6.3–1.10.5.6.7). Rock *RH* is similar to the no-backfill cases, except that *RH* is slightly more humid for drift diameters of 5.5 and 6.5 m than in the no-backfill cases.

After backfill is emplaced, *T* and *RH* on WPs is very sensitive to drift diameter. The drift diameter determines the thickness of the low-K_{th} invert/backfill material that insulates the WP from the near-field rock. A smaller drift diameter provides less insulation, resulting in a smaller temperature difference (ΔT_{drift}) between the WP and drift wall and a smaller drift-ΔRH effect. Peak WP temperatures at the time of backfill are 264–279°C, 223–239°C, and 203–219°C for drift diameters of 6.5, 4.0, and 3.0 m, respectively (Table 1.10.5.6.4). Accordingly, the time to reach the *RH* = 65% and 90% thresholds also decreases with drift diameter. The time to reach the *RH* = 65% threshold is 3760–5450 yr for the WPs in the case with a drift diameter of 6.5 m, which is a factor of 1.3–1.6 greater than the

times for the WPs in the case with a drift diameter of 4.0 m. The time to reach the *RH* = 90% threshold is 35,720–45,940 yr for the WPs in the case with a drift diameter of 6.5 m, which is a factor of 1.6–1.7 greater than the times for the WPs in the case with drift diameter of 4.0 m. The thickness of the backfill/invert insulation for the 6.5-m-diameter case is a factor of 1.6 greater than insulation thickness for the 4.0-m-diameter case. It would appear that the time to reach these *RH* thresholds roughly scales with the thickness of the invert/backfill insulation.

Table 1.10.5.6.1. Temperature and relative humidity in rock at upper drift wall for alternative drift diameters, AML = 83.4 MTU/acre, a line-load design with a 0.1-m gap between WPs, drift spacing = 53.8 m, LML = 1.11 MTU/m, sand invert, no backfill, WP emissivity = 0.8, and percolation flux = 0.3 mm/yr.

Drift diameter	**3.0 m**	**4.0 m**	**5.5 m**	**6.5 m**
T_{peak} (t < 100 yr)	197–241°C	179–217°C	161–184°C	158–180°C
RH_{max} (t < 100 yr)	12–17%	15–20%	21–25%	23–27%
T_{peak} (t > 100 yr)	156–170°C	150–161°C	142–148°C	140–145°C
RH (t = 120 yr)	14–19%	20–22%	23–27%	25–28%
RH (t = 2000 yr)	72–74%	73–75%	76–76%	78–78%
RH (t = 10,000 yr)	99.2–99.2%	99.1–99.1%	99.1–99.1%	99.2–99.2%

Table 1.10.5.6.2. Temperature and relative humidity on upper surface of WP for alternative drift diameters, AML = 83.4 MTU/acre, a line-load design with a 0.1-m gap between WPs, drift spacing = 53.8 m, LML = 1.11 MTU/m, sand invert, no backfill, WP emissivity = 0.8, and percolation flux = 0.3 mm/yr.

Drift diameter	**3.0 m**	**4.0 m**	**5.5 m**	**6.5 m**
T_{peak} (t < 100 yr)	199–243°C	184–223°C	172–203°C	171–203°C
RH_{max} (t < 100 yr)	12–16%	14–19%	16–21%	17–22%
T_{peak} (t > 100 yr)	158–171°C	152–164°C	147–158°C	146–156°C
RH (t = 120 yr)	14–18%	16–21%	18–23%	19–24%
RH (t = 2000 yr)	71–74%	72–74%	72–76%	74–76%
RH (t = 10,000 yr)	97–99.2%	96–98%	94–98%	94–97%
$t(RH$ = 65%)	1460–1660 yr	1460–1640 yr	1450–1620 yr	1320–1480 yr
$t(RH$ = 90%)	3580–3870 yr	3720–4170 yr	4030–4680 yr	3540–3920 yr

Table 1.10.5.6.3. Temperature and relative humidity in rock at upper drift wall for alternative drift diameters, AML = 83.4 MTU/acre, a line-load design with a 0.1-m gap between WPs, drift spacing = 53.8 m, LML = 1.11 MTU/m, sand invert, full sand backfill at 100 yr with K_{th} = 0.6 W/m°C, WP emissivity = 0.8, and percolation flux = 0.3 mm/yr.

Drift diameter	3.0 m	4.0 m	5.5 m	6.5 m
T_{peak} (t < 100 yr)	197–241°C	169–217°C	161–184°C	158–180°C
RH_{max} (t < 100 yr)	12–17%	15–20%	21–25%	23–27%
T_{peak} (t > 100 yr)	157–170°C	149–152°C	135–137°C	134–136°C
RH (t = 120 yr)	18–20%	21–22%	31–31%	32–33%
RH (t = 2000 yr)	74–74%	75–75%	78–78%	80–80%
RH (t = 10,000 yr)	99.2–99.2%	99.2–99.2%	99.1–99.1%	99.2–99.2%

Table 1.10.5.6.4. Temperature and relative humidity on upper surface of WP for alternative drift diameters, AML = 83.4 MTU/acre, a line-load design with a 0.1-m gap between WPs, drift spacing = 53.8 m, LML = 1.11 MTU/m, sand invert, full sand backfill at 100 yr with K_{th} = 0.6 W/m°C, WP emissivity = 0.8, and percolation flux = 0.3 mm/yr.

Drift diameter	**3.0 m**	**4.0 m**	**5.5 m**	**6.5 m**
T_{peak} (t < 100 yr)	199–243°C	184–222°C	172–203°C	169–203°C
RH_{max} (t < 100 yr)	12–16%	14–19%	16–21%	17–22%
T_{peak} (t > 100 yr)	203–219°C	223–239°C	250–266°C	264–279°C
RH (t = 120 yr)	5–7%	4–5%	2–3%	2–2%
RH (t = 2000 yr)	59–63%	55–59%	49–51%	48–51%
RH (t = 10,000 yr)	85–90%	79–84%	73–77%	70–75%
$t(RH = 65\%)$	2180–2710 yr	2820–3320 yr	3730–4600 yr	3760–5450 yr
$t(RH = 90\%)$	10,990–19,860 yr	20,640–29,360 yr	30,480-39,920 yr	35,720–45,940 yr

Table 1.10.5.6.5. Temperature and relative humidity on upper WP surface for AML = 83.4 MTU/acre, a line-load design with a 0.1-m gap between WPs, LML = 1.11 MTU/m, drift spacing = 53.8 m,sand invert, full sand backfill at 100 yr with K_{th} = 0.6 W/m°C, drift diameter = 3.0 m, WP emissivity = 0.8, and percolation flux = 0.3 mm/yr.

Waste package type	Hanford Site DHLW	Savannah River Site DHLW	40-yr-old PWR MPC	26-yr-old BWR MPC	26-yr-old PWR MPC	10-yr-old PWR MPC
T_{peak} (t < 100 yr)	199°C	220°C	196°C	200°C	208°C	243°C
RH_{max} (t < 100 yr)	16%	15%	16%	16%	14%	12%
T_{peak} (t > 100 yr)	203°C	208°C	205°C	203°C	209°C	219°C
RH (t = 120 yr)	7%	6%	7%	7%	6%	5%
RH (t = 2000 yr)	62%	63%	61%	62%	59%	59%
RH (t = 10,000 yr)	89%	90%	87%	88%	86%	85%
$t(RH$ = 65%)	2330 yr	2180 yr	2520 yr	2390 yr	2690 yr	2710 yr
$t(RH$ = 90%)	11,970 yr	10,990 yr	15,320 yr	14,600 yr	18,670 yr	19,860 yr

Table 1.10.5.6.6. Temperature and relative humidity on upper WP surface for AML = 83.4 MTU/acre, a line-load design with a 0.1-m gap between WPs, LML = 1.11 MTU/m, drift spacing = 53.8 m,sand invert, full sand backfill at 100 yr with K_{th} = 0.6 W/m°C, drift diameter = 4.0 m, WP emissivity = 0.8, and percolation flux = 0.3 mm/yr.

Waste package type	Hanford Site DHLW	Savannah River Site DHLW	40-yr-old PWR MPC	26-yr-old BWR MPC	26-yr-old PWR MPC	10-yr-old PWR MPC
T_{peak} (t < 100 yr)	184°C	201°C	182°C	185°C	191°C	223°C
RH_{max} (t < 100 yr)	19%	18%	18%	18%	17%	14%
T_{peak} (t > 100 yr)	224°C	230°C	226°C	223°C	229°C	239°C
RH (t = 120 yr)	5%	4%	4%	5%	4%	4%
RH (t = 2000 yr)	57%	59%	56%	57%	55%	55%
RH (t = 10,000 yr)	83%	84%	81%	82%	80%	79%
$t(RH$ = 65%)	3010 yr	2820 yr	3170 yr	3050 yr	3310 yr	3320 yr
$t(RH$ = 90%)	22,470 yr	20,640 yr	26,170 yr	24,940 yr	28,830 yr	29,360 yr

Table 1.10.5.6.7. Temperature and relative humidity on upper WP surface for AML = 83.4 MTU/acre, a line-load design with a 0.1-m gap between WPs, LML = 1.11 MTU/m, drift spacing = 53.8 m,sand invert, full sand backfill at 100 yr with K_{th} = 0.6 W/m°C, drift diameter = 6.5 m, WP emissivity = 0.8, and percolation flux = 0.3 mm/yr.

Waste package type	Hanford Site DHLW	Savannah River Site DHLW	40-yr-old PWR MPC	26-yr-old BWR MPC	26-yr-old PWR MPC	10-yr-old PWR MPC
T_{peak} (t < 100 yr)	171°C	183°C	169°C	173°C	177°C	203°C
RH_{max} (t < 100 yr)	22%	22%	22%	22%	20%	17%
T_{peak} (t > 100 yr)	265°C	271°C	267°C	264°C	269°C	279°C
RH (t = 120 yr)	2%	2%	2%	2%	2%	2%
RH (t = 2000 yr)	49%	51%	48%	49%	47%	48%
RH (t = 10,000 yr)	73%	75%	72%	73%	70%	70%
t(RH = 65%)	3960 yr	3760 yr	4590 yr	3990 yr	5380 yr	5450 yr
t(RH = 90%)	38,440 yr	35,720 yr	41,940 yr	39,500 yr	45,940 yr	45,390 yr

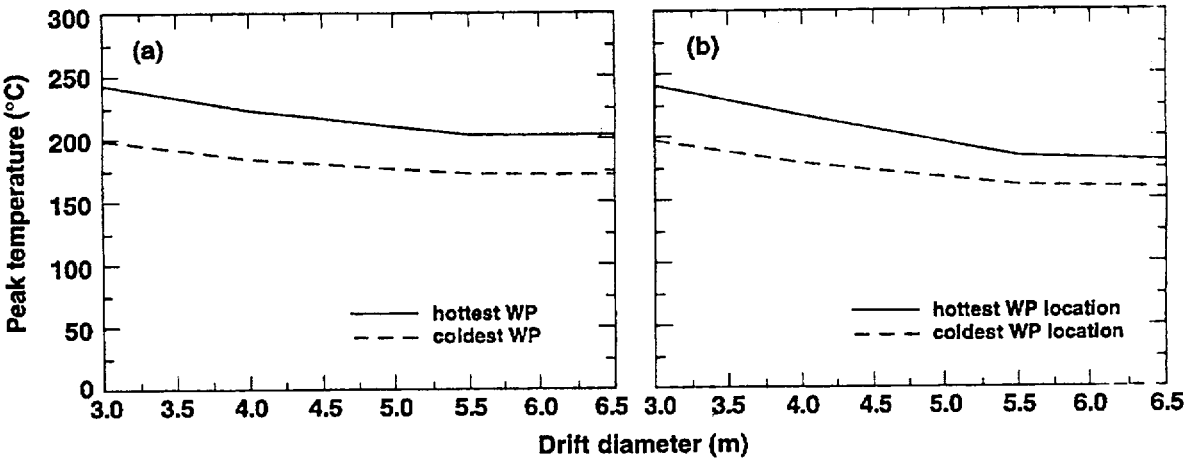

Figure 1.10.5.6.1. Peak temperature on upper WP surface (a) and in rock at upper drift wall (b) for AML = 83.4 MTU/acre, a line-load design with a 0.1-m gap between WPs, LML = 1.11 MTU/m, drift spacing = 53.8 m, sand invert, no backfill, drift diameter = 5.5 m, WP emissivity = 0.8, and ambient percolation flux = 0.3 mm/yr. Peak temperatures are given for the hottest and coldest WP and rock locations. Peak temperatures are also applicable to the pre-closure period for cases that are backfilled at 100 yr.

1.10.5.7 Influence of Areal Mass Loading

In the previous six sections (Sections 1.10.5.1–1.10.5.6), the analysis has focused exclusively on an AML of 83.4 MTU/acre, which is the "reference" thermal load that is assumed for the Advanced Conceptual Design (ACD) rev 00 [TRW, 1996]. Because decay-heat-driven thermal-hydrological flow strongly affects the distribution of temperature T, relative humidity RH, liquid-phase saturation, gas-phase flux, and liquid-phase flux in the altered zone, the near-field, and within the Engineered Barrier System (EBS) itself, it is important to understand how these effects are influenced by AML. Section 10.1 discusses the sensitivity of mountain-scale thermal-hydrological behavior to AML. This section (Section 1.10.5.7) addresses the sensitivity of drift-scale thermal-hydrological behavior to AML. Five AMLs are analyzed in this section, including 25, 45, 83.4, 100, and 120 MTU/acre for the 1.11-MTU/m line-load design (Fig. 1.10.1.1b); and 25, 45 and 83.4 MTU/acre for the 0.46-MTU/m ACD rev 00 axial WP spacing (Fig. 1.10.1.1a). All cases assume a drift diameter of 5.5 m, a WP emissivity of 0.8, and an ambient percolation flux of 0.3 mm/yr. The backfill cases assume that the invert and backfill are filled with a granular sand-like material with a thermal conductivity K_{th} of 0.6 W/m^{o}C. The no-backfill cases assume that the invert is filled with the same granular material. (Note that many of these calculations were conducted in support of the backfill systems study [Balady, 1996], which focused on the evaluation of granular invert and backfill materials.)

One of the primary motivations for considering lower AMLs is to attempt to minimize decay-heat-mobilized condensate flow, and thereby minimize the probability of adding to the liquid-phase seepage flux into the emplacement drifts. There are three ways that advective liquid-phase flux may contact a WP:

Drift seepage: Advective liquid-phase flow of water that enters the drift (and flows through the backfill) as a result of ambient percolation or decay-heat driven condensate flow. This can include episodic nonequilibrium fracture flow or a steady weep.

Wicking: Transport of moisture driven by matric potential gradients (i.e., capillary pressure gradients). This is primarily considered to be an advective liquid-phase transport process (called imbibition); however, binary gas-phase diffusion can also play a role. Because wicking can occur as two-phase flow, it does not necessarily require a continuous liquid phase.

Cold-trap effect: Axial vapor flow and condensation within the drift are driven by axial variations in T and P_V along the drift. Water vapor is transported (by gas-phase advection and diffusion) from areas of higher temperature and P_V to areas of lower temperature and P_V where it condenses, which causes RH to increase (even as high as 100%). Large condensation rates can arise in the cooler areas if the following three conditions are met: (1) high RH in the rock at the drift wall, (2) WP heat output varies substantially from WP to WP, and (3) WPs are thermally isolated from one another.

We start by examining how AML (and WP layout) influence liquid-phase seepage into the drifts (called drift seepage). As in the previous six sections, the model calculations in this section assume a uniform ambient percolation flux of 0.3 mm/yr. (Higher and lower values of ambient percolation flux are addressed in Section 1.10.6.) The calculations do not account for the possibility of episodic fracture flow; rather, ambient percolation flux is assumed to be steady. With the exception of the calculations presented in Section 1.10.7, the calculations do not explicitly represent nonequilibrium fracture flow. However, because an ambient percolation flux of 0.3 mm/yr causes the rock matrix to be fully saturated in the equivalent continuum model (ECM), there can be no matrix imbibition to slow the progress of fracture flow. Consequently, the ECM predicts that all of the decay-heat-mobilized liquid-phase flow will remain in the fractures, resulting in an extremely mobile liquid phase that is highly conducive to the generation of heat pipes and to condensate shedding around the boiling zones.

On the basis of the above-mentioned assumptions, the calculations indicate that the only WPs that could be contacted by advective liquid-phase flow are the DHLW WPs in the ACD rev 00 design. At early time, this contact is dominated by drift seepage; at later time, it is primarily generated by the

cold-trap effect. The calculations indicate (1) zero liquid-phase flux in the vicinity of all of the SNF WPs in the ACD rev 00 and (2) zero liquid-phase flux in the vicinity of all WPs (including the DHLW WPs) in the 0.94- and 1.11-MTU/m line-load designs. It should also be pointed out that had a crushed TSw2 tuff invert been assumed, and had the WPs been assumed to be in direct contact with the invert, then water could have contacted some of the WPs as the result of wicking in the invert. The sand invert does not allow the wicking of moisture to the WPs for an ambient percolation flux of 0.3 mm/yr.

The liquid-phase flux 5 m above the drift for the reference AML of 83.4 MTU/acre and an ambient percolation flux of 0.3 mm/yr is shown in Fig. 1.10.5.7.1. Although most of the WPs in the ACD rev 00 design were indicated to be unaffected by drift seepage (Fig. 1.10.5.1.1), the values of liquid-phase flux, only 5 m above the drift for all WP locations, are much larger than the ambient percolation flux for 2500 yr (Figs. 1.10.5.7.1a,c); the above-ambient liquid-phase fluxes occur immediately after WP emplacement for all but the 10-yr-old PWR WP location. For the 10-yr-old PWR WP location, the liquid-phase flux 5 m above the drift is much greater than ambient starting at 160 yr. From 25–150 yr, the liquid-phase flux above the 26-yr-old PWR WP is between 200 and 300 mm/yr. From 15–120 yr, the liquid-phase flux above the 26-yr-old BWR WP is between 200 and 370 mm/yr. There is also a high degree of spatial variability in the liquid-phase flux above the drift; at 100 yr, above the 26-yr-old PWR WP, the liquid-phase flux is 255 mm/yr, while less than 10 m away (above the Hanford Site DHLW WP), the liquid-phase flux is only 65 mm/yr. The liquid-phase flux 5 m above the drift continues to be much greater than the ambient percolation flux for 2500 yr; at 500 yr, the liquid-phase flux is 112, 99, 59, 37, 56, and 18 mm/yr above the 10-yr-old PWR, 26-yr-old PWR, 26-yr-old BWR, Savannah River DHLW and Hanford Site DHLW WPs, respectively, while at 2000 yr, these values are 22, 18, 11, 8, 2, and 2 mm/yr. The liquid-phase flux 5 m above the drift continues to be above ambient for 8000 yr (Fig. 1.10.5.7.1c).

For the 83.4-MTU/acre, 1.11-MTU/m line-load design, the spatial and temporal distribution of liquid-phase flux 5 m above the drifts is drastically different than in the ACD rev 00 design; the fluxes are much lower and much more spatially uniform above the line-load drift (Figs. 1.10.5.7.1b,d) than above the ACD rev 00 drift (Figs. 1.10.5.7.1a,c). For all WP locations of the line-load design, the liquid-phase flux 5 m above the drift is zero for 3000 yr, then it climbs to only 0.9–1 mm/yr at 4000 yr (when it peaks), which is followed by a uniform steady decline to 0.34–0.38 mm/yr at 6000 yr, and then to below the ambient percolation flux of 0.3 mm/yr at 8000 yr (Fig. 1.10.5.7.1d).

The temporal and spatial distribution of the liquid-phase flux 5 m above the drift for AML = 25 MTU/m (Fig. 1.10.5.7.2) is very different from that for AML = 83.4 MTU/acre. For the ACD rev 00 axial WP spacing, the liquid-phase flux continues to be highly spatially variable; however, the time during which decay-heat-driven liquid-phase fluxes are much greater than the ambient percolation flux is only 120 yr (Fig. 1.10.5.7.2a), as compared with 2000 yr for AML = 83 MTU/acre. For the 25-MTU/acre case with ACD rev 00 axial WP spacing, the liquid-phase flux continues to be above ambient for 2000 yr (Fig. 1.10.5.7.2c), as compared with 8000 yr for AML = 83.4 MTU/acre. Therefore, a reduction in AML from 83.4 to 25 MTU/acre reduces both the magnitude and duration of above-ambient liquid-phase fluxes above the drift for the ACD rev 00 axial WP spacing.

For the 25-MTU/acre, 1.11-MTU/m line-load case, the liquid-phase flux 5 m above the drift is zero for most of the first 100 yr (Fig. 1.10.5.7.2b). For the next 100 yr, the liquid-phase flux is well above ambient, peaking in the range 65–100 mm/yr (at about 120–150 yr). At 220 yr, the liquid-phase flux has declined to the range 0.4–1.7 mm/yr. All locations above the drift return to the ambient percolation flux at 2000 yr. As in the 83.4-MTU/m 1.11-MTU/m line-load case, the spatial distribution of liquid-phase flux is uniform. Therefore, a reduction in AML from 83.4 to 25 MTU/m reduces the duration of above-ambient liquid-phase fluxes above the emplacement drift for the 1.11-MTU/m line-load design; however, the reduction in AML causes an increase in the maximum peak liquid-phase fluxes above the drift during a relatively short interval of time (100–200 yr). The maximum peak liquid-phase fluxes for the 25-MTU/acre 1.11-MTU/m line-load design are less than for either the 25-MTU/acre or 83.4-MTU/acre designs with the ACD rev 00 axial WP spacing.

Tables 1.10.5.7.1 through 1.10.5.7.4 (and Table 1.10.5.1.3) summarize T and RH in the rock at the upper drift wall and on WPs for the cases with LML = 0.46-MTU/m , the ACD rev 00 axial WP, and no

backfill. For all of the AMLs, the ACD rev 00 axial WP spacing results in highly variable *T* and *RH* conditions along the drift. For AML = 25 and 45 MTU/acre, *RH* in the rock is nearly 100%, except at the hottest WP location (the 10-yr-old PWR WP). For AML = 45 MTU/acre, at 100 yr, *T* along much of the drift wall is near the boiling point (96°C). For AML = 25 MTU/acre, at 100 yr, *T* along the entire drift wall is below the boiling point.

For the 25- and 45-MTU/acre cases with the ACD rev 00 axial WP spacing, *RH* on average to cooler-than-average WPs is more humid than in the 83.4-MTU/acre case, while RH on the hotter-than-average WPs is less humid than in the 83-MTU/acre case (Tables 1.10.5.7.2–1.10.5.7.4 and 1.10.5.1.3). This trend is the result of two effects:

Rock dryout decreases with decreasing AML: Lower AMLs result in a smaller volume of rock being heated to superheated conditions (i.e., temperatures above the boiling point and drier-than-ambient *RH*).

Cold-trap effect: Heterogeneous heating conditions cause the axial flow of water vapor along the drift from hotter WPs to cooler WPs, where it condenses. This causes *RH* on the hotter WPs to be much drier (than the homogeneous heating case) and *RH* on the cooler WPs to be much more humid (than the homogeneous heating case).

The decrease in *RH* reduction in the rock with decreasing AML affects all WPs. As regards WP performance (which is degraded with higher *RH*), the cold-trap effect allows the hotter WP to benefit, at the expense of the cooler WPs. This is illustrated by the time to reach the *RH* = 90% threshold; for the 83.4-MTU/acre case, the coolest WP takes 1170 yr to reach this threshold, while the hottest WP takes 2330 yr (Table 1.10.5.7.2). For the 25- and 45-MTU/acre cases, the coolest WP never has a value of *RH* below 90%, while the time for the hottest WP to reach the *RH* = 90% threshold is 9100 and 11,600 yr for the 45- and 25-MTU/acre cases, respectively (Table 1.10.5.7.2). Not only are the coolest WPs never drier than 90%, but the cold-trap effect drives enough vapor and condensation flux onto the surfaces of the coolest WPs to cause their *RH* = 100% on the WP surface for a considerable period of time. For the 45-MTU/acre 0.46-MTU/m case, *RH* = 100% for 2000 and 3000 yr on the Hanford Site and Savannah River Site DHLW WPs, respectively. For the 25-MTU/acre 0.46-MTU/m case, *RH* = 100% for 50 and 1100 yr on the Hanford Site and Savannah River Site DHLW WPs, respectively. Although the WPs are thermally isolated from one another, they are not thermal-hydrologically isolated from one another for the ACD rev 00 axial WP spacing.

Table 1.10.5.7.5 summarizes *T* and *RH* in the rock at the upper drift wall for the five alternative AMLs considered for the 1.11-MTU/acre line-load design with no backfill. The maximum peak drift-wall temperature is only moderately sensitive to AML (varying by only 15°C over this AML range). The insensitivity of maximum peak drift-wall temperature stems from two factors: (1) the drift spacing is relatively wide for all of these cases and (2) the peak drift-wall temperature occurs before thermal interference has developed with the next drift. In other words, peak drift-wall temperatures occur before the thermal field around that drift is even aware of the presence of the neighboring drifts. The 180-m drift spacing in the 25-MTU/acre case and the 100-m drift spacing in the 45-MTU/m case are effectively infinite when drift-wall temperatures peak; this fact is evidenced by both cases having exactly the same range in peak drift-wall temperature (143–172°C). Therefore, the peak-drift wall temperature is effectively that of a single drift in an infinite domain. The range in maximum drift-wall temperatures at 100 yr is much greater (44°C) because there has been sufficient time for the thermal fields around the respective drifts to interfere with each other (Table 1.10.5.7.5).

The extent to which *RH* reduction in the rock (ΔRH_{rock}) contributes to *RH* reduction on WPs varies significantly for the range of AMLs considered. For all AMLs considered, rock dryout provides (to a varying degree) beneficial *RH* reduction on WPs. One very important fact is that rock dryout and *RH* reduction are provided during early time when large condensate fluxes in the near-field rock could possibly result in large drift seepage fluxes (as were seen to occur with the ACD rev 00 design). In effect, for the 1.11-MTU/m line-load design, rock dryout around the drift, even for the 25-MTU/acre case, is sufficient to provide valuable rock dryout, which prevents the large condensate fluxes from entering the drift. The uniform, cylindrical shape of the superheated zone facilitates condensate shedding in the rock pillar, rather than into the drift. Consequently, during the first 100 yr, the liquid-phase flux 5 m

above the drift is zero for the 25-MTU/acre line-load design. For the ACD rev 00 axial WP spacing, the LML is too small to generate any rock dryout; consequently, the large condensate fluxes that occur in the near-field rock at early time result in seepage flux into the emplacement drift.

Table 1.10.5.7.5 shows that rock dryout becomes more uniform with increasing AML. The cause of this trend was discussed in earlier sections. The primary effect is that radiative WP-to-WP heat transfer becomes more efficient with increasing absolute temperature. Because WP temperature increases with AML and because WP-to-WP thermal-radiative heat transfer becomes more efficient with increasing WP temperature, thermal homogenization improves with AML. The improvement of thermal homogenization is also evidenced by the range of WP *RH* and the temporal variability in the time to reach the *RH* = 90% threshold. The temporal variability (from the hottest to the coolest WP) to reach the *RH* = 90% threshold is 7, 8, and 16% for AMLs of 120, 100, and 83.4 MTU/acre, respectively (Table 1.10.5.7.6). The temporal variability (from the hottest to the coolest WP) to reach the *RH* = 90% threshold is a factor of 3.2 and 11.7 for AMLs of 45 and 25 MTU/acre, respectively (Table 1.10.5.7.6). Therefore, the temporal variability in *RH* performance on WPs decreases with increasing AML. Tables 1.10.5.7.7–1.10.5.7.10 and Table 1.10.5.1.4 summarize *T* and *RH* on all of the WPs in the various AML cases using the 1.11-MTU/m line-load design.

While the contribution of ΔRH_{rock} to *RH* reduction on WPs decreases with AML, the magnitude of the drift-ΔRH effect increases modestly with decreasing AML. The drift-ΔRH effect depends on the temperature difference (ΔT_{drift}) between the WP and the drift wall; ΔT_{drift} increases with decreasing AML (Fig. 1.10.5.7.3). The range of ΔT_{drift} increases with decreasing AML (Fig. 1.10.5.7.4) as a result of the less efficient radiative WP-to-WP heat transfer (and less effective thermal homogenization) that occurs at lower absolute temperatures.

Figure 1.10.5.7.5 illustrates how the temporal extent of rock dryout falls into three categories. For the low AML cases, ΔRH_{rock} contributes to *RH* reduction on WPs for a relatively short period of time; for AML = 25 MTU/acre, ΔRH_{rock} is significant for about 200 yr; for AML = 45 MTU/acre, ΔRH_{rock} is significant for about 200 yr. The time that ΔRH_{rock} no longer contributes to *RH* reduction on WPs is indicated by the break in slope for the WP *RH* curves (Fig. 1.10.5.7.5). For the 83.4-MTU/acre case, ΔRH_{rock} contributes to *RH* reduction on WPs for 5000 yr. For the high AML cases (100 and 120 MTU/acre), ΔRH_{rock} contributes to *RH* reduction on WPs for 8000 yr. It is important to point out that because these calculations do not account for edge-cooling/rewetting effects, they are not directly applicable to repository locations that are close enough to the repository edge to be influenced by these effects. It is possible, as shown in Section 1.10.6, to combine the drift-scale model results with results from a mountain-scale model to develop *T* and *RH* curves that are reasonably applicable to the repository edge (or to any location in the repository).

Table 1.10.5.7.11 summarizes *T* and *RH* in the rock at the upper drift wall for the three alternative AMLs considered for LML = 0.46-MTU/m, the ACD rev 00 axial WP, and backfill at 100 yr. For *T* and *RH* in the near-field rock, the above-mentioned observations for the no-backfill cases also apply to the backfill cases, with the minor exception that after backfill, *T* along the drift wall is slightly cooler, and *RH* along the drift wall slightly more humid than in the no-backfill cases (compare Tables 1.10.5.7.1 and 1.10.5.7.11).

Tables 1.10.5.7.12–1.10.5.7.14 and Table 1.10.5.2.3 summarize *T* and *RH* on WPs for the three alternative AMLs considered for LML = 0.46-MTU/m, the ACD rev 00 axial WP, and backfill at 100 yr. During the pre-closure period, *T* and *RH* on WPs are fairly similar over this AML range. A reduction in AML from 83.4 to 45 MTU/acre only reduces the peak temperature on the hottest WP (the 10-yr-old PWR WP) by 17°C; a reduction in AML from 45 to 25 MTU/acre does not reduce the maximum peak WP temperature any further. Therefore, for AML = 45 MTU/acre, the drifts are effectively infinitely apart at the time at which the hottest WP temperatures peak. The average to cooler-than-average WPs take long enough to reach their peak temperatures for their peak temperatures to be sensitive to drift spacing (and AML), as is evidenced by the steady decline in peak temperature for these WPs (compare Tables 1.10.5.7.13, 1.10.5.7.14, and 1.10.5.2.3).

After backfill is emplaced in the cases with the ACD rev 00 axial WP spacing, peak WP temperatures are moderately sensitive to drift spacing (and AML); a reduction of AML from 83.4 to 45

MTU/acre reduces the maximum peak WP temperature by 24°C; a reduction from 45 to 25 MTU/acre reduces the maximum peak WP temperature by 19°C. After backfill is emplaced, there are relatively minor differences in RH_{wp} among these three AML cases. With respect to the influence of AML on WP *RH*, there are two distinct categories of WPs for the ACD rev 00 design with backfill:

SNF WPs: These WPs experience decreasing *RH* with decreasing AML. Because ΔRH_{rock} is negligible for the ACD rev 00 design, *RH* reduction on the SNF WPs depends almost exclusively on ΔRH_{drift}, which is given by the relationship: $RH_{wp}/RH_{dw} = P_{sat}(T_{dw})/P_{sat}(T_{wp})$. Because ΔT_{drift} is independent of AML, and because the ratio $P_{sat}(T_{dw})/P_{sat}(T_{wp})$ decreases moderately with decreasing *T* (which decreases with AML), then RH_{wp} decreases moderately with decreasing AML (particularly at later time). It should be pointed out the percentage of WPs that can be affected by the cold-trap effect increases with decreasing AML. (The cold-trap effect drives water vapor from hotter to cooler WPs, where it condenses, which leaves a surface film of water.) Although lower AMLs allow the average to hotter-than-average WPs to experience slightly lower *RH* than in the higher AML cases, some of the (coolest) WPs (which may include SNF WPs) will experience much higher *RH* (up to 100%) than in the higher AML cases.

DHLW WPs: These WPs experience increasing *RH* with decreasing AML. Because these WPs do not generate enough heat to cause any significant ΔT_{drift} (or ΔRH_{drift}), *RH* reduction on the DHLW WPs depends almost exclusively on ΔRH_{rock}, which decreases strongly with decreasing AML. These WPs are likely to experience the cold-trap effect; moreover, the duration of time that these WPs experience *RH* = 100%, as a result of the cold-trap effect, will increase with decreasing AML.

A comparison of Tables 1.10.5.7.13, 1.10.5.7.14, and 1.10.5.2.3 illustrates these *RH* trends. For the backfill cases, the benefits of reducing the AML include:

- Reducing the magnitude and duration of decay-heat-mobilized condensate flow.
- Modest improvement in the *RH* reduction on SNF WPs.

Table 1.10.5.7.15 summarizes *T* and *RH* in the rock at the upper drift wall for the five alternative AMLs considered for the 1.11-MTU/acre line-load cases with backfill at 100 yr. With regards to *T* and *RH* in the near-field rock, the above-mentioned observations for the no-backfill cases also apply to the backfill cases, with the minor exception that after backfill, *T* along the drift wall is slightly cooler, and *RH* along the drift wall slightly more humid than in the no-backfill cases (compare Tables 1.10.5.7.5 and 1.10.5.7.15).

Tables 1.10.5.7.16–1.10.5.7.20 and Table 1.10.5.2.4 summarize *T* and *RH* on WPs for the five alternative AMLs considered for the 1.11-MTU/m line-load cases with backfill at 100 yr. The pre-closure *T* and *RH* on WPs were discussed earlier in this section. After backfill is emplaced, peak WP temperatures are sensitive to drift spacing (and AML). Increasing the AML from 83.4 to 100 MTU/acre causes a 6°C increase in the maximum peak WP temperature, while increasing the AML to 120 MTU/acre causes an additional 7°C increase. Reducing the AML from 83.4 to 45 MTU/acre causes a 22°C decrease in maximum peak WP temperature, while reducing the AML to 25 MTU/acre causes an additional 9°C decrease. Over the range 25–120 MTU/acre, the maximum peak WP temperature varies by 44°C and the minimum WP *RH* varies by only 2%. Figure 1.10.5.7.6 indicates that the sensitivity of RH_{wp} to AML falls into two distinct time regimes (early and late time), and that for the early time regime, the AML cases fall into three distinct classes (low, intermediate, and high AML). The time regimes are as follows:

Early time regime: During this regime, the sensitivity of RH_{wp} to AML is dominated by the magnitude and duration of ΔRH_{rock}, which increase with AML; consequently RH_{wp} decreases with AML.

Later time regime: During this regime the sensitivity of RH_{wp} to AML is only affected by how the ratio $P_{sat}(T_{dw})/P_{sat}(T_{wp})$ decreases slightly with decreasing *T* (and decreasing AML); consequently, RH_{wp} decreases slightly with decreasing AML.

During the early time regime, RH_{wp} is driest for the high AML cases (100 and 120 MTU/acre), while RH_{wp} is more humid for the low AML cases (25 and 45 MTU/acre). For the intermediate (83.4-MTU/acre) case, RH_{wp} lies right in between RH_{wp} for the low- and high-AML cases.

There has been considerable discussion concerning how the temperature difference (ΔT_{drift}) between the WP and the drift wall generates a substantial *RH* difference (ΔRH_{rock}) between these locations. For the wide drift spacings in the line-load design, there is also a very large temperature difference (ΔT_{pillar}) between the drift wall and the centerline of the rock pillar separating the drifts, which generates a significant *RH* difference (ΔRH_{pillar}) between these locations. Figures 1.10.5.7.7 and 1.10.5.7.8 show the relationship between ΔT_{pillar} and ΔRH_{pillar} as well as their sensitivity to AML. Because thermal interference between drifts decreases with increasing drift spacing, the magnitude of ΔT_{pillar} increases with decreasing AML. During very early time ($t < 60$ yr), ΔRH_{pillar} is similar for all AMLs. At later time ($t > 60$ yr), because the magnitude of rock dryout depends on the extent to which *T* is driven above the nominal boiling point, the magnitude of ΔRH_{pillar} is greater for the higher AML cases. The fact that the 83-MTU/acre case experiences a larger ΔRH_{pillar} than the higher AML cases is due to the fact that the centerline of the pillar in the higher AML cases has become drier (as a result of more intensive thermal interference between drifts), not because *RH* at the drift wall is drier in the 83-MTU/acre case. Because of the somewhat cooler (and more humid) conditions at the pillar centerline in the 83-MTU/acre case (than in the high-AML cases), the 83-MTU/acre case increases the tendency for condensate to drain between the drifts.

Figures 1.10.5.7.7 and 1.10.5.7.8 also clearly illustrate a point made earlier for the line-load design—that the duration of significant ΔRH_{rock} is 5000 yr for the 83.4-MTU/acre case and is 8000 yr for both of the high-AML cases (100 and 120 MTU/acre). This observation applies for a steady uniform percolation flux of 0.3 mm/yr and for repository locations not significantly affected by edge-cooling/rewetting effects.

Figure 1.10.5.7.9 clearly illustrates the insensitivity of ΔT_{drift} to AML. Therefore, because edge-cooling effects effectively cause drifts at the edge to experience conditions that are similar to those at the center of a lower AML repository, ΔT_{drift} is also insensitive to the relative proximity of a drift to the edge of the repository. This implies a model abstraction process whereby the results of a mountain-scale model, which is useful for predicting average rock *T* and *RH* conditions, can be combined with those of a drift-scale model, which is useful for predicting ΔT_{pillar}, ΔRH_{pillar}, and ΔT_{drift}. This model abstraction process is discussed in Section 1.10.6.

Figure 1.10.5.7.10 clearly illustrates how thermal homogenization is extremely effective for the entire range of AMLs considered (25 to 120 MTU/acre). As discussed in Section 1.10.5.2, the "thermal-blanket effect" of the backfill facilitates this homogenization by (1) increasing the ratio of the radial impedance to heat flow (which is controlled by thermal conduction in the backfill) divided by the axial impedance heat flow (which is controlled by thermal radiation between WPs), which forces heat to flow preferentially in the axial direction along the drift; and (2) increasing *T* on the ends of the WPs, which increases the efficiency of radiative WP-to-WP heat transfer.

The possible drift-scale benefits of decreasing the AML for the line-load design include:

- Reducing the duration of decay-heat-mobilized condensate flow.
- Modest improvement in the *RH* reduction on WPs at late time ($t > 6000$ yr).

For both the ACD rev 00 axial WP spacing and the line-load designs, there may be significant mountain-scale benefits in reducing the AML from the reference AML (83.4 MTU/acre). The motivation for considering these benefits is discussed in Sections 1.8.1 and 1.8.3.

Table 1.10.5.7.1. Temperature and relative humidity in rock at upper drift wall for alternative drift spacings and AMLs, ACD rev 00 axial WP spacing, LML = 0.46 MTU/m, drift diameter = 5.5 m, sand invert, no backfill, WP emissivity = 0.8, and percolation flux = 0.3 mm/yr.

AML	25 MTU/acre	45 MTU/acre	83.4 MTU/acre
Drift spacing	75.2 m	41.8 m	22.5 m
T_{peak} (t < 100 yr)	75–137°C	96–140°C	100–165°C
RH_{max} (t < 100 yr)	99.6–99.9%	64–99.9%	36–98%
T_{peak} (t = 120 yr)	68–89°C	94–109°C	100–129°C
RH (t = 120 yr)	99.8–99.9%	72–99.9%	36–97%
RH (t = 2000 yr)	99.9–99.9%	99.9–99.9%	90–97%
RH (t = 10,000 yr)	99.9–99.9%	99.9–99.9%	99.8–99.8%

Table 1.10.5.7.2. Temperature and relative humidity on upper WP surface for alternative drift spacings and AMLs, ACD rev 00 axial WP spacing, LML = 0.46 MTU/m, drift diameter = 5.5 m, sand invert, no backfill, WP emissivity = 0.8, and percolation flux = 0.3 mm/yr.

AML	25 MTU/acre	45 MTU/acre	83.4 MTU/acre
Drift spacing	75.2 m	41.8 m	22.5 m
T_{peak} (t < 100 yr)	86–175°C	99–175°C	107–192°C
RH_{max} (t < 100 yr)	42–100%	40–100%	25–86%
T_{peak} (t > 100 yr)	70–105°C	96–123°C	104–144°C
RH (t = 120 yr)	40–97%	47–100%	29–85%
RH (t = 2000 yr)	83–99.9%	86–100%	86–97%
RH (t = 10,000 yr)	90–99.8%	90–99.9%	92–99.9%
$t(RH = 65\%)$	0–600 yr	0–180 yr	0–630 yr
$t(RH = 90\%)$	0–11,600 yr	0–9100 yr	1170–2330 yr

Table 1.10.5.7.3. Temperature and relative humidity on upper WP surface for AML = 25 MTU/acre, ACD rev 00 axial WP spacing, LML = 0.46 MTU/m, drift spacing = 75.2 m, sand invert, no backfill, drift diameter = 5.5 m, WP emissivity = 0.8, and percolation flux = 0.3 mm/yr.

Waste package type	Hanford Site DHLW	Savannah River Site DHLW	40-yr-old PWR MPC	26-yr-old BWR MPC	26-yr-old PWR MPC	10-yr-old PWR MPC
T_{peak} (t < 100 yr)	86°C	99°C	92°C	107°C	123°C	175°C
RH_{max} (t < 100 yr)	100%	100%	92%	68%	42%	42%
T_{peak} (t > 100 yr)	70°C	74°C	78°C	85°C	93°C	105°C
RH (t = 120 yr)	97%	99%	79%	63%	45%	40%
RH (t = 2000 yr)	99.9%	99.9%	95%	92%	86%	83%
RH (t = 10,000 yr)	99.8%	99.8%	97%	95%	91%	90%
$t(RH$ = 65%)	0 yr	0 yr	0 yr	140 yr	440 yr	610 yr
$t(RH$ = 90%)	0 yr	0 yr	780 yr	1570 yr	6480 yr	11,060 yr
RH = 100% corresponds to the presence of liquid water on the WP						

Table 1.10.5.7.4. Temperature and relative humidity on upper WP surface for AML = 45 MTU/acre, ACD rev 00 axial WP spacing, LML = 0.46 MTU/m, drift spacing = 41.8 m, sand invert, no backfill, drift diameter = 5.5 m, WP emissivity = 0.8, and percolation flux = 0.3 mm/yr.

Waste package type	Hanford Site DHLW	Savannah River Site DHLW	40-yr-old PWR MPC	26-yr-old BWR MPC	26-yr-old PWR MPC	10-yr-old PWR MPC
T_{peak} (t < 100 yr)	99°C	104°C	103°C	111°C	123°C	175°C
RH_{max} (t < 100 yr)	100%	95%	86%	76%	64%	40%
T_{peak} (t > 100 yr)	96°C	98°C	100°C	104°C	109°C	123°C
RH (t = 120 yr)	100%	96%	88%	78%	68%	47%
RH (t = 2000 yr)	100%	100%	96%	93%	89%	86%
RH (t = 10,000 yr)	99.9%	99.9%	97%	96%	92%	90%
$t(RH = 65\%)$	0 yr	0 yr	0 yr	50 yr	100 yr	180 yr
$t(RH = 90\%)$	0 yr	0 yr	150 yr	1060 yr	2890 yr	9100 yr
RH = 100% corresponds to the presence of liquid water on the WP						

Table 1.10.5.7.5. Temperature and relative humidity in rock at upper drift wall for alternative drift spacings and AMLs, a line-load design with a 0.1-m gap between WPs, LML = 1.11 MTU/m, drift diameter = 5.5 m, sand invert, no backfill, WP emissivity = 0.8, and percolation flux = 0.3 mm/yr.

AML	25 MTU/acre	45 MTU/acre	83.4 MTU/acre	100 MTU/acre	120 MTU/acre
Drift spacing	180 m	100 m	53.8 m	44.9 m	37.4 m
T_{peak} (t < 100 yr)	143–172°C	143–171°C	161–184°C	162–187°C	160–183°C
RH_{max} (t <100 yr)	50–62%	37–46%	21–25%	19–22%	17–20%
T_{peak} (t > 100 yr)	110–117°C	119–126°C	135–137°C	147–154°C	154–161°C
RH (t = 120 yr)	63–77%	43–51%	23–27%	20–23%	18–21%
RH (t = 2000 yr)	99.9–99.9%	99.9–99.9%	78–78%	63–64%	58–58%
RH (t =10,000 yr)	99.9–99.9%	99.8–99.8%	99.1–99.1%	98.7–98.7%	99–99%

Table 1.10.5.7.6. Temperature and relative humidity on upper surface of WP for alternative drift spacings and AMLs, a line-load design with a 0.1-m gap between WPs, LML = 1.11 MTU/m, drift diameter = 5.5 m, sand invert, no backfill, WP emissivity = 0.8, and percolation flux = 0.3 mm/yr.

AML	25 MTU/acre	45 MTU/acre	83.4 MTU/acre	100 MTU/acre	120 MTU/acre
Drift spacing	180 m	100 m	53.8 m	44.9 m	37.4 m
T_{peak} (t < 100 yr)	156–195°C	156–195°C	172–203°C	173–209°C	169–206°C
RH_{max} (t <100 yr)	34–51%	27–38%	16–21%	15–19%	14–17%
T_{peak} (t > 100 yr)	116–128°C	125–137°C	147–158°C	153–163°C	160–170°C
RH (t = 120 yr)	44–63%	31–43%	18–23%	16–20%	15–18%
RH (t = 2000 yr)	90–96%	92–97%	72–76%	61–63%	55–57%
RH (t =10,000yr)	93–98%	94–98%	94–98%	94–98%	95–97%
$t(RH = 65\%)$	120–160 yr	210–280 yr	1450–1620 yr	2120–2320 yr	2410–2590 yr
$t(RH = 90\%)$	180–2100 yr	380–1220 yr	4030–4680 yr	7040–7600 yr	7030–7490yr

Table 1.10.5.7.7. Temperature and relative humidity on upper WP surface for AML = 25 MTU/acre, a line-load design with a 0.1-m gap between WPs, LML = 1.11 MTU/m, drift spacing = 180 m,sand invert, no backfill, drift diameter = 5.5 m, WP emissivity = 0.8, and percolation flux = 0.3 mm/yr.

Waste package type	Hanford Site DHLW	Savannah River Site DHLW	40-yr-old PWR MPC	26-yr-old BWR MPC	26-yr-old PWR MPC	10-yr-old PWR MPC
T_{peak} (t < 100 yr)	156°C	171°C	154°C	158°C	164°C	195°C
RH_{max} (t < 100 yr)	51%	48%	50%	48%	43%	34%
T_{peak} (t > 100 yr)	116°C	117°C	117°C	117°C	121°C	128°C
RH (t = 120 yr)	63%	61%	62%	60%	54%	44%
RH (t = 2000 yr)	96%	98%	94%	94%	92%	90%
RH (t = 10,000 yr)	98%	99%	96%	96%	95%	93%
$t(RH = 65\%)$	120 yr	130 yr	130 yr	130 yr	140 yr	160 yr
$t(RH = 90\%)$	200 yr	180 yr	790 yr	830 yr	1500 yr	2100 yr

Table 1.10.5.7.8. Temperature and relative humidity on upper WP surface for AML = 45 MTU/acre, a line-load design with a 0.1-m gap between WPs, LML = 1.11 MTU/m, drift spacing = 100 m,sand invert, no backfill, drift diameter = 5.5 m, WP emissivity = 0.8, and percolation flux = 0.3 mm/yr.

Waste package type	Hanford Site DHLW	Savannah River Site DHLW	40-yr-old PWR MPC	26-yr-old BWR MPC	26-yr-old PWR MPC	10-yr-old PWR MPC
T_{peak} (t < 100 yr)	156°C	171°C	154°C	158°C	163°C	195°C
RH_{max} (t < 100 yr)	38%	37%	38%	37%	33%	27%
T_{peak} (t > 100 yr)	125°C	127°C	126°C	127°C	130°C	137°C
RH (t = 120 yr)	43%	42%	42%	41%	37%	31%
RH (t = 2000 yr)	97%	98%	95%	96%	93%	92%
RH (t = 10,000 yr)	98%	99%	97%	97%	95%	94%
$t(RH$ = 65%)	220 yr	210 yr	230 yr	230 yr	270 yr	280 yr
$t(RH$ = 90%)	450 yr	400 yr	520 yr	560 yr	880 yr	1200 yr

Table 1.10.5.7.9. Temperature and relative humidity on upper WP surface for AML = 100 MTU/acre, a line-load design with a 0.1-m gap between WPs, LML = 1.11 MTU/m, drift spacing = 44.9 m,sand invert, no backfill, drift diameter = 5.5 m, WP emissivity = 0.8, and percolation flux = 0.3 mm/yr.

Waste package type	Hanford Site DHLW	Savannah River Site DHLW	40-yr-old PWR MPC	26-yr-old BWR MPC	26-yr-old PWR MPC	10-yr-old PWR MPC
T_{peak} (t < 100 yr)	173°C	186°C	172°C	175°C	180°C	209°C
RH_{max} (t < 100 yr)	19%	19%	19%	19%	17%	15%
T_{peak} (t > 100 yr)	153°C	154°C	154°C	154°C	157°C	163°C
RH (t = 120 yr)	20%	20%	20%	20%	18%	16%
RH (t = 2000 yr)	63%	63%	62%	62%	61%	61%
RH (t = 10,000 yr)	97%	98%	96%	96%	95%	94%
$t(RH$ = 65%)	2180 yr	2120 yr	2230 yr	2210 yr	2300 yr	2320 yr
$t(RH$ = 90%)	7150 yr	7040 yr	7290 yr	7270 yr	7470 yr	7600 yr

Table 1.10.5.7.10. Temperature and relative humidity on upper WP surface for AML = 120 MTU/acre, a line-load design with a 0.1-m gap between WPs, LML = 1.11 MTU/m, drift spacing = 37.4 m,sand invert, no backfill, drift diameter = 5.5 m, WP emissivity = 0.8, and percolation flux = 0.3 mm/yr.

Waste package type	Hanford Site DHLW	Savannah River Site DHLW	40-yr-old PWR MPC	26-yr-old BWR MPC	26-yr-old PWR MPC	10-yr-old PWR MPC
T_{peak} (t < 100 yr)	170°C	183°C	169°C	173°C	177°C	206°C
RH_{max} (t < 100 yr)	17%	17%	17%	17%	16%	14%
T_{peak} (t > 100 yr)	160°C	161°C	161°C	161°C	164°C	170°C
RH (t = 120 yr)	18%	18%	18%	18%	17%	15%
RH (t = 2000 yr)	57%	57%	56%	56%	55%	55%
RH (t = 10,000 yr)	97%	98%	97%	97%	96%	95%
$t(RH$ = 65%)	2450 yr	2410 yr	2480 yr	2470 yr	2550 yr	2590 yr
$t(RH$ = 90%)	7120 yr	7030 yr	7240 yr	7220 yr	7390 yr	7490 yr

Table 1.10.5.7.11. Temperature and relative humidity in rock at upper drift wall for alternative drift spacings and AMLs, ACD axial WP spacing, LML = 0.46 MTU/m, drift diameter = 5.5 m, sand invert, full sand backfill at 100 yr with K_{th} = 0.6 W/m°C, WP emissivity = 0.8, and percolation flux = 0.3 mm/yr. Temperature and relative humidity in rock at upper drift wall

AML	25 MTU/acre	45 MTU/acre	83.4 MTU/acre
Drift spacing	75.2 m	41.8 m	22.5 m
T_{peak} (t < 100 yr)	85–137°C	96–140°C	100–165°C
RH_{max} (t < 100 yr)	99.5–99.9%	64–99.9%	36–98%
T_{peak} (t = 120 yr)	66–86°C	92–100°C	100–123°C
RH (t = 120 yr)	99.9–99.9%	88–99.9%	45–99%
RH (t = 2000 yr)	99.9–99.9%	99.8–99.9%	92–99%
RH (t = 10,000 yr)	99.9–99.9%	99.8–99.9%	99.8–99.8%

Table 1.10.5.7.12. Temperature and relative humidity on upper surface of WP for alternative drift spacings and AMLs, ACD axial WP spacing, LML = 0.46 MTU/m, drift diameter = 5.5 m, sand invert, full sand backfill at 100 yr with K_{th} = 0.6 W/m°C, WP emissivity = 0.8, and percolation flux = 0.3 mm/yr.

AML	25 MTU/acre	45 MTU/acre	83.4 MTU/acre
Drift spacing	75.2 m	41.8 m	22.5 m
T_{peak} (t < 100 yr)	86–175°C	99–175°C	107–192°C
RH_{max} (t < 100 yr)	42–97%	40–99.4%	25–86%
T_{peak} (t > 100 yr)	82–310°C	106–329°C	117–353°C
RH (t = 120 yr)	1–62%	1–75%	1–57%
RH (t = 2000 yr)	34–99.1%	39–99.4%	43–98%
RH (t = 10,000 yr)	55–99.5%	57–99.6%	60–99.7%
$t(RH$ = 65%)	0–15,900 yr	0–14,840 yr	160*–13,330 yr
$t(RH$ = 90%)	240**–63,990 yr	190**–63,440 yr	860–62,680 yr
** RH is never less than 90% prior to backfill			

Table 1.10.5.7.13. Temperature and relative humidity on upper WP surface for AML = 25 MTU/acre, ACD rev 00 axial WP spacing, LML = 0.46 MTU/m, drift spacing = 75.2 m, sand invert, full sand backfill at 100 yr with K_{th} = 0.6 W/m°C, drift diameter = 5.5 m, WP emissivity = 0.8, and percolation flux = 0.3 mm/yr.

Waste package type	Hanford Site DHLW	Savannah River Site DHLW	40-yr-old PWR MPC	26-yr-old BWR MPC	26-yr-old PWR MPC	10-yr-old PWR MPC
T_{peak} (t < 100 yr)	86°C	99°C	92°C	107°C	123°C	175°C
RH_{max} (t < 100 yr)	100%	100%	92%	68%	42%	42%
T_{peak} (t > 100 yr)	82°C	95°C	135°C	184°C	237°C	310°C
RH (t = 120 yr)	62%	50%	12%	4%	2%	1%
RH (t = 2000 yr)	99.1%	99%	66%	55%	41%	34%
RH (t = 10,000 yr)	99.5%	99%	80%	73%	61%	56%
$t(RH$ = 65%)	130* yr	170* yr	1900* yr	4390 yr	12,380 yr	15,900 yr
$t(RH$ = 90%)	240* yr	290* yr	27,660 yr	37,150 yr	55,940 yr	63,990 yr

* RH is never less than 90% prior to backfill

RH = 100% corresponds to the presence of liquid water on the WP

Table 1.10.5.7.14. Temperature and relative humidity on upper WP surface for AML = 45 MTU/acre, ACD rev 00 axial WP spacing, LML = 0.46 MTU/m, drift spacing = 41.8 m, sand invert, full sand backfill at 100 yr with K_{th} = 0.6 W/m°C, drift diameter = 5.5 m, WP emissivity = 0.8, and percolation flux = 0.3 mm/yr.

Waste package type	Hanford Site DHLW	Savannah River Site DHLW	40-yr-old PWR MPC	26-yr-old BWR MPC	26-yr-old PWR MPC	10-yr-old PWR MPC
T_{peak} (t < 100 yr)	99°C	104°C	103°C	111°C	123°C	175°C
RH_{max} (t < 100 yr)	99.4%	95%	86%	76%	64%	40%
T_{peak} (t > 100 yr)	106°C	120°C	159°C	204°C	253°C	329°C
RH (t = 120 yr)	75%	49%	17%	7%	3%	1%
RH (t = 2000 yr)	99.4%	99%	69%	59%	46%	39%
RH (t = 10,000 yr)	99.6%	99%	81%	74%	63%	57%
$t(RH$ = 65%)	0 yr	150* yr	1560**yr	3150** yr	11,530 yr	14,840 yr
$t(RH$ = 90%)	190* yr	260* yr	26,810 yr	36,610 yr	55,560 yr	63,440 yr

* RH is never less than 90% prior to backfill

**RH is never less than 65% prior to backfill

Table 1.10.5.7.15. Temperature and relative humidity in rock at upper drift wall for alternative drift spacings and AMLs, a line-load design with a 0.1-m gap between WPs, LML = 1.11 MTU/m, drift diameter = 5.5 m, sand invert, full sand backfill at 100 yr with K_{th} = 0.6 W/m°C, WP emissivity = 0.8, and percolation flux = 0.3 mm/yr.

AML	25 MTU/acre	45 MTU/acre	83.4 MTU/acre	100 MTU/acre	120 MTU/acre
Drift spacing	180 m	100 m	53.8 m	44.9 m	37.4 m
T_{peak} (t < 100 yr)	143–172°C	143–171°C	161–184°C	162–187°C	160–183°C
RH_{max} (t <100 yr)	50–62%	37–46%	21–25%	19–22%	17–20%
T_{peak} (t > 100 yr)	106–109°C	115–117°C	135–137°C	141–142°C	147–148°C
RH (t = 120 yr)	86–89%	57–60%	31–31%	26–28%	25–25%
RH (t = 2000 yr)	99.9–99.9%	99.9–99.9%	78–78%	66–67%	60–60%
RH (t =10,000yr)	99.9–99.9%	99.8–99.8%	99.1–99.1%	99–99%	99–99%

Table 1.10.5.7.16. Temperature and relative humidity on upper surface of WP for alternative drift spacings and AMLs, a line-load design with a 0.1-m gap between WPs, LML = 1.11 MTU/m, drift diameter = 5.5 m, sand invert, full sand backfill at 100 yr with K_{th} = 0.6 W/m°C, WP emissivity = 0.8, and percolation flux = 0.3 mm/yr.

AML	25 MTU/acre	45 MTU/acre	83.4 MTU/acre	100 MTU/acre	120 MTU/acre
Drift spacing	180 m	100 m	53.8 m	44.9 m	37.4 m
T_{peak} (t < 100 yr)	154–195°C	154–195°C	172–203°C	172–209°C	169–206°C
RH_{max} (t <100 yr)	34–51%	27–38%	16–21%	15–19%	14–17%
T_{peak} (t > 100 yr)	218–235°C	228–244°C	250–266°C	257–272°C	265–279°C
RH (t = 120 yr)	4–5%	3–4%	2–3%	2–3%	2–3%
RH (t = 2000 yr)	53–60%	57–63%	49–51%	42–44%	38–41%
RH (t =10,000yr)	70–76%	71–77%	73–77%	73–77%	74–79%
$t(RH$ = 65%)	2820–6440 yr	2290–5060 yr	3730–4600 yr	6220–7020 yr	5640–6360 yr
$t(RH$ = 90%)	31,850–41,800yr	31,370–41,250yr	30,480–39,920yr	30,000–39,720yr	29,490–39,060yr

Table 1.10.5.7.17. Temperature and relative humidity on upper WP surface for AML = 25 MTU/acre, a line-load design with a 0.1-m gap between WPs, LML = 1.11 MTU/m, drift spacing = 180 m,sand invert, full sand backfill at 100 yr with K_{th} = 0.6 W/m°C, drift diameter = 5.5 m, WP emissivity = 0.8, and percolation flux = 0.3 mm/yr.

Waste package type	Hanford Site DHLW	Savannah River Site DHLW	40-yr-old PWR MPC	26-yr-old BWR MPC	26-yr-old PWR MPC	10-yr-old PWR MPC
T_{peak} (t < 100 yr)	156°C	171°C	154°C	158°C	164°C	195°C
RH_{max} (t < 100 yr)	51%	48%	50%	48%	43%	34%
T_{peak} (t > 100 yr)	218°C	225°C	220°C	218°C	224°C	235°C
RH (t = 120 yr)	5%	5%	5%	5%	5%	4%
RH (t = 2000 yr)	58%	60%	55%	57%	53%	53%
RH (t = 10,000 yr)	75%	76%	72%	74%	70%	70%
$t(RH = 65\%)$	3410 yr	2820 yr	4580 yr	3810 yr	6000 yr	6440 yr
$t(RH = 90\%)$	34,780 yr	31,850 yr	38,240 yr	36,490 yr	41,800 yr	41,740 yr

Table 1.10.5.7.18. Temperature and relative humidity on upper WP surface for AML = 45 MTU/acre, a line-load design with a 0.1-m gap between WPs, LML = 1.11 MTU/m, drift spacing = 100 m,sand invert, full sand backfill at 100 yr with K_{th} = 0.6 W/m°C, drift diameter = 5.5 m, WP emissivity = 0.8, and percolation flux = 0.3 mm/yr.

Waste package type	Hanford Site DHLW	Savannah River Site DHLW	40-yr-old PWR MPC	26-yr-old BWR MPC	26-yr-old PWR MPC	10-yr-old PWR MPC
T_{peak} (t < 100 yr)	156°C	171°C	154°C	158°C	163°C	195°C
RH_{max} (t < 100 yr)	38%	37%	38%	37%	33%	27%
T_{peak} (t > 100 yr)	228°C	235°C	230°C	228°C	233°C	244°C
RH (t = 120 yr)	4%	3%	4%	4%	4%	3%
RH (t = 2000 yr)	61%	63%	59%	60%	57%	57%
RH (t = 10,000 yr)	75%	77%	73%	75%	71%	71%
$t(RH$ = 65%)	2570 yr	2290 yr	3350 yr	2770 yr	4610 yr	5060 yr
$t(RH$ = 90%)	34,290 yr	31,370 yr	37,770 yr	35,970 yr	41,250 yr	41,150 yr

Table 1.10.5.7.19. Temperature and relative humidity on upper WP surface for AML = 100 MTU/acre, a line-load design with a 0.1-m gap between WPs, LML = 1.11 MTU/m, drift spacing = 44.9 m,sand invert, full sand backfill at 100 yr with K_{th} = 0.6 W/m°C, drift diameter = 5.5 m, WP emissivity = 0.8, and percolation flux = 0.3 mm/yr.

Waste package type	Hanford Site DHLW	Savannah River Site DHLW	40-yr-old PWR MPC	26-yr-old BWR MPC	26-yr-old PWR MPC	10-yr-old PWR MPC
T_{peak} (t < 100 yr)	173°C	186°C	172°C	175°C	180°C	209°C
RH_{max} (t < 100 yr)	19%	19%	19%	19%	17%	15%
T_{peak} (t > 100 yr)	258°C	264°C	260°C	257°C	262°C	272°C
RH (t = 120 yr)	3%	3%	3%	3%	2%	2%
RH (t = 2000 yr)	44%	45%	43%	44%	42%	42%
RH (t = 10,000 yr)	76%	77%	75%	76%	73%	73%
$t(RH$ = 65%)	6480 yr	6220 yr	6760 yr	6540 yr	7020 yr	6760 yr
$t(RH$ = 90%)	33,090 yr	30,000 yr	36,660 yr	34,700 yr	39,720 yr	36,660 yr

Table 1.10.5.7.20. Temperature and relative humidity on upper WP surface for AML = 120 MTU/acre, a line-load design with a 0.1-m gap between WPs, LML = 1.11 MTU/m, drift spacing = 37.4 m,sand invert, full sand backfill at 100 yr with K_{th} = 0.6 W/m°C, drift diameter = 5.5 m, WP emissivity = 0.8, and percolation flux = 0.3 mm/yr.

Waste package type	Hanford Site DHLW	Savannah River Site DHLW	40-yr-old PWR MPC	26-yr-old BWR MPC	26-yr-old PWR MPC	10-yr-old PWR MPC
T_{peak} (t < 100 yr)	170°C	183°C	169°C	173°C	177°C	206°C
RH_{max} (t < 100 yr)	17%	17%	17%	17%	16%	14%
T_{peak} (t > 100 yr)	265°C	271°C	267°C	264°C	269°C	279°C
RH (t = 120 yr)	2%	2%	2%	3%	2%	2%
RH (t = 2000 yr)	39%	41%	39%	40%	38%	38%
RH (t = 10,000 yr)	77%	79%	76%	77%	75%	74%
$t(RH = 65\%)$	5850 yr	5640 yr	6100 yr	5880 yr	6360 yr	6340 yr
$t(RH = 90\%)$	32,260 yr	29,490 yr	35,880 yr	33,800 yr	39,060 yr	38,900 yr

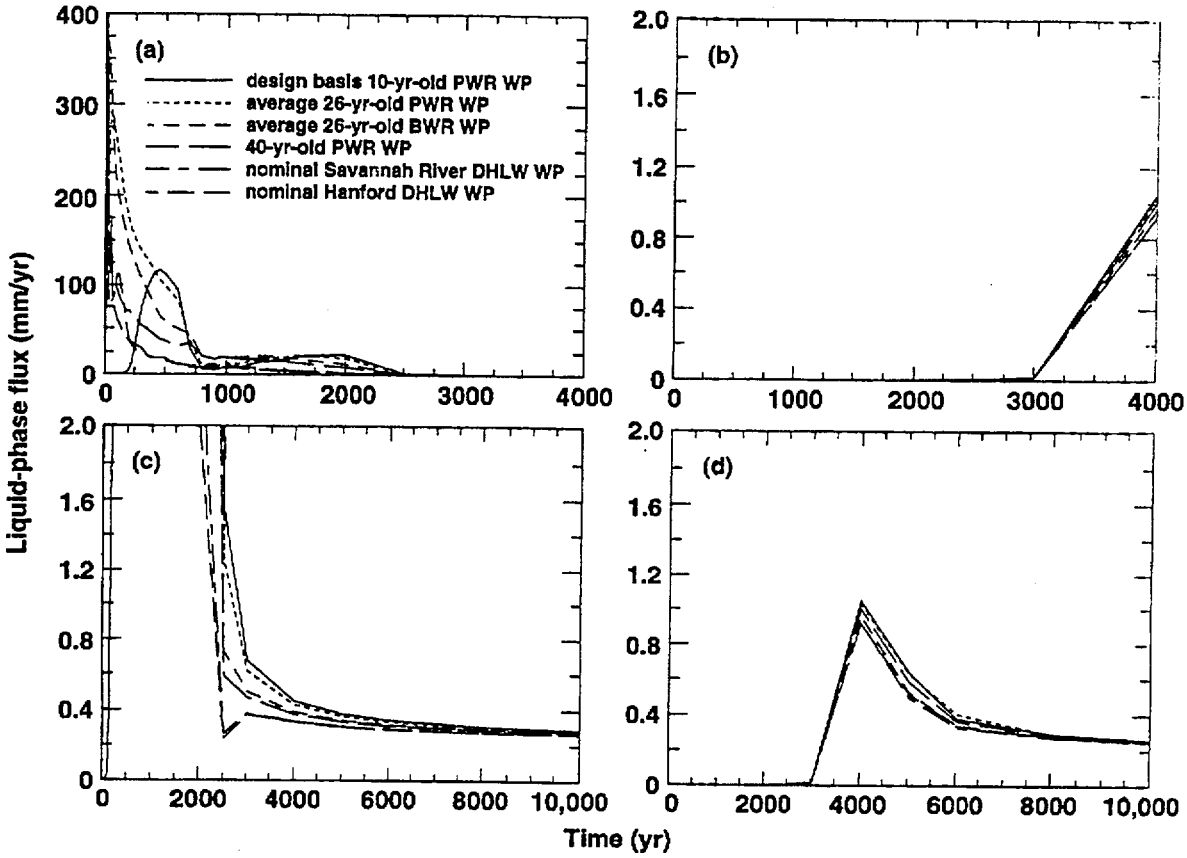

Figure 1.10.5.7.1. Liquid-phase flux 5 m above the emplacement drift at various WP locations for AML = 83.4 MTU/acre, sand invert, no backfill, drift diameter = 5.5 m, WP emissivity = 0.8, and ambient percolation flux = 0.3 mm/yr. Curves are plotted for (a,c) the ACD rev 00 design with LML = 0.46 MTU/m, and drift spacing = 22.5 m; and (b,d) a line-load design with a 0.1-m gap between WPs, LML = 1.11 MTU/m, and drift spacing = 53.8 m. Note the different vertical axis scales for liquid-phase flux.

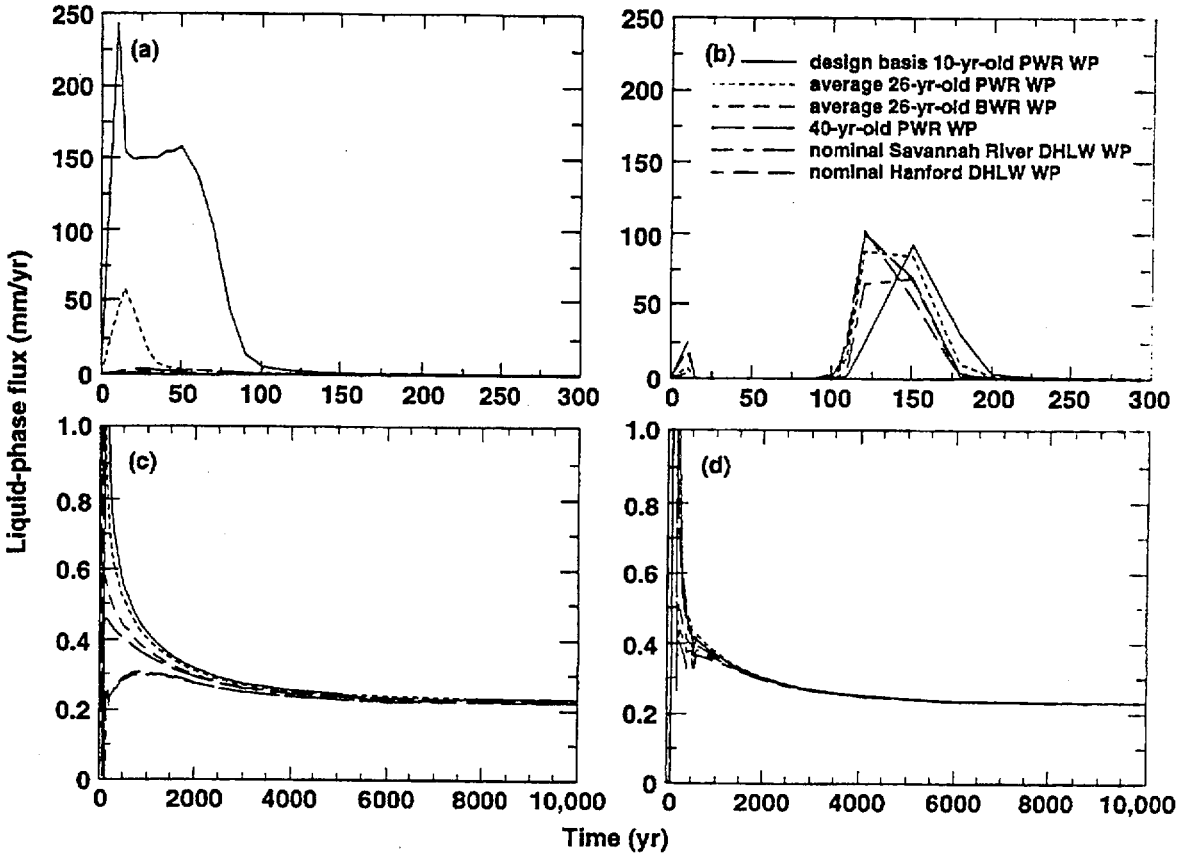

Figure 1.10.5.7.2. Liquid-phase flux 5 m above the emplacement drift at various WP locations for AML = 25 MTU/acre, sand invert, no backfill, drift diameter = 5.5 m, WP emissivity = 0.8, and ambient percolation flux = 0.3 mm/yr. Curves are plotted for (a,c) the ACD rev 00 design with LML = 0.46 MTU/m, and drift spacing = 22.5 m; and (b,d) a line-load design with a 0.1-m gap between WPs, LML = 1.11 MTU/m, and drift spacing = 53.8 m. Note the different vertical axis scales for liquid-phase flux.

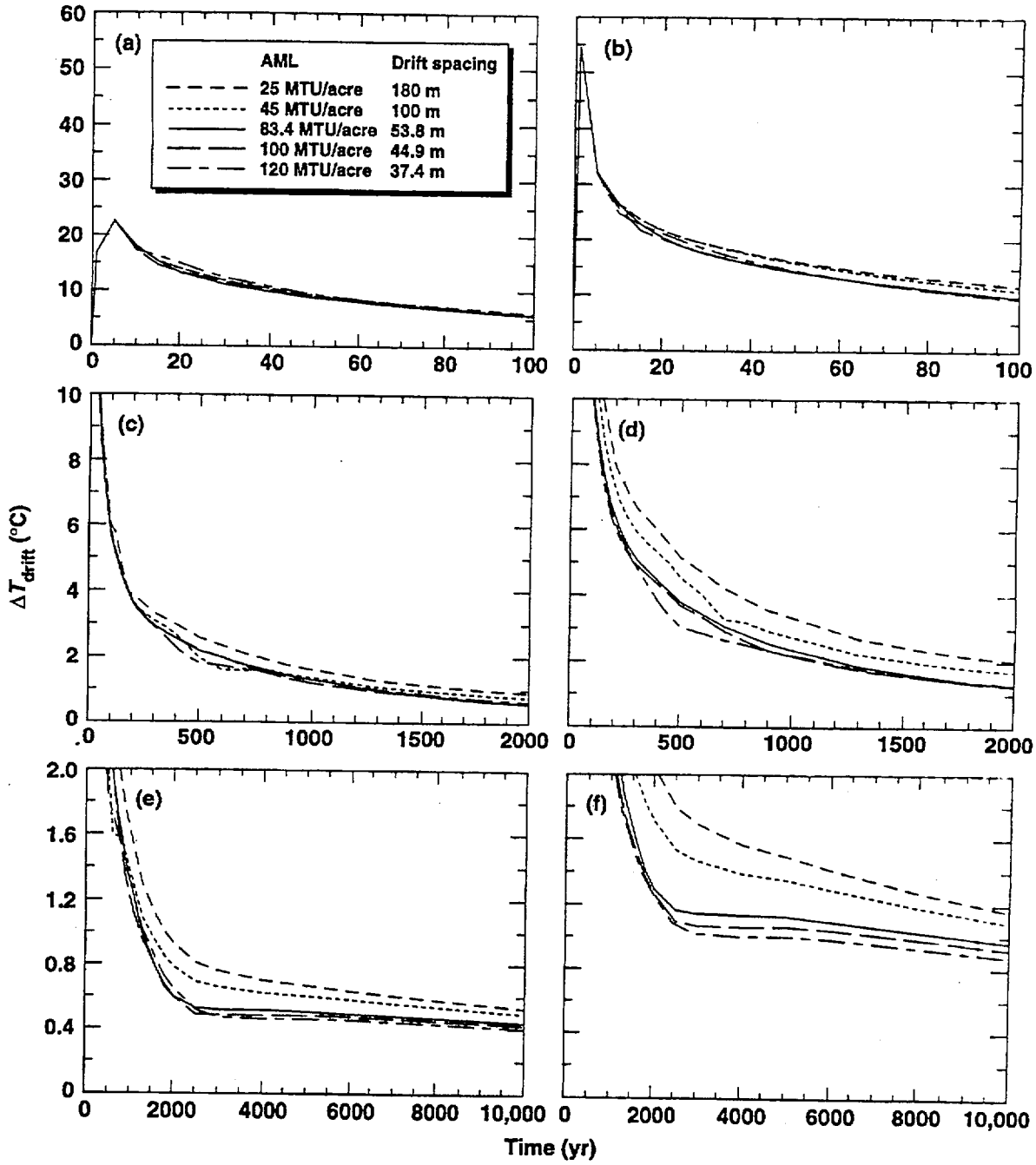

Figure 1.10.5.7.3. Temperature difference between WP surface and drift wall (ΔT_{drift}) for a Hanford Site DHLW WP (a,c) and a "design basis fuel" 10-yr-old PWR WP (b,d) for various AMLs and drift spacings, a line-load design with a 0.1-m gap between WPs, LML = 1.11 MTU/m, sand invert, no backfill, drift diameter = 5.5 m, WP emissivity = 0.8, and ambient percolation flux = 0.3 mm/yr.

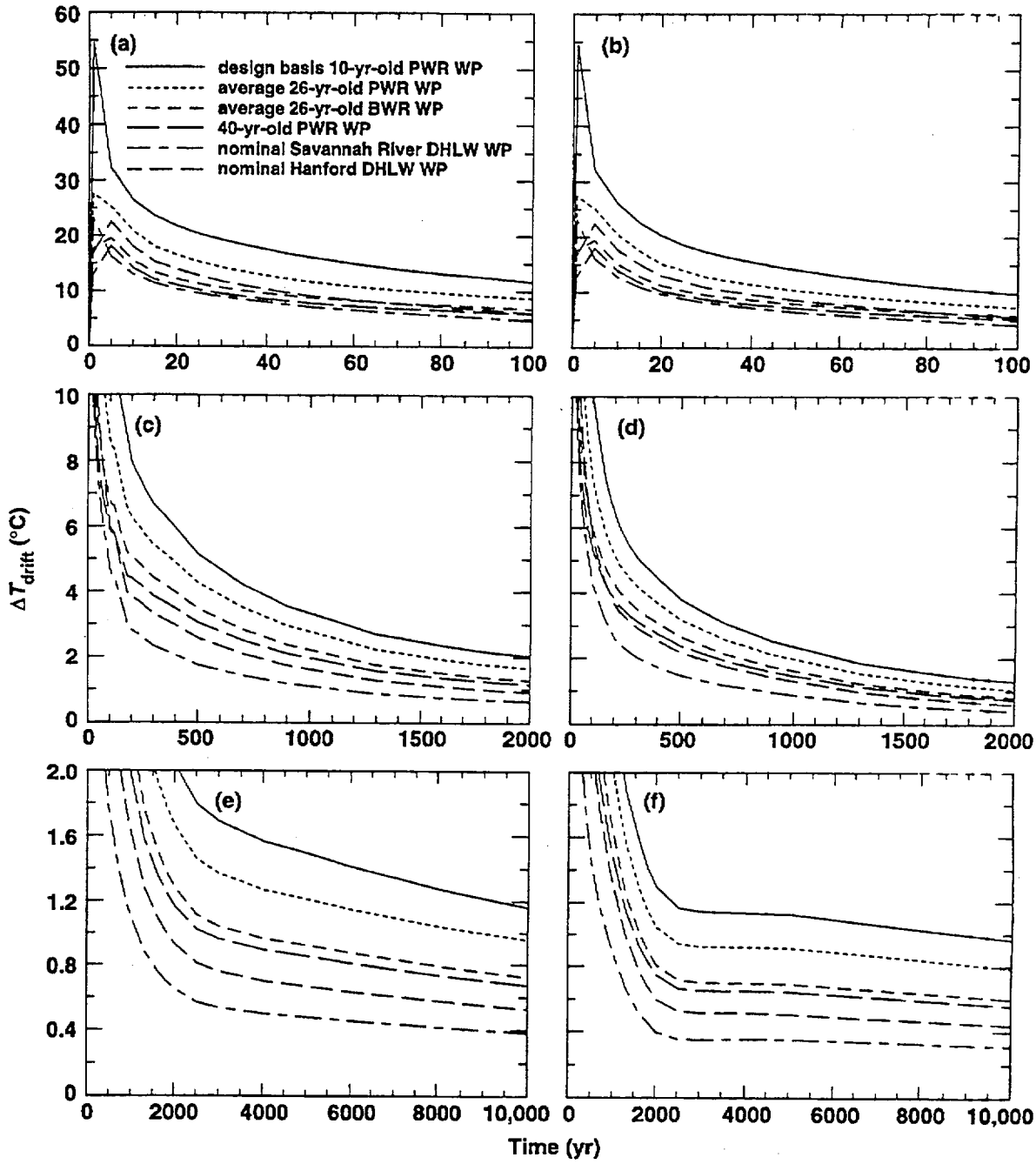

Figure 1.10.5.7.4. Temperature difference between WP surface and drift wall (ΔT_{drift}) for a line-load design with a 0.1-m gap between WPs, LML = 1.11 MTU/m, sand invert, no backfill, drift diameter = 5.5 m, WP emissivity = 0.8, and ambient percolation flux = 0.3 mm/yr. Curves are plotted for (a,c,e) AML =25 MTU/acre and drift spacing = 180 m; and (b,d,f) AML = 83.4 MTU/acre and drift spacing = 53.8 m.

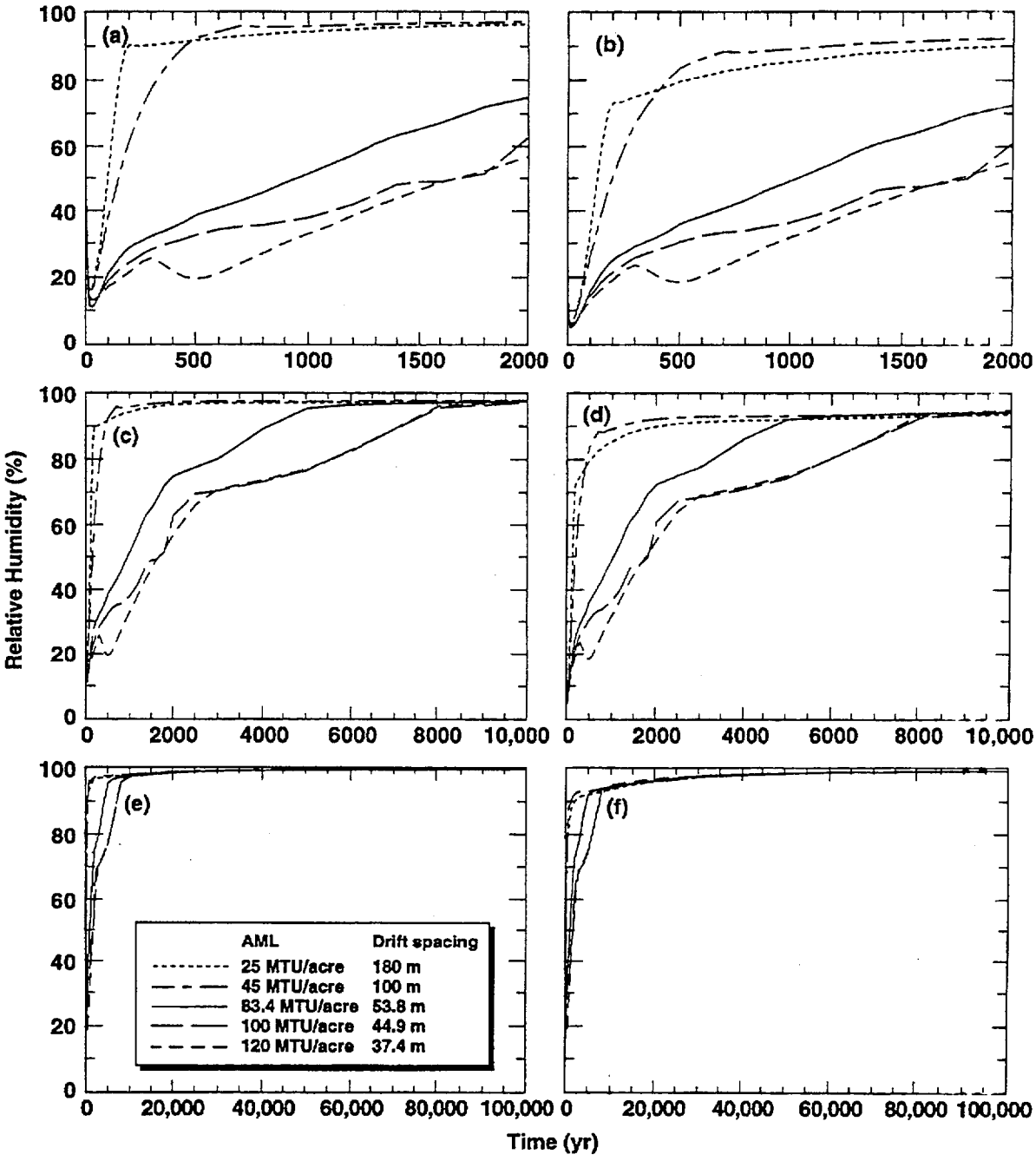

Figure 1.10.5.7.5. Relative humidity on upper surface of a Hanford Site DHLW WP (a,c,e) and a "design basis fuel" 10-yr-old PWR WP (b,d,f) for various AMLs and drift spacings, a line-load design with a 0.1-m gap between WPs, LML = 1.11 MTU/m, sand invert, no backfill, drift diameter = 5.5 m, WP emissivity = 0.8, and ambient percolation flux = 0.3 mm/yr.

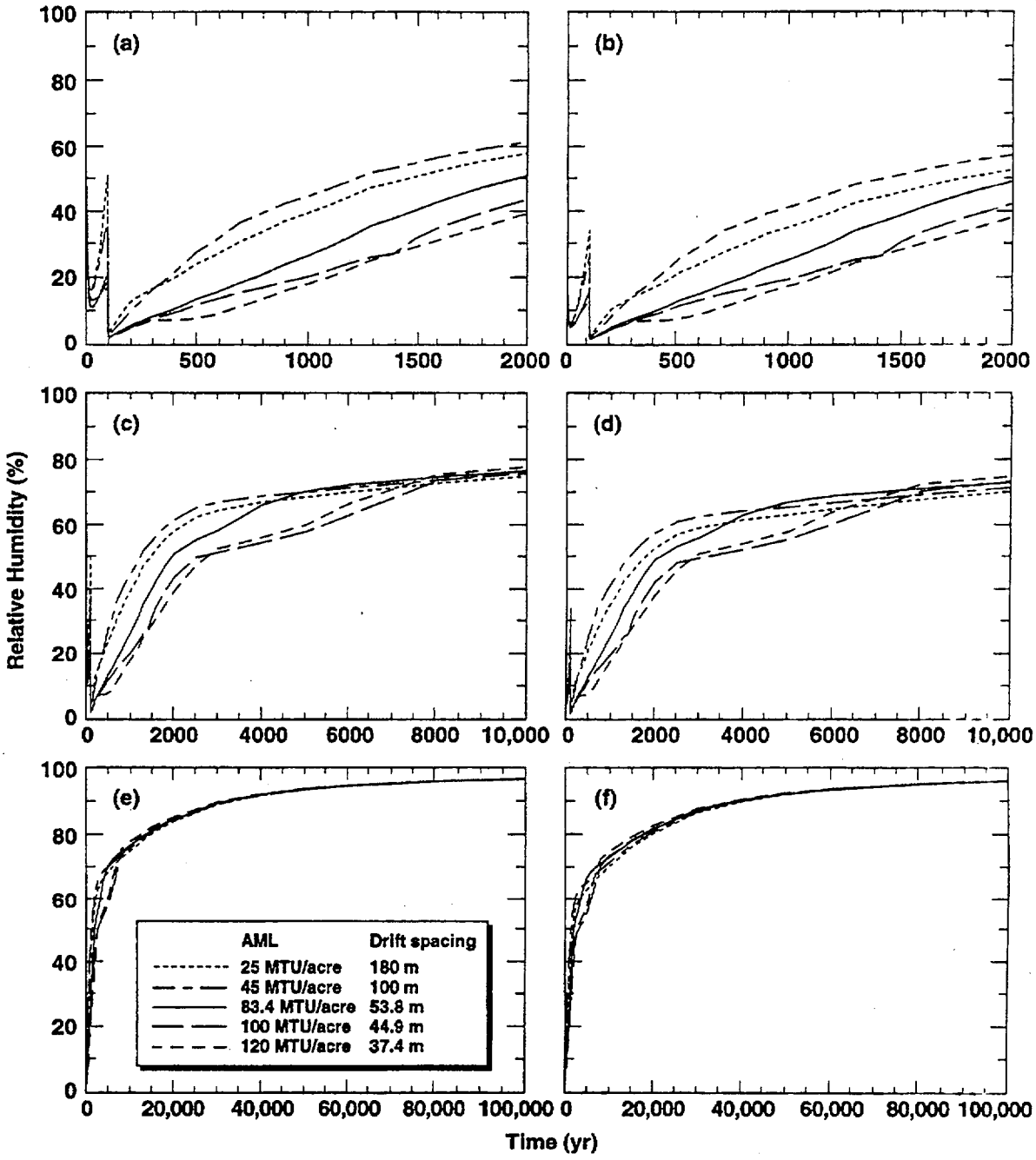

Figure 1.10.5.7.6. Relative humidity on upper surface of a Hanford Site DHLW WP (a,c,e) and a "design basis fuel" 10-yr-old PWR WP (b,d,f) for various AMLs and drift spacings, a line-load design with a 0.1-m gap between WPs, LML = 1.11 MTU/m, sand invert, full sand backfill at 100 yr with K_{th} = 0.6 W/m°C, drift diameter = 5.5 m, WP emissivity = 0.8, and percolation flux = 0.3 mm/yr.

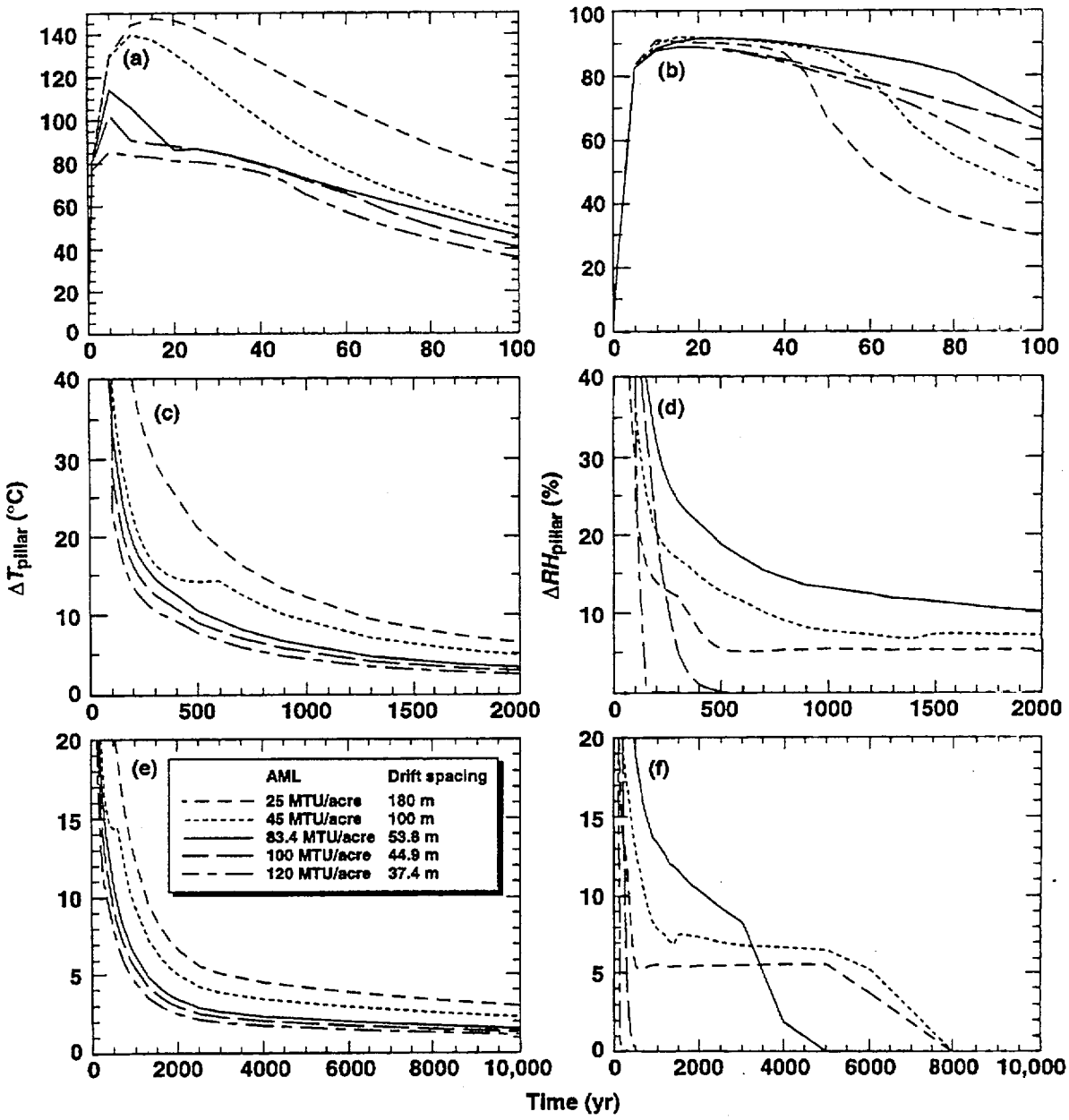

Figure 1.10.5.7.7. Temperature difference (ΔT_{pillar}) between the drift wall (directly above the design basis fuel 10-yr-old PWR WP) and the centerline of the rock pillar (a,c,e) for a line-load design with a 0.1-m gap between WPs, LML = 1.11 MTU/m, sand invert, full sand backfill at 100 yr with K_{th} = 0.6 W/m°C, drift diameter = 5.5 m, WP emissivity = 0.8, ambient percolation flux = 0.3 mm/yr, and various AMLs and drift spacings. Also plotted(b,d,f) is the relative humidity difference (ΔRH_{pillar}) between these same two locations. The temperature and relative humidity differences are taken along a line transverse to the Hanford Site DHLW WP and which is located at the elevation of the crown of the drift.

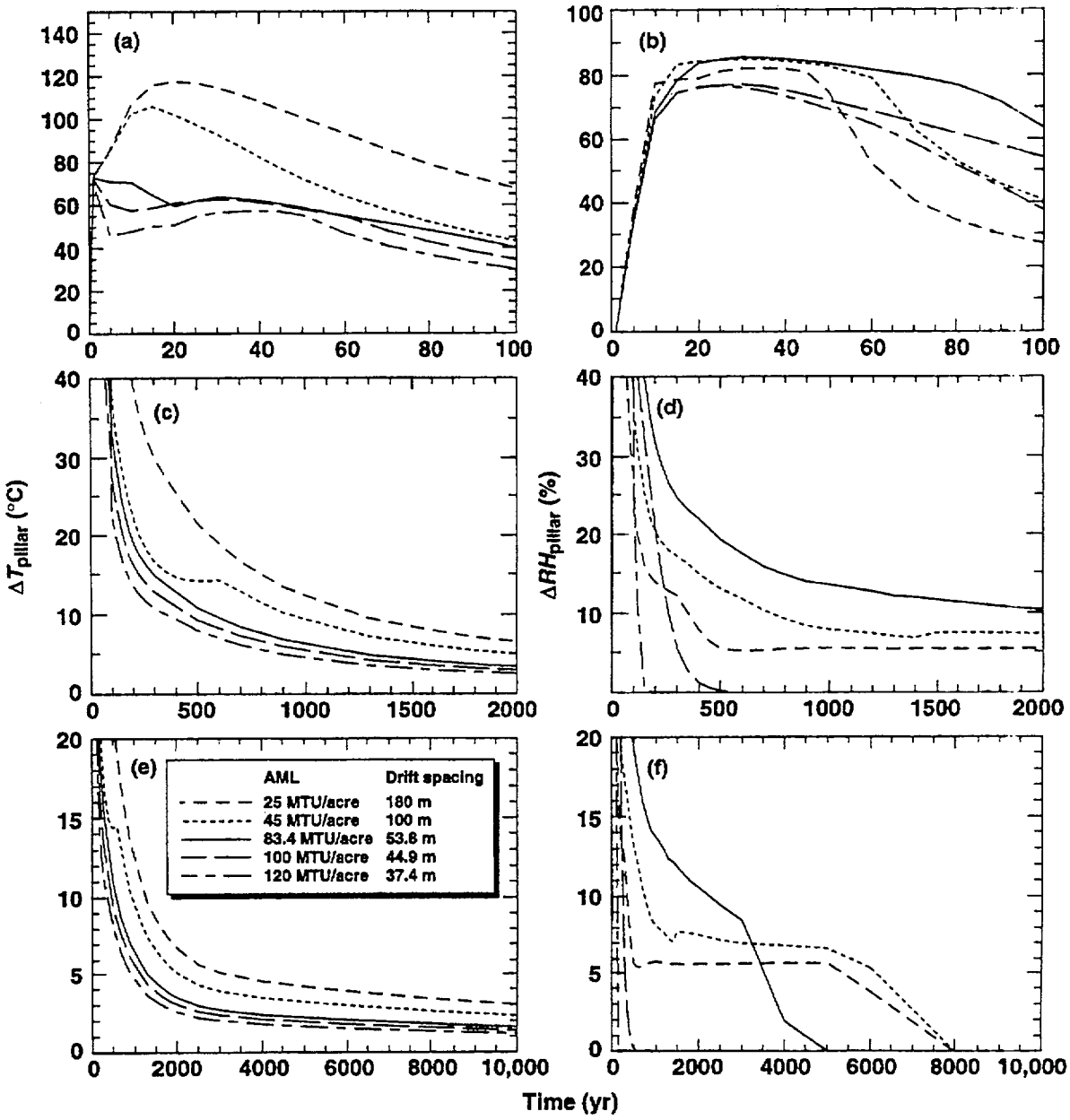

Figure 1.10.5.7.8. Temperature difference (ΔT_{pillar}) between the drift wall (directly above the Hanford Site DHLW WP) and the centerline of the rock pillar (a,c,e) for a line-load design with a 0.1-m gap between WPs, LML = 1.11 MTU/m, sand invert, full sand backfill at 100 yr with K_{th} = 0.6 W/m°C, drift diameter = 5.5 m, WP emissivity = 0.8, ambient percolation flux = 0.3 mm/yr, and various AMLs and drift spacings. Also plotted(b,d,f) is the relative humidity difference (ΔRH_{pillar}) between these same two locations. The temperature and relative humidity differences are taken along a line transverse to the Hanford Site DHLW WP and which is located at the elevation of the crown of the drift.

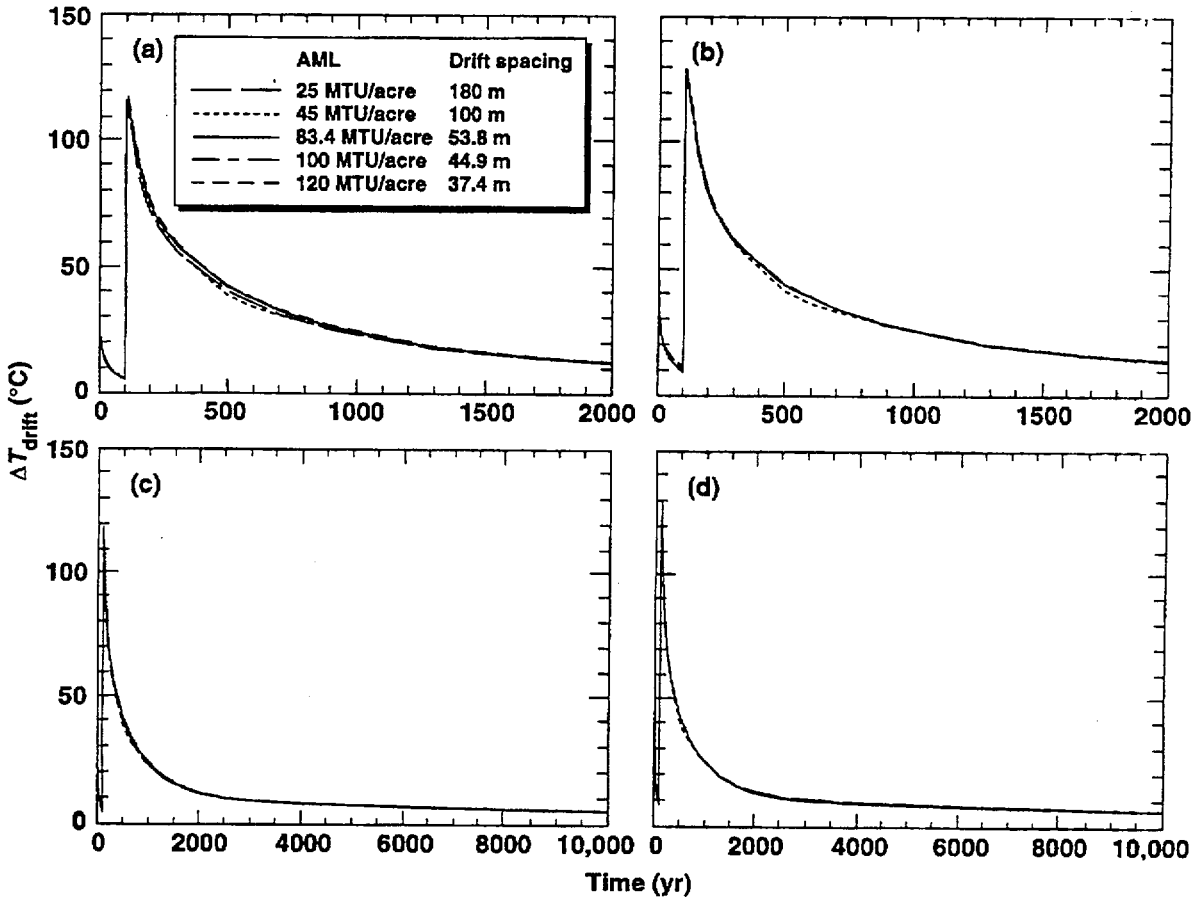

Figure 1.10.5.7.9. Temperature difference between WP surface and drift wall (ΔT_{drift}) for a Hanford Site DHLW WP (a,c) and a "design basis fuel" 10-yr-old PWR WP (b,d) for various AMLs and drift spacings, a line-load design with a 0.1-m gap between WPs, LML = 1.11 MTU/m, sand invert, full sand backfill at 100 yr with K_{th} = 0.6 W/m°C, drift diameter = 5.5 m, WP emissivity = 0.8, and ambient percolation flux = 0.3 mm/yr.

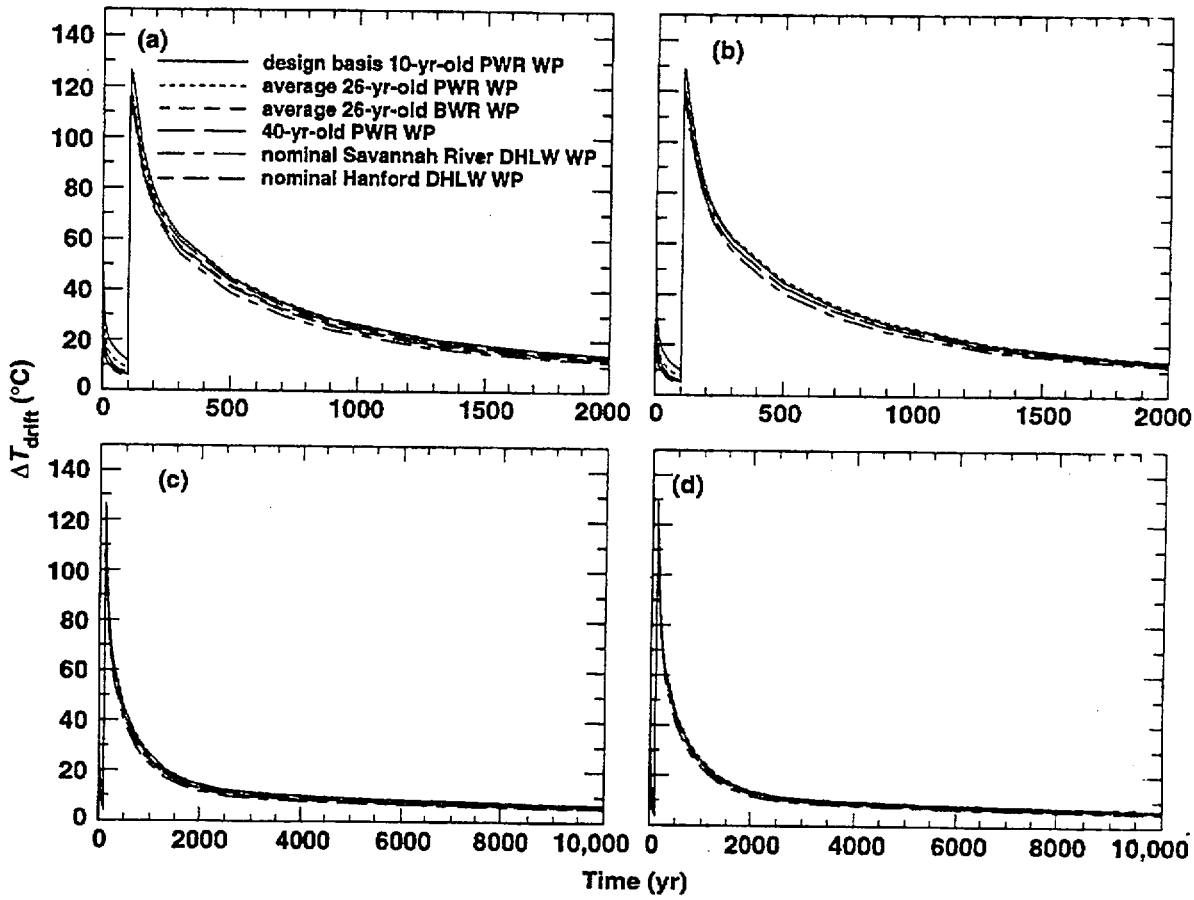

Figure 1.10.5.7.10. Temperature difference between WP surface and drift wall (ΔT_{drift}) for a line-load design with a 0.1-m gap between WPs, LML = 1.11 MTU/m, sand invert, full sand backfill at 100 yr with K_{th} = 0.6 W/m°C, drift diameter = 5.5 m, WP emissivity = 0.8, and ambient percolation flux = 0.3 mm/yr. Curves are plotted for (a,c) AML = 25 MTU/acre and drift spacing = 180 m; and (b,d) AML = 83.4 MTU/acre and drift spacing = 53.8 m.

1.10.6 Influence of Ambient Percolation Flux and Edge-Cooling/Rewetting/Shedding Effects on Thermal-Hydrological Behavior

All of the calculations in Section 1.10.5 assumed an ambient percolation flux of 0.3 mm/yr. This section considers the sensitivity of drift- and mountain-scale thermal-hydrological (T-H) behavior to a wide range of ambient percolation fluxes (0.0 to 5.0 mm/yr). It is important to point out that for most of this flux range (> 0.2 mm/yr) the model predicts fracture-dominated flow that is not reduced by imbibition in the matrix. As in Section 1.10.5, the ambient percolation flux is assumed to be uniform and steady (i.e., episodic fracture flow is not considered). As is discussed in Section 1.3, ambient percolation flux is likely to occur as episodic nonequilibrium fracture-matrix flow, which will need to be addressed in future analyses of T-H behavior. The adequacy of the model assumptions of steady and uniform ambient percolation flux need to be considered in light of some of the primary objectives of this section, which are to examine the following:

- The relative magnitude of heat-mobilized versus ambient liquid-phase flow.
- The sensitivity of the liquid-phase flux distribution above the drifts to WP layout (i.e., square spacing versus line-load spacing).
- The sensitivity of liquid-phase flux to repository location (i.e., proximity to the edge of the repository).

The assumption of a steady and uniform percolation flux makes it easier to discern the contribution of heating heterogeneity on the variability of T-H behavior in the vicinity of emplacement drifts, and to discern the contribution of edge-cooling/rewetting/shedding effects on the variability of T-H behavior in the repository.

For Section 1.10.6, the repository design assumptions are similar to those used in much of Section 1.10.5: drift diameter = 5.5 m; WP emissivity = 0.8; the invert is made up of sand or a "sand-like" granular material; for the backfill cases, the backfill is assumed to be a "sand-like" granular material with a K_{th} of 0.6 W/m^{o}C. (Note that many of these calculations were conducted in support of the backfill systems study [Balady, 1996], which focused on the evaluation of granular invert and backfill materials.) The calculations in this section were conducted with three different types of models: (1) drift-scale models, (2) mountain-scale models, and (3) hybrid drift-scale–mountain-scale models. We start with an analysis of the influence of ambient percolation flux, using the three-dimensional, multiple-WP drift-scale model. The drift-scale model represents detailed three-dimensional T-H behavior in and around the emplacement drifts (including the rock pillar separating the drifts), and one-dimensional mountain-scale T-H behavior that occurs from the water table to the ground surface; it does not represent three-dimensional mountain-scale T-H behavior. This is followed with an analysis of edge-cooling/rewetting/shedding effects using a model that represents three-dimensional mountain-scale T-H behavior with an R–Z coordinate system and represents WP decay heat by uniformly distributing the heat over a disk-shaped area; this is sometimes called a smeared-heat-source model. We continue with some additional analysis of the influence of ambient percolation flux, using the three-dimensional, multiple-WP drift-scale model. This section is concluded with an analysis of edge-cooling/rewetting/shedding effects, using a hybrid drift-scale–mountain-scale model that represents both the detailed three-dimensional drift-scale effects and three-dimensional mountain-scale effects. This model is also used to check the appropriateness of the drift-scale model calculations in analyzing the performance of the entire repository area.

Because of the dominant role decay heat plays in generating liquid-phase flux, it was decided to combine the discussion of ambient percolation flux and the influence of the repository edge on T-H behavior. Depending on the AML, decay heat is capable of generating a zone of counter-current two-phase flow above the repository, which is sometimes called the refluxing zone or the heat-pipe zone; this zone is associated with liquid-phase fluxes that are much larger than ambient. Mountain-scale and drift-scale analyses [Buscheck and Nitao, 1996] have shown that if the AML is high enough, this

zone can be displaced well above the repository horizon by the superheated (above-boiling-temperature) zone. If either the AML is not large enough, or the ambient liquid-phase flux is too large, it is possible for the heat-pipe zone to remain at the repository horizon. The fundamental relationship (see Eq. 1 in Section 1.10.5.1) is between the local heat flux and the heat flux that is required to vaporize the incoming liquid-phase flux. If there is too much liquid-phase flux, then there is insufficient heat flux to generate superheated conditions at the repository horizon. Three effects occur at the edge of the repository that make it more likely for the local heat flux to be overwhelmed by the local liquid-phase flux:

Edge-cooling effect: Because heat flow is two-dimensional (both vertical and lateral) at the repository edge versus one-dimensional at the center of the repository (where it is primarily vertical), cooling is enhanced with proximity to the edge of the repository.

Edge-rewetting effect: Because rewetting is two-dimensional (both vertical and lateral) at the repository edge versus one-dimensional at the center of the repository (where it is primarily vertical), rewetting is enhanced with proximity to the edge of the repository.

Edge-shedding effect: Because the shape of the superheated dryout zone slopes downward toward the repository edge (as a result of edge-cooling effects), there is a tendency for condensate to shed toward the edge of the repository.

The edge-rewetting/shedding effects tend to increase liquid-phase flux with proximity to the repository edge; the edge-cooling effect decreases the local heat flux that is available to vaporize the incoming liquid-phase flux with proximity to the edge. The edge-shedding effect can also increase the tendency for heat pipes to dissipate heat at the repository edge, thereby increasing the edge-cooling rate. Taken together, these effects increase the likelihood of greater-than-ambient liquid-phase fluxes reaching the repository horizon. Before continuing the discussion, it is useful to review the three scales at which condensate shedding occurs:

Waste-package-scale shedding: This is most likely to occur for a square WP spacing and for a highly heterogeneous distribution of heat output from the respective WPs; both of these conditions occur in the ACD rev 00 design. The WPs function like point-heat sources that generate a spherical superheated (and dryout) zone with an overlying hemispherically shaped zone of condensate shedding. As was shown in Section 1.10.5.1, condensate shedding is almost as likely to occur into the drift as into the rock pillar that separates the drifts. The potential for WP-scale shedding causing a nonzero liquid-phase flux at the upper drift wall (called drift seepage) increases with ambient percolation flux.

Drift-scale shedding: This is most likely to occur for a line-load design that facilitates thermal homogenization along the axis of the drift. Thermal homogenization results in a line-heat load that generates a cylindrically shaped superheated (and dryout) zone with an overlying condensate zone that is much more likely to drain into the center of the rock pillar than into the drifts. Drift-scale shedding occurs until the superheated zones have coalesced; for high AMLs, it occurs before and after this coalescence; for AMLs that are too low to cause coalescence, it can occur as long as boiling conditions persist.

Repository-scale shedding: This requires AMLs that are high enough to cause the superheated zones to coalesce between drifts. It also requires that the fracture networks be connected over the necessary length scales (10^2 to 10^3 m) and that the bulk permeability k_b of the network be sufficiently large (> 10^{-1} darcy). Both WP-scale and drift-scale shedding reduce the tendency for repository-scale shedding. An important issue for thermal management is whether to distribute the WPs so that drift-scale shedding is encouraged and repository-scale shedding is thereby minimized.

Figure 1.10.6.1 shows the liquid-phase flux 51 m directly above the drift for the 0.46-MTU/m ACD rev 00 design and the 1.11-MTU/m line-load design and an ambient percolation flux of 0.3 mm/yr. The large liquid-phase flux is the result of this location being in the heart of the heat-pipe zone (i.e., the zone of two-phase counter-current vapor and liquid flow) that overlies the boiling zone. Figure 1.10.6.2a shows the liquid-phase flux at the same location for the 1.11-MTU/m line-load design and five

different values of ambient percolation flux. Figure 1.10.6.2b shows *RH* in the rock at the drift wall directly above the Hanford Site DHLW WP for the 1.11-MTU/m line-load design and the same five values of percolation flux. Notice that the magnitude of the liquid-phase flux is relatively insensitive to a wide range in ambient percolation flux. The one exception is that zero ambient percolation flux is low enough to allow the dryout front to extend more than 51 m above the repository horizon (the elevation at which the liquid-phase flux is plotted in Figs. 1.10.6.1 and 1.10.6.2); for the other ambient percolation-flux cases, the dryout front never gets that far above the repository horizon. On the basis of Figs. 1.10.6.1 and 1.10.6.2 and Table 1.10.6.1, several important observations can be made about T-H behavior for an 83.4-MTU/acre repository:

The magnitude of mountain-scale liquid-phase flow is insensitive to WP layout: If the unthrottled, nonbuoyant, advective rock dryout regime dominates (see Table 1.8-2), then the magnitude of mountain-scale, decay-heat-mobilized vapor and condensate flow depends primarily on AML, and not on the details of the WP layout in the repository (i.e., axial WP spacing and lateral drift spacing). Because the heat-pipe zone 51 m above the repository horizon is far enough away from the drifts to be indicative of mountain-scale thermal-hydrological effects (versus drift-scale effects), the magnitude of liquid-phase flux is the same for these 83.4-MTU/acre designs.

The magnitude of mountain-scale liquid-phase flow is insensitive to ambient percolation flux: The magnitude of mountain-scale, decay-heat-mobilized condensate flux is very large compared with a wide range of possible ambient percolation fluxes. Therefore, the magnitude of the total liquid-phase flux is relatively insensitive to the ambient percolation flux range 0.05 mm–5.0 mm/yr.

Decay heat will significantly mobilize fluid flow for at least several thousand years: If the unthrottled, nonbuoyant, advective rock dryout regime dominates (see Table 1.8-2), then decay heat will significantly mobilize gas- and liquid-phase flow as long as boiling conditions persist (up to 5000 yr). If the unthrottled, buoyant, advective rock dryout regime dominates, then decay-heat-driven mountain-scale T-H effects will last much longer (up to 100,000 yr) whether or not boiling ever occurs. The magnitude of heat-mobilized liquid-phase flux will be one to two orders of magnitude greater than the ambient percolation flux for up to 1000 yr.

Rock dryout depends on ambient percolation flux: For a fairly wide range of ambient percolation flux (0.05–1.0 mm/yr) *RH* reduction resulting from rock dryout (ΔRH_{rock}) is insensitive to ambient flux. For the very low flux range (< 0.05 mm/yr), ΔRH_{rock} may last up to 30,000 yr (Figs. 1.10.6.2b; 1.10.6.6a,b; 1.10.6.7b,d,f; and 1.10.6.8b,d,f). For high fluxes (> 1–5 mm/yr), ΔRH_{rock} will be substantially suppressed (Fig. 1.10.6.8a,c,e).

All of the analyses in Section 1.10.5 were conducted with a drift-scale model that does not account for how the finite size of the repository affects mountain-scale thermal-hydrological effects. Because of the no-heat-flow and no-fluid-flow boundaries of the drift-scale model (see Section 1.10.1.2), it cannot represent the following:

Mountain-scale (or repository-scale) redistribution of condensate: Condensate can flow considerable distances laterally as a result of (1) the hydrological property distribution (e.g., from perched water at hydrostratigraphic contacts and (2) the tendency for condensate to shed around the edge of the boiling zone.

Edge-cooling/rewetting/shedding effects: At the center of the repository, the geometry for cooling is primarily one-dimensional (from above and below), while at the edge it is two-dimensional (from above, from below, and from the side), which enhances the cooling rate. Enhanced edge cooling causes a reduction in the spatial and temporal extent of rock dryout (ΔRH_{rock}); consequently, it takes less time to rewet to ambient (humid) *RH* in the rock. Moreover, while the geometry for rewetting is only one-dimensional at the center of the repository (from above and below the dryout zone), at the edge of the repository, the geometry of rewetting is two-dimensional (from above, from below, and from the side), which enhances the rewetting rate, further reducing the time it takes for the rock to rewet to ambient (humid) *RH* in the rock.

Edge-shedding effects are caused by lateral displacement of condensate from inner regions of the repository to the outer edge of the repository.

Mountain-scale models are required to represent the repository-scale redistribution of condensate and edge-cooling/rewetting effects. Figures 1.10.6.3 and 1.10.6.4 show the liquid-phase flux at six different locations at the repository horizon for two values of ambient percolation flux. The model used in these calculations represents three-dimensional mountain-scale effects with an R–Z coordinate system and assumes that the hydrostratigraphic units are horizontal and of constant thickness [Buscheck and Nitao, 1994]. The repository area is represented by a cylindrical disk with an area of 3.06 km^2; the decay heat from a mixture of 26-yr-old PWR and 26-yr-old BWR WPs (Table 1.10.1.2) is uniformly distributed over the disk shaped repository area.

The repository locations (Figs. 1.10.6.3 and 1.10.6.4) are identified as a function of the repository area that is enclosed, with 0% corresponding to the repository center, and 100% corresponding to the outer perimeter (the repository edge). The 12.5% location is close to the center of the repository with 87.5% of the repository lying outside of that location; the 50% location corresponds to the "median" location of the repository, with half of the repository lying inside that location and half lying outside. For a drift spacing of 53.8 m, the 75% location roughly corresponds to a drift location which is 8 drifts in from the outer edge of the repository. For a drift spacing of 53.8 m, the 97% and 94% locations correspond to the outermost drift and the next drift in from the repository edge.

Tables 1.10.6.1 and 1.10.6.2 complement Figs. 1.10.6.3 and 1.10.6.4 by summarizing the liquid-phase flux conditions at four of the repository locations in the mountain-scale model. These tables also summarize the drift-scale model predictions of liquid-phase flux 5 m above the drift immediately above the 26-yr-old PWR WP for both the 1.11-MTU/m line-load design and the 0.46-MTU/m ACD rev 00 design, thereby allowing a comparison between the smeared-heat-source mountain-scale model and the drift-scale models of the different WP layouts. Note that the geometry of the liquid-phase flow field around the drift results in a "stagnation zone" immediately above the crown of the drift, which reduces the vertical component of flow in the first few meters above the crown. Accordingly, it was decided to compare the vertical component of liquid-phase flux at a location 5 m above the drift, which is nearly outside the zone of stagnating flow. Several important observations can be made about liquid-phase flux in the rock immediately above the drifts:

The zero-flux rock dryout period is followed by a period of condensate-enhanced flux: With the exception of the outermost edge of the repository, the dryout period is associated with zero liquid-phase flux at the repository horizon; the duration of the dryout period decreases with proximity to the repository edge. After the repository rock has been rewetted to ambient liquid saturation conditions, the condensate bank overlying the repository causes a period of greater-than-ambient liquid-phase flux; the magnitude of this flux increases with (1) ambient percolation flux and (2) proximity to the repository edge.

Repository-scale condensate shedding drives large fluxes at the repository edge: If fracture connectivity extends over the width of the repository area (and k_b of the connected fracture network is large enough), then repository-scale redistribution of condensate (the edge-shedding effect) can cause liquid-phase flux at the repository edge to be much greater than the ambient percolation flux for early time (t < 1000 yr); the magnitude of the repository-edge fluxes increases with ambient percolation flux; these fluxes can be two orders of magnitude greater than the ambient percolation flux.

Heating heterogeneity drives much greater fluxes than uniform heating conditions: The highly spatially variable heating in the ACD rev 00 design can cause local liquid-phase fluxes (at the drift scale) to be much greater than those driven by homogeneous heating conditions (at the mountain scale). The fluxes driven by homogeneous heating conditions include those driven by the disk-shaped smeared-heat source (in the mountain-scale model), and those driven by the axially homogenized heating conditions generated by line-load design (represented by the drift-scale model). Therefore, mountain-scale models can drastically underrepresent the magnitude and variability of liquid-phase flux generated by heterogeneous conditions. On the other hand, except for regions affected by edge-shedding effects, the magnitudes of the liquid-

phase fluxes predicted by the mountain-scale, smeared-heat-source model are comparable to those predicted by the drift-scale model for the line-load design.

Figures 1.10.6.5 and 1.10.6.6 show *RH* in the rock at the repository horizon at the same locations considered in the preceding discussion and for ambient percolation fluxes of 0.0, 0.05, and 0.3 mm/yr. The magnitude and duration of *RH* reduction due to rock dryout (ΔRH_{rock}) decrease with:

Ambient percolation flux: A larger liquid-phase flux suppresses the spatial extent of rock dryout and reduces the time to rewet to ambient (humid) *RH*.

Proximity to the edge of the repository: A reduction in ΔRH_{rock} at the repository edge occurs because (1) the edge-cooling effect limits the spatial extent of rock dryout, (2) the edge-rewetting effect decreases the time to rewet to ambient (humid) *RH*, and (3) the edge-shedding effect increases the effective percolation flux at the repository edge, thereby suppressing rock dryout and reducing the time to rewet to ambient *RH*.

The similar *RH* histories for the 12.5% and 50% repository locations (Figs. 1.10.6.5a,b) indicate that (at least) the inner half of the repository is unaffected by edge-cooling and edge-rewetting effects. Edge-cooling/rewetting effects do not affect the minimum rock *RH* at the 75% location (Fig. 1.10.6.5c); however, these effects reduce (by a factor of two) the duration of ΔRH_{rock}. At the 94% repository location, edge-cooling/rewetting and edge-shedding effects (1) increase the minimum RH attained in the rock and (2) reduce (by a factor of nearly 10) the duration of ΔRH_{rock}; at the 97% repository location, these effects cause ΔRH_{rock} to be negligible.

For the inner half of the repository, ΔRH_{rock} persists for periods of 5000, 8000, and 50,000 yr for ambient percolation fluxes of 0.3, 0.05, and 0.0 mm/yr, respectively (Figs. 1.10.6.5a,b and 1.10.6.6a,b). At the 75% repository location, ΔRH_{rock} persists for periods of 2500, 4000, and 25,000 yr for ambient percolation fluxes of 0.3, 0.05, and 0.0 mm/yr, respectively (Figs. 1.10.6.5c and 1.10.6.6c). At the 94% repository location, ΔRH_{rock} persists for periods of 500, 1000, and 3000 yr for ambient percolation fluxes of 0.3, 0.05, and 0.0 mm/yr, respectively (Figs. 1.10.6.5d and 1.10.6.6d). At the 97% repository location, ΔRH_{rock} persists for periods of 300, 700, and 1200 yr for ambient percolation fluxes of 0.3, 0.05, and 0.0 mm/yr, respectively (Figs. 1.10.6.5e and 1.10.6.6e). Therefore, for the two outermost drifts, ΔRH_{rock} will be of limited duration.

We return to the analysis of the influence of ambient percolation flux, using the three-dimensional, multiple-WP model. Tables 1.10.6.3–1.10.6.7 and Figure 1.10.6.7 summarize the influence of ambient percolation flux (over the range 0.0 to 0.3 mm/yr) on *T* and *RH* in the near-field rock and on WPs for the ACD rev 00 design and cases with no backfill. Tables 1.10.6.8–1.10.6.14 and Figure 1.10.6.8 summarize the influence of ambient percolation flux (over the range 0.0 to 5.0 mm/yr) on *T* and *RH* in the near-field rock and on WPs for the 1.11-MTU/m line-load design and cases with no backfill. Several important observations can be made about the influence of ambient percolation flux:

Rock dryout (ΔRH_{rock}) decreases with increasing ambient percolation flux: While this is applicable to both the ACD rev 00 and line-load designs, there are differences between these two designs with regards to the sensitivity of ΔRH_{rock} to ambient percolation flux. For the ACD rev 00 design, a decrease in ambient percolation flux from 0.3 to 0.05 mm/yr results in a large reduction in *RH* , while *RH* for the line-load design is much less sensitive to the same range in ambient percolation flux. In fact, *RH* in the rock is slightly less for the 0.3-mm/yr line-load case than for the 0.05-mm/yr ACD-case (compare Tables 1.10.6.3 and 1.10.6.8). For both designs, a reduction in ambient percolation flux from 0.05 to 0.0 mm/yr results in a large reduction in *RH*, particularly between 2000 and 30,000 yr. During the period 0–2000 yr, there is a steady increase in *RH* for all percolation-flux cases, while at 2000 yr (for all but the 5.0-mm/yr case), the rate of increase slows (Figs 1.10.6.7a,c,e and 1.10.6.8a,c,e); for the 0.0-mm/yr case, this reduction in slope is much more pronounced than for the higher fluxes.

The variability in rock dryout decreases with decreasing ambient percolation flux: This is applicable to the ACD rev 00 design; the line-load experiences a uniform *RH* distribution in the rock along the drift for all values of flux considered.

Rock and WP temperatures increase with decreasing ambient percolation flux: This is applicable to both the ACD rev 00 and line-load designs for the 0.0–0.3 mm/yr ambient percolation flux range; temperatures in the line-load design are insensitive to the 0.3–5.0 mm/yr flux range. Much of the sensitivity of *T* in the 0.05–0.3-mm/yr flux range results from the higher initial liquid saturation associated with the 0.3-mm/yr case; higher initial saturation requires more heat to dry out a given volume of rock. The sensitivity of *T* in the 0.0–0.05-mm/yr flux range and the insensitivity of *T* in the 0.3–5.0-mm/yr flux range are related to the influence of ambient percolation flux on the development of heat pipes. Figure 1.10.6.2a shows how the magnitude of liquid-phase flux in the heat-pipe zone is insensitive to the 0.05–5.0 mm/yr ambient percolation flux range. The liquid-phase flux in the heat-pipe zone determines how efficiently the heat pipe convects heat away from the superheated zone. Lower liquid-phase flux causes less efficient heat transfer in the heat-pipe zone, which allows for the development of a larger superheated zone and higher *T* around the drifts, while higher flux causes more efficient heat transfer in the heat-pipe zone, which limits the development of the superheated zone. For ambient flux greater than 0.05 mm/yr, the efficiency of heat transfer in the heat-pipe zone does not increase strongly with ambient flux; consequently, *T* is less sensitive in the 0.3–5.0-mm/yr ambient flux range.

Greater rock dryout in the line-load design than in the ACD rev 00 design: Regardless of ambient percolation flux, the line-load design always results in lower *RH* in the rock at the drift wall than in the ACD rev 00 design (compare Tables 1.10.6. 3 and 1.10.6.8). The more locally intensive rock dryout for the line-load design always results in lower *RH* on WPs for cases with no backfill than in the ACD rev 00 design (compare Tables 1.10.6. 4 and 1.10.6.9; also compare Tables 1.10.5–7 with Tables 1.10.6.10–12). The differences in rock dryout (and in *RH* on WPs) between the two cases decrease with decreasing ambient percolation flux.

Greater variability in *T* and *RH* in the ACD rev 00 design than in the line-load design: Regardless of ambient percolation flux, the ACD rev 00 design always results in greater spatial variability in *T* and *RH* in the rock at the drift wall than in the line-load design (compare Tables 1.10.6.3 and 1.10.6.8); the variability in *T* and *RH* on WPs is also greater in the ACD rev 00 design than in the line-load design (compare Tables 1.10.6.4 and 1.10.6.9).

Figure 1.10.6.8 and Tables 1.10.6.9 through 1.10.6.14 indicate that there are three ambient percolation flux regimes for the 1.11-MTU/m line-load design, including (1) a low-flux (0.0–0.05-mm/yr) regime, (2) a medium-flux (0.05–1.0-mm/yr), and a high-flux (> 1–5-mm/yr) regime. For the medium-flux range, rock dryout and *RH* on WPs are relatively insensitive to ambient percolation flux. The cause of this insensitivity, which was discussed above, is related to the insensitivity of liquid-phase flux in the heat-pipe zone to the 0.05–5.0-mm/yr ambient percolation flux range (Fig. 1.10.6.2a). Consequently, the liquid-phase flux returning to the boiling front is relatively insensitive to ambient percolation flux. The low-flux regime has lower *RH* in the rock and on WPs because of (1) the lower initial liquid saturation in the rock, which requires less heat to dry out a given volume of rock; and (2) the lower liquid-phase flux that occurs in the heat-pipe zone that overlies the dryout zone. The high-flux regime has higher *RH* in the rock and on WPs because the higher liquid-phase fluxes increase the overall cooling and rewetting rates.

Tables 1.10.6.15 through 1.10.6.19 and Figure 1.10.6.9 summarize the influence of ambient percolation flux (over the range 0.0 to 0.3 mm/yr) on *T* and *RH* in the near-field rock and on WPs for the ACD rev 00 design and the reference case with backfill at 100 yr. Tables 1.10.6.20 through 1.10.6.26 and Figure 1.10.6.10 summarize the influence of ambient percolation flux (over the range 0.0 to 5.0 mm/yr) on *T* and *RH* in the near-field rock and on WPs for the 1.11-MTU/m line-load design and the reference case with backfill at 100 yr. The observations made above for the influence of ambient percolation flux on rock dryout for the cases without backfill are also applicable to the cases with backfill. For the 0.0–0.3-mm/yr ambient percolation flux range considered for the ACD rev 00 backfill cases, there are no additional sensitivities to ambient percolation flux; all of the differences in *RH* on WPs can be attributed to the sensitivity of rock dryout (ΔRH_{rock}) to ambient percolation flux, which was described above.

For the 0.0–5.0-mm/yr ambient percolation flux range considered for the 1.11-MTU/m line-load design, the influence of ambient percolation flux on rock dryout (ΔRH_{rock}), which was described above, can be clearly seen in the *RH* on WPs for the backfill cases. Accordingly, during the first 15,000 yr, there are minor differences in *RH* on WPs for the 0.05–1.0-mm/yr flux range; the one notable exception here is for the 1.0-mm/yr case, which sees an additional increase in *RH* at about 15,000 yr. The 0.0-mm/yr case has a much lower *RH* on WPs during the first 30,000 yr during which time ΔRH_{rock} continues to play a role in *RH* reduction on WPs. While three distinctive ambient percolation flux regimes were noted for rock dryout behavior, there are two distinctive ambient percolation flux regimes that can be identified with respect to the drift-ΔRH effect:

Low-liquid-phase flux regime of negligible wicking in the backfill: In this regime, the liquid-phase flux is low enough and the the matric potential in the near-field rock is low enough to result in negligible wicking of moisture into the backfill. This is very dependent on the hydrological properties of the backfill (the relative permeability and capillary pressure curves). Sand was chosen for the backfill because, for a wide range of conditions, it was found not to wick enough moisture into the backfill to obviate any of the drift-ΔRH effect. Other materials, such as crushed PTn and TSw2 tuff have a much greater tendency to wick moisture into the backfill than sand (or other sand-like granular materials, which have a negligible intragranular porosity); consequently, crushed tuff may not be conducive for the regime of negligible wicking.

High-liquid-phase flux regime of significant wicking in the backfill: In this regime, either the liquid-phase flux is high enough and/or the absolute value of the matric potential in the near-field rock is high enough to allow enough wicking of moisture to cause the partial pressure of water vapor P_v near the WP (in the backfill) to be significantly higher than in the near-field rock; the difference in P_v obviates some (or possibly all) of the drift-ΔRH effect (see Sections 1.8.3.2 and 1.10.5.2).

Given a matric potential that is close enough to zero (nearly fully saturated liquid saturation conditions in the near-field rock), it is even possible for a sand-like material to eventually wick enough moisture into the drift to reduce the drift-ΔRH effect. Both the 1.0- and 5.0-mm/yr cases eventually attain the same level of near-zero matric potential, whereby the sand-like backfill allows some moisture wicking back toward the WP. This is evidenced by the identical *RH* histories for the 1.0- and 5.0-mm/yr cases after 15,000 yr (Fig. 1.10.6.10b,d,f). The 5.0-mm/yr case attains a nearly-fully saturated state in the near-field rock earlier (about 2500 yr) than the 1.0-mm/yr case (about 15,000 yr) because the higher ambient percolation flux (5.0 mm/yr) more quickly overwhelms and rewets the dryout zone than in the 1.0-mm/yr case. A nonzero liquid saturation is attained in the backfill at 2500 and 15,000 yr for the 5.0- and 1.0-mm/yr cases, respectively. Notice that this wicking reduces only a fraction of the drift-ΔRH effect.

The similar early time (t < 15,000 yr) behavior for the 0.3- and 1.0-mm/yr line-load cases is evidenced by the nearly identical times to reach the *RH* = 65% thresholds for these cases (compare Tables 1.10.6.24 and 1.10.6.25). The 0.05-mm/yr case has greater ΔRH_{rock} than the 0.3-mm/yr case; consequently, early-time RH_{wp} is lower for the 0.05-mm/yr case than for the 0.3-mm/yr case. After ΔRH_{rock} has diminished in both the 0.05- and 0.3-mm/yr case, the RH_{wp} for these cases is nearly identical, which is evidenced by the nearly identical times to reach the *RH* = 90% thresholds for these cases (compare Tables 1.10.6.23 and 1.10.6.24). Rock dryout is so persistent for the 0.0-mm/yr case that the time to reach the *RH* = 90% threshold is increased relative to the higher flux cases. Because the 5.0-mm/yr case rewets more quickly than the 1.0-mm/yr case, the time to reach the *RH* = 65% threshold is less than for the 1.0-mm/yr case (compare Tables 1.10.6.25 and 1.10.6.26); however, because wicking in the drift eventually affects both cases to almost the same extent, their late-time RH_{wp} is similar, which is evidenced by the almost identical times to reach the *RH* = 90% threshold for these two cases.

Now we turn to the analysis conducted with the hybrid drift-scale–mountain-scale model. The hybrid model is the result of an abstraction process that combines the results of the mountain-scale T-H model with those of a detailed multiple-WP drift-scale model. The mountain-scale model assumes

that the hydrostratigraphic units are horizontal and of uniform thickness (as in the drift-scale model) and uses an R-Z coordinate system to represent three-dimensional mountain-scale T-H behavior. Because the mountain-scale model extends 1-km below the water table (unlike the drift-scale model, which has a constant-property boundary condition at the water table), it can very accurately represent the temperatures in the repository rock for all time. Note that because the drift-scale model assumes a constant-temperature boundary at the water table, the model predicts repository temperatures that are somewhat cooler (after about 2000 yr) than what they would be with an infinitely deep model domain.

Mountain-scale model: This model accurately accounts for the following important quantities:

Average temperatures in the repository rock: The influence of the edge-cooling effect on the temporal and spatial distribution of average T in the repository rock.

Average relative humidity in the repository rock: The influence of the effects of edge-cooling, edge-rewetting, and edge-shedding on the temporal and spatial distribution of average RH conditions in the repository rock (see Figs. 1.10.6.5 and 1.10.6.6).

Drift-scale model: This model accurately accounts for the following important quantities:

Temperature difference between the WP and the drift wall: This quantity (ΔT_{drift}) has been shown to be independent of AML (and proximity to the repository edge); therefore, ΔT_{drift} can be accurately predicted with the drift-scale model (see Figs. 1.10.5.7.9 and 1.10.5.7.10).

Temperature difference between the pillar centerline and the drift wall: This quantity (ΔT_{pillar}) is dependent on AML and drift spacing. If the effective AML (and drift spacing) are accounted for appropriately in the drift-scale model, then ΔT_{pillar} can be accurately represented with the drift-scale model (see Figs. 1.10.5.7.7 and 1.10.5.7.8).

Relative humidity difference between the pillar centerline and the drift wall: This quantity (ΔRH_{pillar}) is dependent on AML and drift spacing. If the effective AML (and drift spacing) is accounted for appropriately in the drift-scale model, then ΔRH_{pillar} can be accurately represented with the drift-scale model (see Figs. 1.10.5.7.7 and 1.10.5.7.8).

The hybrid model abstraction process involves a three-step process for determining the hybrid-model drift-wall and WP temperatures and a three-step process for determining the hybrid-model drift-wall and WP RH.

Abstracting drift-wall and WP temperatures: The three steps for calculating the temperature at selected repository locations and selected WP locations are as follows:

***T*-1: Average rock temperature at selected repository locations:** Using the mountain-scale model, T is obtained at selected locations, such as the 12.5% location (close to the repository center), and the 97% location (equivalent to the location of the outermost drift). The mountain-scale model temperatures are representative of the average T in the rock at the selected repository location. In the following example, the mountain-scale model is a model that represents mountain-scale T-H behavior with the use of an R-Z model [Buscheck and Nitao, 1994]. To account for the variable overburden thickness (between the repository and the ground surface) and to account for the fact that the major hydrostratigraphic units are not always horizontal and of constant thickness, it would be preferred to utilize a fully three-dimensional mountain-scale model for this step in the abstraction process.

***T*-2: Drift-wall temperature at selected repository and WP locations:** This is determined by taking T from step *T*-1, and adding one-half of ΔT_{pillar} determined from the drift-scale model for each of the selected WP locations. Half of ΔT_{pillar} is used (rather than 100% of it) because ΔT_{pillar} is the temperature difference from the coolest portion of the rock pillar (i.e., the centerline) and the hottest portion of the rock pillar (i.e., at the drift wall). The mountain-scale-model temperature is representative of the average rock pillar temperature (not the coolest rock pillar temperature).

T-3: **Waste package temperature at selected repository and WP locations:** This is determined by taking T from step *T*-2, and adding ΔT_{drift} determined from the drift-scale model for each of the selected WP locations.

Abstracting relative humidity in the rock at the drift wall and on WPs: The three steps for calculating *RH* at selected repository locations and selected WP locations are as follows:

RH-1 **: Average rock relative humidity at selected repository locations:** Using the mountain-scale model, *RH* is obtained at selected locations, such as the 12.5% location (close to the repository center), and the 97% location (equivalent to the location of the outermost drift). The mountain-scale model *RH* is representative of the average *RH* in the rock at the selected repository location. In the following example, the mountain-scale model is a model that represents mountain-scale T-H behavior with the use of an R-Z model [Buscheck and Nitao, 1994]. To account for the variable overburden thickness (between the repository and the ground surface) and to account for the fact that the major hydrostratigraphic units are not always horizontal and of constant thickness, it would be preferred to utilize a fully three-dimensional mountain-scale model for this step in the abstraction process.

RH-2: **Drift-wall relative humidity at selected repository and WP locations:** This is determined by taking *RH* from step *RH*-1, and adding one-half of ΔRH_{pillar} determined from the drift-scale model for each of the selected WP locations. Half of ΔRH_{pillar} is used (rather than 100% of it) because ΔT_{pillar} is the relative humidity difference from the most humid portion of the rock pillar (i.e., the centerline) and the least humid portion of the rock pillar (i.e., at the drift wall). The mountain-scale-model *RH* is representative of the average rock pillar *RH* (not the most humid rock pillar *RH*).

RH-3: **Waste package relative humidity at selected repository and WP locations:** This is determined by taking *RH* from step *RH*-2, and multiplying it by the ratio $P_{sat}(T_{dw})/P_{sat}(T_{wp})$, where $P_{sat}(T)$ is determined from the steam tables, for each of the selected WP locations. The temperature at the drift wall T_{dw} is determined in step *T*-2; the temperature on the surface of the WP T_{wp} is determined in step *T*-3.

There are two additional details about how this abstraction process is executed. The mountain-scale model accounts for the year-by-year WP emplacement schedule by ramping up the heat generation (from 0% to 100% of that generated by the full WP inventory) during the 24-yr emplacement period. Consequently, during the first 50 yr, it tends to underpredict the rate of temperature rise and the rate of *RH* reduction in the repository rock. Because drift-scale T-H behavior is insensitive to drift spacing (and AML) during the first 50 yr, the drift-scale model provides an accurate early-time representation of T and *RH* in the vicinity of the drifts, without requiring any geometric information about the larger-scale system (e.g., proximity to the repository edge). Consequently, the hybrid-model abstraction process involves the direct use of the drift-scale T and *RH* results during the first 50 yr. Incidentally, the drift-scale model and abstracted drift-scale–mountain-scale model results yield very similar T and *RH* at the drift wall and on the surface of the WP over the period 50 to 200 yr.

The second additional detail involves the selection of the appropriate AML and drift spacing for the drift-scale model that is used to determine ΔT_{pillar} and ΔRH_{pillar}. The selection is determined by the extent to which edge-cooling and edge-rewetting effects influence the average T and *RH* in the repository rock at a given repository location. In general, there are two categories of repository locations:

Repository locations not affected by edge-cooling/rewetting/shedding effects: At these locations, the effective AML and effective drift spacing are the same as those for an infinitely-large repository area. The effective AML for the drift-scale model that is used to determine ΔT_{pillar} and ΔRH_{pillar} at these locations is the same as the AML that is represented by the mountain-scale-model. The effective drift spacing for the drift-scale model is the same as the "actual" drift spacing being represented by the abstraction process.

Repository locations significantly affected by edge-cooling/rewetting/shedding effects: At these locations, edge-cooling/rewetting effects reduce the effective AML relative to locations that

experience negligible edge-cooling/rewetting effects. The effective AML for the drift-scale model that is used to determine ΔT_{pillar} and ΔRH_{pillar} at these locations is less than the AML that is represented by the mountain-scale model. The effective drift spacing for the drift-scale model is larger than the "actual" drift spacing being represented by the abstraction process. An example of this selection process is given below.

Figures 1.10.6.11–1.10.6.17 and Tables 1.10.6.27–1.10.6–30 summarize the T and RH results of this hybrid drift-scale–mountain-scale abstraction process for AML = 83.4 MTU/acre, a line-load design with a 0.1-m gap between WP, LML = 1.11 MTU/m, and drift spacing = 53.8 m. The T and RH results were obtained for two repository locations, including (1) the 12.5% location (close to the center of the repository) and (2) the 97% location (which is representative of the outermost drift of the repository). For comparison purposes, T and RH calculated by the "unmodified" drift-scale model are also provided (Figs.1.10.6.11a,b–1.10.6.17a,b).

Because the outermost drift of the repository has a drift spacing of 53.8 m on one of its sides and an infinite drift spacing on its other side, there is an "effective" drift spacing that lies somewhere between 53.8 m and infinity. The 45-MTU/acre drift-scale model with 100-m drift spacing was found to yield T and RH histories at an average rock pillar location that were very similar to those predicted by the mountain-scale model for the 97% location. Accordingly, it was decided that the 45-MTU/acre drift-scale model with 100-m drift spacing yields representative values of ΔT_{pillar} and ΔRH_{pillar} at the outermost drift of the repository.

Figures 1.10.6.11–1.10.6.14 (and Tables 1.10.6.12 and 1.10.6.27) compare the drift-scale and hybrid drift-scale–mountain-scale model for the case with no backfill. For the center of the repository, the drift-scale model yields T and RH results that are similar to those of the hybrid model. The hybrid model predicts slightly lower RH_{wp} for the first 4000 yr than is predicted by the drift-scale model. The slightly lower RH_{wp} in the drift-scale model is related to the waste inventory in the respective models. In the drift-scale model, 88.8% of the nuclear waste mass inventory is from SNF, while the other 11.2% is from DHLW (which produces a negligible amount of heat). In the mountain-scale model, 100% of the nuclear waste mass inventory is from SNF. Therefore, 100% of the inventory in the mountain-scale model is "heat-producing nuclear waste," while only 88.8% of the inventory in the drift-scale model is heat-producing nuclear waste, which causes the effective "heat-producing" AML in the drift-scale model to be 11.2% less than in the mountain-scale model. Consequently, the mountain-scale model predicts somewhat more intensive and more persistent rock dryout (ΔRH_{rock}) than the drift-scale model. Accordingly, as long as ΔRH_{rock} is significant, the hybrid drift-scale–mountain-scale model predicts slightly lower RH_{wp} than the drift-scale model. The effects of slightly greater ΔRH_{rock} are indicated by the longer time to rewet to the RH = 65% threshold, which is 1830–2070 yr for the hybrid model and 1450–1620 yr for the drift-scale model.

After ΔRH_{rock} is no longer significant, the hybrid drift-scale–mountain-scale model predicts slightly higher RH_{wp} than the drift-scale model. This difference is caused by the fact that the hybrid model (appropriately) predicts higher temperatures in the drift than are predicted by the drift-scale model. Recall that the drift-scale model has a constant-temperature boundary at the water table, which results in cooler temperatures after 2000 yr than would have occurred had the model extended "infinitely" below the water table. Because the hybrid model utilizes a mountain-scale model that correctly accounts for the vertical model domain, the hybrid model more accurately accounts for large-scale heat flow, which results in warmer temperatures in the repository than those predicted in the drift-scale model. Because the drift-ΔRH effect is determined by the ratio $P_{sat}(T_{dw})/P_{sat}(T_{wp})$ and because for a given ΔT_{drift}, this ratio is slightly higher for higher T, RH_{wp} in the hybrid model is slightly higher at later times (t > 4000 yr) than in the slightly cooler drift-scale model.

The influence of edge-cooling/rewetting effects on T and RH on WPs is seen by comparing the (d) and (f) panels in Figures 1.10.6.11–14 (and comparing Tables 1.10.6.27 and 1.10.6.28). At the outermost drift, the time to reach the RH = 65% threshold is reduced by a factor of 8.6, relative to the repository center; the time to reach the RH = 90% threshold is reduced by a factor of 5.0, relative to the repository center. A comparison of panels (b) and (f) in Figures 1.10.6.11–14 clearly illustrates the inadequacy of the "unmodified" drift-scale model in representing drift-scale behavior at the edge of the repository. The

hybrid drift-scale–mountain-scale model is a necessary and useful approach to providing an adequate representation of drift-scale T-H behavior at the edge of the repository.

Figures 1.10.6.15–1.10.6.17 (and Tables 1.10.6.24 and 1.10.6.29) compare the drift-scale and hybrid drift-scale–mountain-scale model for the case with no backfill. For the repository center, the drift-scale model yields T and RH results that are very similar to those of the hybrid model. For the reasons given above, the hybrid model predicts slightly lower RH_{wp} for the first 3500 yr than is predicted by the drift-scale model. For intermediate time ($3500 < t < 30{,}000$ yr), the drift-scale model predicts slightly lower RH_{wp} than the hybrid model; this difference arises because of the influence of the slightly higher T in the hybrid model on the ratio $P_{sat}(T_{dw})/P_{sat}(T_{wp})$. For late time ($t > 30{,}000$ yr), the two models predict virtually identical RH_{wp}.

The influence of edge-cooling/rewetting effects on T and RH on WPs is seen by comparing the (d) and (f) panels in Figures 1.10.6.15–17 (and comparing Tables 1.10.6.29 and 1.10.6.30). At the outermost drift, the time to reach the $RH = 65\%$ threshold is reduced by a factor of 1.5 for the coolest WP (the DHLW WP), relative to the repository center; however, the time to reach the $RH = 65\%$ threshold is nearly the same for the hotter-than-average WPs (the 26-yr-old PWR and 10-yr-old PWR WPs). The time to reach the $RH = 90\%$ threshold is nearly the same at the outermost drift as it is for the center of the repository. Because of the influence of the slightly lower T at the repository edge on the ratio $P_{sat}(T_{dw})/P_{sat}(T_{wp})$, the time to reach the $RH = 90\%$ threshold at the edge of the repository is slightly greater than at the center of the repository. A comparison of panels (b) and (f) in Figures 1.10.6.15–17 indicate that when backfill is used, the differences in T and RH predicted by the hybrid model for the repository edge, and T and RH predicted by the "unmodified" drift-scale model are quite similar (especially for $t > 4000$ yr).

Table 1.10.6.1 Liquid-phase flux 5 m above the upper drift wall at the location of the 26-yr-old PWR WP for the drift-scale model and at the repository horizon for the mountain-scale model for AML = 83.4 MTU/acre, and percolation flux = 0.3 mm/yr. The drift-scale model represents (1) the ACD rev 00 design with LML = 0.46 MTU/m and drift spacing = 22.5 m; and (2) the line-load design with a 0.1-m gap between WPs, drift spacing = 53.8 m, LML = 1.11 MTU/m, drift diameter = 5.5 m, sand invert, no backfill, WP emissivity = 0.8, and k_b = 280 millidarcy in all hydrostratigraphic units. The mountain-scale model represents the average conditions at different locations of the repository for k_b = 1 darcy in the TSw1 and TSw2 units.

Model type	Drift-scale		Mountain-scale			
Repository location	NA	NA	12.5%	50%	75%	94%
Repository design	ACD rev 00	Line-load	NA	NA	NA	NA
Time (yr)	Liquid-phase flux (mm/yr)					
0	0.2	0.2	0.3	0.3	0.3	0.3
100	254	0.0	0.0	0.0	0.0	0.2
200	172	0.0	0.0	0.0	0.0	21
500	99	0.0	0.0	0.0	0.0	25
1000	12	0.0	0.0	0.0	0.0	11
2000	18	0.0	0.0	0.0	5.7	1.1
3000	0.4	1.0	0.2	1.5	0.9	0.7
5000	0.36	0.6	1.6	1.0	0.6	0.5
6000	0.33	0.4	1.0	0.8	0.5	0.4
8000	0.30	0.29	0.7	0.5	0.4	0.4
10,000	0.29	0.26	0.5	0.4	0.4	0.4
20,000	0.25	0.24	0.4	0.4	0.39	0.37
100,000	0.20	0.20	0.33	0.33	0.33	0.33

Table 1.10.6.2 Liquid-phase flux 5 m above the upper drift wall at the location of the 26-yr-old PWR WP for the drift-scale model and at the repository horizon for the mountain-scale model for AML = 83.4 MTU/acre, and percolation flux = 0.05 mm/yr. The drift-scale model represents (1) the ACD rev 00 design with LML = 0.46 MTU/m and drift spacing = 22.5 m; and (2) the line-load design with a 0.1-m gap between WPs, drift spacing = 53.8 m, LML = 1.11 MTU/m, drift diameter = 5.5 m, sand invert, no backfill, WP emissivity = 0.8, and k_b = 280 millidarcy in all hydrostratigraphic units. The mountain-scale model represents the average conditions at different locations of the repository for k_b = 1 darcy in the TSw1 and TSw2 units.

Model type	Drift-scale		Mountain-scale			
Repository location	NA	NA	12.5%	50%	75%	94%
Repository design	ACD rev 00	Line-load	NA	NA	NA	NA
Time (yr)	Liquid-phase flux (mm/yr)					
0	0.04	0.04	0.05	0.05	0.05	0.05
100	0.0	0.0	0.0	0.0	0.0	0.0
200	0.0	0.0	0.0	0.0	0.0	0.0
500	0.0	0.0	0.0	0.0	0.0	0.0
1000	0.0	0.0	0.0	0.0	0.0	8
2000	0.0	0.0	0.0	0.0	0.0	1.1
3000	0.0	0.0	0.0	0.0	0.0	0.6
4000	0.2	0.0	0.0	0.0	0.8	0.4
5000	0.3	0.3	0.0	0.0	0.7	0.34
6000	0.6	0.6	0.0	0.1	0.6	0.29
8000	0.30	0.25	0.6	0.5	0.4	0.23
10,000	0.23	0.17	0.5	0.4	0.33	0.19
20,000	0.10	0.09	0.20	0.18	0.14	0.11
100,000	0.04	0.04	0.6	0.06	0.06	0.06

Table 1.10.6.3. Temperature and relative humidity in rock at upper drift wall for 83.4 MTU/acre, the ACD rev 00 design, drift spacing = 22.5 m, LML = 0.46 MTU/m, drift diameter = 5.5 m, sand invert, no backfill, WP emissivity = 0.8, and various percolation fluxes.

Percolation flux	0 mm/yr	0.05 mm/yr	0.3 mm/yr
T_{peak} (t < 100 yr)	127–181°C	111–172°C	100–165°C
RH_{max} (t < 100 yr)	19–40%	27–66%	36–98%
T_{peak} (t = 120 yr)	126–153°C	111–140°C	100–129°C
RH (t = 120 yr)	21–40%	30–65%	36–97%
RH (t = 2000 yr)	61–66%	76–82%	90–97%
RH (t = 10,000 yr)	72–75%	98–98%	99.8–99.8%

Table 1.10.6.4. Temperature and relative humidity on upper surface of WP for 83.4 MTU/acre, the ACD rev 00 design, drift spacing = 22.5 m, LML = 0.46 MTU/m, drift diameter = 5.5 m, sand invert, no backfill, WP emissivity = 0.8, and various percolation fluxes.

Percolation flux	0 mm/yr	0.05 mm/yr	0.3 mm/yr
T_{peak} (t < 100 yr)	130–203°C	116–197°C	107–192°C
RH_{max} (t < 100 yr)	15–38%	20–60%	25–86%
T_{peak} (t > 100 yr)	129–163°C	115–152°C	104–144°C
RH (t = 120 yr)	17–38%	23–59%	29–85%
RH (t = 2000 yr)	58–66%	73–82%	86–97%
RH (t = 10,000 yr)	68–75%	92–99%	92–99.9%
$t(RH = 65\%)$	1940–7630 yr	1050–1580 yr	0–630 yr
$t(RH = 90\%)$	23,690–28,230 yr	4440–7580 yr	1170–2330 yr

Table 1.10.6.5. Temperature and relative humidity on upper WP surface for AML = 83.4 MTU/acre, the ACD rev 00 design with LML = 0.46 MTU/m, drift spacing = 22.5 m, sand invert, no backfill, drift diameter = 5.5 m, WP emissivity = 0.8, and percolation flux = 0 mm/yr.

Waste package type	Hanford Site DHLW	Savannah River Site DHLW	40-yr-old PWR MPC	26-yr-old BWR MPC	26-yr-old PWR MPC	10-yr-old PWR MPC
T_{peak} (t < 100 yr)	130°C	143°C	137°C	148°C	156°C	203°C
RH_{max} (t < 100 yr)	38%	30%	30%	25%	21%	15%
T_{peak} (t > 100 yr)	129°C	136°C	136°C	143°C	148°C	163°C
RH (t = 120 yr)	38%	32%	31%	26%	23%	17%
RH (t = 2000 yr)	66%	65%	63%	62%	59%	58%
RH (t = 10,000 yr)	75%	75%	72%	72%	69%	68%
$t(RH = 65\%)$	1940 yr	1970 yr	3200 yr	4140 yr	6500 yr	7630 yr
$t(RH = 90\%)$	23,690 yr	23,800 yr	25,580 yr	26,150 yr	27,580 yr	28,230 yr

Table 1.10.6.6. Temperature and relative humidity on upper WP surface for AML = 83.4 MTU/acre, the ACD rev 00 design with LML = 0.46 MTU/m, drift spacing = 22.5 m, sand invert, no backfill, drift diameter = 5.5 m, WP emissivity = 0.8, and percolation flux = 0.05 mm/yr.

Waste package type	Hanford Site DHLW	Savannah River Site DHLW	40-yr-old PWR MPC	26-yr-old BWR MPC	26-yr-old PWR MPC	10-yr-old PWR MPC
T_{peak} (t < 100 yr)	116°C	133°C	124°C	136°C	150°C	197°C
RH_{max} (t < 100 yr)	62%	44%	50%	36%	31%	20%
T_{peak} (t > 100 yr)	115°C	124°C	123°C	131°C	135°C	152°C
RH (t = 120 yr)	59%	47%	46%	38%	33%	23%
RH (t = 2000 yr)	82%	82%	78%	77%	74%	73%
RH (t = 10,000 yr)	99%	99%	96%	95%	93%	92%
$t(RH = 65\%)$	1050 yr	1070 yr	1260 yr	1330 yr	1490 yr	1580 yr
$t(RH = 90\%)$	4440 yr	4510 yr	5270 yr	5550 yr	6690 yr	7580 yr

Table 1.10.6.7. Temperature and relative humidity on upper WP surface for AML = 83.4 MTU/acre, the ACD rev 00 design with LML = 0.46 MTU/m, drift spacing = 22.5 m, sand invert, no backfill, drift diameter = 5.5 m, WP emissivity = 0.8, and percolation flux = 0.3 mm/yr.

Waste package type	Hanford Site DHLW	Savannah River Site DHLW	40-yr-old PWR MPC	26-yr-old BWR MPC	26-yr-old PWR MPC	10-yr-old PWR MPC
T_{peak} (t < 100 yr)	106°C	121°C	112°C	127°C	145°C	192°C
RH_{max} (t < 100 yr)	86%	61%	65%	50%	42%	25%
T_{peak} (t > 100 yr)	104°C	114°C	112°C	120°C	125°C	143°C
RH (t = 120 yr)	85%	64%	64%	51%	44%	29%
RH (t = 2000 yr)	97%	97%	93%	91%	88%	86%
RH (t = 10,000 yr)	99.9%	99.9%	98%	96%	93%	92%
$t(RH = 65\%)$	0 yr	130 yr	140 yr	350 yr	520 yr	630 yr
$t(RH = 90\%)$	1170 yr	1190 yr	1650 yr	1850 yr	2200 yr	2330 yr

Table 1.10.6.8. Temperature and relative humidity in rock at upper drift wall for AML = 83.4 MTU/acre, a line-load design with a 0.1-m gap between WPs, drift spacing = 53.8 m, LML = 1.11 MTU/m, drift diameter = 5.5 m, sand invert, no backfill, WP emissivity = 0.8, and various percolation fluxes.

Percolation flux	0.0 mm/yr	0.05 mm/yr	0.3 mm/yr	1.0 mm/yr	5.0 mm/yr
T_{peak} (t < 100 yr)	177–199°C	167–191°C	161–184°C	162–185°C	161–183°C
RH_{max} (t < 100 yr)	15–18%	21–24%	23–25%	20–24%	22–26%
T_{peak} (t > 100 yr)	156–162°C	144–150°C	142–148°C	143–149°C	140–146°C
RH (t = 120 yr)	17–19%	23–27%	23–27%	22–26%	24–28%
RH (t = 2000 yr)	59–59%	73–74%	76–76%	73–74%	91–91%
RH (t = 10,000 yr)	70–71%	98–98%	99.1–99.1%	99.8–99.8%	99.9–99.9%

Table 1.10.6.9. Temperature and relative humidity on upper surface of WP for AML = 83.4 MTU/acre, a line-load design with a 0.1-m gap between WPs, drift spacing = 53.8 m, LML = 1.11 MTU/m, drift diameter = 5.5 m, sand invert, no backfill, WP emissivity = 0.8, and various percolation fluxes.

Percolation flux	0.0 mm/yr	0.05 mm/yr	0.3 mm/yr	1.0 mm/yr	5.0 mm/yr
T_{peak} (t < 100 yr)	187–216°C	178–209°C	172–203°C	173–203°C	172–202°C
RH_{max} (t < 100 yr)	12–16%	16–21%	16–21%	16–21%	17–22%
T_{peak} (t > 100 yr)	160–170°C	149–160°C	147–158°C	148–158°C	146–156°C
RH (t = 120 yr)	14–17%	18–23%	18–23%	18–22%	19–24%
RH (t = 2000 yr)	56–58%	70–72%	72–76%	74–78%	86–89%
RH (t = 10,000 yr)	67–69%	94–97%	94–98%	95–98%	97–99.1%
$t(RH$ = 65%)	6290-8480 yr	1530–1700 yr	1450–1620 yr	1580–1740 yr	1120–1260 yr
$t(RH$ = 90%)	25,850-27,680 yr	5500-6440 yr	4030–4680 yr	4300-4770 yr	2010-2190 yr

Table 1.10.6.10. Temperature and relative humidity on upper WP surface for AML = 83.4 MTU/acre, a line-load design with a 0.1-m gap between WPs, LML = 1.11 MTU/m, drift spacing = 53.8 m,sand invert, no backfill, drift diameter = 5.5 m, WP emissivity = 0.8, and percolation flux = 0 mm/yr.

Waste package type	Hanford Site DHLW	Savannah River Site DHLW	40-yr-old PWR MPC	26-yr-old BWR MPC	26-yr-old PWR MPC	10-yr-old PWR MPC
T_{peak} (t < 100 yr)	187°C	198°C	185°C	188°C	192°C	216°C
RH_{max} (t < 100 yr)	16%	15%	15%	15%	14%	12%
T_{peak} (t > 100 yr)	160°C	162°C	161°C	163°C	164°C	170°C
RH (t = 120 yr)	17%	17%	17%	17%	14%	14%
RH (t = 2000 yr)	58%	59%	57%	58%	57%	56%
RH (t = 10,000 yr)	69%	70%	69%	69%	68%	67%
$t(RH = 65\%)$	6840 yr	6290 yr	7370 yr	7210 yr	8150 yr	8480 yr
$t(RH = 90\%)$	26,250 yr	25,850 yr	26,720 yr	26,680 yr	27,360 yr	27,680 yr

Table 1.10.6.11. Temperature and relative humidity on upper WP surface for AML = 83.4 MTU/acre, a line-load design with a 0.1-m gap between WPs, LML = 1.11 MTU/m, drift spacing = 53.8 m,sand invert, no backfill, drift diameter = 5.5 m, WP emissivity = 0.8, and percolation flux = 0.05 mm/yr.

Waste package type	Hanford Site DHLW	Savannah River Site DHLW	40-yr-old PWR MPC	26-yr-old BWR MPC	26-yr-old PWR MPC	10-yr-old PWR MPC
T_{peak} (t < 100 yr)	178°C	190°C	176°C	180°C	184°C	209°C
RH_{max} (t < 100 yr)	21%	20%	21%	20%	19%	16%
T_{peak} (t > 100 yr)	149°C	151°C	150°C	150°C	153°C	160°C
RH (t = 120 yr)	23%	23%	23%	23%	21%	18%
RH (t = 2000 yr)	72%	73%	71%	72%	70%	70%
RH (t = 10,000 yr)	97%	97%	96%	96%	95%	94%
$t(RH = 65\%)$	1580 yr	1530 yr	1620 yr	1610 yr	1680 yr	1700 yr
$t(RH = 90\%)$	5640 yr	5500 yr	5780 yr	5750 yr	5990 yr	6440 yr

Table 1.10.6.12 Temperature and relative humidity on upper WP surface for AML = 83.4 MTU/acre, a line-load design with a 0.1-m gap between WPs, LML = 1.11 MTU/m, drift spacing = 53.8 m,sand invert, no backfill, drift diameter = 5.5 m, WP emissivity = 0.8, and percolation flux = 0.3 mm/yr.

Waste package type	Hanford Site DHLW	Savannah River Site DHLW	40-yr-old PWR MPC	26-yr-old BWR MPC	26-yr-old PWR MPC	10-yr-old PWR MPC
T_{peak} (t < 100 yr)	171°C	184°C	171°C	174°C	178°C	203°C
RH_{max} (t < 100 yr)	21%	21%	21%	21%	19%	16%
T_{peak} (t > 100 yr)	147°C	149°C	148°C	148°C	151°C	158°C
RH (t = 120 yr)	23%	23%	23%	22%	21%	18%
RH (t = 2000 yr)	75%	76%	76%	74%	73%	72%
RH (t = 10,000 yr)	97%	98%	98%	96%	95%	94%
$t(RH = 65\%)$	1510 yr	1450 yr	1550 yr	1540 yr	1610 yr	1620 yr
$t(RH = 90\%)$	4180 yr	4030 yr	4320 yr	4290 yr	4540 yr	4680 yr

Table 1.10.6.13. Temperature and relative humidity on upper WP surface for AML = 83.4 MTU/acre, a line-load design with a 0.1-m gap between WPs, LML = 1.11 MTU/m, drift spacing = 53.8 m,sand invert, no backfill, drift diameter = 5.5 m, WP emissivity = 0.8, and percolation flux = 1.0 mm/yr.

Waste package type	Hanford Site DHLW	Savannah River Site DHLW	40-yr-old PWR MPC	26-yr-old BWR MPC	26-yr-old PWR MPC	10-yr-old PWR MPC
T_{peak} (t < 100 yr)	173°C	184°C	172°C	175°C	179°C	203°C
RH_{max} (t < 100 yr)	21%	20%	20%	20%	19%	16%
T_{peak} (t > 100 yr)	148°C	149°C	149°C	149°C	152°C	158°C
RH (t = 120 yr)	22%	22%	22%	22%	20%	18%
RH (t = 2000 yr)	72%	73%	72%	72%	71%	70%
RH (t = 10,000 yr)	98%	99%	97%	97%	96%	95%
$t(RH = 65\%)$	1630 yr	1580 yr	1670 yr	1650 yr	1720 yr	1740 yr
$t(RH = 90\%)$	4400 yr	4300 yr	4510 yr	4490 yr	4660 yr	4770 yr

Table 1.10.6.14. Temperature and relative humidity on upper WP surface for AML = 83.4 MTU/acre, a line-load design with a 0.1-m gap between WPs, LML = 1.11 MTU/m, drift spacing = 53.8 m,sand invert, no backfill, drift diameter = 5.5 m, WP emissivity = 0.8, and percolation flux = 5.0 mm/yr.

Waste package type	Hanford Site DHLW	Savannah River Site DHLW	40-yr-old PWR MPC	26-yr-old BWR MPC	26-yr-old PWR MPC	10-yr-old PWR MPC
T_{peak} (t < 100 yr)	172°C	183°C	171°C	174°C	178°C	202°C
RH_{max} (t < 100 yr)	22%	21%	22%	21%	20%	17%
T_{peak} (t > 100 yr)	146°C	147°C	146°C	147°C	150°C	156°C
RH (t = 120 yr)	24%	24%	24%	23%	22%	19%
RH (t = 2000 yr)	89%	90%	88%	88%	86%	86%
RH (t = 10,000 yr)	99.1%	99.4%	98%	98%	97%	97%
$t(RH = 65\%)$	1170 yr	1120 yr	1190 yr	1190 yr	1240 yr	1250 yr
$t(RH = 90\%)$	2060 yr	2010 yr	2100 yr	2090 yr	2160 yr	2190 yr

Table 1.10.6.15. Temperature and relative humidity in rock at upper drift wall for 83.4 MTU/acre, the ACD rev 00 design, drift spacing = 22.5 m, LML = 0.46 MTU/m, drift diameter = 5.5 m, sand invert, full sand backfill at 100 yr with K_{th} = 0.6 W/m°C, WP emissivity = 0.8, and various percolation fluxes.

Percolation flux	**0 mm/yr**	**0.05 mm/yr**	**0.3 mm/yr**
T_{peak} (t < 100 yr)	127–181°C	111–172°C	100–165°C
RH_{max} (t < 100 yr)	19–40%	27–66%	36–98%
T_{peak} (t = 120 yr)	125–149°C	110–136°C	100–123°C
RH (t = 120 yr)	23–43%	3470%	45–99%
RH (t = 2000 yr)	62–67%	77–83%	92–99%
RH (t = 10,000 yr)	73–76%	98–98%	99.8–99.8%

Table 1.10.6.16. Temperature and relative humidity on upper surface of WP for 83.4 MTU/acre, the ACD rev 00 design, drift spacing = 22.5 m, LML = 0.46 MTU/m, drift diameter = 5.5 m, sand invert, full sand backfill at 100 yr with K_{th} = 0.6 W/m°C, WP emissivity = 0.8, and various percolation fluxes.

Percolation flux	**0 mm/yr**	**0.05 mm/yr**	**0.3 mm/yr**
T_{peak} (t < 100 yr)	130–203°C	116–197°C	107–192°C
RH_{max} (t < 100 yr)	15–38%	20–60%	25–86%
T_{peak} (t > 100 yr)	141–374°C	127–362°C	117–353°C
RH (t = 120 yr)	0.5–28%	0.5–42%	1–57%
RH (t = 2000 yr)	30–66%	37–82%	43–98%
RH (t = 10,000 yr)	44–75%	60–98%	60–99.7%
$t(RH$ = 65%)	1830–22,010 yr	1080–13,740 yr	160*–13,330 yr
$t(RH$ = 90%)	23,530–72,820 yr	4310–66,490 yr	860–62,680 yr

Table 1.10.6.17. Temperature and relative humidity on upper WP surface for AML = 83.4 MTU/acre, the ACD rev 00 design with LML = 0.46 MTU/m, drift spacing = 22.5 m, sand invert, full sand backfill at 100 yr with K_{th} = 0.6 W/m°C, drift diameter = 5.5 m, WP emissivity = 0.8, and percolation flux = 0.0 mm/yr.

Waste package type	Hanford Site DHLW	Savannah River Site DHLW	40-yr-old PWR MPC	26-yr-old BWR MPC	26-yr-old PWR MPC	10-yr-old PWR MPC
T_{peak} (t < 100 yr)	130°C	143°C	137°C	148°C	156°C	202°C
RH_{max} (t < 100 yr)	44%	30%	36%	25%	21%	14%
T_{peak} (t > 100 yr)	141°C	158°C	195°C	245°C	296°C	374°C
RH (t = 120 yr)	28%	19%	8%	3%	2%	1%
RH (t = 2000 yr)	66%	66%	49%	43%	35%	30%
RH (t = 10,000 yr)	75%	75%	61%	56%	48%	44%
$t(RH = 65\%)$	1830 yr	1860 yr	12,590 yr	15,310 yr	19,660 yr	22,010 yr
$t(RH = 90\%)$	23,530 yr	24,090 yr	37,890 yr	45,580 yr	65,290 yr	72,820 yr

Table 1.10.6.18. Temperature and relative humidity on upper WP surface for AML = 83.4 MTU/acre, the ACD rev 00 design with LML = 0.46 MTU/m, drift spacing = 22.5 m, sand invert, full sand backfill at 100 yr with K_{th} = 0.6 W/m°C, drift diameter = 5.5 m, WP emissivity = 0.8, and percolation flux = 0.05 mm/yr.

Waste package type	Hanford Site DHLW	Savannah River Site DHLW	40-yr-old PWR MPC	26-yr-old BWR MPC	26-yr-old PWR MPC	10-yr-old PWR MPC
T_{peak} (t < 100 yr)	116°C	133°C	124°C	136°C	150°C	197°C
RH_{max} (t < 100 yr)	62%	44%	50%	36%	31%	20%
T_{peak} (t > 100 yr)	127°C	146°C	182°C	232°C	282°C	362°C
RH (t = 120 yr)	42%	26%	10%	4%	2%	1%
RH (t = 2000 yr)	82%	82%	60%	52%	42%	37%
RH (t = 10,000 yr)	98%	98%	81%	75%	65%	60%
$t(RH$ = 65%)	1100 yr	1080 yr	2970 yr	4760 yr	9910 yr	13,740 yr
$t(RH$ = 90%)	4310 yr	4470 yr	27,890 yr	37,590 yr	57,810 yr	66,490 yr

Table 1.10.6.19. Temperature and relative humidity on upper WP surface for AML = 83.4 MTU/acre, the ACD rev 00 design with LML = 0.46 MTU/m, drift spacing = 22.5 m, sand invert, full sand backfill at 100 yr with K_{th} = 0.6 W/m°C, drift diameter = 5.5 m, WP emissivity = 0.8, and percolation flux = 0.3 mm/yr.

Waste package type	Hanford Site DHLW	Savannah River Site DHLW	40-yr-old PWR MPC	26-yr-old BWR MPC	26-yr-old PWR MPC	10-yr-old PWR MPC
T_{peak} (t < 100 yr)	106°C	121°C	112°C	127°C	145°C	192°C
RH_{max} (t < 100 yr)	86%	61%	65%	50%	42%	25%
T_{peak} (t > 100 yr)	117°C	136°C	172°C	222°C	272°C	353°C
RH (t = 120 yr)	57%	34%	13%	5%	2%	1%
RH (t = 2000 yr)	98%	97%	71%	62%	50%	43%
RH (t = 10,000 yr)	99.7%	99.2%	82%	76%	66%	60%
$t(RH = 65\%)$	160* yr	210* yr	1590 yr	2250 yr	9480 yr	13,660 yr
$t(RH = 90\%)$	950 yr	860 yr	25,870 yr	35,690 yr	54,680 yr	62,670 yr
* RH is never less than 65% prior to backfill						

Table 1.10.6.20. Temperature and relative humidity in rock at upper drift wall for AML = 83.4 MTU/acre, a line-load design with a 0.1-m gap between WPs, drift spacing = 53.8 m, LML = 1.11 MTU/m, drift diameter = 5.5 m, sand invert, full sand backfill at 100 yr with K_{th} = 0.6 W/m°C, WP emissivity = 0.8, and various percolation fluxes.

Percolation flux	0.0 mm/yr	0.05 mm/yr	0.3 mm/yr	1.0 mm/yr	5.0 mm/yr
T_{peak} (t < 100 yr)	177–199°C	167–191°C	161–184°C	162–185°C	161–183°C
RH_{max} (t < 100 yr)	15–18%	21–24%	21–25%	21–24%	22-26%
T_{peak} (t > 100 yr)	150–151°C	138–140°C	135–137°C	136–138°C	134–135°C
RH (t = 120 yr)	22–22%	30–31%	31–31%	30–30%	32–32%
RH (t = 2000 yr)	61–61%	76–76%	78–78%	76–76%	94–94%
RH (t = 10,000 yr)	72–72%	98.5–98.5%	99.1–99.1%	99.8–99.8%	99.9–99.9%

Table 1.10.6.21. Temperature and relative humidity on upper WP surface for AML = 83.4 MTU/acre, a line-load design with a 0.1-m gap between WPs, drift spacing = 53.8 m, LML = 1.11 MTU/m, drift diameter = 5.5 m, sand invert, full sand backfill at 100 yr with K_{th} = 0.6 W/m°C, WP emissivity = 0.8, and various percolation fluxes.

Percolation flux	**0.0 mm/yr**	**0.05 mm/yr**	**0.3 mm/yr**	**1.0 mm/yr**	**5.0 mm/yr**
T_{peak} (t < 100 yr)	187–216°C	178–209°C	172–203°C	173–203°C	172–202°C
RH_{max} (t < 100 yr)	12–16%	16–21%	16–21%	16–21%	17–22%
T_{peak} (t > 100 yr)	263–278°C	252–268°C	250–266°C	251–267°C	249–264°C
RH (t = 120 yr)	2–2%	2–3%	2–3%	2–3%	2–3%
RH (t = 2000 yr)	39–40%	48–49%	49–51%	48–50%	57–59%
RH (t = 10,000 yr)	52–55%	72–76%	73–76%	73–77%	81–84%
$t(RH$ = 65%)	15,520-17,520 yr	4850–5830 yr	3730–4600 yr	3820–4610 yr	2080–2180 yr
$t(RH$ = 90%)	41,840-50,660 yr	33,580-43,430 yr	30,480–39,920 yr	19,790-27,390 yr	19,930-27,490 yr

Table 1.10.6.22. Temperature and relative humidity on upper WP surface for AML = 83.4 MTU/acre, a line-load design with a 0.1-m gap between WPs, LML = 1.11 MTU/m, drift spacing = 53.8 m,sand invert, full sand backfill at 100 yr with K_{th} = 0.6 W/m°C, drift diameter = 5.5 m, WP emissivity = 0.8, and percolation flux = 0.0 mm/yr.

Waste package type	Hanford Site DHLW	Savannah River Site DHLW	40-yr-old PWR MPC	26-yr-old BWR MPC	26-yr-old PWR MPC	10-yr-old PWR MPC
T_{peak} (t < 100 yr)	187°C	198°C	185°C	188°C	192°C	216°C
RH_{max} (t < 100 yr)	16%	15%	15%	15%	14%	12%
T_{peak} (t > 100 yr)	264°C	270°C	266°C	263°C	268°C	278°C
RH (t = 120 yr)	2%	2%	2%	2%	2%	2%
RH (t = 2000 yr)	40%	41%	39%	40%	38%	39%
RH (t = 10,000 yr)	55%	56%	53%	54%	52%	52%
$t(RH$ = 65%)	16,170 yr	15,520 yr	16,850 yr	16,380 yr	17,540 yr	17,520 yr
$t(RH$ = 90%)	44,480 yr	41,840 yr	47,720 yr	46,020 yr	51,080 yr	50,660 yr

Table 1.10.6.23. Temperature and relative humidity on upper WP surface for AML = 83.4 MTU/acre, a line-load design with a 0.1-m gap between WPs, LML = 1.11 MTU/m, drift spacing = 53.8 m,sand invert, full sand backfill at 100 yr with K_{th} = 0.6 W/m°C, drift diameter = 5.5 m, WP emissivity = 0.8, and percolation flux = 0.05 mm/yr.

Waste package type	Hanford Site DHLW	Savannah River Site DHLW	40-yr-old PWR MPC	26-yr-old BWR MPC	26-yr-old PWR MPC	10-yr-old PWR MPC
T_{peak} (t < 100 yr)	178°C	190°C	176°C	180°C	184°C	209°C
RH_{max} (t < 100 yr)	21%	20%	21%	20%	19%	16%
T_{peak} (t > 100 yr)	253°C	260°C	255°C	252°C	258°C	268°C
RH (t = 120 yr)	3%	3%	3%	3%	3%	2%
RH (t = 2000 yr)	49%	51%	48%	50%	47%	48%
RH (t = 10,000 yr)	76%	77%	74%	75%	72%	72%
$t(RH = 65\%)$	5150 yr	4850 yr	5500 yr	5220 yr	5800 yr	5830 yr
$t(RH = 90\%)$	36,130 yr	33,580 yr	39,450 yr	37,740 yr	43,590 yr	43,430 yr

Table 1.10.6.24. Temperature and relative humidity on upper WP surface for AML = 83.4 MTU/acre, a line-load design with a 0.1-m gap between WPs, LML = 1.11 MTU/m, drift spacing = 53.8 m,sand invert, full sand backfill at 100 yr with K_{th} = 0.6 W/m°C, drift diameter = 5.5 m, WP emissivity = 0.8, and percolation flux = 0.3 mm/yr.

Waste package type	Hanford Site DHLW	Savannah River Site DHLW	40-yr-old PWR MPC	26-yr-old BWR MPC	26-yr-old PWR MPC	10-yr-old PWR MPC
T_{peak} (t < 100 yr)	171°C	184°C	171°C	174°C	178°C	203°C
RH_{max} (t < 100 yr)	21%	21%	21%	21%	19%	16%
T_{peak} (t > 100 yr)	252°C	258°C	250°C	251°C	256°C	266°C
RH (t = 120 yr)	3%	3%	3%	3%	3%	2%
RH (t = 2000 yr)	51%	52%	50%	51%	49%	49%
RH (t = 10,000 yr)	76%	77%	74%	76%	73%	73%
$t(RH$ = 65%)	3930 yr	3730 yr	4250 yr	3960 yr	4580 yr	4600 yr
$t(RH$ = 90%)	33,320 yr	30,480 yr	36,800 yr	34,890 yr	39,920 yr	39,820 yr

Table 1.10.6.25. Temperature and relative humidity on upper WP surface for AML = 83.4 MTU/acre, a line-load design with a 0.1-m gap between WPs, LML = 1.11 MTU/m, drift spacing = 53.8 m,sand invert, full sand backfill at 100 yr with K_{th} = 0.6 W/m°C, drift diameter = 5.5 m, WP emissivity = 0.8, and percolation flux = 1.0 mm/yr.

Waste package type	Hanford Site DHLW	Savannah River Site DHLW	40-yr-old PWR MPC	26-yr-old BWR MPC	26-yr-old PWR MPC	10-yr-old PWR MPC
T_{peak} (t < 100 yr)	173°C	184°C	172°C	175°C	179°C	203°C
RH_{max} (t < 100 yr)	21%	20%	20%	20%	19%	16%
T_{peak} (t > 100 yr)	252°C	258°C	254°C	251°C	257°C	267°C
RH (t = 120 yr)	3%	3%	3%	3%	3%	2%
RH (t = 2000 yr)	50%	51%	48%	50%	47%	48%
RH (t = 10,000 yr)	77%	78%	75%	76%	74%	73%
$t(RH = 65\%)$	3990 yr	3820 yr	4300 yr	4040 yr	4590 yr	4610 yr
$t(RH = 90\%)$	21,750 yr	19,790 yr	24,790 yr	23,600 yr	27,240 yr	27,390 yr

Table 1.10.6.26. Temperature and relative humidity on upper WP surface for AML = 83.4 MTU/acre, a line-load design with a 0.1-m gap between WPs, LML = 1.11 MTU/m, drift spacing = 53.8 m,sand invert, full sand backfill at 100 yr with K_{th} = 0.6 W/m°C, drift diameter = 5.5 m, WP emissivity = 0.8, and percolation flux = 5.0 mm/yr.

Waste package type	Hanford Site DHLW	Savannah River Site DHLW	40-yr-old PWR MPC	26-yr-old BWR MPC	26-yr-old PWR MPC	10-yr-old PWR MPC
T_{peak} (t < 100 yr)	172°C	183°C	171°C	174°C	178°C	202°C
RH_{max} (t < 100 yr)	22%	21%	22%	21%	20%	17%
T_{peak} (t > 100 yr)	250°C	256°C	252°C	249°C	254°C	264°C
RH (t = 120 yr)	3%	3%	3%	3%	3%	2%
RH (t = 2000 yr)	60%	62%	58%	60%	57%	58%
RH (t = 10,000 yr)	84%	85%	83%	84%	82%	81%
$t(RH$ = 65%)	2120 yr	2080 yr	2160 yr	2130 yr	2190 yr	2180 yr
$t(RH$ = 90%)	21,760 yr	19,930 yr	24,820 yr	23,530 yr	27,340 yr	27,490 yr

Table 1.10.6.27 Temperature and relative humidity on upper WP surface at the 12.5% repository location (close to the center of the repository) for AML = 83.4 MTU/acre, a line-load design with a 0.1-m gap between WPs, LML = 1.11 MTU/m, drift spacing = 53.8 m,sand invert, no backfill, drift diameter = 5.5 m, WP emissivity = 0.8, and percolation flux = 0.3 mm/yr. Calculations were done with the hybrid mountain-scale–drift-scale model.

Waste package type	Hanford Site DHLW	Savannah River Site DHLW	40-yr-old PWR MPC	26-yr-old BWR MPC	26-yr-old PWR MPC	10-yr-old PWR MPC
T_{peak} (t < 100 yr)	172°C	184°C	171°C	174°C	178°C	203°C
RH_{max} (t < 100 yr)	9%	9%	9%	9%	8%	7%
T_{peak} (t > 100 yr)	147°C	149°C	148°C	148°C	151°C	158°C
RH (t = 120 yr)	14%	14%	14%	14%	13%	11%
RH (t = 2000 yr)	66%	67%	66%	66%	65%	64%
RH (t = 10,000 yr)	98%	98%	97%	97%	96%	95%
$t(RH$ = 65%)	1890 yr	1830 yr	1940 yr	1930 yr	2020 yr	2070 yr
$t(RH$ = 90%)	4220 yr	4140 yr	4280 yr	4280 yr	4400 yr	4470 yr

Table 1.10.6.28 Temperature and relative humidity on upper WP surface at the 97% repository location (at the outer edge of the repository) for AML = 83.4 MTU/acre, a line-load design with a 0.1-m gap between WPs, LML = 1.11 MTU/m, drift spacing = 53.8 m,sand invert, no backfill, drift diameter = 5.5 m, WP emissivity = 0.8, and percolation flux = 0.3 mm/yr. Calculations were done with the hybrid mountain-scale–drift-scale model.

Waste package type	Hanford Site DHLW	Savannah River Site DHLW	40-yr-old PWR MPC	26-yr-old BWR MPC	26-yr-old PWR MPC	10-yr-old PWR MPC
T_{peak} (t < 100 yr)	156°C	171°C	154°C	158°C	163°C	195°C
RH_{max} (t < 100 yr)	42%	42%	42%	41%	38%	33%
T_{peak} (t > 100 yr)	127°C	127°C	127°C	128°C	131°C	137°C
RH (t = 120 yr)	47%	48%	47%	46%	43%	38%
RH (t = 2000 yr)	97%	98%	96%	95%	94%	93%
RH (t = 10,000 yr)	97%	98%	97%	97%	96%	95%
$t(RH = 65\%)$	190 yr	180 yr	200 yr	200 yr	220 yr	240 yr
$t(RH = 90\%)$	430 yr	370 yr	490 yr	530 yr	660 yr	890 yr

Table 1.10.6.29 Temperature and relative humidity on upper WP surface at the 12.5% repository location (close to the center of the repository) for AML = 83.4 MTU/acre, a line-load design with a 0.1-m gap between WPs, LML = 1.11 MTU/m, drift spacing = 53.8 m,sand invert, full sand backfill at 100 yr with K_{th} = 0.6 W/m°C, drift diameter = 5.5 m, WP emissivity = 0.8, and percolation flux = 0.3 mm/yr.

Waste package type	Hanford Site DHLW	Savannah River Site DHLW	40-yr-old PWR MPC	26-yr-old BWR MPC	26-yr-old PWR MPC	10-yr-old PWR MPC
T_{peak} (t < 100 yr)	172°C	184°C	171°C	174°C	178°C	203°C
RH_{max} (t < 100 yr)	10%	9%	10%	10%	9%	7%
T_{peak} (t > 100 yr)	252°C	258°C	253°C	251°C	256°C	266°C
RH (t = 120 yr)	2%	2%	2%	2%	2%	1%
RH (t = 2000 yr)	45%	46%	44%	45%	43%	43%
RH (t = 10,000 yr)	78%	80%	77%	78%	76%	75%
$t(RH$ = 65%)	3810 yr	3700 yr	3920 yr	3830 yr	4030 yr	4030 yr
$t(RH$ = 90%)	33,910 yr	30,950 yr	37,510 yr	35,630 yr	41,020 yr	40,780 yr

Table 1.10.6.30 Temperature and relative humidity on upper WP surface at the 97% repository location (at the outer edge of the repository) for AML = 83.4 MTU/acre, a line-load design with a 0.1-m gap between WPs, LML = 1.11 MTU/m, drift spacing = 53.8 m,sand invert, full sand backfill at 100 yr with K_{th} = 0.6 W/m°C, drift diameter = 5.5 m, WP emissivity = 0.8, and percolation flux = 0.3 mm/yr.

Waste package type	Hanford Site DHLW	Savannah River Site DHLW	40-yr-old PWR MPC	26-yr-old BWR MPC	26-yr-old PWR MPC	10-yr-old PWR MPC
T_{peak} (t < 100 yr)	156°C	171°C	154°C	158°C	163°C	195°C
RH_{max} (t < 100 yr)	42%	42%	42%	41%	38%	33%
T_{peak} (t > 100 yr)	236°C	242°C	238°C	236°C	241°C	251°C
RH (t = 120 yr)	5%	4%	4%	5%	4%	4%
RH (t = 2000 yr)	61%	63%	59%	60%	57%	57%
RH (t = 10,000 yr)	76%	78%	75%	75%	73%	72%
$t(RH$ = 65%)	2530 yr	2310 yr	3080 yr	2710 yr	3850 yr	4010 yr
$t(RH$ = 90%)	35,770 yr	33,050 yr	39,060 yr	37,440 yr	43,050 yr	42,830 yr

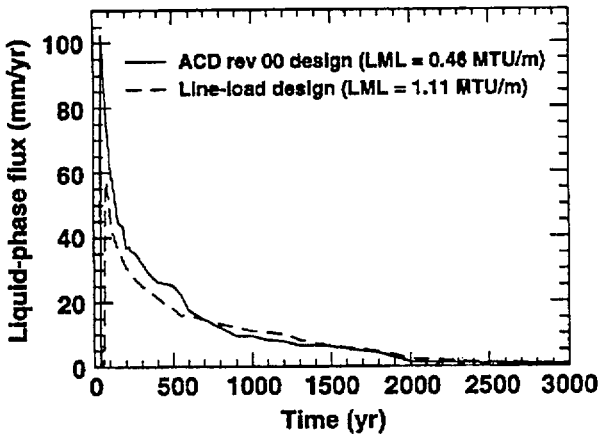

Figure 1.10.6.1. Liquid-phase flux 51 m directly above the emplacement drift for AML = 83.4 MTU/acre, sand invert, no backfill, drift diameter = 5.5 m, WP emissivity = 0.8, and various ambient percolation fluxes. Curves are plotted for the ACD rev 00 design with LML = 0.46 MTU/m and drift spacing = 22.5 m; and for a line-load design with a 0.1-m gap between WPs, LML = 1.11 MTU/m, and drift spacing = 53.8 m. Curves are plotted for conditions directly above the Hanford Site DHLW WP.

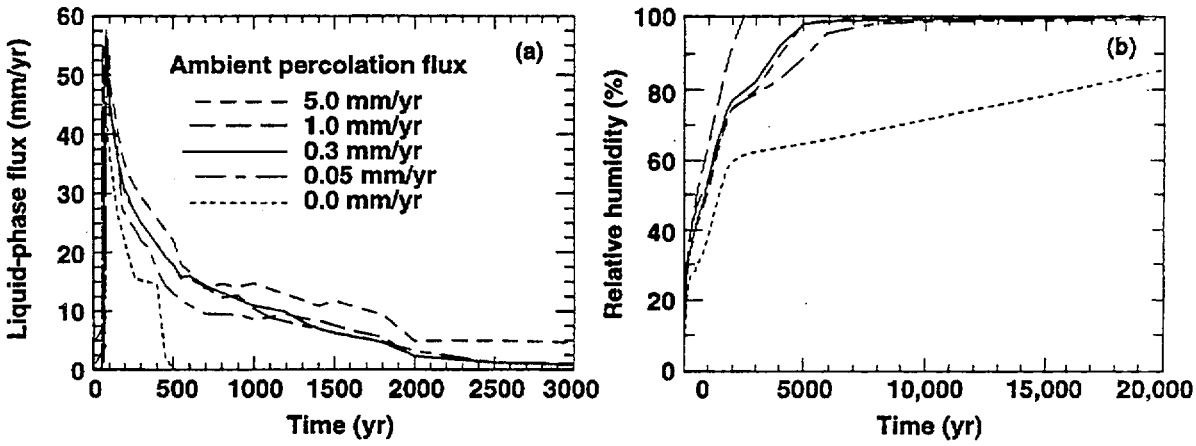

Figure 1.10.6.2. Liquid-phase flux 51 m above the repository horizon (a) and relative humidity in rock at the upper drift wall (b) for the line-load design with AML = 83.4 MTU/acre, a 0.1-m gap between WPs, LML = 1.11 MTU/m, drift spacing = 53.8 m, sand invert, no backfill, drift diameter = 5.5 m, WP emissivity = 0.8, and various ambient percolation fluxes. Curves are plotted for conditions directly above the Hanford Site DHLW WP. Note the different time scales.

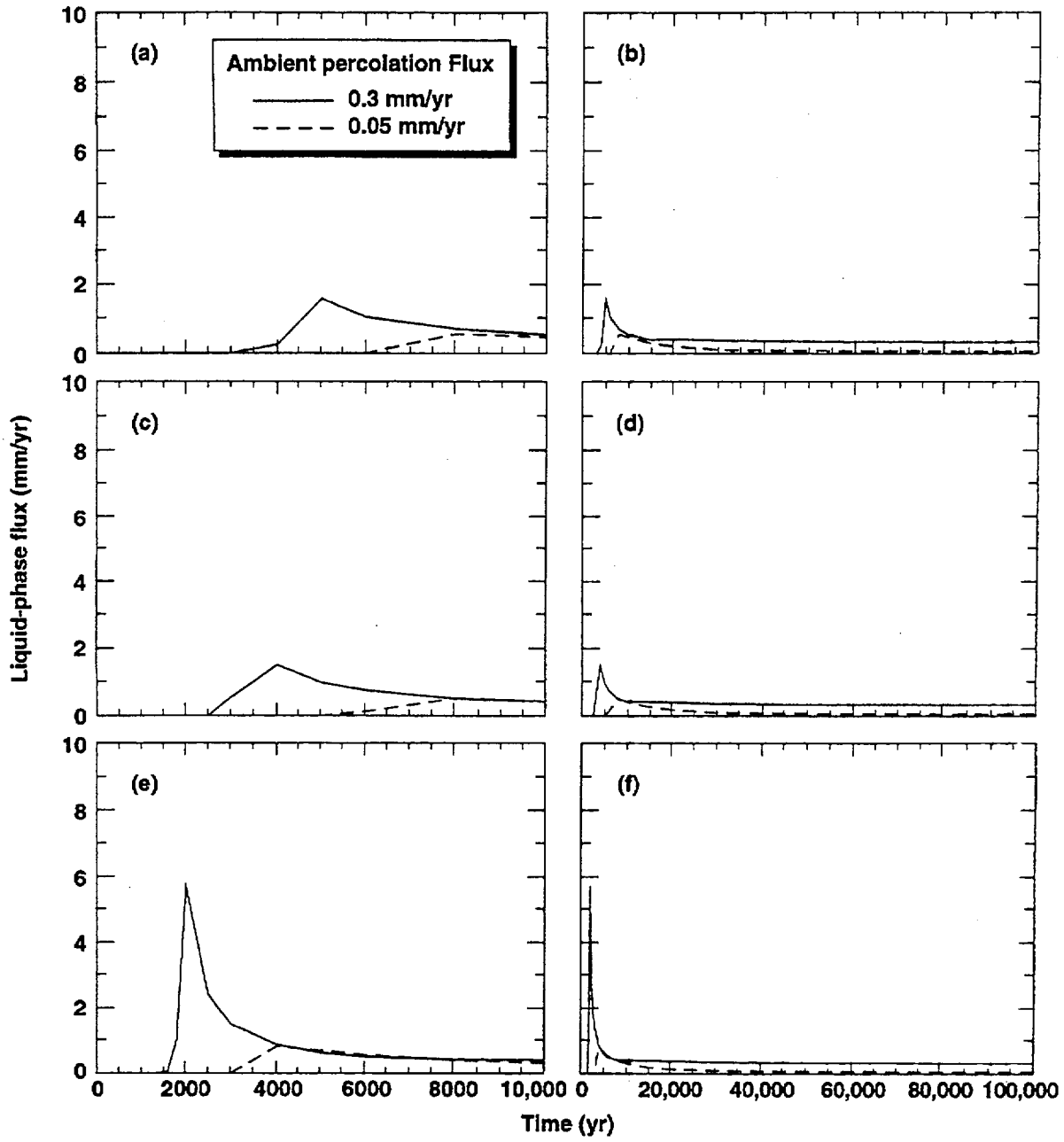

Figure 1.10.6.3. Liquid-phase flux at the repository horizon at various repository locations, including: (a,b) 12.5%, (c,d) 50%, and (e,f) 75%, for AML = 83.4 MTU/acre, repository area = 3.06 km^2, and various ambient percolation fluxes. The repository locations are identified as the percentage of the repository area enclosed, with 0% corresponding to the repository center, and 100% corresponding to the outer perimeter. Calculations were done with a mountain-scale, smeared-heat-source model that uniformly distributes the decay heat from a mixture of 26-yr-old BWR WPs and 26-yr-old PWR WPs over the 3.06-km^2 repository area.

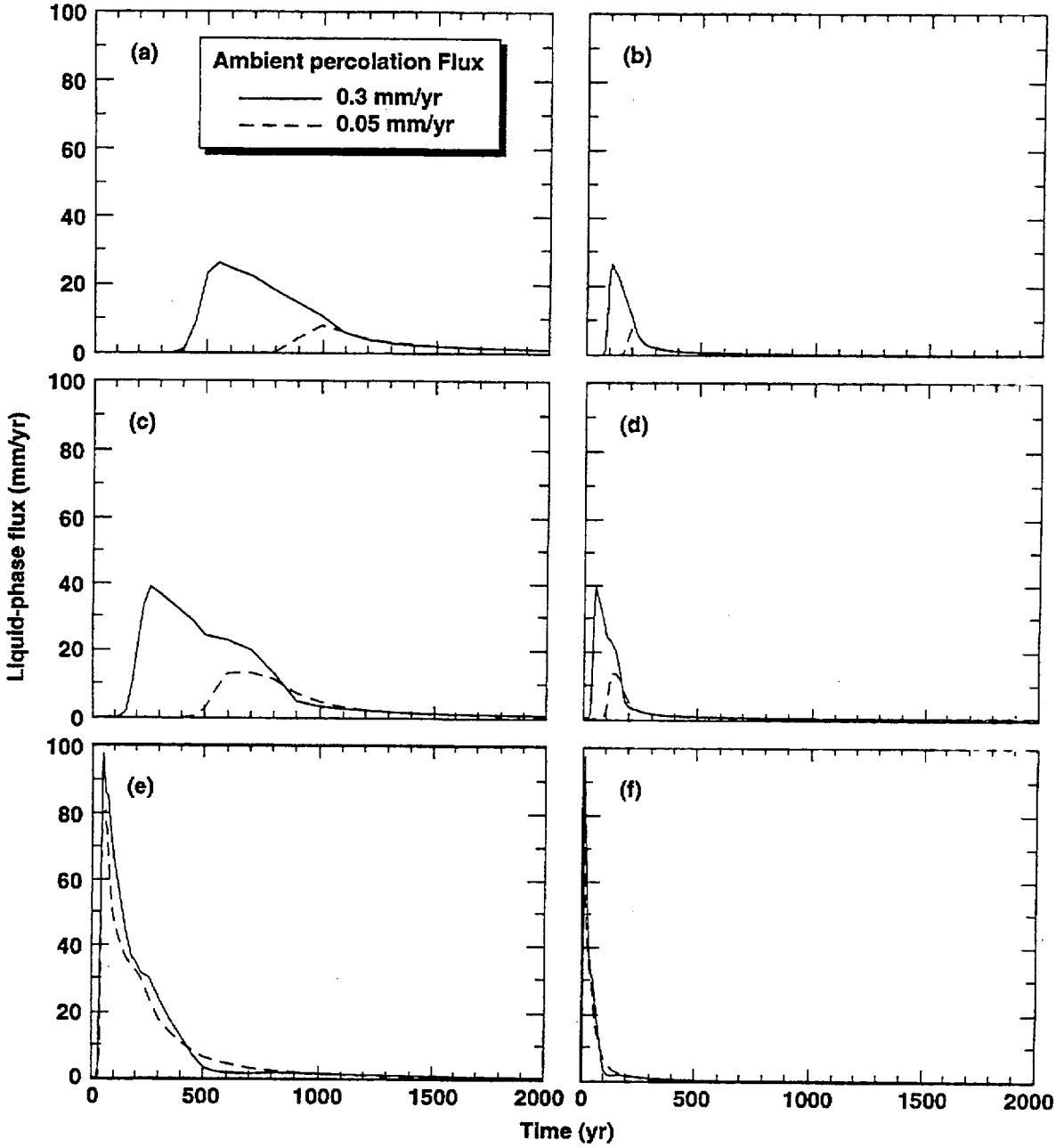

Figure 1.10.6.4. Liquid-phase flux at the repository horizon at various repository locations, including: (a,b) 94%, (c,d) 97%, and (e,f) 100% for AML = 83.4 MTU/acre, repository area = 3.06 km^2, and various ambient percolation fluxes. The repository locations are identified as the percentage of the repository area enclosed, with 0% corresponding to the repository center, and 100% corresponding to the outer perimeter. Calculations were done with a mountain-scale, smeared-heat-source model that uniformly distributes the decay heat from a mixture of 26-yr-old BWR WPs and 26-yr-old PWR WPs over the 3.06-km^2 repository area.

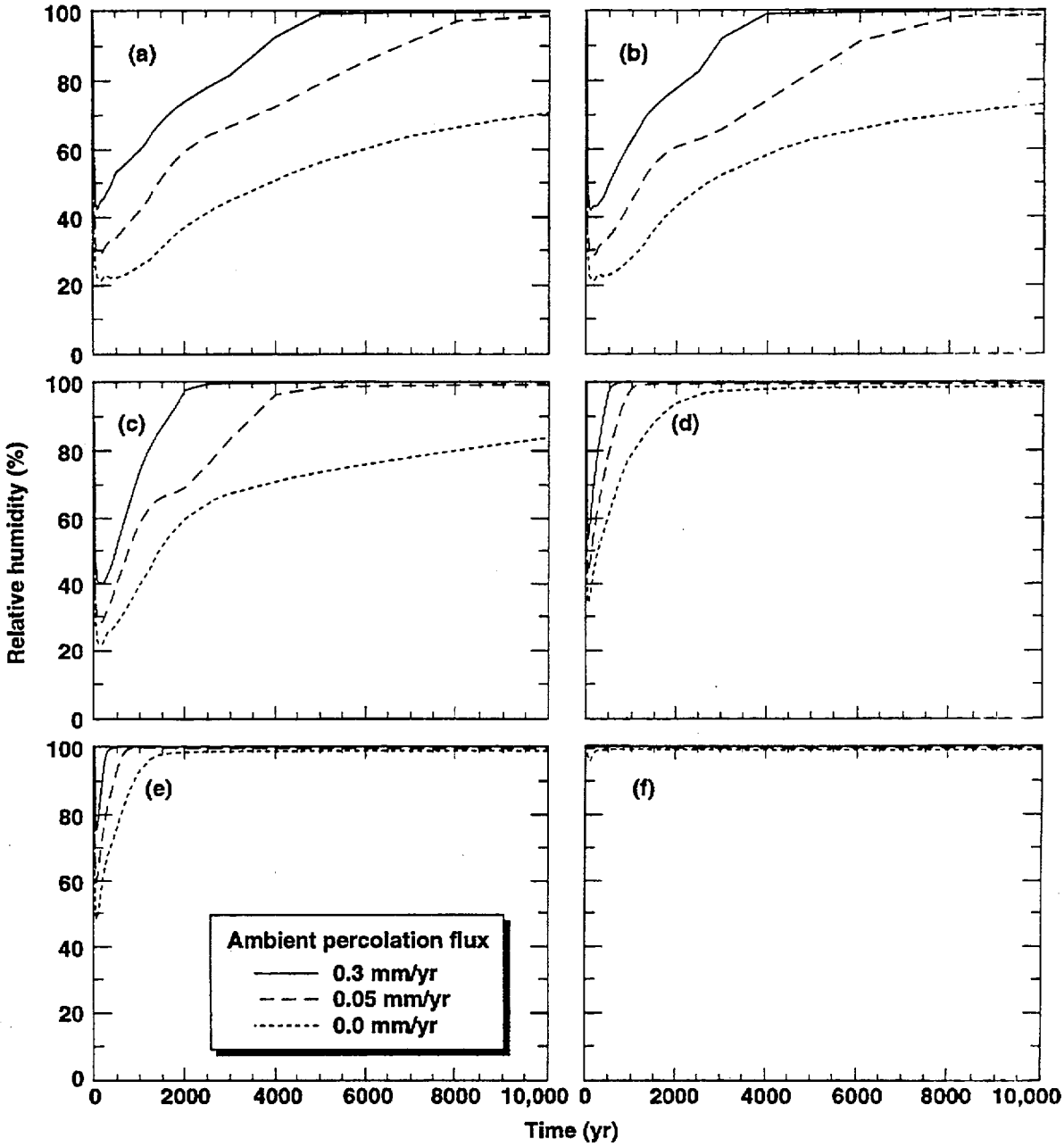

Figure 1.10.6.5. Relative humidity in the rock at the repository horizon at various repository locations, including: (a) 12.5%, (b) 50%, (c) 74%, (d) 94%, (e) 97%, and (f) 100% for AML = 83.4 MTU/acre, repository area = 3.06 km^2, and various ambient percolation fluxes. The repository locations are identified as the percentage of the repository area enclosed, with 0% corresponding to the repository center, and 100% corresponding to the outer perimeter. Calculations were done with a mountain-scale, smeared-heat-source model that uniformly distributes the decay heat from a mixture of 26-yr-old BWR WPs and 26-yr-old PWR WPs over the 3.06-km^2 repository area.

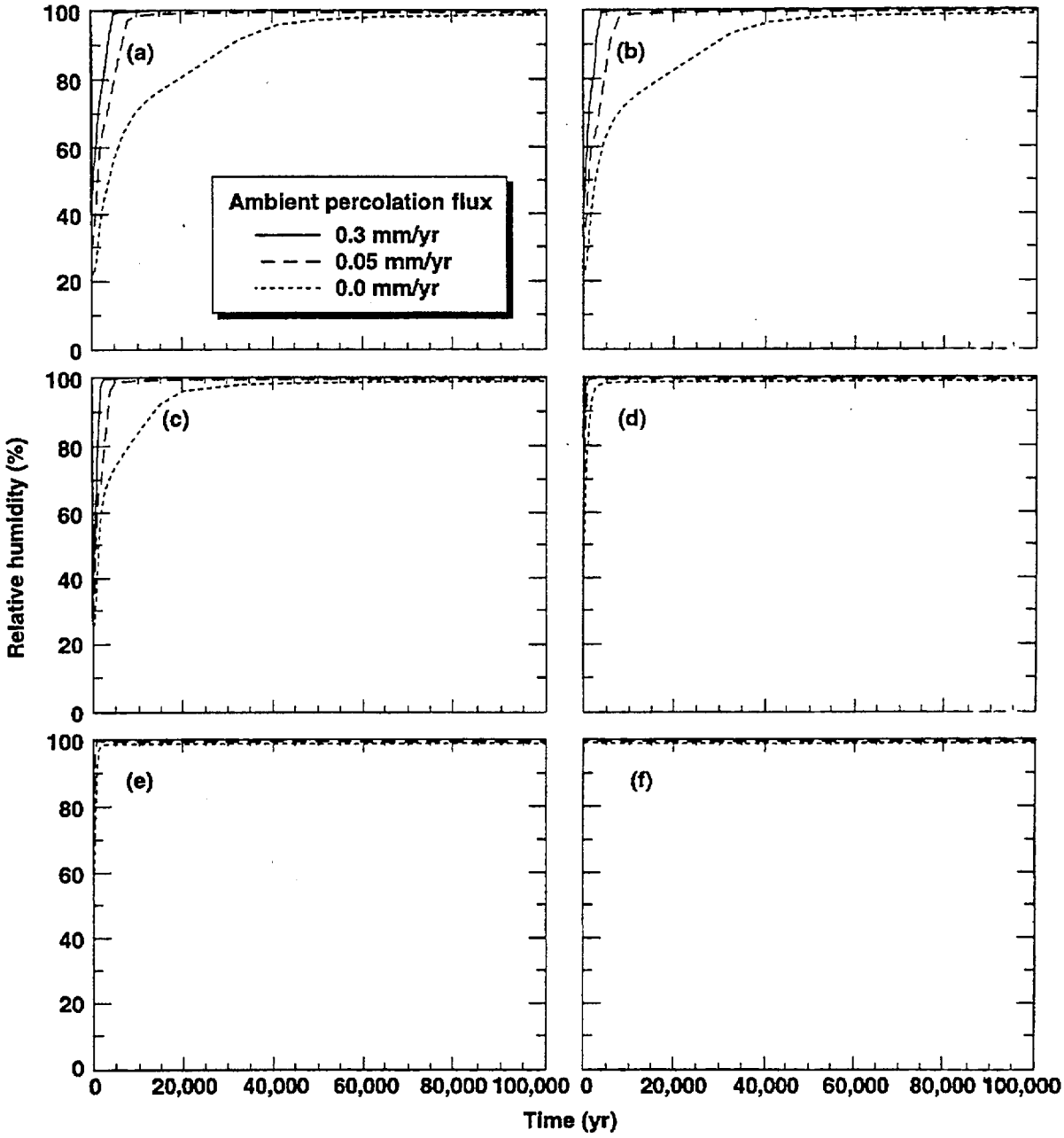

Figure 1.10.6.6. Relative humidity in the rock at the repository horizon at various repository locations, including: (a) 12.5%, (b) 50%, (c) 74%, (d) 94%, (e) 97%, and (f) 100% for AML = 83.4 MTU/acre, repository area = 3.06 km^2, and various ambient percolation fluxes. The repository locations are identified as the percentage of the repository area enclosed, with 0% corresponding to the repository center, and 100% corresponding to the outer perimeter. Calculations were done with a mountain-scale, smeared-heat-source model that uniformly distributes the decay heat from a mixture of 26-yr-old BWR WPs and 26-yr-old PWR WPs over the 3.06-km^2 repository area.

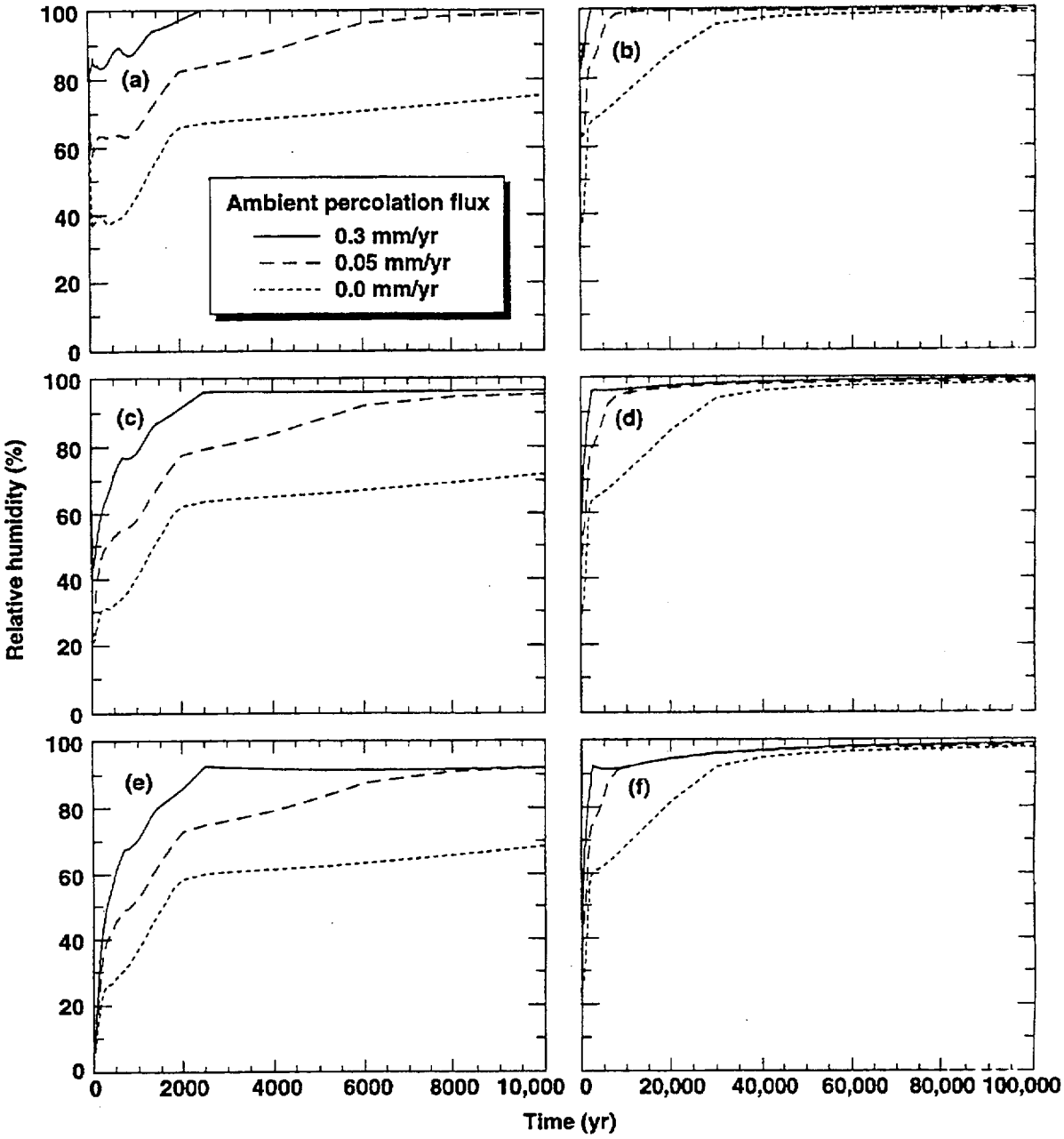

Figure 1.10.6.7. Relative humidity on the upper surface of a Hanford Site DHLW WP (a,b), a 26-yr-old BWR WP (c,d), and a "design basis fuel" 10-yr-old PWR WP (e,f) for AML = 83.4 MTU/acre, the ACD rev 00 design, LML = 0.46 MTU/m, drift spacing = 22.5 m, sand invert, no backfill, drift diameter = 5.5 m, WP emissivity = 0.8, and various values of ambient percolation flux.

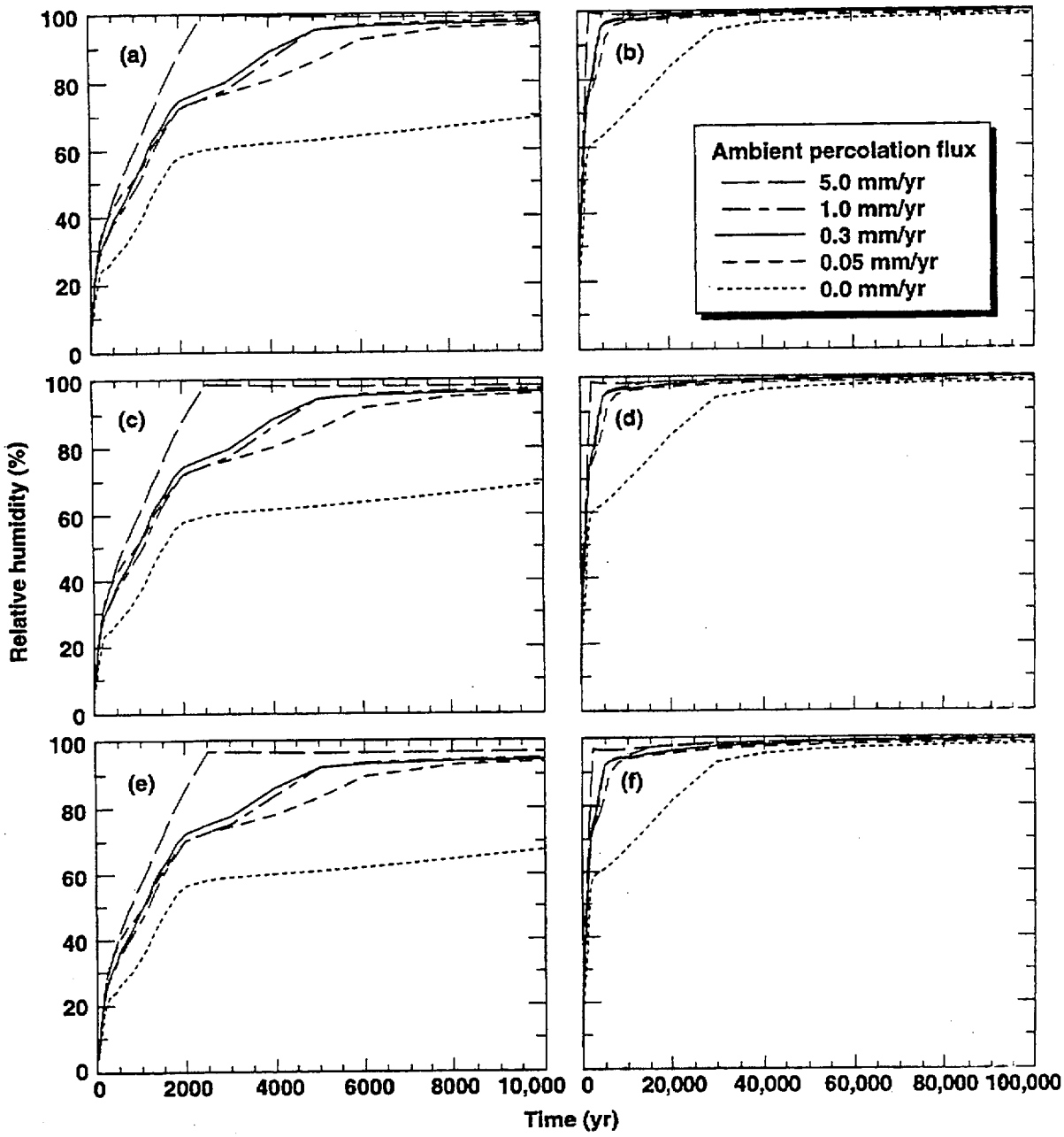

Figure 1.10.6.8. Relative humidity on the upper surface of a Hanford Site DHLW WP (a,b), a 26-yr-old BWR WP (c,d), and a "design basis fuel" 10-yr-old PWR WP (e,f) for AML = 83.4 MTU/acre, a line-load design with a 0.1-m gap between WPs, LML = 1.11 MTU/m, drift spacing = 53.8 m, sand invert, no backfill, drift diameter = 5.5 m, WP emissivity = 0.8, and various values of ambient percolation flux.

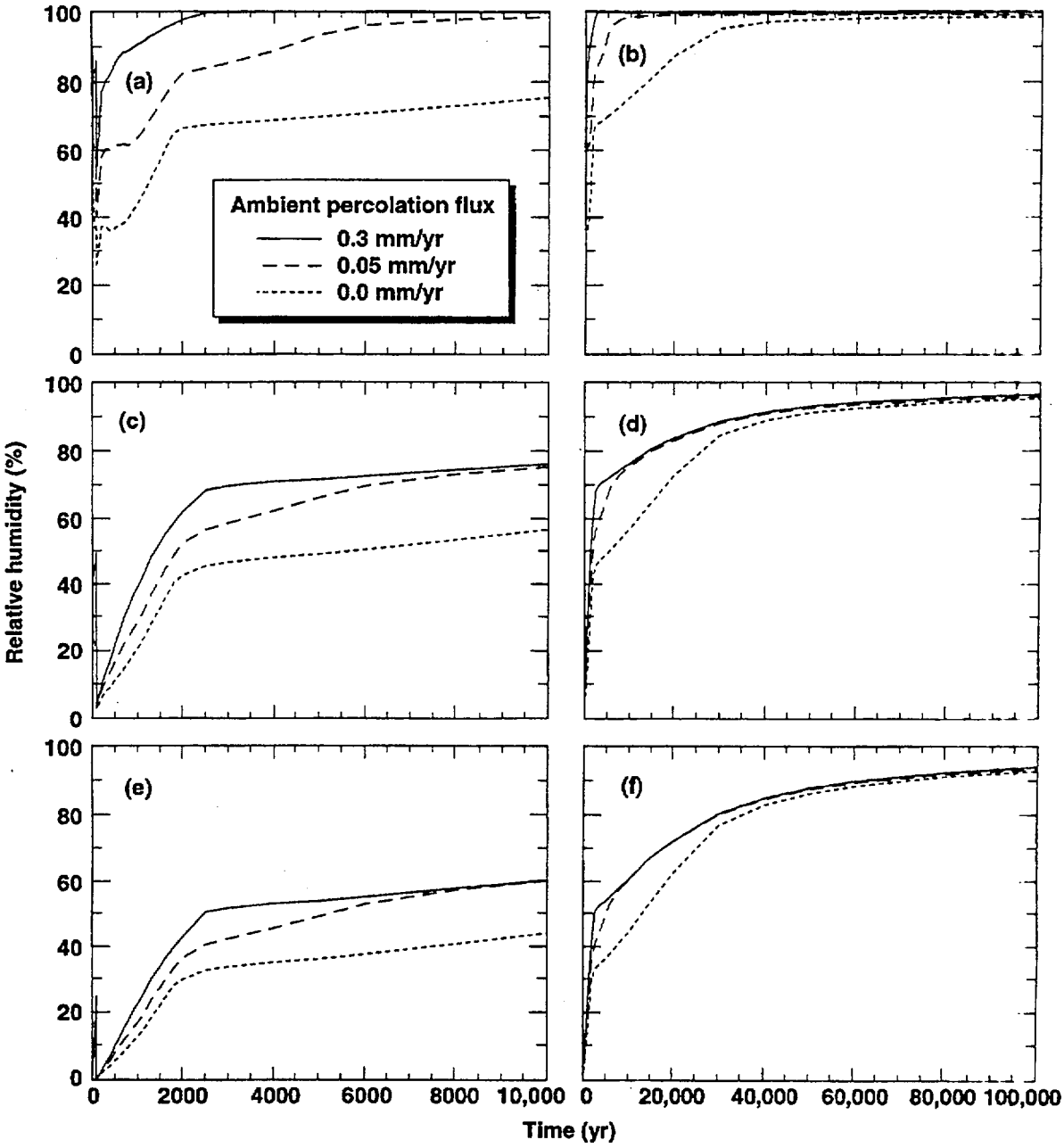

Figure 1.10.6.9: Relative humidity on the upper surface of a Hanford Site DHLW WP (a,b), a 26-yr-old BWR WP (c,d), and a "design basis fuel" 10-yr-old PWR WP (e,f) for AML = 83.4 MTU/acre, the ACD rev 00 design, LML = 0.46 MTU/m, drift spacing = 22.5 m, sand invert, full sand backfill at 100 yr with K_{th} = 0.6 W/m°C, drift diameter = 5.5 m, WP emissivity = 0.8, and various values of ambient percolation flux.

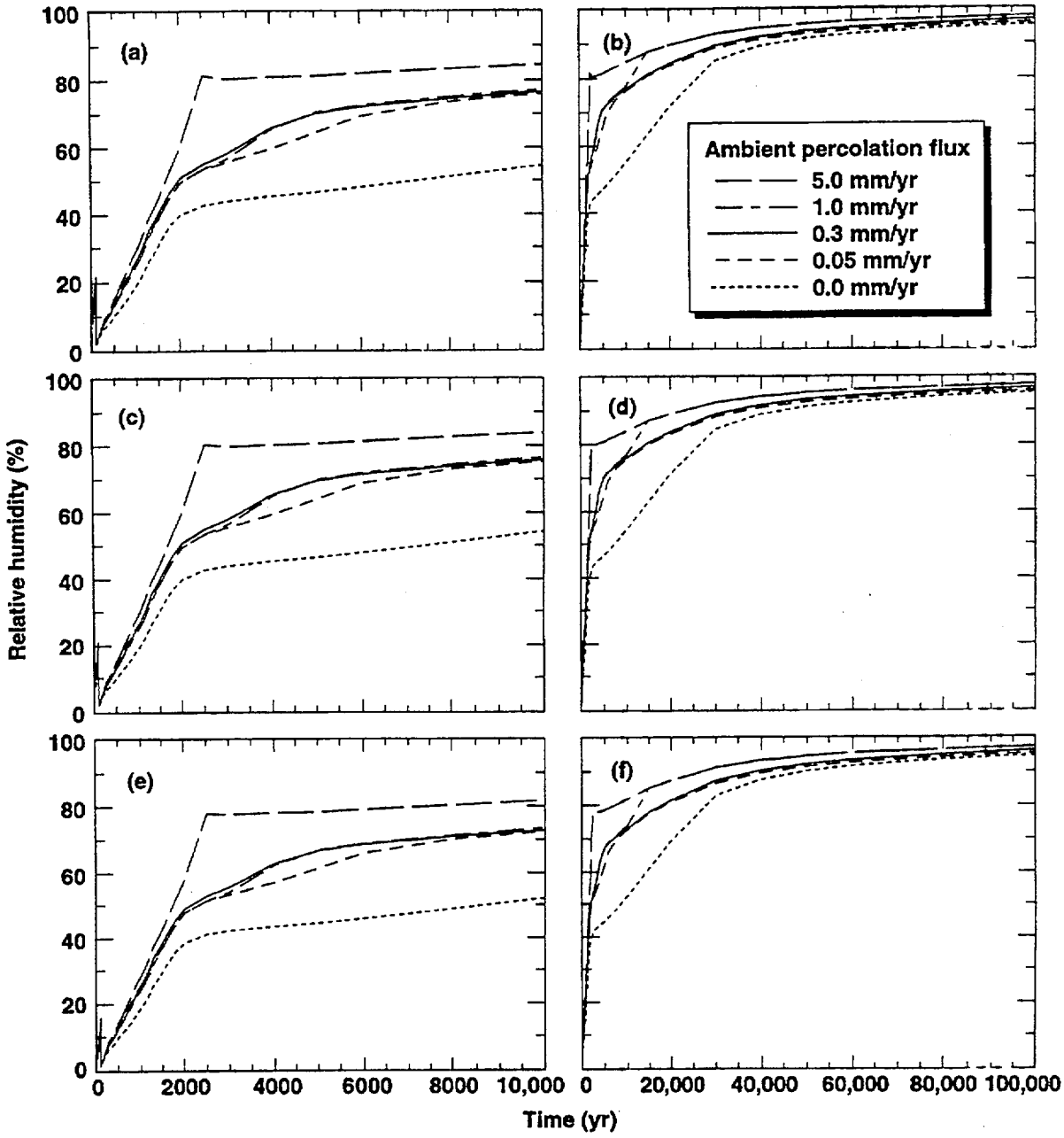

Figure 1.10.6.10. Relative humidity on the upper surface of a Hanford Site DHLW WP (a,b), a 26-yr-old BWR WP (c,d), and a "design basis fuel" 10-yr-old PWR WP (e,f) for AML = 83.4 MTU/acre, a line-load design with a 0.1-m gap between WPs, LML = 1.11 MTU/m, drift spacing = 53.8 m, sand invert, full sand backfill at 100 yr with K_{th} = 0.6 W/m°C, drift diameter = 5.5 m, WP emissivity = 0.8, and various values of ambient percolation flux.

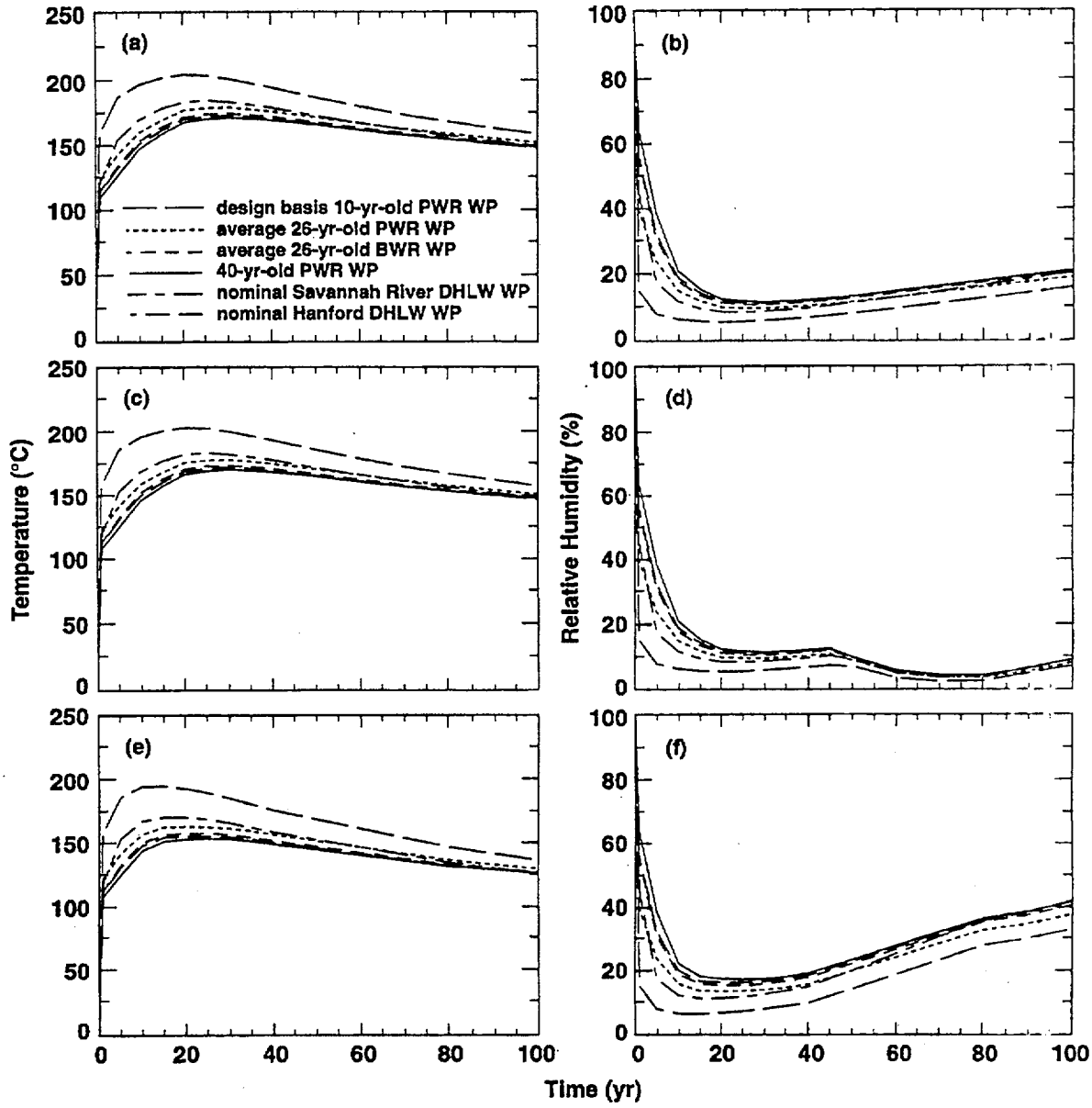

Figure 1.10.6.11. Temperature (a,c,e) and relative humidity (b,d,f) on upper surface of WP for AML = 83.4 MTU/acre, a line-load design with a 0.1-m gap between WPs, LML = 1.11 MTU/m, sand invert, drift diameter = 5.5 m, WP emissivity = 0.8, and percolation flux = 0.3 mm/yr. Curves are plotted for drift-scale model calculations (a,b). Also plotted are hybrid mountain-scale–drift-scale model calculations for two repository locations, including the 12.5% location (b,d), which is near the center of the repository; and the 97% location (e,f), which is equivalent to the outermost drift location. The repository locations are identified as the percentage of the repository area enclosed, with 0% corresponding to the repository center, and 100% corresponding to the outer perimeter.

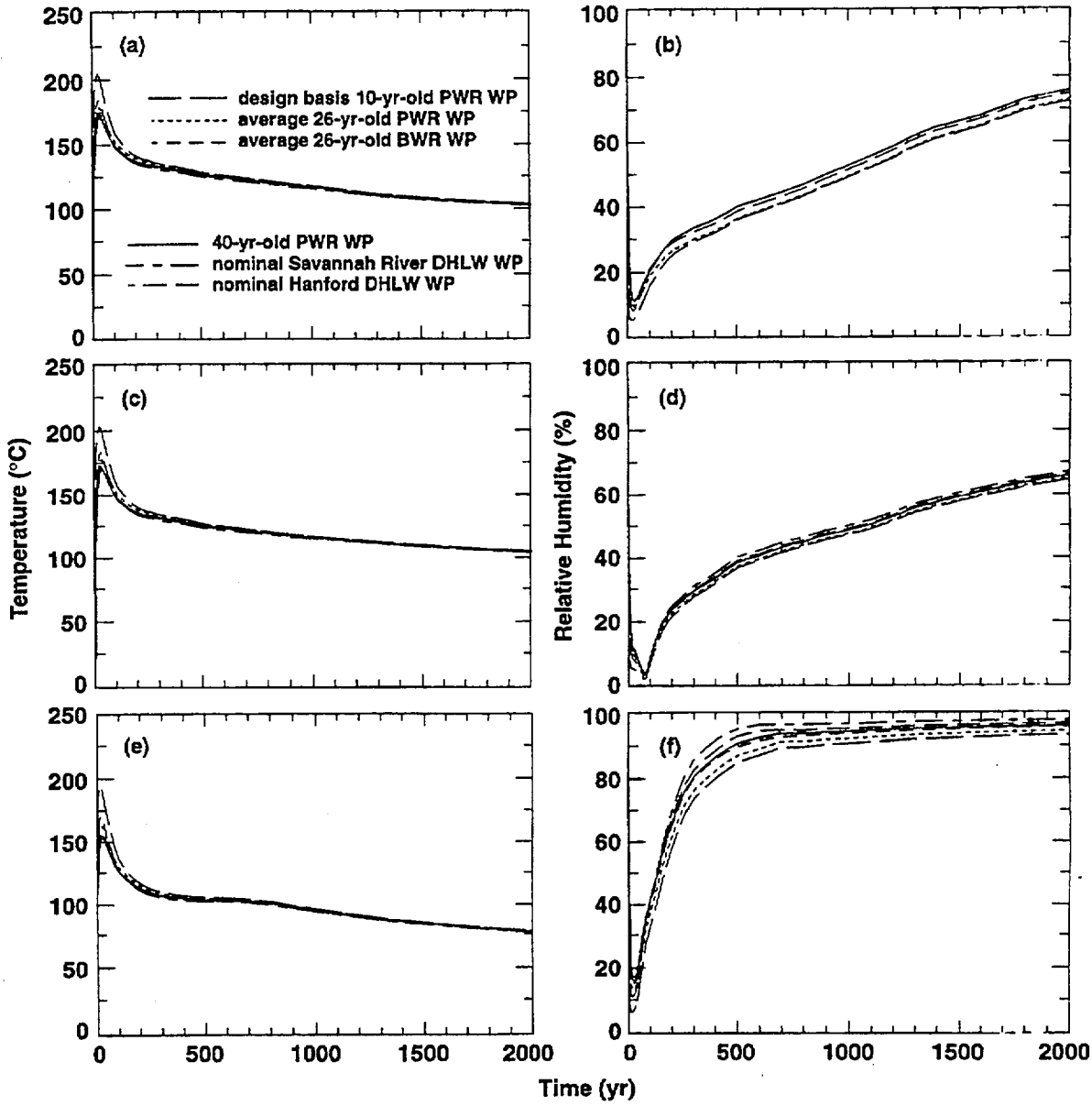

Figure 1.10.6.12. Temperature (a,c,e) and relative humidity (b,d,f) on upper surface of WP for AML = 83.4 MTU/acre, a line-load design with a 0.1-m gap between WPs, LML = 1.11 MTU/m, sand invert, no backfill, drift diameter = 5.5 m, WP emissivity = 0.8, and percolation flux = 0.3 mm/yr. Curves are plotted for drift-scale model calculations (a,b). Also plotted are hybrid mountain-scale–drift-scale model calculations for two repository locations, including the 12.5% location (b,d), which is near the center of the repository; and the 97% location (e,f), which is equivalent to the outermost drift location. The repository locations are identified as the percentage of the repository area enclosed, with 0% corresponding to the repository center, and 100% corresponding to the outer perimeter.

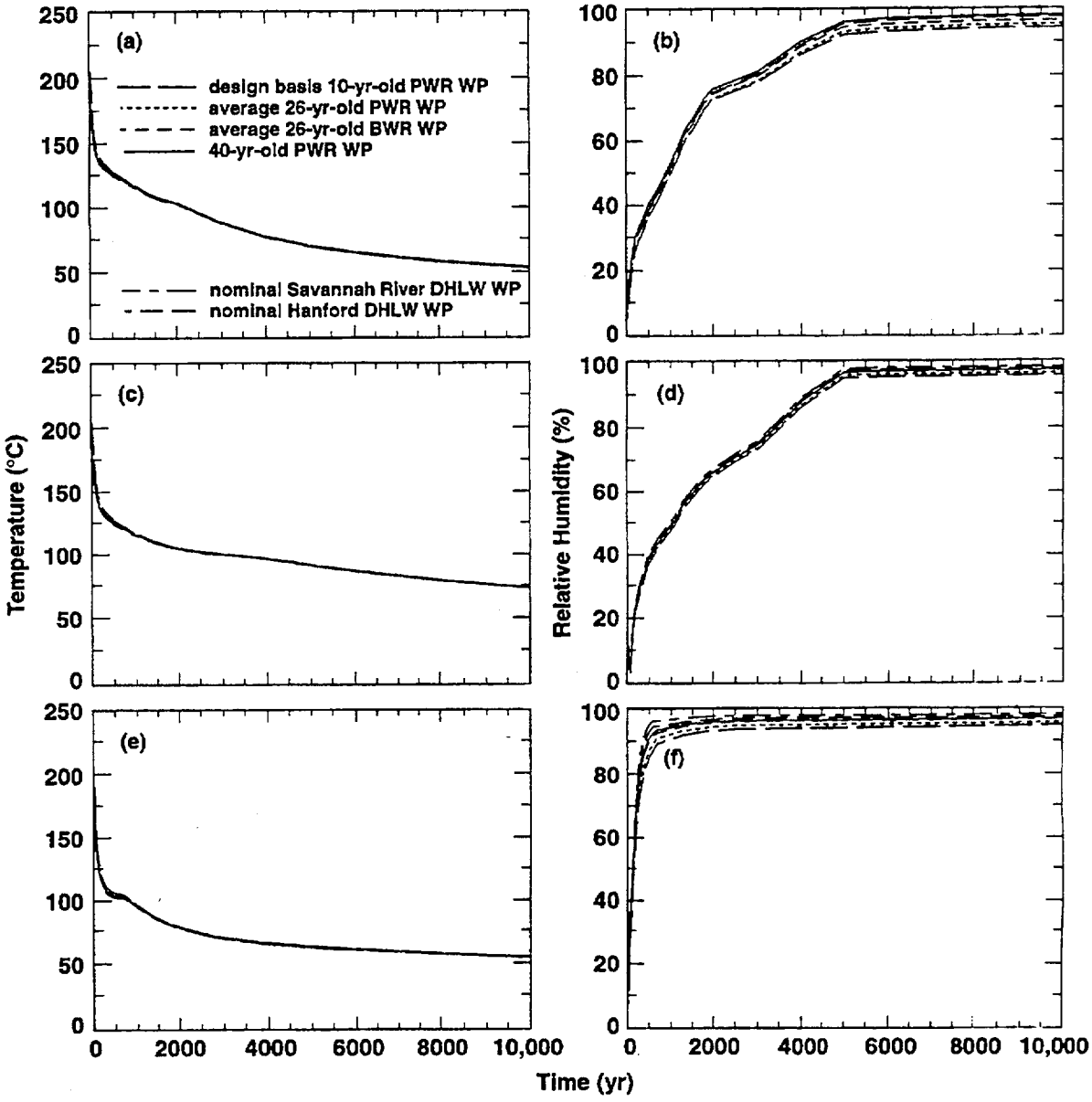

Figure 1.10.6.13. Temperature (a,c,e) and relative humidity (b,d,f) on upper surface of WP for AML = 83.4 MTU/acre, a line-load design with a 0.1-m gap between WPs, LML = 1.11 MTU/m, sand invert, no backfill, drift diameter = 5.5 m, WP emissivity = 0.8, and percolation flux = 0.3 mm/yr. Curves are plotted for drift-scale model calculations (a,b). Also plotted are hybrid mountain-scale–drift-scale model calculations for two repository locations, including the 12.5% location (b,d), which is near the center of the repository; and the 97% location (e,f), which is equivalent to the outermost drift location. The repository locations are identified as the percentage of the repository area enclosed, with 0% corresponding to the repository center, and 100% corresponding to the outer perimeter.

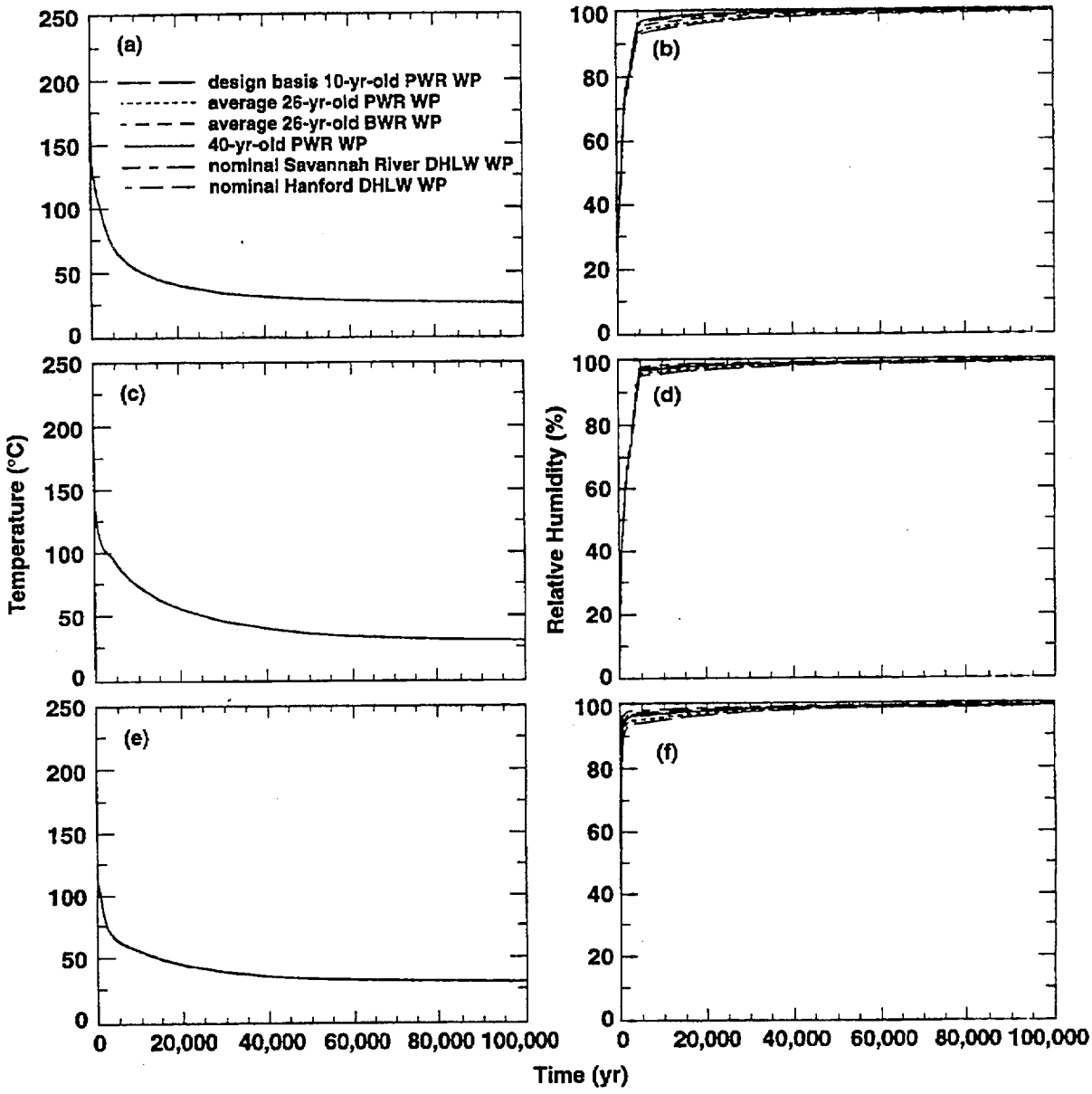

Figure 1.10.6.14. Temperature (a,c,e) and relative humidity (b,d,f) on upper surface of WP for AML = 83.4 MTU/acre, a line-load design with a 0.1-m gap between WPs, LML = 1.11 MTU/m, sand invert, no backfill, drift diameter = 5.5 m, WP emissivity = 0.8, and percolation flux = 0.3 mm/yr. Curves are plotted for drift-scale model calculations (a,b). Also plotted are hybrid mountain-scale–drift-scale model calculations for two repository locations, including the 12.5% location (b,d), which is near the center of the repository; and the 97% location (e,f), which is equivalent to the outermost drift location. The repository locations are identified as the percentage of the repository area enclosed, with 0% corresponding to the repository center, and 100% corresponding to the outer perimeter.

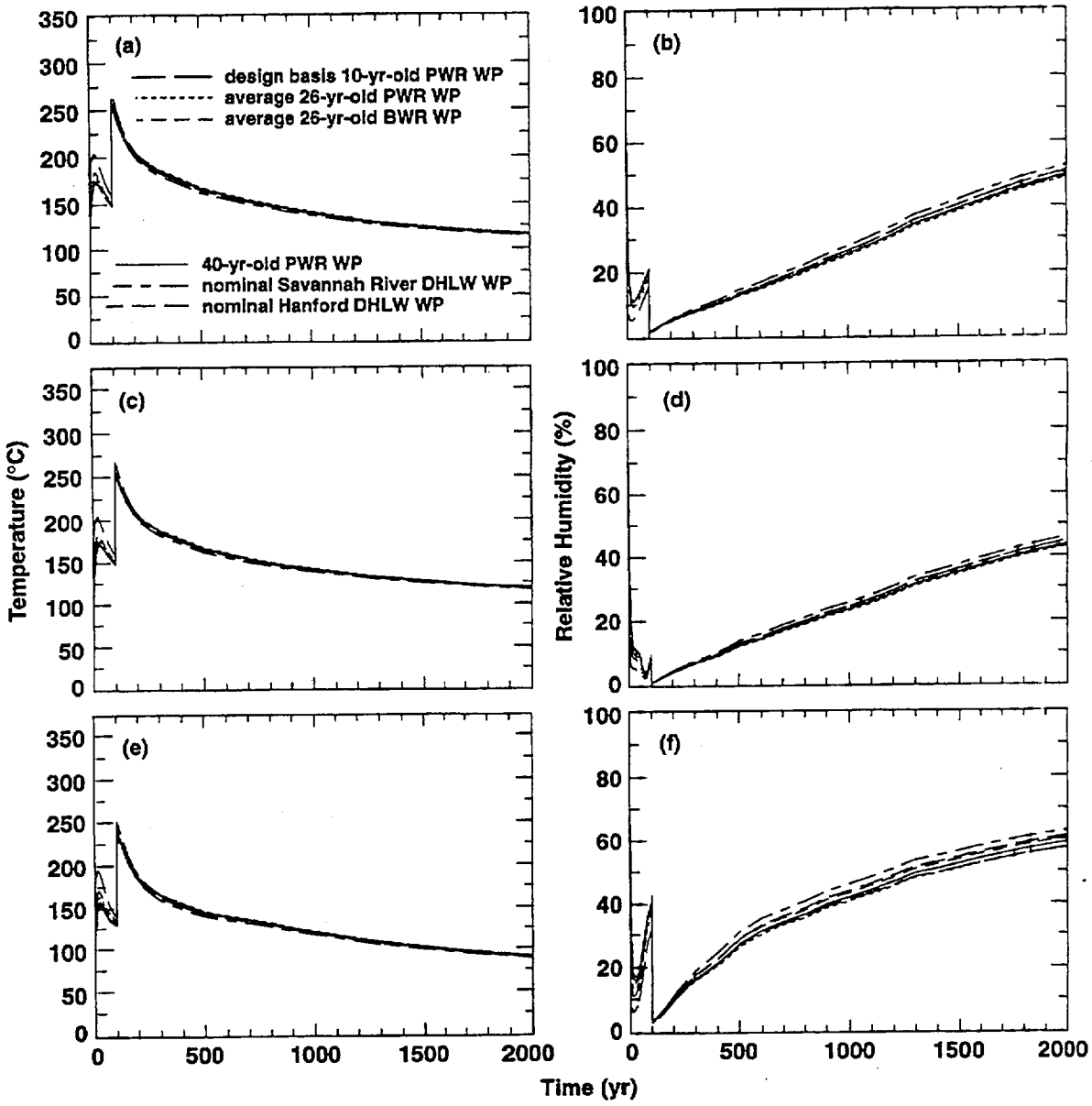

Figure 1.10.6.15. Temperature (a,c,e) and relative humidity (b,d,f) on upper surface of WP for AML = 83.4 MTU/acre, a line-load design with a 0.1-m gap between WPs, LML = 1.11 MTU/m, sand invert, full sand backfill with K_{th} = 0.6 W/m°C, drift diameter = 5.5 m, WP emissivity = 0.8, and percolation flux = 0.3 mm/yr. Curves are plotted for drift-scale model calculations (a,b). Also plotted are hybrid mountain-scale–drift-scale model calculations for two repository locations, including the 12.5% location (b,d), which is near the center of the repository; and the 97% location (e,f), which is equivalent to the outermost drift location. The repository locations are identified as the percentage of the repository area enclosed, with 0% corresponding to the repository center, and 100% corresponding to the outer perimeter.

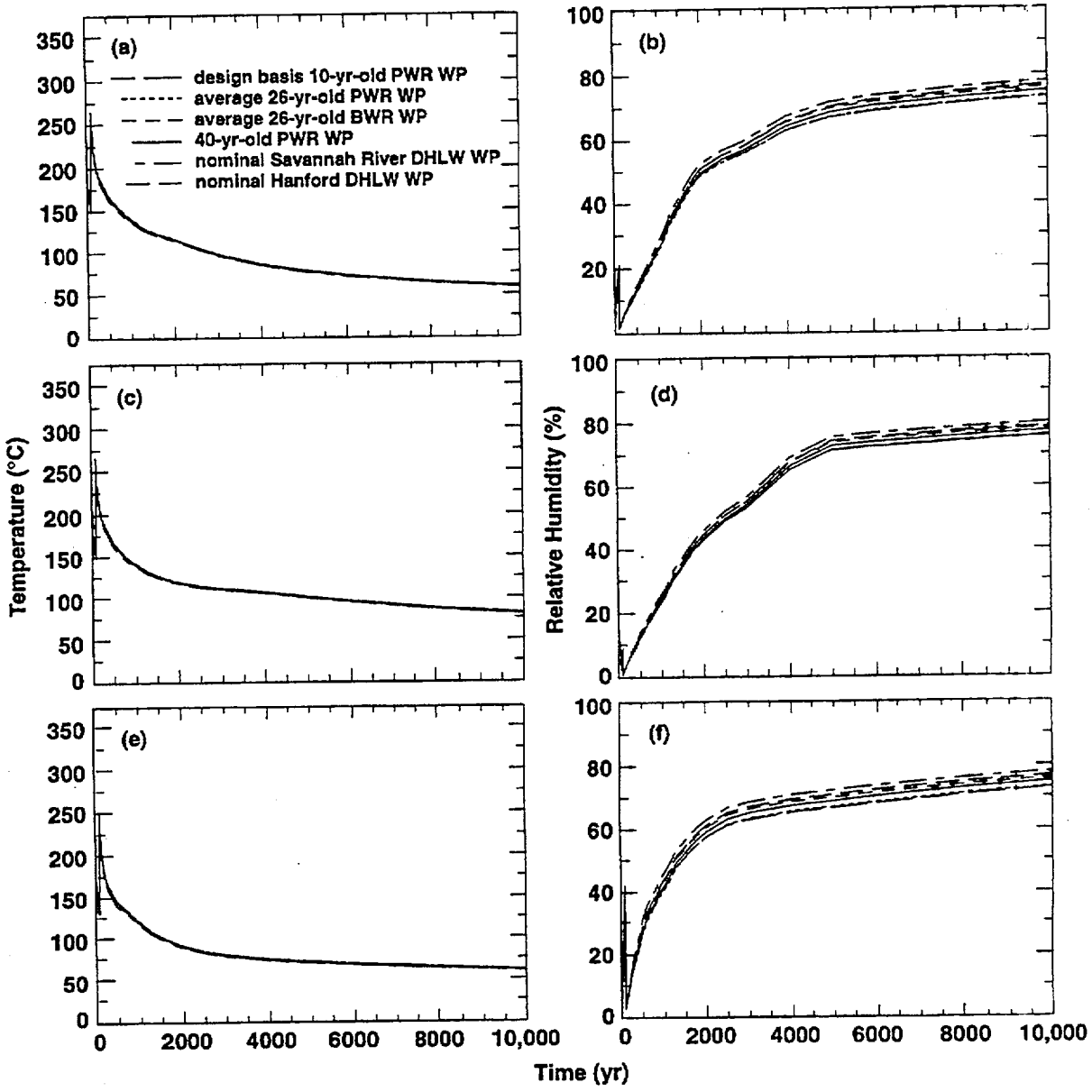

Figure 1.10.6.16. Temperature (a,c,e) and relative humidity (b,d,f) on upper surface of WP for AML = 83.4 MTU/acre, a line-load design with a 0.1-m gap between WPs, LML = 1.11 MTU/m, sand invert, full sand backfill with K_{th} = 0.6 W/m°C, drift diameter = 5.5 m, WP emissivity = 0.8, and percolation flux = 0.3 mm/yr. Curves are plotted for drift-scale model calculations (a,b). Also plotted are hybrid mountain-scale–drift-scale model calculations for two repository locations, including the 12.5% location (b,d), which is near the center of the repository; and the 97% location (e,f), which is equivalent to the outermost drift location. The repository locations are identified as the percentage of the repository area enclosed, with 0% corresponding to the repository center, and 100% corresponding to the outer perimeter.

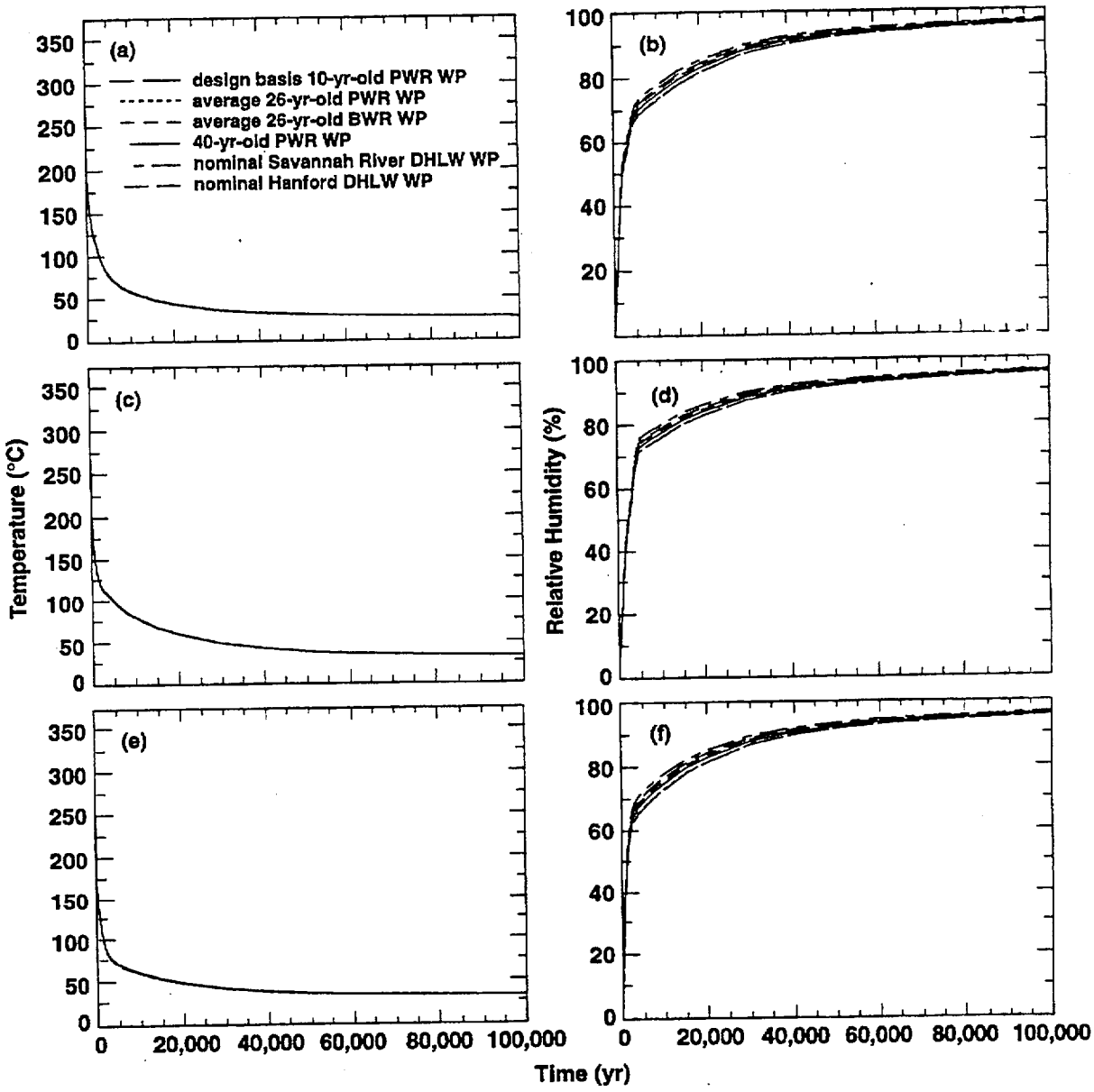

Figure 1.10.6.17. Temperature (a,c,e) and relative humidity (b,d,f) on upper surface of WP for AML = 83.4 MTU/acre, a line-load design with a 0.1-m gap between WPs, LML = 1.11 MTU/m, sand invert, full sand backfill with K_{th} = 0.6 W/m°C, drift diameter = 5.5 m, WP emissivity = 0.8, and percolation flux = 0.3 mm/yr. Curves are plotted for drift-scale model calculations (a,b). Also plotted are hybrid mountain-scale–drift-scale model calculations for two repository locations, including the 12.5% location (b,d), which is near the center of the repository; and the 97% location (e,f), which is equivalent to the outermost drift location. The repository locations are identified as the percentage of the repository area enclosed, with 0% corresponding to the repository center, and 100% corresponding to the outer perimeter.

1.10.7 Comparison of Discrete-Fracture Model with Equivalent Continuum Model

A discrete-fracture model (DFM) was developed (refer to Section 1.9.7 and Nitao and Buscheck [1995] for further details) to simulate drift-scale thermal-hydrological behavior at the repository site at Yucca Mountain. A single symmetry cell from an infinite array of drifts was modeled with discrete fracture planes spaced 0.33 m apart transverse to the drift. Fractures of various apertures were modeled. Areal mass loadings of 40, 48, and 60 MTU/acre were considered, corresponding to drift spacings of 120, 100, and 80 m, respectively. Calculations were done with a two-dimensional model that averages the heat output from a mixture of 26-yr-old BWR WPs and 26-yr-old PWR WPs into a uniform line-heat load (refer to Section 1.10.1.2 and Buscheck and Nitao [1995] for further details). The 40-MTU/acre case is characterized by cylindrical boiling zones that never coalesce between drifts, the boiling zones in the 48-MTU/acre case barely coalesce, and the boiling zones in the 60-MTU/acre case coalesce into a single tabular boiling zone centered at the repository horizon. The effect of repository ventilation on the moisture and heat transport was not considered. The model extends from the ground surface to the water table. Various units described by Peters et al. [1984] were treated as horizontal layers of constant thickness, as was done by Buscheck et al. [1995], along with uniform fracture aperture over all hydrostratigraphic units. For all cases, the equivalent continuum model (ECM) was also used to calculate drift-scale thermal-hydrological behavior [Refer to Section 1.1.3.2 for the discussion of the DFM and the ECM].

Figure 1.10.7.1 shows the vertical profile of bulk liquid saturation intersecting the WP axis. An interesting result is that the bulk saturations predicted by the ECM and the DFM eventually agree within a few hundred years. During approximately the first 100 yr after emplacement, the DFM predicts significant nonequilibrium fracture flow, resulting in considerable condensate drainage from above to below the repository horizon, as indicated by the vertically asymmetric bulk saturations profile in Fig. 1.10.7.2, while the ECM predicts very little net drainage of condensate through the repository horizon during this period. After less than 100 yr, the nonequilibrium condensate shedding behavior (as characterized by drainage around and below the boiling zones) ceases in the DFM, and the system approaches nearly the same state as that predicted by the ECM; both the ECM and DFM predict condensate refluxing (of virtually the same magnitude) in fractures above the repository for thousands of years after boiling fronts between drifts coalesce. The close agreement of the ECM with the DFM despite the presence of fracture flow is the result of the matrix becoming saturated in the condensation zone. Our model assumed homogeneous connectivity in the fracture, but long-term refluxing can occur without boiling zone coalescence if horizontal fracture connectivity above the boiling zone is poor. The characteristic time for the eventual quasi-equilibrium between the fractures and matrix would be longer if a larger fracture spacing were used; this effect will be investigated in future work.

The tendency for downward drainage of condensate flow in fractures to decrease with time is related to the decrease in specific thermal flux (i.e., thermal flux per unit area of outer boiling boundary) at the boiling zone. The causes of the decrease are (1) decrease in WP heat output and (2) increase in the area of the boiling boundary as the boiling front expands. The local condensate flux, which is approximately proportional to the thermal flux, eventually becomes so small that the matrix imbibes most or all of the condensate (as quickly as it is generated). The point at which this transition occurs can be expressed in terms of the critical flux for fracture-dominated flow [Nitao et al., 1993]. Heterogeneous distributions of fracture and matrix properties may delay the transition by increasing local condensate flux through vapor and condensate flow focusing [Buscheck and Nitao, 1994a].

A higher initial matrix saturation than that assumed here will decrease imbibition fluxes and prolong the period of significant condensate shedding.

DFM drift-scale repository simulations suggest that nonequilibrium condensate shedding ceases less than 100 yr after waste emplacement; the period of significant condensate shedding may increase for heterogeneous fracture and matrix property distributions or for higher initial liquid saturations than were assumed in the calculations presented in this section [Nitao and Buscheck, 1995]. The ECM is found to agree with the DFM after this early period of significant condensate shedding. Refluxing of condensate in fractures above the repository predicted by ECM agrees with that predicted by DFM. In future work we will determine the sensitivity of our simulation results to fracture spacing and heterogeneous matrix and fracture distributions and extend the calculations to larger repository scales.

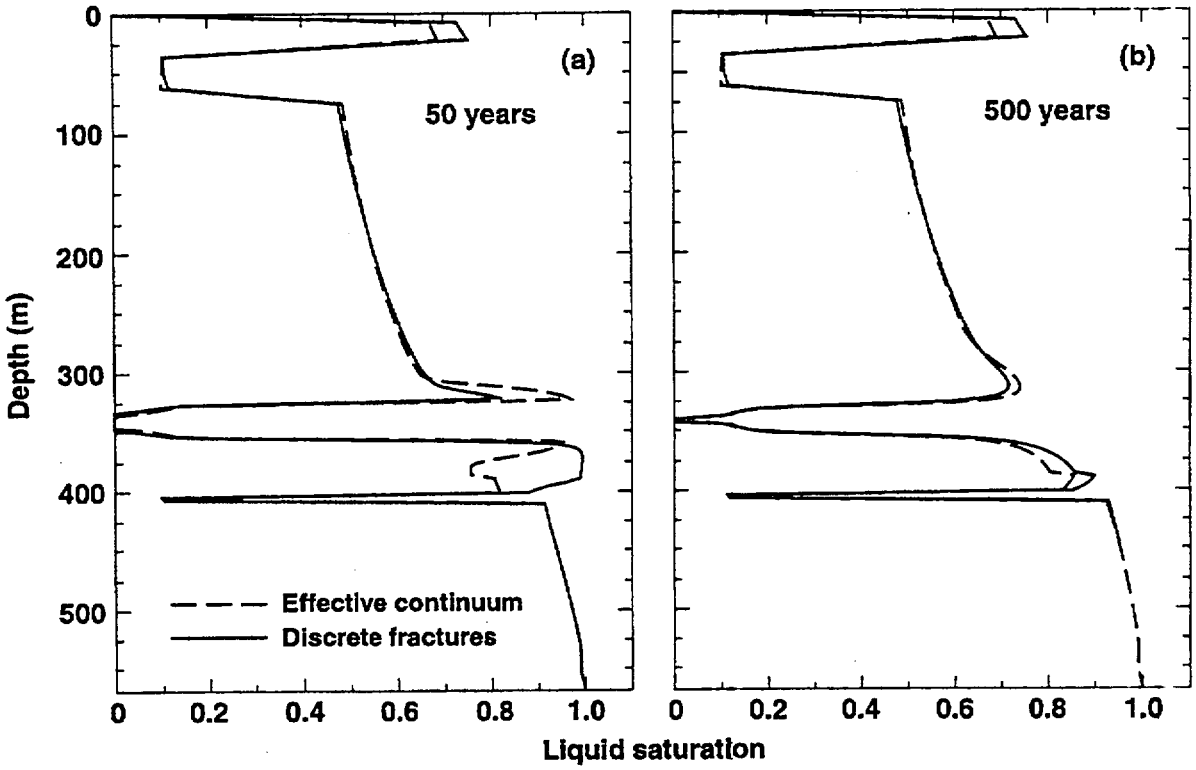

Figure 1.10.7.1. Vertical profile of ECM bulk liquid saturation and DFM matrix-averaged liquid saturation in transverse plane to drift (a) at 50 years and (b) 500 years from emplacement for drift-scale repository model using k_b = 280 millidarcy (corresponding to 100 μm fractures) and areal mass loading of 48 MTU/acre.

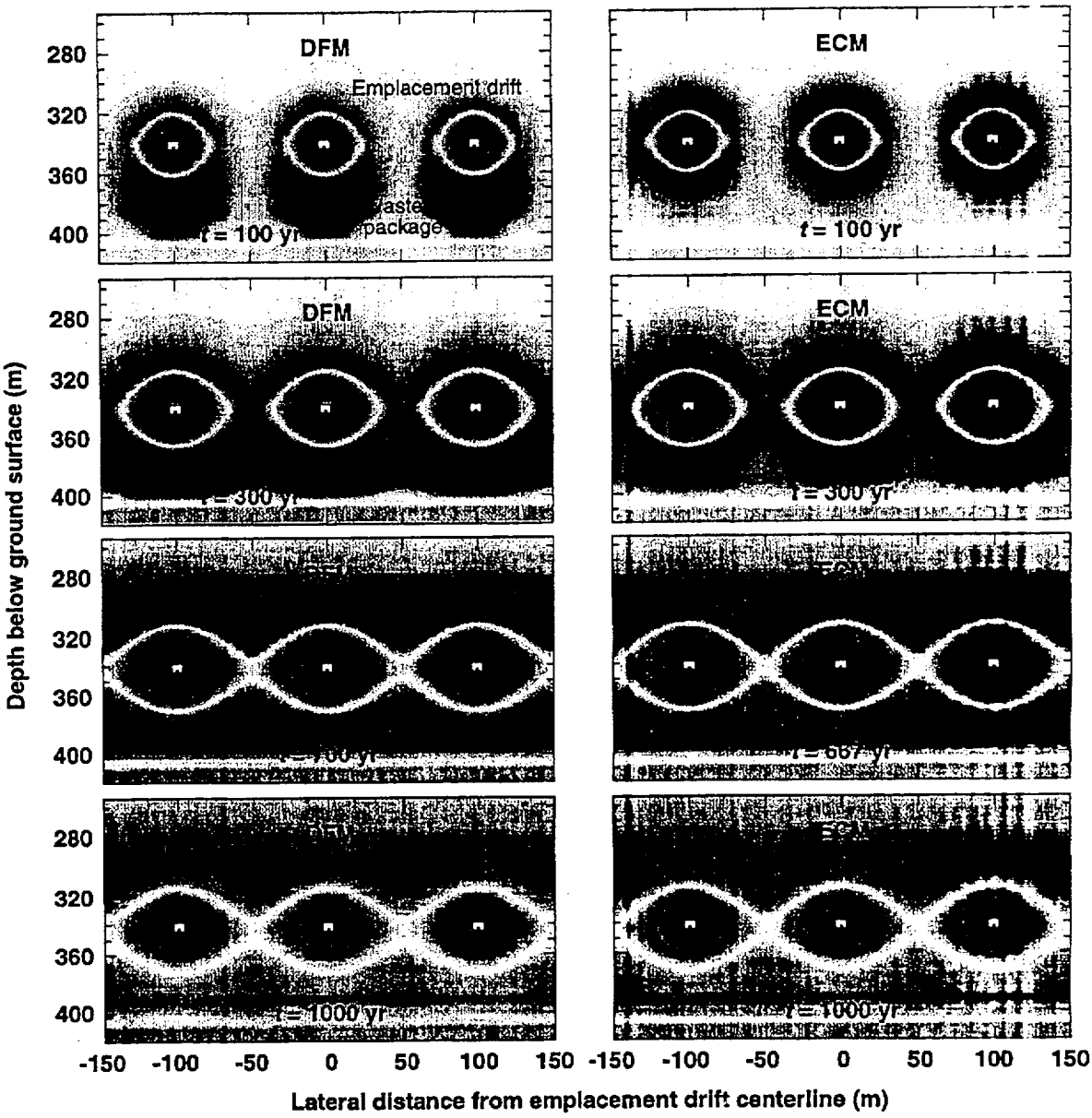

Figure 1.10.7.2. ECM bulk dimensionless liquid saturation and DFM matrix-averaged dimensionless liquid saturation in plane transverse to drift for the repository model at various times for k_b = 280 millidarcy and areal mass loading of 48 MTU/acre. Same shading as used for Figure 4.

References

Abelin, H., Birgersson, L., and Neretnieks, I., (1987), "Some Recent Observations of Channeling in Fractured Rocks — Its Potential Impact on Radionuclide Migration," *Proceedings, DOE/AECL Conference*, September 15–17, San Francisco, CA, pp. 387–410.

Abelin, H., L. Birgersson, J. Gidlund, and I. Neretnieks, "A Large-Scale Flow and Tracer Experiment in Granite, 1. Experimental Design and Flow Distribution," *Water Resources Research* 27, 3107–3117 (1991).

Buscheck, T. A., and J. J. Nitao, *Nonequilibrium Fracture-Matrix Flow During Episodic Infiltration Events in Yucca Mountain*, Lawrence Livermore National Laboratory, Livermore, CA, UCRL-ID-108311 (1991).

Chesnut, D. A., Alan L. Flint, , and Joseph S. Y. Wang, *Coordinated Exploratory Studies Facility (ESF) Construction-Phase Testing and Monitoring Program*, Scientific Programs Operations, Management and Operating Contractor Milestone Report M4-TR31K5M, May 28, 1996.

Chesnut, D. A., D. O. COX, and G. L. ASAKI, "A Practical Method for Waterflood Performance Prediction and Evaluation," *Proceedings, Pan American Congress of Petroleum Engineering*, Mexico City, March 19-23 (1979).

Chesnut, Dwayne A., "Characterizing the Altered Zone at Yucca Mountain: The Beginning of a Testing Strategy," *Proceedings, Third International High-Level Radioactive Waste Management Conference*; American Nuclear Society, Inc.: Las Vegas, NV, pp. 1026–1039 (1992).

Chesnut, Dwayne A., and Dale G. Wilder, Foreign Trip Report: Åspö Hard Rock Laboratory Workshop on Design and Construction of Deep Repositories, Såstaholm Conference Center, Täby, Sweden, March 30-April 1, 1993 (Submitted to Lawrence Livermore National Laboratory, May 7, 1993).

Cox, Dave O., and Nick Stellavato, "Analysis of Air Permeability Tests at Yucca Mountain, Nevada," *Proceedings, ??? Annual International High-Level Radioactive Waste Management Conference, Las Vegas, Nevada.* April 29–May 3, 1996.

Fabryka-Martin, J. T., P. R. Dixon, S. Levy, B. Liu, H. J. Turin, and A. V. Wolfsberg, *Summary Report of Chlorine-36 Studies: Systematic Sampling for Chlorine-36 in the Exploratory Studies Facility.* Level 4 Milestone Report 3783AD, Los Alamos National Laboratory, March 29, 1996.

Flint, Lorraine E., *Matrix Properties of Hydrogeologic Units at Yucca Mountain, Nevada*, U.S. Geological Survey, Water Resources Investigations Report 96-xx (in review, 7/22/96).

Gauthier, John H., Michael L. Wilson, and Franz C. Lauffer, "Estimating the Consequences of Significant Fracture Flow at Yucca Mountain," *Proceedings, Third International High-Level Radioactive Waste Management Conference*, American Nuclear Society, Inc.: Las Vegas, NV, pp. 891–898 (1992).

Harr, M. E., *Reliability-Based Design in Civil Engineering*, McGraw-Hill Book Company (1987).

Hudson, David B., and Alan L. Flint, *Estimation of Shallow Infiltration and Presence of Potential Fast Pathways for Shallow Infiltration in the Yucca Mountain Area, Nevada.* U.S. Geological Survey, Water Resources Investigations Report xx-xxx, 1996 (in press).

LeCain, G. D., and J. N. Walker, "Results of Air Permeability Testing in a Vertical Borehole at Yucca Mountain, Nevada," *Radioactive Waste Management*, pp. 2782–2788, 1994.

Liu, Beiling, June Fabryka-Martin, Andy Wolfsberg, Bruce Robinson, and Pankaj Sharma, "Significance of Apparent Discrepancies in Water Ages Derived from Atmospheric Radionuclides at Yucca Mountain, Nevada," *Water Resources at Risk*, American Institute of Hydrology Conference, Denver, Colorado, May 14–18, 1995.

Loeven, Colleen, *A Summary and Discussion of Hydrologic Data from the Calico Hills Nonwelded Hydrogeologic Unit at Yucca Mountain, Nevada*, Report LA-12376-MS, Los Alamos National Laboratory 1993.

Moreno Luis, Ivars Neretnieks, and Björn Gylling, "Modeling of Fluid and Solute Transport in Fractured Rock," *Proceedings, Fourth International High-Level Radioactive Waste Management Conference*, American Nuclear Society, Inc.: Las Vegas, NV, pp. 1128–1133 (1993).

Nativ, Ronit, Eilon Adar, Ofer Dahan, and Mebus Geyh, "Water recharge and solute transport through the vadose zone of fractured chalk under desert conditions," *Water Resources Research* 31, No. 2, pp. 253-261, (Feb. 1995).

Rousseau, Joseph P., Edward M. Kwicklis, and Daniel C. Gillies, editors: *Hydrogeology of the Unsaturated Zone, North Ramp Area of the Exploratory Studies Facility, Yucca Mountain, Nevada*, U.S. Geological Survey, Water Resources Investigations Report 96-xx (in review, 8/96).

Russel, C.E., J.W. Hess, and S.W. Tyler, *Hydrolgeologic Investigation of Flow in Fractured Tuffs, Rainier Mesa, Nevada Test Site,* Flow and Transport through Unsaturated Fractured Rock, D. D. Evans and T. J. Nicholson (editors), Geophysical Monograph #42, AGU, Washington, DC, 1987.

Wang, J. S. Y., N. G. W. Cook, H. A. Wollenberg, C. L. Carnahan, I. Javandel, and C.F. Tsang, "Geohydrologic Data and Models of Rainier Mesa and Their Implications to Yucca Mountain," *Proceedings, Fourth Annual International High-Level Radioactive Waste Management Conference,* Las Vegas, NV, April 26–30, 1993.

Wilder, D. G., *Influence of Stress-Induced Deformations on Observed Water Flow in Fractures at the Climax Granitic Stock,* Rock Mechanics: Proceedings of 28th U.S. Symposium, Tucson, AZ; Edited by I.W. Farmer, J.J.K. Daemen, C.S. Desai, C.E. Glass and S.P. Neuman; A.A. Balkema, Rotterdam, 1987.

University of California
Lawrence Livermore
National Laboratory

UCRL-LR-124998

Volume II: Near-Field and Altered-Zone Environment Report

Chapters 2–11 and Appendix

Dale G. Wilder

August 23, 1996